LOCKHEED MARTIN ENERGY RESEARCH LIBRARIES

3 4456 0445258 0

ORNL/TM-13565

ornl

OAK RIDGE
NATIONAL
LABORATORY

LOCKHEED MARTIN

High Temperature Materials Laboratory

Tenth Annual Report: October 1996 Through September 1997

A. E. Pasto
B. J. Russell

OAK RIDGE NATIONAL LABORATORY
CENTRAL RESEARCH LIBRARY
CIRCULATION SECTION
4500N ROOM 175
LIBRARY LOAN COPY
DO NOT TRANSFER TO ANOTHER PERSON.
if you wish someone else to see this report, send in name with report and the library will arrange a loan.
ORNL-118 (6-97)

MANAGED AND OPERATED BY
LOCKHEED MARTIN ENERGY RESEARCH CORPORATION
FOR THE UNITED STATES
DEPARTMENT OF ENERGY

ORNL-27 (3-96)

This report has been reproduced directly from the best available copy.

Available to DOE and DOE contractors from the Office of Scientific and Technical Information, P.O. Box 62, Oak Ridge, TN 37831; prices available from (615) 576-8401, FTS 626-8401.

Available to the public from the National Technical Information Service, U.S. Department of Commerce, 5285 Port Royal Rd., Springfield, VA 22161.

This report was prepared as an account of work sponsored by an agency of the United States Government. Neither the United States Government nor any agency thereof, nor any of their employees, makes any warranty, express or implied, or assumes any legal liability or responsibility for the accuracy, completeness, or usefulness of any information, apparatus, product, or process disclosed, or represents that its use would not infringe privately owned rights. Reference herein to any specific commercial product, process, or service by trade name, trademark, manufacturer, or otherwise, does not necessarily constitute or imply its endorsement, recommendation, or favoring by the United States Government or any agency thereof. The views and opinions of authors expressed herein do not necessarily state or reflect those of the United States Government or any agency thereof.

ORNL/TM-13565

High Temperature Materials Laboratory

TENTH ANNUAL REPORT: OCTOBER 1996 THROUGH SEPTEMBER 1997

A. E. Pasto
B. J. Russell

Date Published—August 1998

Research sponsored by the
Department of Energy
Assistant Secretary for Energy Efficiency
and
Renewable Energy
Office of Transportation Technologies
as part of the
High Temperature Materials Laboratory
User and Fellowship Programs
Oak Ridge National Laboratory
managed by
LOCKHEED MARTIN ENERGY RESEARCH CORP.
for the
U.S. DEPARTMENT OF ENERGY
under contract DE-AC05-96OR22464

LOCKHEED MARTIN ENERGY RESEARCH LIBRARIES

3 4456 0445258 0

CONTENTS

LIST OF FIGURES v
LIST OF TABLES vii
ACRONYMS AND ABBREVIATIONS ix
ABSTRACT xiii

1. INTRODUCTION 1-1

2. MAJOR ACCOMPLISHMENTS IN FY 1997 2-1
   2.1 HTML PROGRAM ITEMS 2-1
      2.1.1 Total Quality Management Effort 2-1
      2.1.2 A New HTML Database 2-1
      2.1.3 HTML Celebrated its Tenth Anniversary 2-1
   2.2 SPECIAL VISITORS, HONORS, AND AWARDS 2-2
      2.2.1 Efforts to Brief the U.S. Military 2-2
      2.2.2 Other DOE Offices 2-2
      2.2.3 Conference and Exhibition Participation 2-3
      2.2.4 HTML Written Up in Navy "Best Manufacturing Process" Document 2-3
      2.2.5 Honors, Awards, and Appointments 2-4
   2.3 MATERIALS ANALYSIS USER CENTER (MAUC) HIGHLIGHTS 2-5
      2.3.1 DOE2000 Program Awarded to ORNL with Participation of HTML 2-5
      2.3.2 Industrial Catalyst Company Makes Successful Use of Ex Situ Reactor 2-5
      2.3.3 Remote Microscopy Developments 2-6
   2.4 DIFFRACTION USER CENTER (DUC) HIGHLIGHTS 2-6
      2.4.1 High Temperature X-ray Diffraction Capabilities Installed at X14 Beamline 2-6
      2.4.2 Intensity Enhanced at HFIR Beamline HB-4 2-7
      2.4.3 New Software Developed for High-Temperature X-ray Data Collection 2-7
   2.5 RESIDUAL STRESS USER CENTER (RSUC) HIGHLIGHTS 2-7
      2.5.1 First In Situ Neutron Diffraction Strain Measurements on Electrostrictive Ceramics 2-7
      2.5.2 HTML Works to Establish International Standards for Residual Stress Mapping by Neutron Diffraction Methods 2-8
      2.5.3 New Monochromator Yields a Doubling of Flux, and New Data Collection Routine Put into Productive Use 2-8
   2.6 THERMOPHYSICAL PROPERTIES USER CENTER (TPUC) HIGHLIGHTS 2-8
      2.6.1 Michigan State University (MSU) and HTML Collaborate to Enhance Thermal Diffusivity Data Analysis Methods 2-8
      2.6.2 Ford Research Laboratory Studies Aluminum Metal Matrix Composite Thermal Transport Properties at HTML 2-9
      2.6.3 Thermophysical Property Data for Improving Lost Foam Process Obtained 2-9
   2.7 MECHANICAL CHARACTERIZATION AND ANALYSIS USER CENTER (MCAUC) HIGHLIGHTS 2-9
      2.7.1 Development of a Virtual Instrumentation Laboratory 2-9
      2.7.2 Efforts to Calibrate Indenter Shapes Other Than Berkovich Are Successful 2-9
      2.7.3 Infrared Imaging Used to Identify Onset of Cracking During Cyclic Fatigue 2-10
   2.8 MACHINING AND INSPECTION RESEARCH USER CENTER (MIRUC) HIGHLIGHTS 2-10
      2.8.1 Cylindrical Grinding Used to Produce Two-Component Fuel Injector Plunger Specimens 2-10

2.8.2 High-Speed Diamond Grinding Wheel Allows Major Grinding Time Reduction 2-10
2.8.3 Improved Grindability Test Machine Received 2-11
2.9 HTML FELLOWSHIP PROGRAM HIGHLIGHTS 2-11

3. HTML USER STATISTICS 3-1
3.1 USER DAYS 3-1
3.2 USER AGREEMENTS AND PROPOSALS 3-3

4. HTML USER CENTERS 4-1
4.1 MATERIALS ANALYSIS USER CENTER 4-1
4.1.1 Staff and Current Capabilities 4-1
4.1.2 Highlights 4-1
4.2 MECHANICAL CHARACTERIZATION AND ANALYSIS USER CENTER 4-3
4.2.1 Staff and Current Capabilities 4-3
4.2.2 Major Research Areas 4-4
4.2.3 Major Activities in FY 1997 4-6
4.3 THERMOPHYSICAL PROPERTIES USER CENTER 4-8
4.3.1 Background 4-8
4.3.2 Staff and Major Instruments 4-8
4.3.3 Developments and New Capabilities 4-9
4.4 RESIDUAL STRESS USER CENTER 4-11
4.4.1 Background 4-11
4.4.2 Staff and Major Instruments 4-11
4.4.3 New Capabilities 4-12
4.4.4 Major Activities 4-13
4.5 DIFFRACTION USER CENTER 4-16
4.5.1 Background 4-16
4.5.2 Staff and Major Instruments 4-16
4.5.3 New Capabilities 4-17
4.6 MACHINING AND INSPECTION RESEARCH USER CENTER 4-18
4.6.1 Staff and Major Instruments 4-18
4.6.2 New Capabilities 4-20
4.6.3 Major Activities in FY 1997 4-20

5. HTML FELLOWSHIP PROGRAM 5-1
5.1 INDUSTRIAL FELLOWSHIPS 5-1
5.1.1 Background 5-1
5.1.2 Industrial Fellowships for FY 1997 5-2
5.2 GRADUATE FELLOWSHIPS 5-9
5.3 FACULTY FELLOWSHIPS 5-18
5.3.1 Background 5-18

APPENDIX A. STANDARD NONPROPRIETARY USER AGREEMENTS A-1
APPENDIX B. FY 1997 NONPROPRIETARY RESEARCH PROPOSALS B-1
APPENDIX C. FY 1997 RESEARCH PROJECT SUMMARIES, INDUSTRIES AND UNIVERSITIES C-1
APPENDIX D. PUBLICATIONS AND PRESENTATIONS D-1

LIST OF FIGURES

Figure		Page
3.1	A history of user days of research expended in HTML since its inception	3-3
3.2	Numbers of materials-related User Agreements received by the ORNL Office of Science and Technology Partnerships	3-4
3.3	Cumulative number of User Agreements received by the ORNL Office of Science and Technology Partnerships	3-4
3.4	History of technical proposals received by HTML	3-5
3.5	Cumulative history of technical proposals received by HTML	3-5
3.6	Cumulative technical proposals and User Agreements received	3-7
5.1	Nanoindentation hardness profile	5-6
5.2	Wear volume correlation with coating thickness	5-7
5.3	High resolution electron micrograph of (a) PrO_2-ZrO_2 coated alumina particles and (b) the arrows showing damage to the particle during EDS measurements	5-8
5.4	Nanoindentation loading/displacement curve of the TiN thin film coating sample	5-9
5.5	Z-contrast STEM image of NiO-ZrO_2(Y_2O_3) interface with structural model superimposed	5-10
5.6	Profiles of Ni, Zr, and O normalized EELS intensities taken across the NiO-ZrO_2 interface in steps of interplanar spacing	5-11
5.7	Normal stresses in NiO lamellae	5-11
5.8	Normal stresses in ZrO_2 (cubic) lamellae	5-12
5.9	Parabolic plot of continuous thermogravimetry measurements comparing the steady-state oxidation kinetics (at 950–1150°C) of bare LPPS Ni-22Co-18Cr-12Al-0.3Y bond coatings with the same bond coatings coated with a 125-mm TBC (a commercial EB-PVD TBC system)	5-13
5.10	Metallographic section showing internal fracture of an interfacial Al_2O_3 scale on a failed APS TBC (100 h + 270 1-h cycles at 1150°C)	5-14
5.11	Fracture section of an interfacial Al_2O_3 scale (exposed by YSZ spallation) on an APS TBC showing microstructural evidence of localized Al_2O_3 scale healing by sintering across an internal crack (arrows); 360 1-h cycles at 1150°C	5-14
5.12	A portion of the alumina-cubic zirconia phase diagram as determined in this investigation. The solvus line was fit using a logarithmic curve	5-18
5.13	Bright-field TEM image of alumina scale on isothermally oxidized PtAl+Zr	5-19
5.14	EDS spectra from alumina grains and grain boundary showing segregation of Zr to grain boundaries	5-19
C.1	The geometry and pass sequence of weld	C-6
C.2	Thermal conductivity of the base metal in an HY-100 weldment	C-6
C.3	Shows failure data points for two different materials and a run-out point (not a failure) from the current testing method	C-10
C.4	Lattice strains due to change in composition in the aluminum weld specimen	C-12
C.5	Average values of thermal diffusivity for several Al MMCs measured via laser flash	C-13
C.6	Diffusion of iron into $MoSi_2$ substrate	C-16
C.7	Diffusion of iron into Si substrate	C-17
C.8	Composite sample of spray-found H-13 steel (center) with LENS deposits of H-13 on polished (left) and as-formed (right) spray-formed surfaces	C-19
C.9	Residual stresses determined by neutron diffraction in LENS-spray-LENS composite	C-20
C.10	Thermal diffusivity of APS coatings before and after thermal aging	C-24
C.11	Experimental layout	C-28

C.12 Strain in the <220> direction measured normal and transverse to the applied field direction C-28
C.13 Unit cells of (a) 312 and (b) 211 phases C-29
C.14 Lattice parameter changes as a function of temperature for Ti_3SiC_2 ..... C-30
C.15 Experimental and predicted in-plane temperature ratios of SiC-BN-Nicalon/BMAS C-31
C.16 A $\sin^2\psi$ plot showing tensile stresses in the Mo_2C layer using the (213) reflection C-35
C.17 Effect of yttria content on thermal conductivity C-37
C.18 The atomic configurations consistent with the Pitsch orientation and relationship between Fe and Cu, where A, B, C, and D denote the four possible in-plant orientations C-39
C.19 Comparison of the (110) pole figures for (a) Fe, (b) FeTa, and (c)–(d) FeTaN epitaxial films C-40
C.20 Conductivity of lost foam coatings C-41
C.21 Specific heat capacity of casting sands C-41
C.22 Results summary of residual stress analyses of the hot-pressed and the heat-treated SiC-AlN specimens C-43
C.23 Lattice image of the heat-treated SiC-25 Mol% AlN with its corresponding EDS spectra from different locations C-44
C.24 Differences in lattice parameters a and c for the hot pressed and the heat-treated SiC-AlN specimens C-44
C.25 HREM image of $NiO-Y_2O_3$ interface showing an atomically abrupt transition between the two phases C-46
C.26 Model of $NiO-Y_2O_3$ interface in which the phases share a common oxygen plane C-46
C.27 Tensile stress-strain behaviors of the as-received and crept specimens C-48

LIST OF TABLES

Table		Page
3.1	History of HTML user days by fiscal year	3-1
3.2	HTML user days for FY 1997 by User Center	3-2
5.1	Hardness and size data of alloy and boron-treated steels	5-3
5.2	Results of axial cyclic fatigue testing	5-4
5.3	NT154 specimen test matrix for compressive creep	5-4
5.4	Minimum creep rates in compression measured at the end of approximately 150 h, or after approximately 100 h of steady-state creep	5-5
C.1	Surface profilometry	C-15
C.2	Test	C-15
C.3	CBCF samples measured at ORNL 800°C analysis with the nonpenetrating model	C-34
C.4	CBCF samples measured at ORNL at 800°C analysis with the penetrating model	C-34
C.5	Sample identification and layer description	C-35
C.6	Hydrostatic stresses measured by X-ray diffraction and macro-Raman spectroscopy	C-36

ACRONYMS AND ABBREVIATIONS

ABET	Accrediting Board for Technology
ACR	Advanced Ceramics Research
AEM	analytical electron microscope
AFM	atomic force microscope
Al MMC	aluminum metal matrix composite
AlN	aluminum nitride
APS	air plasma sprayed/spraying
ASM-TMS	American Society of Materials-the Minerals, Metals, and Materials Society
ASME	American Society for Mechanical Engineers
ASTM	American Society for Testing and Materials
atm	atmosphere
bcc	body-centered cubic
BES	U.S. Department of Energy, Office of Basic Energy Sciences
CBCF	carbon-bonded carbon fiber
CBN	cubic boron nitride
CCMD	Committee on Cost Methods Development
CFCC	continuous fiber ceramic composites
CMC	Ceramic Manufacturability Center
CMM	coordinate measuring machine
CNC	computer numerically controlled
CRADA	cooperative research and development agreement
CVD	chemical vapor deposition
DARPA	Defense Advanced Research Projects Agency
DCB	double cantilever beam
DMSNT	Diffraction Management Software for Windows®
DOE	U.S. Department of Energy/design of experiment
DOE-FE	U.S. Department of Energy, Fossil Energy
DOE-HQ	U.S. Department of Energy, Headquarters
DOE-ORO	U.S. Department of Energy, Oak Ridge Operations
DOT	Department of Transportation
DSC	differential scanning calorimetry
DSE	directionally solidified eutectic
DTA	differential thermal analysis
DUC	Diffraction User Center
EB-PVD	electron beam–physical vapor deposition
ECAE	equal channel angular extension
ECR	electron cyclotron resonance
EDS	energy dispersive spectroscopy
EERC	Energy and Environmental Research Center
EERE	U.S. Department of Energy, Office of Energy Efficiency and Renewable Energy
EELS	electron energy loss spectroscopy
EGA	evolved gas analysis
EMD	electronic measuring device
ER	U.S. Department of Energy, Office of Energy Research
EXAFS	extended X-ray absorption fine structure
FIB	focused ion beam
FM	fibrous monolithic
FTIR	Fourier Transfer Infrared
FY	fiscal year
GIXRD	grazing incidence X-ray diffraction

GSAS	General Structure Analysis System
HAZ	heat-affected zone
HFCVD	hot filament chemical vapor deposition
HFIR	High Flux Isotope Reactor
HREM	high-resolution electron microscope/microscopy
HRTEM	high-resolution transmission electron microscopy
HTLC	hydrotalcite-like compounds
HTML	High Temperature Materials Laboratory
HTSC	high-temperature superconductivity
HTXRD	high-temperature X-ray diffraction
I&C	Instrumentation & Controls Division
IEA	International Energy Agency
INEEL	Idaho National Environmental and Engineering Laboratory
IOF	industries of the future
IR	infrared
JIS	Japanese Industrial Standard
KC	Kyocera Corporation
KICC	Kyocera Industrial Ceramics Corporation
LDRD	Laboratory Director's Research and Development
LENS	laser engineering net shaping
LF	lost foam
LFTD	laser flash thermal diffusivity
LMER	Lockheed Martin Energy Research Corp.
LMES	Lockheed Martin Energy Systems, Inc.
LPPS	low pressure plasma spray
LSU	Louisiana State University
M&C	Metals & Ceramics Division
MAUC	Materials Analysis User Center
MCAG	Mechanical Characterization and Analysis Group
MCAUC	Mechanical Characterization and Analysis User Center
MICS	Mathematics, Information, and Computation Division
MIRUC	Machining and Inspection Research User Center
MMC	metal matrix composite/materials macrocharacterization collaboratory
MOR	modulus of rupture
MSU	Michigan State University
MTS	mechanical testing systems
NASA	National Aeronautics and Space Administration
NAVSEA	U.S. Department of the Navy, Naval Sea Systems
NDE	nondestructive examination
NE	negative electrode
NGI	next generation internet
NRSF	Neutron Residual Stress Facility
NSLS	National Synchrotron Light Source
OCV	open circuit voltage
OHVT	Office of Heavy Vehicle Technologies (DOE)
OIT	Office of Industrial Technologies
ORISE	Oak Ridge Institute for Science and Education
ORNL	Oak Ridge National Laboratory
OTT	Office of Transportation Technologies
PC	personal computer
PE	positive electrode
PFBR	pressurized fluidized bed reactor
PMN	lead-manganese niobate
PPG	Pittsburgh Plate Glass

PPUC	Physical Properties User Center
PRT	participating research team
PSD	position-sensitive detector
PTS	polycrystalline texture stress
PVD	physical vapor deposition
PZT	lead-zirconate titanite
R&D	research and development
RABiTS™	Rolling Assisted Biaxial Textured Substrate
RH	relative humidity
RHEED	reflecting high energy electron diffraction
RSUC	Residual Stress User Center
RT	room temperature
RTXRD	room-temperature X-ray diffraction
RUS	resonant ultrasound facility
SAD	selected area diffraction
SAE	Society of Automotive Engineers
SAM	scanning auger microscope
SBIR	Small Business Innovative Research
SEM	scanning electron microscope
SENS	stress evaluation by neutron and synchrotron radiation
SERS	Science and Engineering Research Semester
SIMS	secondary ion mass spectroscopy
SLH	sandwiched layered hydroxide
SNL	Sandia National Laboratory
SP	porous separation
SSD	Solid-State Division
STA	simultaneous thermal analysis
STEM	scanning transmission electron microscopy
TBC	thermal barrier coating
TEM	transmission electron microscope
TG	thermogravimetry
TG/IR	thermal gravimetrical infrared
TGO	thermally grown oxide
THF	tetra hydro furan
TPUC	Thermophysical Properties User Center
TQM	total quality management
UAB	University of Alabama-Birmingham
UND	University of North Dakota
USACA	United States Advanced Ceramics Society
UT	University of Tennessee
VAMAS	Versailles Project on Advanced Materials and Standards
XPS	X-ray photoelectron spectroscopy
XRD	X-ray diffraction
YBCO	yttrium-barium-copper xode
YSZ	yttrium stabilized zirconia

ABSTRACT

The High Temperature Materials Laboratory (HTML) has completed its tenth year of operation as a designated U.S. Department of Energy User Facility at Oak Ridge National Laboratory. This document profiles the historical growth of the HTML User and Fellowship Programs since their inception in 1987. Growth of the HTML programs has been demonstrated by the number of institutions executing user agreements and by the number of days of instrument use (user days) since the HTML began operation. A total of 380 nonproprietary agreements (211 industry, 160 university, and 9 other federal agency) and 67 proprietary agreements are now in effect. This represents an increase of 114 nonproprietary user agreements since the last reporting period (FY 1995 and FY 1996). A state-by-state summary of these nonproprietary user agreements is given in Appendix A. Forty-six states are represented by these users.

During FY 1997, the HTML User Program evaluated 73 nonproprietary proposals (35 from industry, 34 from universities, and 4 from other government facilities) and several proprietary proposals. The HTML User Advisory Committee approved about 95% of those proposals, frequently after the prospective user revised the proposal based on comments from the committee.

This annual report discusses activities in the individual user centers, as well as plans for the future. It also gives statistics about users, proposals, and publications as well as summaries of the nonproprietary research projects active during FY 1997.

1. INTRODUCTION

The High Temperature Materials Laboratory (HTML) is a modern research facility at the Oak Ridge National Laboratory (ORNL) that houses a unique collection of instruments for characterizing materials. The instruments in the six user centers provide a comprehensive set of tools for performing state-of-the-art determination of the structure and properties of solids and some liquids at high temperature. A dedicated staff trains and guides users in conducting the research.

Highly computerized instrumentation is used to improve the efficiency of data collection and interpretation. Research projects start as submitted proposals that, when approved, provide the user access to any of the HTML instruments needed to perform the work. User projects typically include research to relate materials properties to structure or to manufacturing processes, or to train users and provide them access to the equipment necessary to perform their own materials research.

An external oversight advisory committee and an on-site proposal review committee assist in the successful operation of the HTML User Program. The external committee, known as the HTML Programs Senior Advisory Committee, provides guidance on strategic issues facing HTML. During the FY 1997 reporting period, the HTML Programs Senior Advisory Committee was composed of the following members:

- Dr. Ronald H. Chand (1992), Chand Kare Technical Ceramics, Worcester, Mass.;
- Mr. Bryan J. McEntire (1992), St. Gobain/Norton Industrial Ceramics Corp., East Granby, Conn.;
- Dr. James W. Patten (1991), Cummins Engine Co., Columbus, Ind.;
- Dr. Maxine L. Savitz (1990), AlliedSignal Ceramic Components, Torrance, Calif.;
- Dr. Andrew M. Sherman (1997), Ford Research Laboratory, Dearborn, Mich.; and
- Dr. Wendell S. Williams (1996), Dept. of Materials Science and Engineering, Case Western Reserve University, Cleveland, Ohio.

Early in the User Program, user agreements were developed that established the intellectual property and liability rights of the user institution and Martin Marietta Energy Systems, Inc. (MMES)/Lockheed Martin Energy Systems, Inc. (LMES) [before the establishment of Lockheed Martin Energy Research Corp. (LMER)]. Two types of standard agreements are used: a nonproprietary agreement and a proprietary agreement. The nonproprietary user agreement requires that users, along with HTML technical staff, jointly publish the results of their research within 6 months of completing the user project. Proprietary agreements do not require users to publish with HTML staff but do require payment on a full-cost recovery basis. The first user agreement was signed on July 15, 1987; since that time, 380 nonproprietary agreements have been executed. In Appendix A, a state-by-state listing is provided of the approved nonproprietary user agreements that involve materials research and provide access to HTML.

These 380 nonproprietary user agreements have yielded 740 project proposals since the inception of the HTML. In the current reporting period, 73 nonproprietary research proposals were received, and these are listed in Appendix B.

Work was performed on numerous projects during the reporting period, including several that were initiated in previous years. Summary descriptions of these projects are given in Appendix C. Several presentations and publications were produced as a result of these projects; they are listed in Appendix D.

Since shortly after the beginning of the User Program, a user logbook has been kept for each instrument in the user centers. Entries in the logbooks are tallied annually by each user center for each instrument, and the totals are rolled into one set of data for HTML. Each 8-h period of time, or fraction of an 8-h period, that an instrument is being used is tallied as a "user day." Over the years since 1987, the user-day data have been collected for industry and university users, as well as for internal ORNL staff. In FY 1997, there were 22,162 user days of effort. A complete tabulation of user days by user center, instrument, and user type is contained in Appendix E. A full discussion of these statistics is presented in Sect. 3.

2. MAJOR ACCOMPLISHMENTS IN FY 1997

During the FY 1997 reporting period, the HTML experienced continued growth, both in the number of users performing research and in the number of proposals received. The User Centers undertook activities in new areas and expanded their existing expertise and capabilities. The following sections contain summaries of many accomplishments at HTML during this time.

2.1 HTML PROGRAM ITEMS

2.1.1 Total Quality Management Effort

Continuous improvement of processes is essential to the continued health of programs and facilities at HTML. For that reason, HTML staff began in 1995 a thorough internal evaluation to cut and control costs and to improve efficiency. In 1995, we initiated a total quality management (TQM) effort with meetings of staff and management to discuss our mission and vision and to agree upon a set of guiding principles and goals to lead us into a secure future. This effort was expanded in FY 1996, through the leadership of Mary Rawlins and Connor Matthews of the U.S. Department of Energy Oak Ridge Operations Office (DOE-ORO). In FY 1997, we began a thorough examination of the processes by which users are located, proposals are received and processed, and work is accomplished. The goal of this effort is to locate those processes that are redundant or otherwise unnecessary and costly in time or funding, and eliminate them if possible. One of the processes we have modified is the external review process for proposals, which previously involved quarterly proposal review meetings wherein two staff members from private industry and one from a university traveled to HTML and conferred with the director and the user center leaders. We saved $58,000 per year by eliminating the external reviewers, their associated travel and per diem expenses, and our internal preparation time. Also, we now review proposals monthly, thus providing much quicker turn-around time than previously. We are now concentrating on eliminating or speeding up the other processes involved in getting proposals and users into HTML. One major improvement has been in controlling and tracking the user and proposal paperwork (see next item).

2.1.2 A New HTML Database

Ted Nolan and Billie Russell have developed and implemented a new, comprehensive HTML database. Previously, two separate databases existed, each unrelated to the other. The new system connects the proposal database to the instrument use database, and it is located on the server so that it is accessible to HTML group leaders and administrative staff. This year several new features have been added, including built-in letters of proposal receipt, approval, etc., so that when information is added to the database on new users or proposals, the necessary correspondence can be printed directly and instantly.

2.1.3 HTML Celebrated Its Tenth Anniversary

On July 15, 1997, HTML hosted a celebration of its founding ten years ago and its successful operation since then. Public events were held from 8 a.m. to 12:30 p.m. at the Pollard Auditorium on the campus of Oak Ridge Associated Universities and from 2 to 5 p.m. at Oak Ridge's Garden Plaza Hotel.

The morning session provided several perspectives on the history of HTML and its research accomplishments. The speakers included Dr. Arvid Pasto, HTML director; Dr. Douglas Craig, director of ORNL's Metals and Ceramics Division; Mr. Al Chesnes, former director of DOE's Office of Transportation Systems; Dr. Victor Tennery, HTML's original director; Dr. Alex Zucker, former ORNL associate director and one-time acting laboratory director; Dr. Wendell Williams, retired

professor from the University of Illinois; Ms. Mary Rawlins, program manager for DOE's Oak Ridge Operations; and Dr. Jim Eberhardt, director of DOE's Office of Heavy Vehicle Technologies.

Speakers from user institutions included Dr. Abhaya Datye, director of the Center for Micro-Engineered Ceramics at the University of New Mexico; Dr. Jim Patten, executive director of Materials Engineering at Cummins Engine Co.; Dr. Gregg Wagner of Westinghouse; and Dr. Michael Readey of Caterpillar. Displays representing Allison Engine Company, Chand Kare Technical Ceramics, Caterpillar, Detroit Diesel Corporation, Cummins Engine Company, and AlliedSignal Aerospace Engine Company were available in the HTML lobby. A poster and vendor display was open in the Garden Plaza Hotel lobby during the afternoon of July 15.

2.2 SPECIAL VISITORS, HONORS, AND AWARDS

2.2.1 Efforts to Brief the U.S. Military

Efforts are being made to bring HTML to the attention of the United States military services, since our capabilities are often complementary to those of the service branches and the Defense Advanced Research Projects Agency (DARPA). Numerous visits to HTML were made this fiscal year, including: Lt. General Ronald Hite, Military Deputy to the Assistant Secretary of the Army, on October 9; Major Steve Bruttig and his staff of the U.S. Army Medical Research and Material Command, on October 9; USAF Colonel Michael Wiedemer, Commander of Arnold Engineering Development Center, on October 11; Brigadier General James Boddie of Picatinny Arsenal, on November 26; Mr. Richard Rumpf, ex-Assistant Secretary of the Navy for research and development (R&D), on December 18; Dr. Dennis Wend of TARDEC, on February 25; General Johnny Wilson, U.S. Army, on March 11; Dr. Fenner Milton, Deputy Assistant Secretary of the Army for Research and Technology, on April 11; Cpt. Martin Kosiek, Jacksonville Naval Aviation Depot, and many of his scientific and engineering staff, on April 30; staff of the Naval Sea Systems Command (NAVSEA), representing the technology office, and the Aegis, CVX, and SC-21 Programs, on July 15; General Gordon Sullivan, retired Chief of Staff of the U.S. Army, on August 19; staff of the U.S. Army TACOM and Focus: HOPE of Detroit, on August 25; and Rear Admiral of the Navy Michael T. Coyle, with responsibility for NAVSEA, on October 31.

A particular highlight was the visit by Lieutenant General of the Army Ronald V. Hite, Military Deputy to the Assistant Secretary of the Army—Research, Development, and Acquisition, and 24 of his staff and program executive officers on April 10 and 11, 1997. General Hite's office has a budget of $14B (larger than NASA's) and covers every Army weapon system. Present were 2 three-star generals, 4 two-star generals, and 5 one-star generals, along with several colonels and civilians. They represented aviation, tactical wheeled vehicles, tactical missiles, etc. Several of them were impressed with the programs and capabilities of HTML and requested follow-on visits for their staffs to probe means of and areas for collaboration.

Arvid attended the Defense Manufacturing Conference in Miami Beach during the first week of December and presented a paper on HTML to the "Best Manufacturing Practices" symposium there.

2.2.2 Other DOE Offices

In a similar vein, HTML has been brought to the attention of several other offices of DOE, with visits including those of Dr. Pandit Patil, director of the DOE Office of Advanced Automotive Technologies, on October 17; numerous researchers and management representatives of the refractories industry attending an OIT-sponsored workshop in the HTML, who were given a presentation of HTML capabilities and a tour on November 7; Howard Feibus, the director of the Office of Advanced Research in DOE-Fossil Energy; Fred Glaser, the deputy to this office, and Marvin Singer, senior advisor for the Advanced Policy and Planning Team at DOE-FE, on December 10; Mr. Bill O'Connor, [Oak Ridge liaison in the Office of Field Management, DOE-Headquarters (HQ)], on March 5; and a large group of DOE staff representing the DOE Committee on Cost Methods Development (CCMD) on June 19.

A particular highlight was the visit by Energy Secretary Pena and Mr. Tom Gross, director of the Office of Transportation Technologies, on May 30. The secretary was shown around HTML and was briefed on our neutron residual stress activities.

2.2.3 Conference and Exhibition Participation

Arvid participated in the SAE Truck and Bus Show and Exposition in Detroit on October 14–16, 1996, where the HTML was represented by a display booth and was featured in a presentation given by Arvid.

Arvid and several HTML staff attended the annual DOE Customer's Coordination Meeting in Dearborn, October 28–November 1. Several posters illustrating work at the HTML were displayed in the poster exhibition, and a display booth highlighting ORNL's accomplishments in the heat engine topic area included HTML. A live demonstration of remote microscopy was given during two of the meeting days by members of the Materials Analysis User Center.

Arvid attended the OIT EXPO in Washington February 4–26, 1997, where the HTML shared an exposition booth with the OIT Advanced Industrial Materials Program display. The purposes for attending the conference/exposition were (a) to inform the attendees of the availability and capabilities of the HTML and (2) to gain insight into the research, development, and technology needs of the various industries represented there. Arvid brought back the names of several key contacts, and literature representing all of the OIT "Industries of the Future" (IOFs): steel, aluminum, glass, chemicals, refining, forest products, and metal casting, as well as from several industrial segments represented there that are not yet full-fledged IOFs—heat-treating, agriculture, and forging.

Arvid attended the American Ceramic Society Annual Meeting in Cincinnati, Ohio on May 4–7, 1997, where he hosted a display booth at the conference's exposition and presented a paper on the HTML's capabilities at a symposium on NDE. He also moderated a panel discussion on NDE.

Arvid participated in the Ph.D. thesis defense of one of the HTML Fellowship Program participants at Pennsylvania State University. Arvid served on the thesis committee of this student, Dr. Matt Stough, who has taken a position at Osram Sylvania in New Hampshire.

Arvid also attended a Materials Research Conference at Northwestern University and presented a paper on HTML and its capabilities.

The director and/or staff of the HTML attended numerous other conferences and exhibitions this period, including the ASM/TMS Materials Exposition in Indianapolis, September 16–19, where HTML had an exhibition booth, and Discover Ceramics "97," September 23–26, a conference in Columbus, Ohio, where HTML also had an exhibition booth. Staff also attended and/or presented papers at the Conference on Transportation Technologies, Department of Transportation (DOT) Volpe Center, Cambridge, Massachusetts, September 16–18, 1997; the USACA Meeting in Washington, September 23–24, 1997; the National Conference on the Advancement of Research in Oak Ridge, to which Arvid was invited, September 21–24, 1997; the International Symposium on Ceramic Material for Engines in Japan, October 1997; and the Annual CCM in Dearborn, October 27–30, 1997.

2.2.4 HTML Written Up in Navy "Best Manufacturing Process" Document

The HTML and its programs were reviewed by the U.S. Navy's Best Manufacturing Processes Survey Team on November 5, 1996, spending a full day in the facility hearing presentations and seeing the equipment. We were rewarded with the following HTML-related items being designated "best practices:"

- The Overall HTML Concept, including User/Fellowship programs
- Remote Microscopy: The Virtual Laboratory Concept
- Revolutionary High Speed Infrared Camera System For Quantitative Thermal Diffusivity Mapping and Nondestructive Evaluation

The four remaining HTML presentations are:

- In Situ High Temperature Thermal Analysis and Diffraction,
- Through Thickness and Surface Residual Stress Measurement,
- Mechanical Properties Microprobe, and
- Machining and Inspection Research User Center

and will also be prominently included in the Navy's write-up, but were not designated as best practices. The published report should be available within a couple of months.

2.2.5 Honors, Awards, and Appointments

Several HTML staff received special honors or awards and/or were appointed or elected to office in scientific organizations during this fiscal year.

Kristin Breder

Award from the Association for Women in Science, East Tennessee Chapter, for Distinguished Scientific Achievement.

Third prize from the American Ceramic Society, Engineering Ceramics Division, for Student Technical Presentation by Ron Ott, Kristin Breder, Mattison K. Ferber, and J. M. Rigsbee (Characterization of Machining Induced Subsurface Damage of a High Strength Silicon Nitride).

Donna Conger

Designated recording secretary for IEA Annex II—IEA Cooperative Programme on Ceramics for Advanced Engines and Other Conservation Applications.

Ralph Dinwiddie

American Ceramic Society Ceramographic Award, First Place for Optical Techniques, with Hsin Wang.

Elected for a second 2-year term as vice chair of the board of governors of the International Thermal Conductivity Conferences.

Elected for a second term as chair of the Thermosense Working Group, a 150-member international organization of thermographers.

Edgar Lara-Curzio

"Outstanding Technical Achievements Award," Hispanic Engineer National Achievement Awards Conference, Houston, Texas, October 11, 1997.

Award of Appreciation, American Society for Testing and Materials (ASTM), Committee C28 on Advanced Ceramics for authoring standard C1337, Test Method for Creep and Creep Rupture of Continuous Fiber-Reinforced Composites Under Tensile Loading at Elevated Temperatures, January 1997.

Best of Show and First Place Poster Award, American Ceramic Society, in recognition of the poster presentation entitled "Characterization of Nicalon™/SiC Composites with BN/Al2O3 Fiber Coatings," presented at the 99th Annual Meeting & Exposition, Cincinnati, Ohio, May 4–7, 1997 (A. Clark and K. L. More, co-authors).

Vice Chairman and secretary of the ASTM Subcommittee C28.07 on Ceramic Composites, January 1995–to date.

Cochairperson of Coordination Group on Test Methods for Ceramic Matrix Composites, Military Handbook-17, November 1995–to date.

Leader of Task Group on Rules Governing Testing, American Society for Mechanical Engineers (ASME) Boiler and Pressure Vessel Code for Ceramic Matrix Composites, August 1996–to date.

Chairperson of Session on Mechanical Test Methods and NDE, 21st Annual Cocoa Beach Conference and Exposition, Cocoa Beach, Florida, January 15, 1997.

Chairperson and Session Developer, Stress Rupture of Ceramic Matrix Composites, Fourth International Conference on Composites Engineering, ICCE/4, Kohala Coast, Hawaii, July 6–12, 1997.

Hsin Wang

Award of First Prize in the American Ceramic Society Ceramographic Contest at the 99th Annual Meeting, May 1997, with Frank A. Modine and Ralph B. Dinwiddie. Entitled "Infrared Micrograph of a ZnO Varistor During Electrical Breakdown."

Xun-Li Wang

Elected as Member of International Scientific Committee, Meca-SENS 1 (Stress Evaluation by Neutron and Synchrotron Radiation), to be held in Remis, France, December 1999.

Member of Youth Committee, Chinese Materials Research Society.

Co-recipient of a 1997 ORNL Laboratory Directed Research and Development grant.

Best Paper Award, 1996 TAPPI Engineering Conference.

Invited presentation in October 1997, The Sixth Materials Research Conference for Young (Chinese) Scientists, Jinan, China (unable to attend).

Invited presentation in June 1997, Institut Laue-Langevin, Grenoble, France.

Invited presentation in June 1997, Laboratoire Léon Brillouin, Saclay, France.

2.3 MATERIALS ANALYSIS USER CENTER (MAUC) HIGHLIGHTS

2.3.1 DOE2000 Program Awarded to ORNL with Participation of HTML

Two pilot programs selected to be funded as a part of the DOE2000 initiative were announced in 1997. A proposal co-submitted by OTT Office of Heavy Vehicle Technologies (OHVT) entitled "Materials MicroCharacterization Collaboratory" was one of these pilot programs selected by the Mathematical, Information, and Computational Sciences (MICS) Division of Energy Research (ER) for the DOE2000 initiative. This pilot program is demonstrating the use of activities such as remote electron microscope operation, video teleconferencing, and the use of electronic white boards in collaborative materials research. Research focuses on the characterization of NOx reduction catalysts (of major importance to OHVT) and materials interfaces (of general interest for many EE and ER materials programs). The collaboratory brings together combinations of unique characterization tools and experts to provide real-time insights into the performance of materials, thus demonstrating a new paradigm in the conduct of materials research. The Materials Analysis User Center and the Residual Stress User Center are major participants in this project in two ways. Hardware and software are being implemented to facilitate use of HTML instruments that are already available for remote operation and to bring on-line other instruments. HTML personnel are providing principal guidance for research using virtual laboratory tools that will relate catalyst microstructure to performance.

2.3.2 Industrial Catalyst Company Makes Successful Use of Ex Situ Reactor

Dow Chemical Company users began work in the MAUC studying the effects of sequential reactions on the growth of palladium (Pd) particles in Pd/carbon (C)-based model catalyst specimens. These samples formed the basis of a series of experiments aimed at determining whether or not our new ex-situ catalyst reactor system was suitable to provide useful information about reaction mechanisms and the development of catalyst morphologies that might affect performance. This was

the first time our reactor system was tested under the most stringent of working conditions that might be used in any study. Over the course of four days, more than 20 separate reactions were conducted at temperatures from 100°C to 800°C and in both nitrogen and hydrogen atmospheres. In every case, the reactor system and the procedure for transfer of the specimen into the microscope and subsequently back into the reactor without exposure to the atmosphere worked perfectly. The system proved to be facile and easy to use, and the Dow users were clearly impressed with the efficiency of the operation. Some dramatic micrographs were obtained showing, for example, the formation of nanoparticles of Pd uniformly distributed over the carbon support surface as a critical temperature was reached. We are now in discussions that may lead to the initiation of proprietary work on real catalyst systems with Dow.

2.3.3 Remote Microscopy Developments

Staff of the Materials Analysis User Center continued to develop and demonstrate remote microscopy tools. Full funding for the Materials MicroCharacterization Collaboratory (MMC, a DOE2000 demonstration project, noted above) was received from the MICS branch of DOE-ER. These funds and the matching EE funds from the OHVT are being used to support the activities described below.

- The MMC has been designated as a Next Generation Internet (NGI) application. This can be expected to provide infrastructure support by increasing communication speed between collaboratory partners and industrial and university researchers participating in MMC-related research.
- We are developing a research relationship with the National Aeronautics and Space Administration's (NASA's) Ames Laboratory, Moffett Field, California. NASA is creating an Astrobiology Center located at Ames. The center will rely heavily on virtual laboratory concepts, and we at HTML have the opportunity to provide microstructural characterization for this center. A demonstration project is already under way, wherein scientists at Ames will be observing the famous Mars meteorite remotely using our high resolution SEM, looking for fossilized signs of life. The Astrobiology Center will rely heavily on NGI developments; Ames is the principal laboratory for all of NASA's involvement in the NGI project. On July 10, 1997, at Ames, HTML and NASA personnel demonstrated to NASA management the use of the HTML microscopes for such studies. The head of all of NASA's NGI programs was in attendance. Although not directly related to EE missions, these activities provide us with experience performing very high resolution SEM remotely, helping cement our role in NGI, and possibly leading to significant financial support in the future.
- Educational activities continued to increase. Remote microscopy and video teleconferencing are being used to provide microscopy instruction for courses at Lehigh University and the University of Tennessee. The University of Wisconsin-Milwaukee is next in line to be set up for educational programs.
- An MMC demonstration took place at the DOE Research Integration Workshop in Reston, Virginia on July 16, 1997, during which time Secretary of Energy Pena was offered the opportunity to run electron microscopes at HTML and at Berkeley National Laboratory.

2.4 DIFFRACTION USER CENTER (DUC) HIGHLIGHTS

2.4.1 High Temperature X-ray Diffraction Capabilities Installed at X14 Beamline

Two HTML researchers extended the instrument capabilities at the National Synchrotron Light Source beamline X14, where HTML has a post-doc stationed, by utilizing a programmable Micristar temperature controller. A test sample material, bismuth strontium oxide, was selected for study. This material is of interest as it is a fast oxygen ion conductor, with a poorly characterized phase transformation at elevated temperatures (around 650°C), and has potential applications in solid-

oxide fuel cells and solid-state sensors. The Micristar unit was successfully substituted for the Bühler controller, which allowed the adjustment of the control settings, digital readout of temperature, and programming of temperature schedule. This unit may be controlled via an RS-232 interface, and it is hoped that such an interface will be set up in the future between the VAX computer and the Micristar to integrate the temperature control with the goniometer software.

2.4.2 Intensity Enhanced at HFIR Beamline HB-4

This year, the Solid-State Division at ORNL installed a vertically focusing Ge(511) monochromator on the HB-4 diffractometer that resulted in a flux increase of a factor of three for small samples. For large samples, a 20% increase in flux was also realized, thanks to the better performance of the new monochromator. This upgrade opens new opportunities for all HTML users, especially in the areas of high temperature studies, where the peak intensities are inherently low due to broadening and thermal diffuse scattering and for cases where a large sample is not available.

2.4.3 New Software Developed for High-Temperature X-ray Data Collection

The capabilities offered by DUC were enhanced by the development of new software for temperature control and data acquisition by an engineering student from Michigan Technological University employed at the HTML under the Science and Engineering Research Semester (SERS) program. The new software, written in C++ with a graphical user interface and running under Windows NT, better utilizes the rapid data acquisition rates made possible by an existing position sensitive detector. Data download times have been reduced by a factor of twenty, which was the slow step in existing commercial software. This same software is capable of controlling HTXRD experiments using an identical position sensitive detector and temperature controller at the ORNL X14A synchrotron beamline at BNL. The next development phase will add scanning capabilities to the data collection package. This development allows real-time studies of phase transformations by high temperature X-ray diffraction at HTML.

2.5 RESIDUAL STRESS USER CENTER (RSUC) HIGHLIGHTS

2.5.1 First In Situ Neutron Diffraction Strain Measurements on Electrostrictive Ceramics

Electrostrictive materials are considered good candidates to replace piezoelectrics because of their increased strain response with electric field, but the application of these materials has been limited by poor electromechanical coupling. Users from Alfred University and the University of Cincinnati recently utilized the strain-mapping facilities of the HTML to study samples of polycrystalline $Pb(Mg_{1/3}Nb_{2/3})O_3$-$PbTiO_3$-$(Ba,Sr)TiO_3$ (PMN) produced by Lockheed-Martin Syracuse. Neutron diffraction provides a means of determining strain as a function of direction and *hkl* within bulk electrostrictive materials under applied dc fields, which may be used to correlate microscopic strains with macroscopic strains measured using strain gages. Strain components normal and parallel to the field were measured as a function of applied field up to 1.2 kV/mm. The (400), (220), (310), and (222) reflections of PMN were measured and used to determine the maximum microscopic strain response of polycrystalline PMN. The neutron diffraction strain data will be compared to the macroscopically-measured strains determined using strain gauges as an initial step towards understanding the poor electromechanical coupling of PMN materials. Future research proposals are anticipated to study the electrostrictive response as a function of dopant levels, processing, and even under ac fields.

2.5.2 HTML Works to Establish International Standards for Residual Stress Mapping by Neutron Diffraction Methods

HTML's active participation in the Versailles Project on Advanced Materials and Standards (VAMAS), Technical Working Group 20 (TWA20), aims to standardize accurate and reliable procedures for making nondestructive residual stress measurements in crystalline materials by neutron diffraction. At this year's meeting held in Nykoping, Sweden, the prime theme was a review of round-robin results on a shrink-fitted aluminum ring and plug assembly measured by various neutron scattering laboratories around the world. ORNL's instrumentation and measurement experience contributed to the outstanding quality of the HTML submitted data. In addition to the required data set, HTML also reported data obtained with finer steps and with finer slits (higher spatial resolution). The TWA20 group considered this an important contribution as the additional data revealed new features in the sample and showed the effect of sampling volume on the measurement results. A comparison of results indicates that three laboratories, including ORNL, achieved consistent results that were in line with predictions. Other laboratories, however, exhibited results disagreeing by as much as 100%. Three more specimens are planned for the next phase of round-robin studies: a two-phase composite sample, a shot-peened sample dealing with measurement of near-surface residual stresses, and a weld specimen. Because of ORNL's expertise and experience, HTML will help to define the measurement procedure for the composite material and will be consulted regarding the preparation of the weld specimen(s).

2.5.3 New Monochromator Yields a Doubling of Flux, and New Data Collection Routine Put into Productive Use

Neutron residual stress measurements at HFIR were delayed for two months due to an unscheduled downtime. During this downtime, we installed a new monochromator on our beamline. Tests on the new focusing monochromator for stress mapping indicated a flux gain of approximately a factor of two. The peak profiles were also narrower, which should improve sensitivity to strain. During the outage, data collection software was modified to enable studies of large grained alloys by introducing multi-axis oscillations that assure that valid polycrystalline averages are obtained during data collection. This software modification was necessary for two upcoming studies: stresses in stator vane segments with Ni superalloy turbine blades, and a Cummins Engine Study of subsurface stresses from induction furnace heat treatment of a diesel cam shaft.

2.6 THERMOPHYSICAL PROPERTIES USER CENTER (TPUC) HIGHLIGHTS

2.6.1 Michigan State University (MSU) and HTML Collaborate to Enhance Thermal Diffusivity Data Analysis Methods

An improved thermal diffusivity data analysis program has been developed at MSU for opaque and semitransparent solids. The program utilizes all the data points in a thermal diffusivity measurement, a significant improvement over most existing analysis models that frequently use just ten of the several thousand measured data points. Heat loss due to sample radiation and light penetration in semitransparent materials were also taken into account in the model. Six carbon-bonded-carbon fiber specimens with systematic changes in thickness were tested to 2400°C. Thermal diffusivity measurements of steels, alumina, and zirconia were also performed. The data are currently being analyzed by the MSU program. Once validated, the code will be made available for use at HTML, expanding the range of materials studied and improving the accuracy of each measurement.

2.6.2 Ford Research Laboratory Studies Aluminum Metal Matrix Composite Thermal Transport Properties at HTML

A scientist from Ford Research Laboratory used TPUC/HTML facilities to characterize the thermal transport properties of aluminum metal matrix composite (Al-MMC) materials proposed for use in automotive brake hardware. The specific goal was to investigate the effects of particle reinforcement phase and volume fraction on thermal transport in these materials. Specimens were cut from actual brake hardware provided by two manufacturers, representing seven different materials: four SiC particle reinforced alloys, two Al_2O_3 particle reinforced alloys, and the unreinforced Al alloy. Room temperature thermal diffusivity, measured by the laser flash method, varied from 0.43 cm^2/s for the Al_2O_3 materials to 0.89 cm^2/s for the SiC materials. The vol% of SiC (10–30%) did not significantly change the thermal diffusivity. It was found that at 475°C, the thermal diffusivity of the SiC reinforced materials dropped by 40% of its room temperature value, and the Al_2O_3 reinforced materials diffusivity dropped by 10%. The specific heat capacity of these Al-MMCs was also measured via differential scanning calorimetry. The data will be used for modeling potential future brake systems and the performance during braking. Results will be compared to results for traditional gray cast iron currently used as brake system hardware.

2.6.3 Thermophysical Property Data for Improving Lost Foam Process Obtained

With the drive to reduce wall thicknesses and eliminate rejects, great emphasis is being placed on casting modeling. However, thermal property data of the ceramic coatings and the supporting sand are not available in the literature. The casting group at University of Alabama at Birmingham (UAB) came to HTML to characterize thermal transport properties of materials used in the lost foam casting process. This process is heavily used to cast engine blocks in the transportation industry. Thermal conductivity of the porous ceramic coatings were measured up to 1000°C by the laser flash and differential scanning calorimetry (DSC) techniques. Four types of casting sands were tested by the same techniques. Special holders were developed for the loose sands, and thermal conductivity of the sands was measured to 1000°C. To improve accuracy, a heat probe technique is being developed to measure large volumes of casting sand.

2.7 MECHANICAL CHARACTERIZATION AND ANALYSIS USER CENTER (MCAUC) HIGHLIGHTS

2.7.1 Development of a Virtual Instrumentation Laboratory

During this fiscal year, considerable progress has been made by Dr. Matt Ferber of the Mechanical Characterization and Analysis User Center in the development of LabVIEW*-based server/client software for accessing instruments in the group over the internet. This software has been designed to easily interface with existing LabVIEW control software currently in use on a number of MCAUC instruments including the Interface Test System, the Refractory Creep Facility, and the Mechanical Property Microprobe. The newly developed server/client software allows a remotely located user to monitor various instrument signals, view the instrument through a series of cameras, and control key aspects of the instrument's functions.

2.7.2 Efforts to Calibrate Indenter Shapes Other Than Berkovich Are Successful

For some materials, thin films in particular, a flat punch or a spherical indenter tip may be more suitable for elastic modulus measurement. Extensive scanning force microscopy work was done on indents made with 2μm and 20μm spherical indenters to study the shape of such indenters. A method

*Manufactured by National Instruments, Austin, Texas.

for calibrating such indenters was also developed. The results were presented at the Annual Meeting of the American Ceramic Society in May 1997.

2.7.3 Infrared Imaging Used to Identify Onset of Cracking During Cyclic Fatigue

Tom Fitzgerald, Westinghouse Electric Power Division, Orlando, Florida, performed room temperature cyclic testing on zirconia-coated MAR-M substrates using MCAUC's MTS® Servohydraulic Tester. The intent of Westinghouse's study was to determine the onset of crack formation as a function of the number of cycles for this coating system. A problem with the coating was that it was white, so it was difficult to detect the formation of the typically miniscule cracks. However, MCAUC's infrared imaging system was successfully used in conjunction with the mechanical testing to identify crack formation. The substrate material warmed during mechanical tests, so when cracks formed on the coating, a temperature discontinuity was created, which the infrared imaging system was able to unequivocally detect. With the aid of a VCR, Dr. Fitzgerald was able to identify the cycle in which crack formation occurred.

2.8 MACHINING AND INSPECTION RESEARCH USER CENTER (MIRUC) HIGHLIGHTS

2.8.1 Cylindrical Grinding Used to Produce Two-Component Fuel Injector Plunger Specimens

The Weldon cylindrical grinder was used in a plunge-grinding mode to produce several dozen mock-up diesel engine fuel injector plungers. The objectives of the experiment were (1) to develop and demonstrate a grinding process for the specimens using a variable composition grinding wheel and (2) to determine the grinding ratio in order to estimate grinding costs in a production environment. The specimens started as cylindrical rods approximately 50 mm long by 8 mm in diameter, with one end being composed of type M2 tool steel and the other of zirconia. Approximately 1 mm of radial stock was removed from the rods in a plunge-grinding operation.

Because diamond abrasive does not perform well on steel work pieces, a cubic boron nitride (CBN) abrasive wheel was used. Although CBN is softer than diamond, the abrasive performs extremely well on steel and is still capable of grinding ceramic materials. CBN wheels are generally more expensive than comparable-sized diamond wheels. The grinding wheel was custom engineered for this specific work piece, so that the surface used to grind the steel would have a different concentration and bond filler material from that used to grind the ceramic. Initially, the test specimens tended to fail during the grinding process by breaking at the steel-zirconia interface zone. However, this problem was overcome by providing additional support of the work piece during the grinding process.

Although there are still some minor problems to be solved with the final geometry of the work piece, extremely fast cycle times were demonstrated. Grinding ratio (the volume of work piece material removed by grinding divided by the volume of grinding wheel consumed by grinding) is difficult to calculate in a laboratory environment because of the small volumes of material involved. The volume of material removed from each specimen can be calculated based on the initial and final geometry of the specimen. The volume of material worn from the grinding wheel must be calculated indirectly, based on the change in diameter of a graphite wear rod. Data are being analyzed to determine the grinding ratio for the process.

2.8.2 High-Speed Diamond Grinding Wheel Allows Major Grinding Time Reduction

An experimental grinding wheel from Cincinnati Milacron was purchased and installed for use on the instrumented centerless grinder. Previous studies have shown the need to grind ceramic materials at much higher wheel speeds than are currently available using "conventional superabrasive" (diamond and cubic boron nitride) grinding wheels. The maximum safe operating speed of

conventional wheels is limited by the construction material used for the wheel core, which is typically a vitrified material with a large mass. Should such a wheel fail catastrophically, it would be very difficult to contain the wheel fragments within the machine enclosure because of the high energy levels involved. The new Milacron wheel has a much lower mass and higher strength because of the use of composite materials for the wheel core. Small, low-mass, abrasive coupons are cemented to the periphery of the wheel core. Should wheel damage occur during grinding experiments, the amount of energy released can be easily contained within the machine enclosure. The new wheel can be operated at speeds up to 100 m/s (20,000 surface feet per minute). In order to accommodate the higher wheel speed, several modifications had to be made to the centerless grinder. A variable speed motor/controller with appropriate safety features was added, and changes were made to the hydrostatic spindle bearing lubrication system. Temperature sensors have been installed on the bearing housings, and the equipment is ready for a final safety review prior to being used at the higher grinding speeds. Initial centerless grinding tests with the new wheel indicate that drastic reductions in per-piece grinding cycle time can be achieved. An AlliedSignal GS-44 silicon nitride tensile specimen, which previously required a 35-min cycle time to grind on a centerless grinder at conventional wheel speeds, was ground to the required finished geometry in approximately two minutes. The new wheel was operated at a surface speed of 97 m/s (19,000 surface feet per minute).

2.8.3 Improved Grindability Test Machine Received

A prototype grindability tester, which uses a diamond abrasive belt to measure the relative grindability of ceramic specimens, was delivered last year to HTML by Chand Kare Technical Ceramics. The equipment was recently replaced by a second-generation grindability tester that incorporates improvements in construction resulting from our experience with the prototype unit. The new equipment has been installed and is available under the HTML User and Fellowship Programs and to other users wishing to perform grindability studies.

2.9 HTML FELLOWSHIP PROGRAM HIGHLIGHTS

Most of our fellowship program projects, like the user projects, involve users coming to HTML to do their work; however, some of our equipment is portable. In the case of the fellowship program project with James W. Fash of Ford Motor Company, Dr. Ralph Dinwiddie of TPUC took the high-speed infrared camera to the Ford Scientific Research Laboratories and participated in the project aimed at improving brakes and braking systems for automobiles. The process of sending HTML staff to fellowship program participant sites has been dubbed the "reverse fellowship" process. This process was essentially repeated this year, with the participation of Dr. Kwang-Jin Lee of Delphi Chassis Systems, who utilized the expertise and equipment of HTML on a brake system project.

This period, several HTML graduate fellowship program students have completed their studies and graduated. Elizabeth Dickey of Northwestern University completed her dissertation defense and is now employed as an assistant professor at the University of Kentucky. Ron Ott of UAB successfully defended his thesis on March 14, 1997, concluding his fellowship. He has taken a position as a post-doctoral researcher at UAB. Allen Haynes of UAB successfully completed his thesis defense, which ends his fellowship. Dr. Haynes is now employed by Oak Ridge Institute for Science and Education and works in a postdoctoral position in the Ceramic Surface Systems Group at ORNL. Matt Stough of Pennsylvania State University had his dissertation defense successfully performed on June 23, 1997. The ex-graduate fellow is now employed at Osram Sylvania, Exeter, New Hampshire. His work has led to an important new understanding of the zirconia-alumina phase diagram, with better definition of solubilities of the Zr and Al species in each other's oxide lattices.

3. HTML USER STATISTICS

This section provides tables and graphs that summarize selected HTML user, fellowship, and other statistics, including user demographics, user agreements, and user proposal history.

3.1 USER DAYS

Individuals from industrial companies, universities, other DOE laboratories, and other agencies, along with internal users from HTML, the Metals and Ceramics Division, and other ORNL divisions, utilize the equipment within HTML. Since shortly after the beginning of the User Program, there has been a user logbook for each instrument in the User Centers. The entries from these logbooks are tallied annually by each User Center for each instrument, then the totals are rolled into one set of data for the HTML. Each 8-h period, or fraction of an 8-h period, that an instrument is being used is tallied as a "user day." Over the years since 1987 (with the exceptions of 1987 and 1995), the user day data have been collected for industry and university users as well as for internal ORNL staff.

Recently, with the advent of a new FileMaker PRO* relational database, we have been collecting more complete user-day data on each instrument. We now collect data on industry, university, and internal ORNL users, but also include numerous other uses. We have also separated the HTML Fellowship Program data, whereas previously it had been included in the user activity. Table 3.1 contains all of the data since the second full year of operation (data for the first full year do not exist). Empty cells in the table indicate that no data were recorded, not that a given type of user work was not performed.

The complete tabulation of user days by User Center, instrument, and user type for FY 1997 is contained in Appendix F. Data for FY 1997 are included from the HTML Fellowship Program in all three of its operational categories: "industrial," "graduate," and "faculty." User-day data are compiled according to User Centers in Table 3.2.

Table 3.1. History of HTML user days by fiscal year

	1989	1990	1991	1992	1993	1994	1996	1997	Total
User									
Industry	581	956	3,201	3,692	2,695	4,719	5,326	1,672	22,842
University	248	607	674	880	1,353	2,163	2,181	1,801	9,907
Proprietary	31						256	166	453
Other Agency	9						20	3	32
Fellowship									
Industry							622	1,844	2,466
Graduate							1,417	932	2,349
Faculty							148	4	152
Subtotal	869	1,563	3,875	4,572	4,048	6,882	9,970	6,422	38,201
Work for Others							158	70	228
ORNL	1,427	1,758	5,309	4,661	9,666	7,301	8,958	13,683	52,763
CRADA							2,706	1,877	4,583
Total	2,296	3,321	9,184	9,233	13,714	14,183	21,792	22,052	95,775

* Subsidiary of Apple Computer, Inc.

Table 3.2. HTML user days for FY 1997 by User Center

	User Center						
	DUC[a]	MAUC[b]	MCAUC[c]	MIRUC[d]	RSUC[e]	TPUC[f]	Total
User							
Industry	21	95	1,018	45	337	156	1,672
University	148	193	853	25	400	182	1,801
Proprietary	26	122	0	0	6	12	166
Other Agency	0	0	0	0	0	3	3
Fellowship							
Industry	10	62	1,565	2	39	166	1,844
Graduate	70	363	209	11	50	229	932
Faculty	0	4	0	0	0	0	4
Subtotal	275	839	3,645	83	832	748	6,422
Work for Others	0	0	0	0	48	22	70
ORNL	317	996	10,783	1,003	463	121	13,683
CRADA	6	21	1,817	6	0	27	1,877
Total	598	1,856	16,245	1,092	1,343	918	22,052

[a]DUC = Diffraction User Center
[b]MAUC = Materials Analysis User Center
[c]MCAUC = Mechanical Characterization and Anaylsis User Center
[d]MIRUC = Machining and Inspection Research User Center
[e]RSUC = Residual Stress User Center
[f]TPUC = Thermophysical Properties User Center

The data for total, industrial, university, and internal ORNL user days are plotted in Fig. 3.1. As the figure shows, although there is some irregularity in the growth pattern, in general the HTML experienced a steady increase in the number of user days performed for each category through FY 1996, leveling off in FY 1997.

The increase in use of HTML facilities has been partially attributable to continuing efforts towards providing lower-cost service (making the program more cost effective). It is also attributable to the continuing commitment to customers exhibited by the HTML staff—by pleasing the customer we get repeat business (see Sect. 3.2), and we get new business because customers spread the word about us. Also, the continued growth can be attributed to our ongoing marketing, in which we inform potential customers of our services through in-house visits, tours, and presentations at universities, conferences and expositions, and to our World Wide Web site. Major growth has occurred this year in the ORNL internal use category, in which we support several other DOE programs, including the Heavy Vehicle Propulsion Materials Program, the Continuous Fiber Ceramic Composites Program, the Advanced Turbine Systems Program, and others. However, this growth has been offset by shrinkage in the number of external industrial user days and to a lesser extent by a decrease in the external university user days, after years of steady growth in these areas. There is no ready answer to why this has occurred, as university and industry interest levels remain high (see the increased numbers of proposals submitted, described below).

To meet the continuing demand for some instruments, we have purchased duplicates (e.g., a second nanoindenter and several tensile test machines). However, we occasionally have to delay the user's visit to HTML because of difficulties in scheduling our limited staff and equipment. We are now very close to or have reached a "saturation" in user day capability at the current budget level.

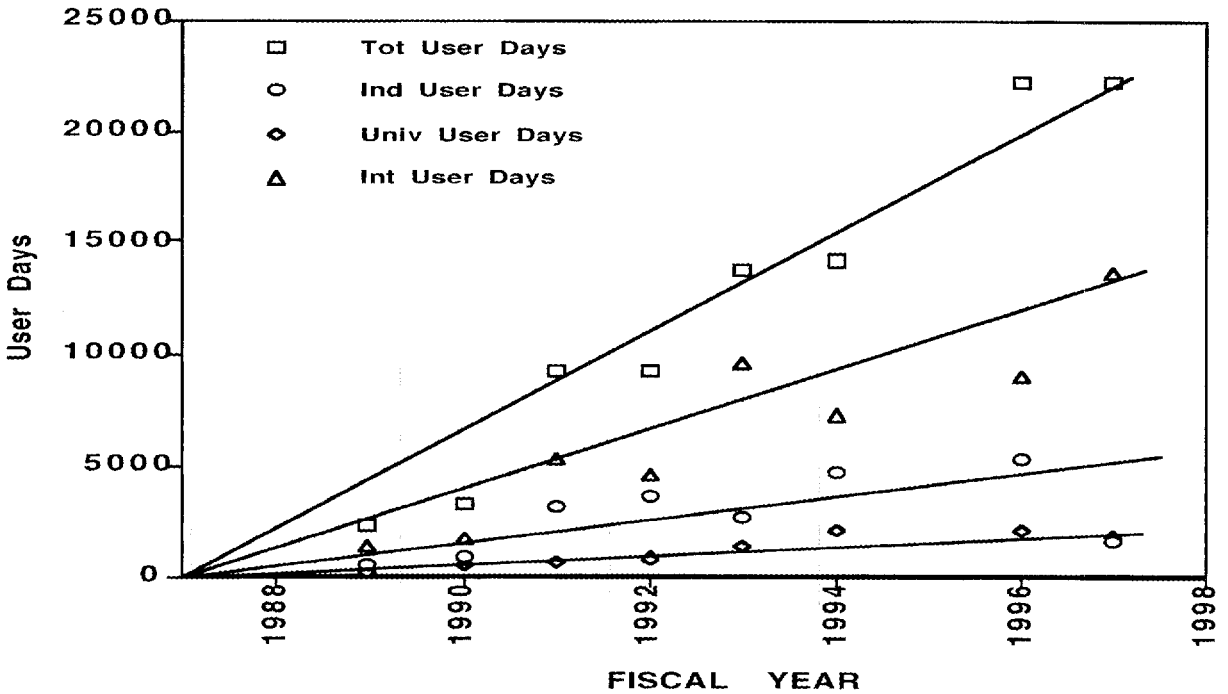

Fig. 3.1. A history of user days of research expended in HTML since its inception.

3.2 USER AGREEMENTS AND PROPOSALS

A "User Agreement" between LMER and the user institution is the legal vehicle that allows a user to perform work in HTML; it specifies the handling of intellectual property and personal liability. The agreements are handled and tracked by the ORNL Office of Science and Technology Partnerships (OSTP), which provides a listing of all of the User Agreements within LMER.

A User Agreement allows a company or university access to any of the 15 user facilities at ORNL. The user completes another document, called a "technical proposal," after both parties have signed the User Agreement. Technical proposals are handled and tracked by the HTML Program Office. Figures. 3.2 through 3.5 illustrate User Agreements received by OSTP and technical proposals received by HTML (see the tables in Appendix B).

Figure 3.2 illustrates the history of total User Agreements received at OSTP. Many are written expressly for interaction with HTML User Centers, although some were written for multiple-user facility access or for access to other ORNL facilities, such as the Materials Processing Laboratory User Centers (MPLUS) or the Surface Modification and Characterization Facility (SMAC). After a quick rise in the numbers of User Agreements during HTML start-up, the annual number stabilized at about 30, with approximately equal numbers of industrial and university agreements. The industrial numbers increased in the years 1994 through 1996 because HTML program and research staff aggressively marketed the facility; because new customer interest in HTML was stimulated by word of mouth; and because new User Centers at ORNL, such as MPLUS and SMAC, brought in new users. The increased number of User Agreements bodes well for the future. During FY 1997, however, the number of new agreements decreased slightly.

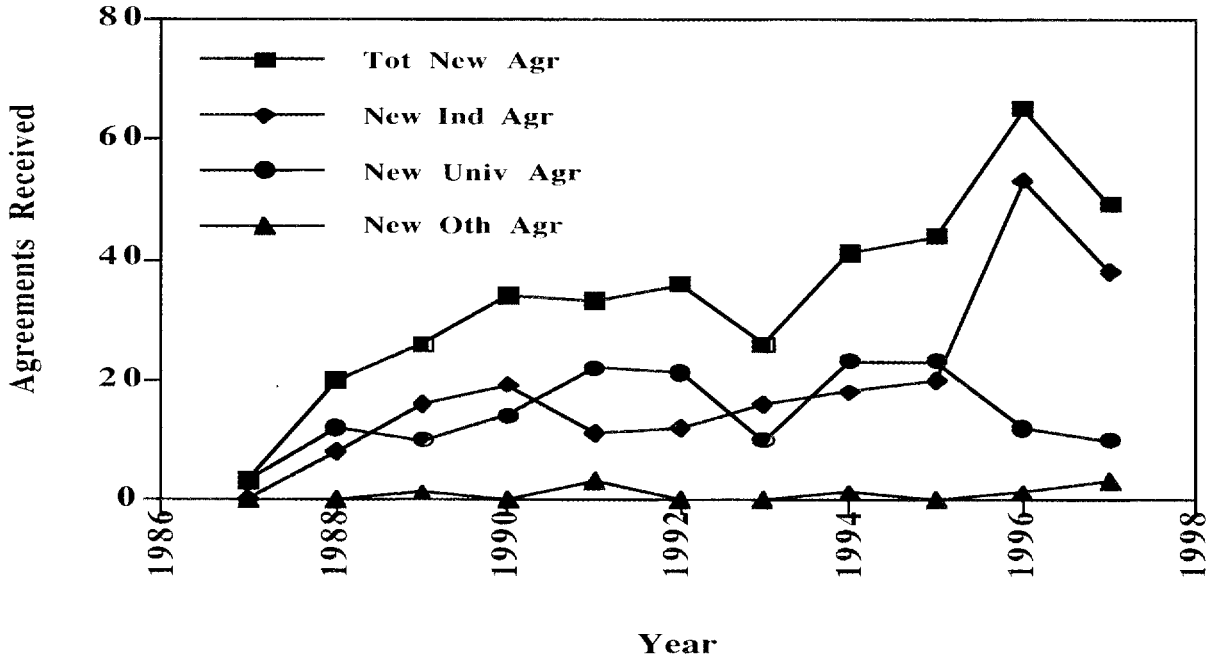

Fig. 3.2. Numbers of materials-related User Agreements received by the ORNL Office of Science and Technology Partnerships.

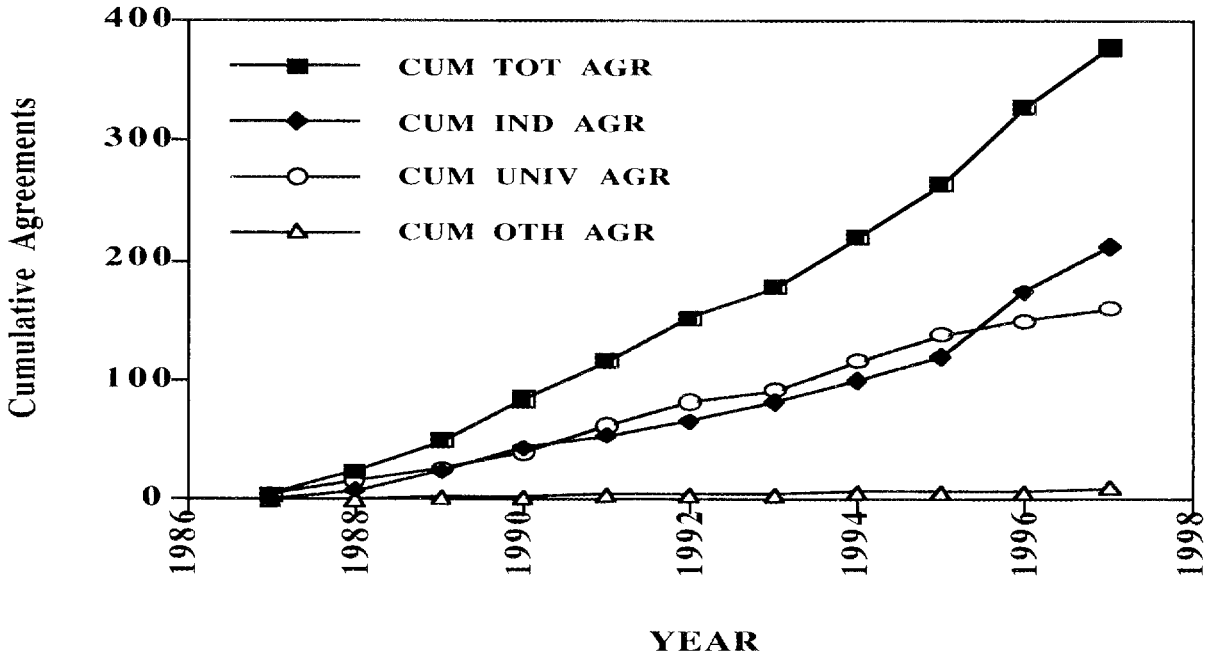

Fig. 3.3. Cumulative number of User Agreements received by the ORNL Office of Science and Technology Partnerships.

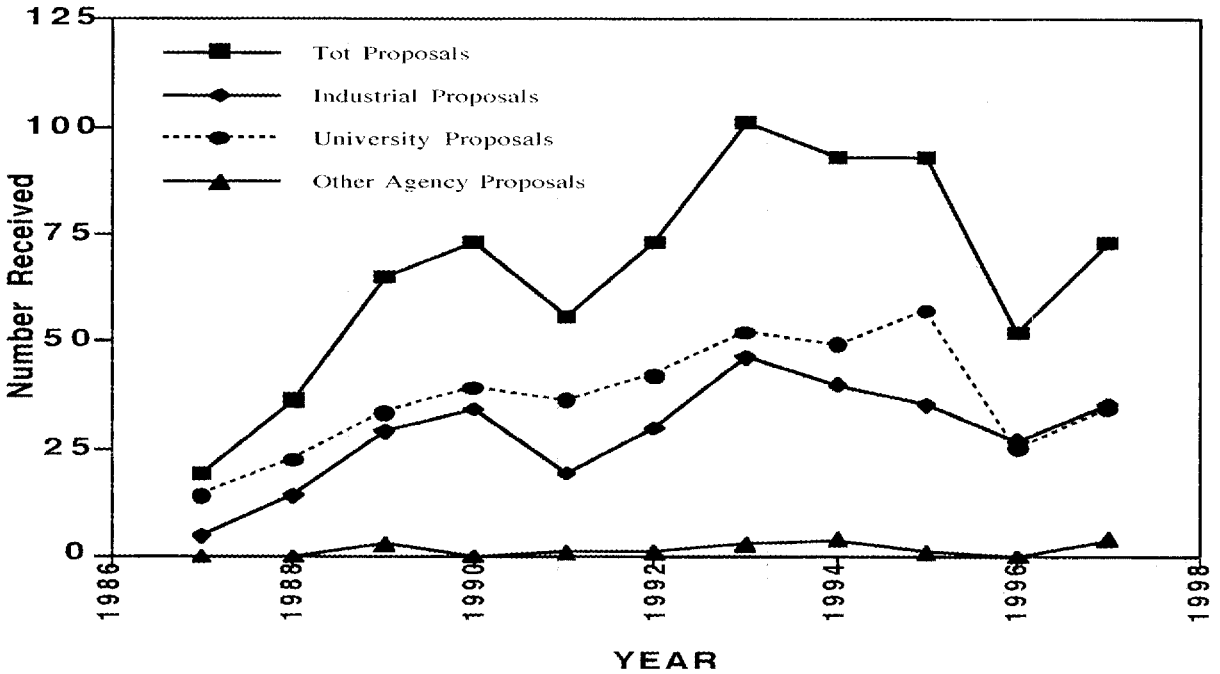

Fig. 3.4. History of technical proposals received by HTML.

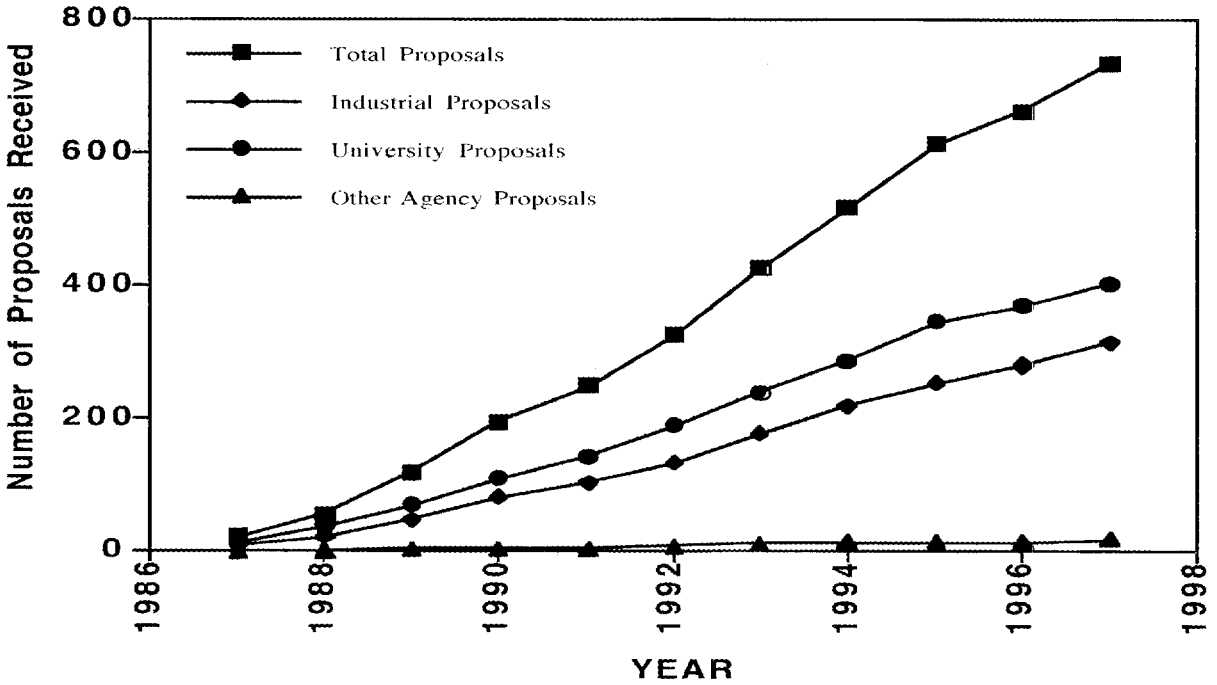

Fig. 3.5. Cumulative history of technical proposals received by HTML.

Figure 3.3 shows the cumulative number of User Agreements: the total is approaching 400. Industrial User Agreements have now surpassed university User Agreements.

The history of technical proposals is illustrated in Fig. 3.4. Like the User Agreements, proposals increased until about 1990 as the HTML programs were starting up. Since then, however, the rates for proposals have varied quite widely. The rate of receipt of user proposals decreased noticeably from about 1993 through 1996, especially industrial proposals, which showed a steady 4-year decline. The possible reasons for this were numerous.

One factor was that many companies were continuing to work under previously existing proposals. New proposals were not being written, and no specific means to close out old proposals existed. Meanwhile, companies maintained their presence at HTML, which caused a problem because the HTML user program is charged a quarterly fee for each "active" user clearance into ORNL. Therefore, money was sometimes being spent needlessly on clearances for projects that had been closed.

A new mechanism was instituted in FY 1996 to close out old proposals, cause new ones to be written, and eliminate the clearance costs for users who were no longer active. At the end of each year, a letter is sent to each user institution thought to be active, inquiring about its status and asking for a written summary if the work is completed (for our annual report) and to provide the publications that resulted from the work. In this way, we get a clear understanding of their project status, a summary, and a paper if the work has been completed. This action may be partly responsible for the increase in the number of proposals submitted in FY 1997.

A second possible reason is that in 1993 companies took advantage of the new openness of the Democratic administration in Washington and its encouragement of CRADAS and other industry-laboratory interactions. Several companies "tested the waters" in 1993 and 1994, and as a result we saw an increase in the number of proposals. We are now returning to a steadier rate.

A third possible reason is that HTML staff members are concentrating their efforts on a few, relatively important projects as the HTML program approaches saturation.

Whatever the reasons, the turnaround in FY 1997 is quite dramatic.

Figure 3.5. presents a picture of the cumulative history of technical proposals, showing that the total number of proposals received has now exceeded 730. Universities continue to lead industries in the submission rate.

Figure 3.6 depicts the cumulative history of User Agreements and technical proposals received, illustrating that the ratio of proposals to agreements is 734/377, or about 2. This figure indicates that, on the average, users tend to come to the ORNL User Facilities about twice to perform research and development projects. This repeat business is evidence of the satisfaction we provide to our customers.

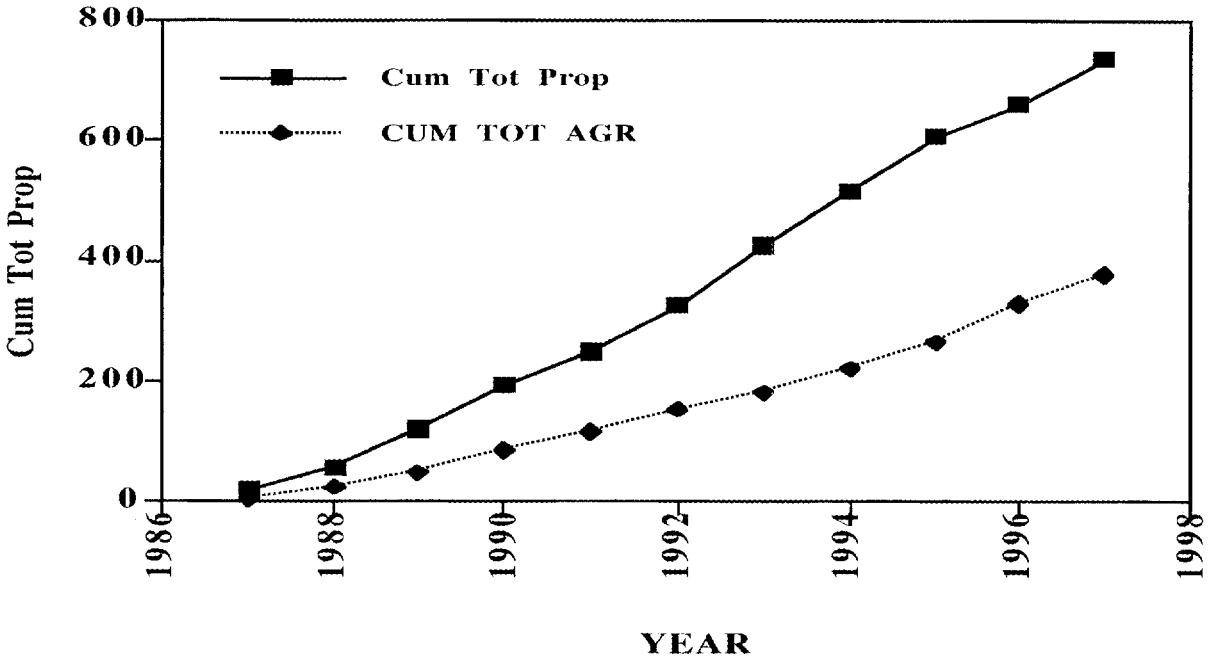

Fig. 3.6. Cumulative technical proposals and User Agreements received.

4. HTML USER CENTERS

4.1 MATERIALS ANALYSIS USER CENTER

4.1.1 Staff and Current Capabilities

The MAUC uses electron microscopy and surface chemical analysis techniques to characterize the structure and chemistry of advanced structural materials. The information obtained from these characterizations is used to elucidate the mechanisms that control material performance.

T. A. (Ted) Nolan is group leader of MAUC. Additional MAUC staff members are listed below, along with the instruments for which they have primary operating responsibility:

- Dr. L. F. (Larry) Allard—Hitachi HF-2000 field emission gun transmission electron microscope (FEG-TEM);
- Ms. D. W. (Dorothy) Coffey—Hitachi S-800 FEG SEM and S-4500 800 FEG-SEM;
- Mr. L. (Larry) Walker—JEOL 733 electron microprobe (on loan from the LMES Y-12 Plant);
- Dr. K. L. (Karren) More—JEOL 4000EX 4000EX high-resolution transmission electron microscope (HREM) and 2000FX analytical electron microscope and Topometrix scanning probe microscope;
- Dr. E. (Edgar) Völkl—electron holography, digital and remote microscopy.

4.1.2 Highlights

4.1.2.1 Remote and digital microscopy

Some time ago we recognized the value of a capability for our users to interact directly with the scientists and instruments in our laboratory by Internet connections during microscopy sessions. Therefore, the concept of "remote microscopy" in a "virtual laboratory" was a natural next step to improve performance and to make our facilities available to a much-expanded user base. To this end, we have successfully developed control and image-processing algorithms for the digital imaging and control system of the Hitachi HF-2000 FEG-TEM, our "flagship" instrument. The Hitachi S-4500 SEM and the JEOL 733 super electron probe are now remotely operable as well. Typical functions that can be controlled remotely include focus, specimen position, magnification, and acquisition of a high-definition image.

A new initiative sponsored by the Mathematics, Information, and Computation Division (MICS) of DOE called DOE 2000 is under way; this initative seeks to develop and demonstrate "collaboratory" concepts such as remote instrument operation, electronic whiteboards and notebooks, and telepresence tools. We participated with Argonne and Lawrence Berkeley national laboratories in the submission of a proposal to MICS to perform a pilot project called the Materials Microcharacterization Collaboratory (MMC). This proposal was one of two selected for funding, and it is supporting the continued development of remote microscopy. The MMC has as its principal mission the use of the abovementioned tools to solve materials problems that are important to DOE and the nation. The problem being addressed by HTML researchers is that of using the microstructural characterization tools available through the MMC to assist in producing a better NOx reduction catalyst. This effort is strongly supported by the Office of Heavy Vehicle Technologies, and this office has authorized the reallocation of a portion of the user funds to match the MICS funds for using collaboratory tools on this important problem. We have teamed with researchers at Ford Research Laboratory who are making new experimental catalyst formulations for NOx reduction. This work is described in some detail in the next section.

Within the past year, the remote microsocopy concept has begun to move from demonstration phase to beneficial use. Three universities are using remote operation of our microscopes in microscopy and materials science courses. Ford Research Laboratory is on-line, and several other

industrial institutions are planning to set up PCs with cameras and software to be ready to perform remote microscopy with us.

4.1.2.2 Ex situ reactor for catalyst studies

The ex situ reactor system is currently being used extensively for studies of catalyst reactions by users such as Dow Chemical and Ford Research Laboratory. The Ford work comprises studies of several catalysts being tested as candidates for reduction of NOx emissions from diesel truck engines. Dow scientists are using the capability of the specimen holder to be transferred between the reactor and the microscope without atmospheric exposure to study carbon-based catalysts designed for chemical industry applications.

The Ford work is being conducted largely via remote microscopy, as a component of the DOE2000 Materials MicroCharacterization Collaboratory and the HTML user program. In order to be able to react catalysts such as platinum (Pt) on mixed alumina-titania supports in oxidizing atmospheres, we had to make technological improvements in our system. The use of standard holey carbon support films proved impossible, because the thin carbon films oxidized and degraded rapidly under our reaction conditions. We needed a stable, oxidation-resistant, conductive film to replace the carbon and found that amorphous films of conductive $LaCrO_3$ deposited in our ion sputter-deposition system satisfied all our requirements. Samples of as-prepared Pt/TiO_2 catalyst material showed a uniform distribution of Pt clusters 0.5 to 1.0 nm in size over the support surface in the as-prepared condition. These particles were shown to grow in size to the 2–3 nm range after 2 h at 450°C in a 14% O_2/N_2 base gas environment. The same sample areas were observed in the before and after reaction conditions. This work is thus providing useful information on the mechanisms of catalyst degradation with treatment.

In the Dow work, we experienced problems with the reactor when HCl gas was used as a reaction gas. Copper components were found to form volatile $CuCl_2$ which was picked up strongly by the carbon catalyst support material, and was subsequently reduced to Cu particles under the reducing treatment to which the catalyst was being subjected. To prevent this problem in future studies, we replaced Cu gaskets with Viton in the chamber flanging, and had a feedthrough comprising 4 Cu posts plated first with Ni then a gold flashing to protect from HCl attack. Other components such as the Cu sample retainer plate were replaced with stainless steel. These modifications have thus provided a better capability to conduct reactions in corrosive gas environments, such as we expect to encounter in future work.

4.1.2.3 Characterization of electronic materials

Characterization of electronic materials has been identified as a new thrust area for MAUC. We have previously reported results of successful user projects with Coors Electronic Packaging and Vamistor Corp. Collaborations are developing with Intel wherein we will use electron holography and remote microscopy to determine materials causes for defects in processor chips. Our electron holography capabilities provide yet another tool for the analysis of electronic components. Electron holography combined with unique electron lens configurations and special algorithms enables measurement of electric and magnetic fields with high spatial resolution quantitatively in free space and in suitably prepared electronic devices. We have demonstrated this technique by mapping the electrical field across *pn* junctions in semiconductor devices. Ours is the only laboratory in the nation capable of high-resolution electric and magnetic field imaging. We are developing a relationship with SEMATECH. They are developing technology that will replace aluminum conductors on semiconductor devices with copper. Copper has the advantage of lower resistivity but the disadvantage that it diffuses into silicon, thus changing the electronic properties of the silicon. A diffusion barrier is required to separate the copper from the silicon. Our laboratory has the capability to determine thickness and continuity of diffusion barrier coatings that can be as thin as 5 nm.

4.2 MECHANICAL CHARACTERIZATION AND ANALYSIS USER CENTER

4.2.1 Staff and Current Capabilities

The Mechanical Characterization and Analysis Group (MCAG) specializes in the mechanical characterization of structural materials, including high-temperature materials. MCAG performs mechanical testing and analysis, develops test methods and supplemental analytical techniques, and conducts finite-element and life-prediction analyses of monolithic ceramics, ceramic composites, and ceramic coatings. Numerous mechanical test frames are available to visiting researchers from industry and academia. Also available are capabilities to conduct tension, compression, flexure, shear, and micromechanical tests in controlled environments and at elevated temperatures on standard and customized specimens. Staff has expertise with a wide range of materials, mechanical test designs, finite-element and analytical modeling, life-prediction analysis, statistical design, and failure analysis.

Staff and their areas of expertise are as follows:

Dr. Kristin Breder, group leader
Mechanical/environmental testing, fractography and failure analysis, statistical analysis
E-mail: brederk@ornl.gov, telephone (423) 574-5089

Dr. Mattison K. Ferber, senior research staff member
Characterization of creep, stress-rupture, and fatigue behavior of structural ceramics in tension, flexure, and special test configurations; data acquisition software and hardware
E-mail: ferbermk@ornl.gov, telephone (423) 576-0818

Mr. Timothy P. Kirkland, principal technologist
Measurement of mechanical properties of structural materials
E-mail: kirklandtp@ornl.gov, telephone (423) 574-2588

Dr. Edgar Lara-Curzio, development staff member
Characterization of mechanical behavior of composites and their constituents (fibers, fiber coatings, interfaces), environmental effects, reliability and durability, modeling of mechanical behavior and constitutive relations, standard test methods and special test configurations
E-mail: laracurzioe@ornl.gov, telephone (423) 574-1749

Ms. Laura Riester, development associate
Micro-mechanical testing, atomic force microscopy, microscopy, and imaging
E-mail: riesterl@ornl.gov, telephone (423) 574-2588

Mr. Stephan Russ, student intern
Ceramic composites
E-mail: russse@ornl.gov, telephone (423) 241-4571

Dr. Andrew A. Wereszczak, development staff member
Creep, fatigue and corrosion behavior, life-prediction, and reliability analysis; finite-element analysis, fracture mechanics, and testing methodologies
E-mail: wereszczakaa@ornl.gov, telephone (423) 574-7601

Ms. Jessie B. Whittenbarger, group administrative support
E-mail: whittenbarjb@ornl.gov, telephone (423) 576-1818

Mr. Mark J. Andrews, HTML graduate fellow
Mechanical testing and reliability analysis
E-mail: andrewsmj1@ornl.gov, telephone (423) 241-4571

4.2.2 Major Research Areas

4.2.2.1 High-temperature tensile test facility

- Eleven 35-kN capacity electromechanical test machines equipped with self-aligning grips for accommodating a wide array of specimen geometries, including button-head tensile, and flat specimens.
- Two servohydraulic test machines capable of monotonic, static, dynamic, and cyclic testing of a wide variety of specimen geometries.
- All test machines equipped with integral, electronic controllers and function generators, and compact two-zone resistance-heated furnaces (maximum temperature, 1700°C; sustained testing in ambient air, 1500°C).
- All machines equipped with low-contact force, capacitance extensometers (accuracy, ~0.1 mm at room temperature and ~0.5 mm at 1500°C).

4.2.2.2 Tensile creep/stress rupture and stress relaxation facility

- Creep and stress rupture
  - — Nine electromechanical tensile machines designated for long-duration creep-stress rupture and low frequency tension-tension fatigue testing.
  - — Computerized control and data acquisition using in-house-developed software application.
  - — Compact two-zone furnaces (maximum temperature, 1700°C).
  - — Low-contact force capacitance extensometers.
- Stress relaxation
  - — Two stress-relaxation test frames devoted to metals and superalloy testing equipped with averaging extensometers and furnaces capable of 1100°C.
  - — Two stress-relaxation test frames devoted to ceramics testing equipped with averaging extensometers and furnaces capable of 1500°C.

4.2.2.3 Ceramic flexure test facility

- Six test frames with pneumatic actuators, each with loading capacity 2.2 kN to test simultaneously three flexure samples, C-rings, or compression specimens.
- Standard mechanical property tests (room temperature to 1500°C):
  - — Static fatigue (time to failure measured as a function of static stress).
  - — Dynamic fatigue (fracture stress measured as a function of loading rate).
  - — Low cycle flexural fatigue.

4.2.2.4 Electromechanical test facility

- 200 kN universal (electromechanical) test machine with high-temperature (1800°C) furnace.
- Small universal test machine dedicated to room-temperature testing of flexure specimens and C-rings, as well as fracture toughness testing.
- Standard mechanical property tests (using standard as well as specially designed test fixtures):
  - — Static fatigue (time to failure measured as a function of static stress).
  - — Dynamic fatigue (fracture stress measured as a function of loading rate).
  - — Cyclic fatigue (cycles to failure measured as a function of cyclic stress).
  - — Fast-fracture tensile and compressive strength.
  - — Shear strength.
  - — Fracture toughness.
  - — Capability for compression creep tests with straight cylindrical specimens and contact extensometer (accuracy, ~0.5 μm) and compressive creep rates (room temperature to 1800°C; stresses, as low as 0.05 MPa).

- Rotary bend fatigue machine equipped with small furnace for testing small (~75 mm long and ~10 mm in diameter) cylindrical specimens in fully reversed cyclic loading.

4.2.2.5 Electromechanical test facilities with environmental testing

- High-temperature clamshell furnace and ceramic retort, for both compression and flexure tests in air, inert gas, or vacuum at temperatures up to 1500°C.
- Environmental tensile test facility: envionmental chamber mounted on test machine (screw-driven), mechanical pump, diffusion pump, regenerative gettering furnace, and temperature controller. High-temperature static, tension-tension cyclic, or dynamic loading in vacuum or inert environments (room temperature to 1600°C using button-head tensile specimen geometry).

4.2.2.6 Test facility for composites and their constituents

- Six in-house-developed electromechanical, universal test machines.
  - — 10-kN load capacity, 150-mm stroke, and 8-nm displacement resolution.
  - — Computerized data acquisition and control.
  - — Environmental chambers to conduct tests in controlled atmospheres (e.g., inert gases with less than 10 ppm O_2, oxidizing and reducing environments, water vapor).
  - — Noncontact laser extensometry.
  - — Various specimen geometries, gripping arrangements, and fixtures (e.g., shoulder-loaded tensile specimens, minincomposites, single small diameter fibers and filaments, double-notched shear specimens, Iosipescu shear specimen).
- Micromechanical universal testing machine.
  - — 1000-N load capacity, 25-mm stroke, and 100-nm displacement resolution.
  - — Equipped with miniature load cells, encoders, and capacitance gauges.
  - — Specially suited for composite interfacial testing by means of single-fiber push-in and push-out tests.
  - — Array of indenter geometries (e.g., Vickers, Knoop, Cube Corner, Diamond, and WC flat punch) to conduct indentation tests.

4.2.2.7 Mechanical properties and scanning force microprobes

- Special microhardness tester capable of operating at four load ranges (0–4, 0–20, 0–100, 0–650 mN).
- Sensitive capacitance gage for constant monitoring of position of indenter relative to surface of specimen.
- Constant monitoring of load as a function of displacement.
- Plastic and elastic components of displacement are separated either by continuous sensing of sample stiffness while force is being applied, or by calculating the hardness based on the recorded measurements of load vs displacement.
- The scanning force microprobe gives information on the response of materials to indentation by compiling a three-dimensional (3-D) image from an array of single-line profile scans.

4.2.2.8 Life-prediction analysis

- Work station with two life-prediction algorithms and integrated finite element programs for performing finite-element analysis (FEA) and reliability modeling work to predict probability of component survivability in known service environment and stress level:
  - — Mechanical test data from standard specimens.
  - — FEA data for stress in actual components.
  - — FEA support provided for other mechanical testing of monolithic ceramics and composites.

4.2.2.9 Resonant ultrasound spectroscopy (RUS) facility

- Characterization and inspection of mechanical integrity of ceramic specimens and components.
- Resonance spectrum generated by sweeping frequency of ultrasound signal applied to component and by detecting resonance frequencies of component.
- Applicable to determining with high accuracy the full elastic constants of isotropic and anisotropic materials (e.g., single crystals, textured polycrystals, and composites).

4.2.2.10 Additional capabilities

- Infrared imaging used in situ with mechanical testing.
- Acoustic emission capabilities.
- Strain gaging facilities.
- Testing of ceramic-ceramic joints.
- Testing of intermetallics.
- Thermal shock testing.
  - — Failure analysis.
  - — Tube testing and test of tubular filters.

4.2.3 Major Activities in FY 1997

Sixteen new proposals were submitted to MCAUC in FY 1997. The year was a very active one in terms of user hours as well as hours logged by industrial and academic fellows. Some new capabilities were developed, and improvement to equipment is a continuous effort.

The test facilities described above are all computerized in terms of controls and data acquisition. As the opportunity rises in terms of upgrading of computers or facilities, several applications using Labview software (National Instruments) have been added. Labview is a flexible, modular software system from which one can customize one's applications. This can be made to interface with the internet such that with a fairly small client application, a user can operate or check on an experiment remotely. This was successfully demonstrated for a few of the applications in MCAG this year; a demonstration tensile test experiment was performed from the University of Tennessee as part of a class. For the users in MCAG where long term testing is common, it would be very useful to be able to observe remotely the test in progress and to download data on regular intervals without having to travel. These possibilities increase as the equipment gets updated.

Through a productive synergism between the user program, the fellowship program, and the Advanced Turbine Systems program, the activities on thermal barrier coatings (TBC) have increased substantially. Through the user program, Westinghouse has an on-going project to generate fatigue life data on TBC specimens to assist in development and validation of TBC life prediction models. The approach is to perform a compression/compression fatigue test on a tubular substrate/bond coat/thermally grown oxide (TGO)/TBC in a strain controlled mode to a series of preselected strains at two temperatures. Failures are expected to consist of coating spallation. In a recently finished graduate fellowship project, the purpose was to investigate the isothermal oxidation and thermocyclic degradation of various TBC systems (both APS and EB-PVD) with particular emphasis on the growth kinetics, microstructures, flaw content, fracture behavior, and micromechanical properties of the interfacial Al_2O_3 scales that formed on APS TBCs. Several important findings on the failure modes and microstructural development of the TBCs under cyclic loading were made, and this is reported in more detail in the summary of the project given later. In another graduate fellowship project, Raman piezospectroscopy was used to study TBCs. Piezospectroscopy is particularly useful for analyzing the failure behavior of TBCs, since stress can be measured in both the zirconia thermal barrier and the oxide scale that forms at high temperatures. For plasma-sprayed TBCs, the bulk compressive stress in the zirconia gradually decreases with the number of cycles indicating cracking during cool down. Tensile stresses normal to the interface at the peaks of asperities in the bond coat were measured indicating that cracking in the zirconia is highly dependent upon interface roughness. Similar results were obtained for TBCs produced by PVD with the bulk

compressive stress in the zirconia gradually decreasing with the number of thermal cycles. A bimodal stress distribution was measured in the oxide scale; either stress was close to zero or over 2 GPa of compression for delaminated or intact scales, respectively. This shows that piezospectroscopy can be used to measure damage accumulation nondestructively in thermal barrier coatings. In order to study the development of cracks in TBCs, a four-point flexure rig was combined with a microscope in such a manner that the development of microcracks as a function of applied strain could be followed. Using this, it was demonstrated how spallation cracks develop in some of these systems.

Thermal shock capabilities are being developed in a project funded by the Heavy Vehicle Propulsion System Materials Program as part of an international collaboration under the International Energy Agency (IEA). It was determined to compare different up-shock techniques (e.g., laser heating, blow torch heating, contact heating) and to establish relationships to other thermal shock methods. This project, when completed, will result in additional capabilities for the user center.

The life prediction and reliability analysis capabilities now consist of a computer workstation running two finite element analysis (FEA) programs and two life prediction cones (CARES/CARES LIFE and CERAMIC/ERICA). The FEA has been used in support of user and program activities. We have been able to provide support in failure analysis, combining fracture analysis, fractography, and FEA.

In the nanoindentation area, the capabilities have been expanded to include indenters of different shape. Especially, our work with a Vickers indenter has been successful. The Vickers indenter will produce indentation cracking in certain materials even at the micron scale, and work is on-going to use this for measurement of fracture toughness of coatings and layered structures.

Several proposals in the nanonidentation area were related to coatings and also to near surface characterization. In a project with Lehigh University, the properties of the subsurface zone of an alloy exposed to solid particle erosion was studied. Erosive wear of materials is a problem in several energy-related applications, and the idea would be to use an alloy that during erosion would deform plastically and yield a surface with improved properties. Several cross sections of specimens that had been eroded under different conditions have been studied, and changes in properties and size of the plastically deformed layer is being determined. An additional goal of this project is to perform more fundamental investigations of the properties of these highly deformed layers.

In a user project with Kennametal, we are studying high-temperature contact fatigue. This is related to understanding the wear mechanisms in cutting tools and has allowed us to combine our knowledge of indentation with our experience in high-temperature creep. A system is being set up in which a SiC spherical indenter is combined with SiC push rods in one of the creep testing machines to produce a load-controlled indentation system. This project is continuing in 1998.

Our capabilities to test ceramic/ceramic or ceramic/metal joints has been expanded. Tubular specimens of SiC joined in a butt-joint with a supporting sleeve were successfully tested in tension at 1100°C. Rectangular ceramic/metal joints were tested both in flexure and in tension at temperatures up to 1000°C. The need for testing of joined specimens will likely increase as more ceramics and ceramic composites are being integrated into systems.

In a project with Inco, we are measuring the stress relaxation behavior of a superalloy that undergoes dimensional changes due to phase transformation. The phase transformation will actually lead to a stress increase when the stress relaxation experiment is performed at the critical temperature. The accurate extensometry and stable furnaces available in MCAUC made it possible to precisely map the behavior of these alloys in a way that had not been done previously. This project is continuing into 1998.

In addition to the work in the User Center, researchers in MCAUC are performing extensive research in other DOE programs, and within these we have extensive collaborations with other groups at ORNL, as well as with industry.

4.3 THERMOPHYSICAL PROPERTIES USER CENTER

4.3.1 Background

The TPUC is dedicated to measuring thermophysical properties as a function of temperature and correlating these properties with the processing, microstructure, and performance of materials. Specifically, the TPUC staff works with users to determine thermophysical properties such as thermal diffusivity, thermal conductivity, specific heat, and thermal expansion and to characterize the thermal stability, high-temperature reactions and compatibility, and high-temperature oxidation and corrosion properties of materials. The materials studied include structural ceramics, engineering alloys, ceramic and metal matrix composites, superconducting materials, ceramic precursors, carbon materials, and carbon fiber composites.

4.3.2 Staff and Major Instruments

4.3.2.1 Staff

TPUC is one component of the Diffraction and Thermophysical Properties Group. Members of the group with prime responsibilities for thermophysical properties activities include the following:

- Dr. Ralph B. Dinwiddie—thermal transport and thermal imaging;
- Mr. Wallace (Wally) D. Porter—thermal analysis;
- Dr. Hsin Wang—thermal transport and thermal imaging;
- Ms. Joy L. Kilroy—group administrative support; and
- Dr. Camden (Cam) R. Hubbard—group leader.

Dr. Hsin Wang was an ORISE postdoctoral appointee throughout the period but became a staff member in early FY 1998. He received his Ph.D. from Alfred University's College of Ceramics. His thesis research emphasized measurement of properties of ZnO ceramics.

4.3.2.2 Major instruments

The major facilities of TPUC are divided into three areas: thermal analysis, thermal transport, and the new focus of thermal imaging.

Thermal Analysis

- Stanton Redcroft STA1500 simultaneous thermal analyzer (STA).
  - — differential thermal analysis (DTA)
  - — thermogravimetry (TG)
  - — evolved gas analysis (EGA) by mass spectrometry.
- Stanton Redcroft DSC1500 differential scanning calorimeter.
- Theta dual push rod dilatometer.
- Cahn TG.

The simultaneous thermal analyzer (STA = DTA + TG + EGA) and the differential scanning calorimeter both are capable of operation to 1500°C in 1-atm inert or oxidizing atmospheres. The thermal analysis laboratory also contains a dual push rod dilatometer for bulk thermal expansion measurements to 1500°C. The Cahn large-mass, high-temperature, high-sensitivity TG, with concurrent DTA attachment, provides measurement capability to 1700°C for samples having masses up to 100 g. This instrument supports measurements in vacuum, inert, oxidizing, reducing, and corrosive atmospheres, and thus considerably extends TPUC's capabilities in thermal analysis.

Thermal Transport

- Anter laser flash thermal diffusivity system.
- Xenon flash thermal diffusivity system.
- Longitudinal bar thermal conductivity system.
- Topometrix scanning thermal conductivity microscope (STCM).
- 3-Omega system thin-film thermal conductivity of nonelectrically conductive materials.

The laser flash and xenon flash systems measure thermal diffusivity of materials under a variety of conditions. With the laser flash system (discussed in more detail in Sect. 4.3.3), researchers can make measurements as a function of temperature to 2500°C, measurement of thermal diffusivity of molten metals, and analyses of two- and three-layer samples. The xenon flash system is optimized for room-temperature thermal diffusivity measurements.

The longitudinal bar thermal conductivity system provides for steady-state measurement of thermal conductivity from 80 K to 500 K. These measurements, coupled with the elevated-temperature measurements, are important in modeling thermal conductivity in solids (in terms of grain size, impurities, and crystal defects).

The Topometrix STCM maps thermal conductivity variations in materials such as composites on a submicrometer scale, providing microstructural information not available by other means.

The 3-Omega system was recently assembled to provide a means to measure thermal conductivity as a function of temperature directly. The greatest strength of this technique is the ability to measure the thermal conductivity of electrically insulating thin films and bulk specimens.

Thermal Imaging

- Amber infrared (IR) camera.
- Selected germanium lenses for both microscopic and broad field imaging.
- Image processing software.
- Portable system including computer and triggering circuitry.

A high-speed IR camera for two-dimensional (2-D) thermal diffusivity and nondestructive thermography is the newest instrument in TPUC. The camera was purchased by the DOE-OIT Advanced Turbine Systems program to study thermal-transport characteristics of TBCs on turbine blades and to assess its applicability to detection of defects (see Sect. 4.3.3).

Supporting Facilities

- Five-cell helium pycnometer for density.
- Sample preparation facilities, including the following:
  - — diamond core drill
  - — low-speed diamond cutoff saw
  - — diamond band saw
  - — vacuum deposition chamber
  - — polisher

4.3.3 Developments and New Capabilities

4.3.3.1 Thermal conductivity of coatings

Coatings are being widely used to increase the performance life of gas turbine engine hot-section components, with a future goal of increasing operating temperatures and, hence, fuel efficiency. Thin films are also widely used as protective oxide coatings, wear-resistant coatings, and corrosion-resistant coatings, and as active elements in electronic components. The 3-Omega technique is used to determine thermal conductivity of electrically nonconductive coatings. A photolithographic

method is used to deposit a small heater on the surface of the specimen. Using a variable-frequency ac power supply, a lock-in amplifier, and a furnace enables measurement of thermal conductivity as a function of both depth and to 500°C. The new 3-Omega capability enhances HTML's ability to study the effects of processing conditions, thermal history, and microstructure on the thermal conductivity of high-performance coatings.

4.3.3.2 Laser flash thermal diffusivity system

TPUC purchased a state-of-the-art laser flash thermal diffusivity (LFTD) system in FY 1996 that significantly expanded TPUC's thermal-transport measurement capabilities. This highly flexible system can operate from RT up to 2500°C in vacuum or inert gas. Two furnaces are used to achieve this: one for the range from RT to 500°C and a carbon furnace for the 500 to 2500°C range. In addition, measurements of thermal diffusivity may be made in oxidizing or reducing atmospheres from 25 to 1700°C using a third alumina tube furnace. Six-sample carousels on the two-vacuum/inert-atmosphere furnaces greatly increase the number of tests that can be made in a single day. In addition to standard disc-shaped samples, the new system will also measure square plates, powders, molten metals, and coatings. Completion of installation of accessory attachments and debugging of the measurement software was followed by significant growth in productive user activity.

4.3.3.3 Thermophysical properties of molten and semisolid metals

In FY 1996 TPUC carefully assessed industry's current and future needs for knowledge of thermophysical properties. Based on that study, TPUC expanded its focus to include measuring the properties of molten and semisolid metals. These data have recently become very valuable in the national efforts to model materials processes such as welding, casting, quenching, and hot forging or rolling. TPUC has contributed to several user and DOE projects needing properties of molten metals. The new laser flash thermal diffusivity system has demonstrated the capability to determine the thermal diffusivity of difficult-to-measure molten alloys. TPUC also developed and applied techniques for determining the density of molten metals utilizing our existing dilatometer. These data are often coupled with studies on casting modeling.

4.3.3.4 Infrared camera for two-dimensional thermal diffusivity mapping and thermography

TPUC has developed a system capable of producing quantitative thermal diffusivity maps of test coupons, plates, and tubes, as well as thermal effusivity maps of components with complex shapes, such as turbine blades and vanes. This system is ideal for the study of composites and coatings. At the heart of the system is a high-speed, high-sensitivity IR camera with a 256 × 256 pixel focal plane array operating in snapshot mode. Each one of the 65,536 detectors that make up the focal plane array is exposed at the same time and for the same length of time. This allows for a straightforward pixel-to-pixel comparison in each image. With Ge lenses, the spatial resolution can be adjusted down to 7.5 μm, and the temperature resolution can be as sensitive as 0.015°C. The camera can operate at speeds up to 130 full frames per second, or up to 1480 images per second at a resolution of 64 × 64 pixels. The exposure time for each image can be adjusted down to 2 μs, allowing the study of very hot and/or fast-moving targets, such as cutting tools, boilers, and brake rotors, during operation. The camera can be calibrated for absolute temperature measurement.

For 2-D thermal diffusivity mapping, the sample or part is heated by 1000-W quartz lamps, a 1000-W xenon illuminator, or a 4800-W xenon flash lamp. The camera is used to record the temperature response of the heated surface with time. In some cases the thermal response of the back side of the sample is recorded. Custom software is then used to calculate the thermal diffusivity or thermal effusivity for each point in the image. The result is a thermal diffusivity or effusivity map of the object under test. This data can be viewed in a variety of ways, including a spreadsheet format, a 2-D false-color image, or a 3-D surface plot.

In addition to the measurement of temperature and thermal properties, the camera can also be used for thermography applications for nondestructive evaluation of components. The use of IR transmitting fibers coupled to the camera was demonstrated and has great potential for temperature measurement within systems such as dies during liquid metal insertion.

TPUC developed a portable camera-control capability to allow off-site field work. The first demonstration of this portability was in a reverse HTML fellowship with the Ford Scientific Research Laboratory. The purpose of this investigation is to simultaneously image hot spots on the inboard and outboard sides of a brake rotor during braking on a dynamometer. These hot spots result in localized thermal expansion of the rotor that cause the torque variations we know as brake roughness or brake judder. During the three visits to Ford, the TPUC staff was able to record thousands of images of this hot-spotting phenomenon as a function of initial rotor temperature and speed, brake pad manufacturer and design, and braking behavior (i.e., dragging or stopping). In addition to the qualitative images, which show the spatial and time evolution of the hot spots, a calibration was performed that allowed the quantitative measurement of temperature as a function of time and location.

These results have both short- and long-term benefits. In the short term, brake system components that are less likely to cause hot spotting can be selected for cars about to be introduced into the market. In the long term, the thermoelastic models that describe hot spotting may be refined and used to evaluate future designs before they go into production. Visits to GM Delphi Chassis Systems and the University of Southern Illinois are currently being planned for additional work on brake systems and materials.

4.4 RESIDUAL STRESS USER CENTER

4.4.1 Background

User projects and DOE programs are increasingly concerned with life prediction and failure analysis of engineering structures. In many of these cases, knowledge of residual stress gradients (sign and magnitude) as a function of location at both the surface and throughout the volume of a component is critical information for failure analysis and life prediction models. The Residual Stress User Center (RSUC) was established to meet this need and to provide a facility for research into controlling residual stresses, either through modifying the forming and finishing processes, by changes in the design, or through stress-relief procedures. RSUC activities now include both the X-ray residual stress facility, the neutron residual stress facility (discussed in detail in Sect. 4.4.3), and the developing use of synchrotron radiation and Raman microprobe. The diffraction facilities can be utilized to measure macro (long-range) and micro (short-range) residual stresses in polycrystalline materials. Raman microprobe is currently focused on alumina stress measurement in TBCs.

RSUC also characterizes the nonrandom grain distribution or texture in materials and relates this to directionally dependent materials properties. Texture is very common in materials subject to deformation and also in thin films, both areas of increasing importance.

4.4.2 Staff and Major Instruments

4.4.2.1 Staff

The Neutron Residual Stress Facility (NRSF) is operated in a team mode, with members of the Metals and Ceramics (M&C), Solid-State (SSD), and Instrumentation and Controls (I&C) divisions participating. Unless otherwise noted, the following staff members are from the Diffraction and Thermophysical Properties Group, Metals and Ceramics Division. At the end of FY 1996 two group members took positions in industry, and a new postdoc and University of Tennessee (UT) subcontractor were added to the group during the year.

- Dr. E. Andrew Payzant—residual stress mapping, instrument specification;
- Dr. Roberta (Robbie) Peascoe—texture (UT);
- Dr. Steve Spooner—residual stress mapping by neutron diffraction (SSD);
- Dr. Christina Hoffmann—residual stress mapping by neutron diffraction, refractory corrosion;
- Dr. Xun-Li Wang—micro and macro residual stress by neutron diffraction;
- Dr. Thomas R. Watkins—X-ray residual stress and grazing incidence diffraction;
- Dr. Michael Wright—instrumentation design for neutron strain mapping (I&CD);
- Ms. Joy L. Kilroy—group administrative support; and
- Dr. Camden R. Hubbard—group leader and NRSF project leader.

Dr. Hoffmann is an Oak Ridge Institute for Science and Education (ORISE) postdoc who received her Ph.D. in Mineralogy and Crystallography from the University of Bern, Switzerland. Dr. Peascoe received her degree from Texas A&M University in Inorganic Chemistry and Crystallography.

4.4.2.2 Major instruments

- Scintag PTS four-axis goniometer with 18-kW rotating-anode generator.
- Scintag PTS four-axis goniometer with 2-kW sealed-tube generator.
- Neutron spectrometer with XYZ mapping system for macroresidual stress mapping.
- Neutron powder diffraction spectrometer and furnace for microresidual stress analysis.
- X14A beam line at the National Synchrotron Light Source (NSLS) [RSUC is a participating research team (PRT) member on this ORNL beam line].

Both of the neutron spectrometers are owned and managed by the Neutron Scattering Section of the SSD at ORNL. RSUC is provided a portion of the time on these instruments to establish and operate the neutron residual stress effort based on an agreement between DOE's Basic Energy Sciences (BES) and Energy Efficiency (EERE) programs and ORNL's Solid State and Metals and Ceramics divisions. The long-term goal is to establish a dedicated stress mapping instrument at HFIR.

4.4.2.3 Accessory instrumentation

- Position-sensitive and Peltier Si(Li) X-ray detectors;
- Laser position sensor for X-ray polycrystalline-texture-stress (PTS) units;
- Grazing incidence optics;
- Strain gage capabilities;
- Tensile load frame for use on the neutron diffraction, residual stress mapping facility;
- Huber full-circle Eulerian cradle for use on the neutron diffraction, residual stress mapping facility; and
- High-temperature furnace.

4.4.3 New Capabilities

4.4.3.1 Grazing incidence X-ray diffraction

Following an earlier demonstration of the application of grazing incidence X-ray diffraction (GIXRD) methods for depth-profiling residual stresses over a very shallow, near-surface region of specimens, the user interest in this technique has exceeded the capacity at which we can make measurements on our laboratory systems. Numerous proposals and inquiries related to grinding-induced subsurface stresses and to stresses in thin coatings have been received. GIXRD employs low angles of X-ray incidence to control the depth of X-ray penetration. By approaching the angle of total external reflection, the depth of sampling can range from tens of angstroms to a few micrometers. With this technique, diffraction information about phase content, texture, and residual stress can be obtained as a function of sampling depth.

Of particular importance is the nondestructive measurement of strains induced by grinding and the range of depth profiling. RSUC continues to pursue projects to provide a scientific basis for aspects of this technique and to support further development of this technique and instrumentation. The particular limiting aspect is slow data collection, which limits the extent of user proposals we can address and further limits the number of specimens that can be studied. To address this shortfall, we have assessed several options to increase the flux and instrument time or to develop alternate instrument access. These include multilayer X-ray mirrors, focusing capillary optics, and synchrotron radiation. We demonstrated that a 30-fold enhancement could be achieved with use of a multilayer X-ray mirror. A capillary optics device did not look promising for this application. Tests using the ORNL X14A beam line at NSLS have been encouraging, and additional testing and optimization of the facilities there are under way.

4.4.3.2 Neutron residual stress facility

A cooperative joint effort—signed in April 1994 between DOE's Office of Energy Efficiency and Renewable Energy (EE), OTT, and ER/BES, Division of Material Sciences—established NRSF. As part of the HTML's RSUC, NRSF is a collaborative effort to meet expressed industrial and academic needs for through-thickness strain mapping. This joint program is a direct result of a multiyear Laboratory Director's Research and Development (LDRD) project proposed and led by HTML staff at HFIR. NRSF is operated by a team consisting of staff from HTML in the M&C Division, the Neutron Scattering Group of the SSD, and the I&C Division.

The goal of the joint program is to establish and operate user facilities for macroresidual and microresidual stress analysis in conjunction with the existing RSUC X-ray facilities in HTML and the neutron scattering facilities program at HFIR. We currently are meeting this goal by using a portion of the beam time on two SSD spectrometers (HB-2 and HB-4). Another goal is to develop a dedicated instrument at HFIR optimized for macroresidual stress analysis, and thus to greatly expand both the capabilities and speed of measurement.

HFIR operation in FY 1997 was significantly reduced compared to FY 1995 and FY 1996 because of operational problems. In FY 1997 there were just 99 measurement days available compared to an average of 143 days per year in the preceeding two fiscal years.

4.4.4 Major Activities

4.4.4.1 Complimentary projects

In the reporting period, the residual stress facilities have also been used on a number of DOE and Work for Others projects. The former include measurement of stresses in clad boiler tubes, weld overlays, and thermal barrier coatings. The Work for Others projects include studies for a commercial airline company, Weyerhauser, and the Navy. DOE projects have led to additional nonproprietary user projects, as well as proprietary projects from industrial users. The NRSF was used in several proprietary projects during the period, and the staff is currently working with candidate users in conducting research and developing additional proposals.

Advanced computer simulations for the design of neutron scattering instrumentation. Teaming up with Dr. J. L. Roberson of SSD, Dr. X.-L. Wang of RSUC has recently won a LDRD project on Monte Carlo simulation of neutron beam optics. The LDRD effort aims to develop sophisticated computational models for various neutron optical components commonly used in the construction of neutron scattering instruments. By linking these modules together, it will be possible to design and optimize instruments in a much more powerful way than is currently achievable. Computational models are also a necessary first step in the development of data analysis and visualization tools, and are fundamental to a coherent approach to data analysis that includes experimental considerations such as instrumental resolution and multiple scattering, which cannot be readily addressed in any other way. The successful completion of this project will strengthen ORNL's posture with regard to the Spallation Neutron Source (SNS) and the HFIR upgrade projects. HTML

will utilize the models to evaluate the design options for its instruments at the themal neutron guide hall of the upgraded HFIR and at the SNS.

4.4.4.2 Macroresidual stress mapping instrumentation

The demand for macroresidual stress mapping by neutron diffraction continues to exceed the time available. We can schedule approximately 40 experiment days every three months (2 of every 3 fuel cycles at HFIR). However, we encountered a demand typically 100% in excess of the available days. To meet this demand as soon as possible, we have given high priority to the development of an enhanced, dedicated stress-mapping facility. This effort has been stretched out by several factors:

- the decision by DOE to spread the capital funding over three years;
- design analysis that recommended a horizontal beam arrangement;
- SSD's need to continue to use HB-2, and in the future to split that beam to support four major research instruments (including the stress mapping);
- a proposal to build a thermal guide hall using HB-2 beam as the source; and
- a DOE decision to upgrade HB-2 but not to build the thermal guide hall at this time.

In the guide hall plans, the neutron-based residual stress program would have had two stations on a thermal guide. The thermal guide hall proposal had been rated as the number one proposal for the upgrade of DOE's neutron facilities by an independent committee, but the proposal faced tough budgetary concerns and ultimately was not funded.

HTML and SSD staff have been working within this picture of uncertainty to improve the existing instrumentation and simultaneously plan for the possibilities of the thermal guide hall or the fallback of a multi-instrumented HB-2. We have divided the new instrument development task into several components. The first component involves expanding the number of neutron detectors from one to seven to increase detection efficiency and produce data on the strain tensor without specimen rotation. The second involves developing new monochromators that deliver a significantly higher flux at the specimen. The third component is to specify and order two new goniometers for use at HFIR and, potentially, the thermal guide hall. The fourth component involved assessing the requirements for a multi-instrumented HB-2 based on new shielding and monochromators. The fifth is the DOE 2000 Pilot Project, Materials Microcharacterization Collaboratory, which aims to improve user access and collaboration via use of the internet and new computational tools. Progress on each of these is described in the following sections.

4.4.4.3 Seven-detector array for neutron residual stress mapping

One action we have taken to increase our measurement capacity is to expand the number of position sensitive detectors (PSDs) from one to seven. A vertically stacked array of seven PSDs was designed; the seven detectors, shielding, and electronics were installed; and software was developed. Testing demonstrates that the seven-detector array has increased our measurement capability by at least three; however, limitations of the HB-2 goniometer prevent full utilization of this detector array. An improved design for shielding and stable detector mounting will be developed when we have acquired the new goniometer system.

Each detector in the array has an active area of 4 × 10 cm and a linear resolution of 1 mm. They are spaced at 7° intervals on an arc having an 80-cm radius. Each detector can be rotated about the normal to the detector face to compensate for the apparent curvature of the Debye Scherrer cone at 2q angles away from 90°. A numerical model to correct the data for geometric errors and irregularities in the alignment of the detector array has been developed. Calibration data are collected on diffraction lines of a nickel powder standard. A least-squares fitting method is used to minimize the error between observed and calculated peak positions simultaneously in all seven detectors. The variables include sample-to-detector distance, spacing of the detectors along the array arc, tilt of the array from vertical, variation of the height of the array with 2q, 2q zero offset, and neutron

wavelength. With profile fitting of the diffraction peak plus background, reproducibility of the peak position measurement of better than 0.003° of 2q has been demonstrated. For typical data, the calibration procedure provides measured 2qs with an absolute accuracy of 0.02° for all detectors. The seven-detector system was further improved during early FY 1997 and then placed into productive use. Results to date all show increased accuracy in measurement along with a reduction in data collection time.

4.4.4.4 Neutron monochromator design for stress mapping

Neutron flux increases on the gage volume in a residual stress sample combined with reduced diffraction peak width can be achieved simultaneously with the use of a vertically focusing, horizontally curved perfect silicon monochromator, according to the calculations made for us by the University of Missouri (Columbia). Flux improvements as large as a factor of 7 have been predicted with the instrumental diffraction peak width reduced by 2. To achieve this increase will require an enlargement of the beam dimension at HB-2. Without the taller beam, a gain of a factor of 2 to 3 was expected. A doubly-bent silicon monochromator that is elastically bent in the scattering plane and mechanically focused out of the scattering plane was ordered in FY 1996 and was installed with its own monochromator plug at the HB-2 beam port in FY 1997. The monochromator was designed and built by the University of Missouri. The new monochromator achieved a gain in peak intensity of 60% and a measurable reduction in peak breadth.

4.4.4.5 New goniometer specifications

Specifications for new goniometers for use at HFIR for neutron residual stress were completed in FY 1996. The goal is to provide for larger specimens (~2 × larger than currently possible to study), achieve higher accuracy in the rotational axes via use of absolute encoders, permit ready exchange of detector systems, enable for the first time routine single-crystal strain and polycrystalline texture measurements, and support various accessories such as tensile frames and furnaces. One of the two systems will have a sample orienter (Kappa geometry) for studies of strain in single-crystal or highly oriented polycrystalline materials. This sample orienter will also permit texture-mapping experiments and the ability to characterize the variation of texture as a function of processing parameters throughout the volume of a specimen. The two instruments were ordered in FY 1997 with delivery anticipated by late FY 1998.

4.4.4.6 Dedicated NRSF installation

Since the thermal neutron guide hall construction proposal was not funded, the alternate plan is to increase the beam size, design a new shutter, and install thermal neutron guides at HB-2 to support various scattering instruments of SSD and NRSF. The modified beam delivery concept will provide a dedicated location at HFIR for the NRSF, utilizing a taller beam than is currently available.

Monte Carlo analysis indicates a potential of significant intensity gains via redesign of the beryllium reflector tube and shutter and use of thermal neutron guides. Considerable debate and changes continue to occur in the plans for which instruments will be accommodated at the upgraded HB-2. However, all designs to date provide for the large specimen residual stress mapping instrument.

4.4.4.7 DOE 2000, materials microcharacterization collaboratory

Late in FY 1997 the DOE office of Mathematics, Information, and Computer Science joined OTT-HTML in initiating a pilot project to develop, install, and test tools for conducting "Science at a Distance" with focus on materials microcharacterization. Besides several DOE electron microscopy facilities, two beam lines at major national facilities were included. These are the Neutron Residual Stress Mapping facility at HFIR and ORNL's X14A beam line at BNL, both operated by the RSUC. Initial efforts were to establish the foundation for enhanced remote instrument operation for video

images of the experimental area as well as video conferencing between scientists. Equipment and networking were ordered and will be installed and tested in FY 1998.

4.5 DIFFRACTION USER CENTER

4.5.1 Background

The DUC uses room- and high-temperature X-ray and neutron diffraction methods to characterize crystalline phase(s) and stability of advanced structural ceramics, alloys, catalysts, and other industrially relevant materials. The data, obtained individually as a function of temperature and environment and frequently in conjunction with data from thermal analysis or electron microscopy, are used to relate materials processing and performance with phase transformations, reactions (solid-solid, liquid-solid, and gas-solid), lattice expansion, atomic structure, crystallization from the melt, and phase stability.

In addition to supporting users' diffraction needs, the XRD facilities are extensively used by qualified staff in the M&C Division who are conducting a wide variety of ceramic and alloy R&D efforts. DUC also provides technical expertise in diffraction and materials science in support of a number of DOE-funded projects.

4.5.2 Staff and Major Instruments

4.5.2.1 Staff

DUC is a central part of the Diffraction and Thermophysical Properties Group. Members who had prime responsibilities for activities in this User Center during the reporting period include the following:

- Dr. E. A. (Andrew) Payzant—development staff member, RT & HTXRD, neutron diffraction, synchrotron;
- Mr. O. B. (Burl) Cavin—subcontractor, RT & HTXRD;
- Dr. R (Robbie) Peascoe—(UT subcontractor), RTXRD and zeolites;
- Dr. C. J. (Claudia) Rawn—(ORISE postdoc), RT and HTXRD;
- Dr. T. R. (Tom) Watkins—research staff member, RT & HTXRD;
- Ms. J. L. (Joy) Kilroy—group administrative support; and
- Dr. C. R. (Cam) Hubbard—group leader.

Mr. Cavin, who had been with DUC since the beginning of the HTML, retired in September 1993. Fortunately, he has continued to participate in the operation of the X-ray facilities by supporting users and assisting ORNL staff members. Dr. Misture (ORISE postdoc) left ORNL to take a faculty position at Alfred University. Dr. Payzant, formerly an ORISE postdoc in RSUC, became a staff member with prime responsibility for the DUC. Dr. Rawn joined the group as a postdoc. Her expertise is in use of XRD for phase equilibria and solid-state chemistry. Drs. Hubbard and Watkins, whose primary focus is the RSUC, helped fill the transition in User Center staff.

4.5.2.2 Major instruments

- Scintag θ-2θ PAD V goniometer with Peltier cooled Si(Li) detector;
- Scintag θ-θ PAD X goniometer with Buehler high-temperature furnace system and a position-sensitive, liquid-nitrogen-cooled Ge detector;
- High-resolution neutron powder diffractometer (HB-4) at HFIR with furnace and cryostats; and
- X14A beam line at the NSLS with Buehler high-temperature furnace system.

The neutron powder diffractometer facilities are part of the NSRF at HFIR sponsored by ER. HTML user projects that also require neutron powder diffraction are accommodated under a collaborative arrangement.

DUC became a member of the PRT for the X14A beam line at NSLS. This beam line was constructed with funding from the ER, ORNL, and industrial members of the PRT. As part of the PRT, we are developing high-temperature diffraction and stress analysis as well as adding extended X-ray absorption fine structure (EXAFS) capabilities at X14A for research use by HTML users. The extremely high flux, several orders of magnitude greater than our laboratory-based systems, will enable users to study smaller specimens, to study rapid reactions and kinetics, and to resolve subtle phase transformations that cannot be determined with the laboratory-based systems.

4.5.3 New Capabilities

4.5.3.1 Rietveld full-pattern refinement method

The Rietveld full-pattern-fitting structural refinement method has become a frequently requested data analysis method. The Rietveld method has developed as a powerful new method for extracting detailed structural information from powder diffraction data that could previously only be extracted from single crystal data. This enables polycrystalline powders with known compositions to be analyzed and the structural changes and defects to be correlated to physical (electrical, thermal, etc.) properties. The Rietveld method refines lattice parameters, profile shapes, atomic coordinates, thermal motion parameters, site occupancies, and instrumental aberrations. For a multiphase sample the user can obtain accurate information on the volume fraction of each phase in a mixture. The User Center now has several codes operational for Rietveld refinement [General Structure Analysis System (GSAS), Rietan, RIQAS, FullProf]. Each code has different advantages and limitations, thus requiring mastery of several by DUC staff. The GSAS software package can accommodate multiple data sets combining laboratory X ray, synchrotron X ray, and neutron diffraction data, all available through the diffraction user center. Synchrotron X-ray powder diffraction data can be collected where the wavelength has been tuned near and away from the absorption edges of different cations, having a similar number of electrons, allowing identification of cations that are hard to distinguish using conventional laboratory X rays. Using GSAS to combine data sets collected at different wavelengths provides valuable information for understanding the defect chemistry from the site occupancies of similar cations. GSAS also allows the combination of X-ray and neutron diffraction data allowing the combination of neutron data (highly penetrating, the ability to "see" lighter atoms like H, C, and O, and the ability to disclose both the magnitude and direction of magnetic moments) with laboratory and/or synchrotron X-ray powder diffraction data. Using full-pattern-fitting HTXRD users are able to accurately determine lattice parameters without use of an internal standard, thus avoiding possible chemical interactions between the standard and the sample. Users can subsequently calculate bond distances and angles from the atomic coordinates.

4.5.3.2 Neutron powder diffraction

High-resolution neutron powder diffraction capabilities managed by the Neutron Scattering Group, SSD, are now available to HTML users. This became possible by developing a cooperative understanding and referral process. When an HTML project would benefit by including neutron powder diffraction, users can include this request in the HTML proposal; members of the DUC team then will obtain the necessary additional review by the SSD's neutron powder diffraction staff. When the HTML staff receives a request for extensive neutron powder diffraction research, they forward this request to the Neutron Scattering Group for consideration under the BES's Neutron Scattering Facilities Program. HTML and the Neutron Scattering Group have jointly acquired a high-temperature vacuum furnace (1600°C) for neutron powder diffraction measurements and made it operational. We have jointly tested and demonstrated this furnace facility and successfully made it available to HTML and Neutron Scattering Group users at HFIR.

4.5.3.3 High-temperature XRD furnace for X14A

A Buehler high-temperature furnace and power supply essentially identical to the system used at HTML was donated to HTML for use at NSLS. Methods to attach the furnace and a temperature controller for the furnace have been developed and tested during one experimental cycle at NSLS. This preliminary experimental cycle was used productively with several DUC and RSUC users to study a phase transformation oxide growth and distortions from a cubic lattice that could not be detected on conventional instruments. Detailed plans for further modification were developed from this preliminary effort and are being implemented.

4.5.3.4 Zeolites for highly selective chemical sensors

A Seed Money project to develop methods for using zeolites as chemically selective coatings for chemical sensors was started in collaboration with the Life Sciences Division. Recent work at ORNL has proved the ability of microcantilevers to detect chemical vapors. By coating commercially available microcantilevers with a sensitizing overlayer, it is possible to measure chemical exposures. In a recent experiment, gold-coated microcantilevers were used to detect mercury vapors. The change in mass due to absorption shifted the resonant frequency, allowing the detection of mercury vapor with picogram sensitivity. Using zeolites as chemical absorbers, we intend to expand the range of chemicals that can be detected using microcantilevers and assist in developing sensors to monitor emissions from engines, land mines, ammunition stores, explosives, and contraband.

4.5.3.5 Advanced data collection and analyses

The XRD instruments in DUC and RSUC were converted to networked Pentium PCs running Scintag's Diffraction Management Software for Windows NT® (DMSNT) software. DUC also employs a variety of state-of-the-art powder diffraction software packages. By the end of FY 1996 the RTXRD and HTXRD systems are operating under Windows-NT control. The transition enhances HTML's data collection and analysis capabilities, keeping them state-of-the-art.

4.6 MACHINING AND INSPECTION RESEARCH USER CENTER

The MIRUC provides basic facilities for investigation of grinding processes for high-performance ceramic materials, design and fabrication of mechanical property test specimens, dimensional characterization of test specimens and other components, and tribology.

4.6.1 Staff and Major Instruments

4.6.1.1 Staff

B. (Sam) McSpadden, leader of the Machining and Inspection Research Group, has overall responsibility for MIRUC. His technical specialty is dimensional metrology. Other group members and the equipment and technologies for which they have primary responsibility are as follows:

- Dr. Peter Blau—a nationally recognized expert in the field of tribology (friction, wear, and lubrication). Dr. Blau is responsible for all tribological research performed in MIRUC. Numerous custom-designed friction and wear-testing instruments, scratch testers, and repetitive-impact testers are now available for use by guest researchers;
- Mr. Tyler Jenkins—responsible for operation of the Harig surface grinders; coolant management; health, safety, and environmental issues;
- Mr. Tom Morris—a technical specialist in grinding and ceramics machining, principal investigator on CRADAs involving cost-effective machining of ceramics;

- Mr. Lawrence O'Rourke—responsible for operation of the Weldon cylindrical grinder, Nicco creep-feed cylindrical grinder, grinding wheel management, and procurement;
- Mr. Randy Parten—responsible for dimensional metrology, with emphasis on programming and operation of the coordinate measuring machine (CMM), Mahr form tester, Taylor-Hobson Talysurf surface profile measuring instrument, and the Rodenstock noncontact laser surface topography measuring instrument;
- Mr. Earl Shelton—responsible for operation and computer numerically controlled (CNC) programming of the Cincinnati Milacron centerless grinder and the Sabre vertical grinding center;
- Ms. Jessie Whittenbarger—group administrative support.

4.6.1.2 Major instruments

Five types of numerically controlled grinders are available to guest researchers for their projects at MIRUC. The grinders were selected for their similarity to those used in manufacturing facilities throughout the United States. Grinders are instrumented to permit real-time measurement of key grinding process parameters including grinding forces, spindle horsepower, spindle vibration, acoustic emission, and coolant temperature. Data may be collected, displayed, stored, and analyzed using specialized Labview programs and other analysis software. Major machining equipment includes:

- Weldon Cylindrical Grinder
- Bridgeport/Harig Surface Slicer/Grinder
- Nicco Creep-Feed Surface Grinder
- Cincinnati Milacron Twingrip Centerless Grinder with high-speed spindle
- Cincinnati Milacron Sabre Multiaxis Grinder with high-speed spindle
- Ded-Tru centerless grinding attachment for use with surface grinders to grind small components
- SmartCAM Production Turning Package
- SmartCAM Production Milling Package
- Autodesk Mechanical Desktop with AutoCAD R13
- DADiSP (data analysis and display software)
- Statistica (statistical analysis software)

The center maintains state-of-the-art dimensional and surface texture measuring equipment for use by guest researchers. Our technical staff is available to assist researchers in the operation of the more complex equipment, such as the CMM. Our equipment is computer controlled, and inspection data can be easily exported to advanced analysis software and CAD/CAM software using a laboratory-wide network. Major inspection equipment includes:

- Electronic Measuring Devices (EMD) Legend Integrated Metrology Center, a precision CMM with both contact and noncontact scanning capability
- Mahr/Perthen Formtester
- Talysurf Model 120 Stylus Surface Texture Measurement System
- EOIS Mini-moiré Sensor
- Nikon Optical Comparator
- Rodenstock RM600 Laser Surface Texture Measurement System

Physical testing and material analysis constitute a major portion of the work in the tribology laboratory. Experiments are designed to screen materials, effect simulations of components, or study the basic relationships between the microstructures and compositions of surfaces and their friction and wear behavior. Available machines fall into three categories: (1) commercially developed testing machines, (2) machines designed under subcontract, and (3) machines designed and built by ORNL for special purposes. Most of the testing machines are aimed at sliding wear, but abrasive wear, impact wear, and rolling-contact wear tests are also available. Tribology testing at high temperatures and controlled atmospheres is also within the capabilities of the user center. Major tribology equipment includes:

- Reciprocating Friction and Wear Tester
- Repetitive Impact Testing System
- Friction Microprobe
- Cameron-Plint TE-77 Reciprocating Sliding Wear Tester
- Instrumented Scratch Tester
- High-Temperature Pin-on-Disk System
- Multimode Friction and Wear Tester
- Micro-Abrasive Wear Tester
- Sather Lubricant Load-Carrying Capacity Screening Rig
- Teledyne-Taber Portable Scratch Tester
- Wilson Microindentation Hardness Tester
- Talysurf 10 Surface Roughness Measuring System

4.6.2 New Capabilities

4.6.2.1 Cincinnati Milacron Twingrip centerless grinder

Extensive modifications to the Cincinnati Milacron Twingrip centerless grinder have made it possible to increase safely grinding wheel speeds to 100 m/s (~20,000 surface feet per minute). A variable speed motor/controller with appropriate safety features was added, and changes were made to the hydrostatic spindle bearing lubrication system. Temperature sensors were installed on the hydrostatic spindle-bearing housings to ensure that bearing temperature remains well below 140°F during operation.

4.6.2.2 AutoDesk Mechanical Desktop

The Machining and Inspection Research Group has obtained Autodesk Mechanical Desktop software as a general purpose tool to prepare and display CAD drawings, provide 3-D visualization tools, generate machining tool paths, and evaluate inspection results. This particular software was chosen because of its moderate price, ease of use and maintenance, easy integration with other software packages, and wide acceptance throughout industry. The software includes self-paced instruction modules and is available for use by group members and HTML guest researchers.

4.6.2.3 Improved grindability test machine

A prototype grindability tester, which uses a diamond abrasive belt to measure the relative grindability of ceramic specimens, was developed by Chand-Kare Technical Ceramics and installed at HTML. The prototype equipment has been replaced by a second-generation grindability tester that incorporates improvements in construction resulting from our experience with the prototype unit. The new equipment has been installed and is available to HTML users wishing to perform grindability studies.

4.6.3 Major Activities in FY 1997

4.6.3.1 High-speed centerless grinding

Studies at ORNL and elsewhere strongly suggested that for silicon nitride workpieces, wheel wear, material removal rates, and mechanical properties are all improved by grinding at higher-than-conventional wheel speeds. The maximum safe operating speed for conventional grinding wheels is limited by the construction material used for the wheel core, which is typically a vitrified material with a large mass. Should such a wheel fail catastrophically, it would be very difficult to contain the wheel fragments within the machine enclosure because of the high energy levels involved. A composite-core, 180-grit, vitrified-bond, 100-concentration, diamond-abrasive grinding wheel was

installed on the grinder. The new wheel has a much lower mass and higher strength than a conventional wheel because of the use of composite materials for the wheel core. Small, low-mass, abrasive coupons are cemented to the periphery of the wheel core.

Initial centerless grinding tests demonstrated that drastic reductions in per-piece grinding cycle time can be achieved. An AlliedSignal GS-44 silicon nitride tensile specimen, which previously required a 35-min cycle time to grind on a centerless grinder at conventional wheel speeds, was ground to the required finished geometry in under 1 min. The new wheel was operated at a surface speed of 97 m/s (19,000 surface feet per minute). The test specimens used were premachined to a "near net shape" condition, in which the specimen blanks were 3 mm (0.130 in.) oversized on the diameter. Once the high speed centerless grinding process has been thoroughly investigated and optimized for tensile specimens, the technology can be applied to grinding silicon nitride diesel engine valves.

4.6.3.2 Cylindrical grinding used to produce fuel systems specimens

The Weldon cylindrical grinder was used in a plunge grinding mode to produce mock-up fuel system components. The objectives of the experiment were to develop and demonstrate a grinding process for the specimens using a variable-composition grinding wheel and to determine the grinding ratio in order to estimate grinding costs in a production environment. The specimens started as cylindrical rods approximately 50 mm long by 8 mm in diameter, with one end being composed of type M2 tool steel and the other of zirconia. Approximately 1 mm of radial stock was removed from the rods in a plunge grinding operation.

Because diamond abrasive does not perform well on steel work pieces, a CBN abrasive wheel was used. Although CBN is softer than diamond, the abrasive performs extremely well on steel and is still capable of grinding ceramic materials. CBN wheels are generally more expensive than comparable-sized diamond wheels. The grinding wheel was custom-engineered for this specific work piece, so that the surface used to grind the steel would have a different concentration and bond filler material from that used to grind the ceramic. Initially, the test specimens tended to fail during the grinding process by breaking at the steel-zirconia interface zone. However, this problem was overcome by providing additional support of the work piece during the grinding process.

4.6.3.3 CRADA signed with Cummins Engine Company

A CRADA, entitled *Precision Grinding of Components for Diesel Fuel Systems Applications*, was signed with Cummins Engine Company, and work is in progress. Mr. Tom Morris is the principal investigator for the Machining and Inspection Research Group, and Dr. Albert Shih is the principal investigator for Cummins. High-speed grinding tests are being performed on the instrumented Weldon cylindrical grinder using a CBN wheel manufactured by Cincinnati Milacron.

4.6.3.4 User from Cummins Engine Company performs cylindrical grinding studies

Dr. Albert Shih conducted grinding research on a user proposal entitled *High Speed Cylindrical Grinding of a Silicon Nitride Fuel System Component Using a Cubic Boron Nitride (CBN) Wheel.* Using the instrumented Weldon cylindrical grinder, he conducted a series of tests under various operating conditions to evaluate the performance of a state-of-the-art, composite-core, variable concentration, CBN grinding wheel on silicon nitride specimens.

Of particular interest was the effect of the truing/dressing operation on part quality. Various wheel-dressing methods were evaluated and compared, and subsequent grinding tests were conducted to simulate the production of ceramic fuel system components for diesel engines using high-speed grinding. Surface texture and roundness, two good indicators of part quality, were measured on specimens that were ground under various conditions. Sixteen baseline grinding tests were conducted to determine the effects of wheel truing and surface speed on the grinding process.

4.6.3.5 User from Caterpillar performs instrumented creep-feed grinding studies under HTML user program

Dr. Michael Haselkorn, of Caterpillar's Advanced Materials Technology group, performed extensive grinding tests on the instrumented Nicco Creep-Feed surface grinder. Dr. Haselkorn's research proposal, entitled *Cost Effective Machining of Silicon Nitride Diesel Engine Components*, involved aggressive creep-feed grinding of over 100 billets (50 mm × 50 mm) under various conditions. The objective of the research was to determine the effect of diamond type (friable/nonfriable), bond type (resin/vitreous), diamond grit size (100/150), concentration (75/125) and material removal rate (high/low) on the machinability and the quality of ceramic specimens. Caterpillar obtained eight new diamond grinding wheels of various types from wheel manufacturer Diacraft for use in the tests. Two materials, AlliedSignal GS-44 sintered silicon nitride and Ceradyne 147-3 Ceraloy sintered reaction bonded silicon nitride were used in the studies. Machinability was determined qualitatively by measuring grinding forces and spindle power under the various grinding conditions. Quality metrics included surface texture measurements, optical and SEM microscopy evaluations, and flexure strength measurements.

4.6.3.6 Users from Louisiana State University investigate wear mechanisms and associated responses of a fine-abrasive, resinoid-bond, diamond wheel used in creep feed grinding

Dr. Warren Liao and graduate student Kun Li visited the HTML to continue their studies of wheel-wear mechanisms in the creep-feed grinding process. The Nicco instrumented creep-feed grinder was used to perform the grinding and various inspection instruments, including the Legend coordinate measuring machine, the Rank-Taylor-Hobson surface analyzer, and the Nikon optical comparator, were used to characterize surface texture and wheel wear. Specific issues addressed in the current user proposal were abrasive wear mechanisms in the transition and steady-state stages, effects of different grinding widths on surface texture and strength of the ground specimen, and relationships between instrument sensor responses and wheel wear.

4.6.3.7 Users from Kyocera perform comparative surface texture measurements

MIRUC staff members worked with users from Kyocera to perform surface texture measurements on groups of modulus of rapture (MOR) bars. Comparative measurements were made parallel and perpendicular to the grinding direction using both the Rodenstock laser and the Rank-Taylor-Hobson stylus surface analyzers.

4.6.3.8 User agreement signed with 3M Corporation

A nonproprietary user agreement was signed with the 3M Corporation. A research proposal entitled *Quantification of the Effects of Machining Variables, Wafer Fixturing Methods, and Residual Stress on the Properties (Flatness and Parallelism) of 3M AlTiC Wafers Face Ground on a Cincinnati Milacron Sabre Machining Center* was submitted by Michael J. Besser, of the 3M Advanced Ceramics Program. The work was designed to evaluate the benefits of high-speed grinding of 3M's 310 AlTiC 4_ square wafers. This work represents the first use of Cincinnati Milacron owned equipment in the HTML User Program.

5. HTML FELLOWSHIP PROGRAM

The HTML Fellowship Program was created in FY 1992 to

- provide a mechanism for training of industrial and university researchers in state-of-the-art advanced characterization techniques,
- encourage research in areas of interest to DOE,
- improve the quality and output of DOE programs, and
- help make U.S. industry more competitive in a world market.

Four categories of fellowships currently exist: industrial, faculty, graduate, and postdoctoral. This program is administered for HTML by ORISE. Research must relate to the following DOE Transportation Technology Program areas of interest:

- processing of advanced materials;
- machining of hard materials;
- structure of materials;
- physical and thermophysical properties of materials;
- mechanical properties of materials;
- corrosion of materials;
- gas-phase reactions with solids;
- tribology of solid surfaces;
- characterization of materials for energy-related applications; and
- high-temperature structural materials (ceramics, composites, intermetallics, and metals).

5.1 INDUSTRIAL FELLOWSHIPS

5.1.1 Background

To apply for a fellowship, industrial researchers must submit an application to the HTML Fellowship Program coordinator. While projects under the User Program are typically short-term and limited to two weeks of hands-on work at the HTML, the Fellowship Program provides an opportunity for longer-term research (which can be performed at intermittent intervals) and often covers more basic research studies. One advantage of a fellowship appointment is that travel, lodging, research expenses, and salaries (graduate and faculty fellowships) are covered by the HTML Fellowship Program. Another mechanism that exists for industrial fellowships is the reverse fellowship. Using this mechanism, an HTML researcher can travel to a company or university to perform on-site research.

Fellowship applications are reviewed by the HTML director along with an external committee that represents university, industrial, and private sectors. The current committee members are Gary Fischman (Food and Drug Administration), Bob Powell (General Motors), Andy Sherman (Ford Motor Co.), Bob Bitting (Alfred University), Joe Panzarino (JNP, formerly of Norton), and Gene Haertling (Clemson University). As with the User Program, a standard nonproprietary user agreement must be in place before work can be performed at HTML. Once a fellowship appointment has been made, HTML staff work with the respective fellow to schedule instrument time.

As of the end of FY 1997, a total of 36 HTML fellows have been appointed (15 industrial, 14 graduate, and 7 faculty).

5.1.2 Industrial Fellowships for FY 1997

James Fash, Ford Scientific Research Laboratory, "Thermal Elastic Instability in Automotive Brake Systems" [FEL96-046(31)-16I]

TPUC

Techniques for the observation of thermal hot spotting during operation of automotive disk brake systems are being developed in this program. During braking, uniform temperature and consequently pressure distributions are desired for smooth brake operation. Occasionally, nonuniform distributions, or hot spots, will form. Local thermal expansion at the hot spots results in variations in the thickness and surface properties that in turn leads to nonuniform friction forces.

Over the past year, the expertise in TPUC has been applied to observation of operating brake systems. The TPUC infrared camera has been integrated into an operating brake dynamometer to allow time resolved infrared images to be collected. During the review period, two specific studies were performed. In each, materials and test parameters were varied to assess the influence of various design variables on hot spotting. This has led to design guidelines that should reduce potential for hot spot behavior.

During the later part of this review period, extension of the full field IR techniques to local single point measurements was prototyped and evaluated. A fiber optic cable was located such that thermal energy from the brake entering from one end of the cable would transmit the energy to a single point IR detector. This system was then interfaced directly to Ford's brake dynamometer conventional data acquisition processes. The proof of concept for this measurement technique was successful and provided good measurement of local temperatures, although uncalibrated in this exercise. Further work will be pursued in the coming year to carry this concept forward. When completed, this will greatly improve the capability to observe thermal behavior in brake systems.

C. Guo, Chand Kare Technical Ceramics, "Determination of Dominant Factors Controlling Ceramic Grindability" [FEL96-44(29)-14I]

MIRUC

Recent ceramic grindability measurements have shown that ceramic materials have very different grinding characteristics. The objectives of this research include: studying correlations between ceramic grindabilities and their material properties such as hardness, fracture toughness, and thermal diffussivity; identifying dominant factors of ceramic grindability; and evaluating diamond wheels for grinding ceramics.

In order to study the correlation between ceramic property and grindability, reliable property data are needed. Elastic modulus, hardness, fracture toughness, density, and thermal diffussivity of more than 70 ceramics have been measured at HTML. Correlation, if any, between the grindability and material property is being investigated.

Diamond wheel variation is an important contributing factor to process variation in ceramic grinding. Four diamond wheels of same specifications from different wheel manufacturers were evaluated when grinding SiC MOR bars. Power consumption, grinding force, grinding ratio (G-ratio), surface finish, and flexural strength are the parameters investigated. Results clearly showed that diamond wheels of the same specification performed significantly different. These results imply that the current wheel specification does not provide enough information to qualify a diamond wheel for technical ceramic machining.

Cynthia Hsieh, Caterpillar, Inc., "Particle Characterization of Modified S5 Tool Steels & Boron and/or Vanadium Treated Steels" [FEL96-45(30)-15I]

MAUC

In order to develop new high-strength steels that will provide improved wear resistance while withstanding brittle fracture, this work is part of the efforts at Caterpillar to understand the mechanisms that can bring about those improved properties. A more-defined goal of this proposal is to establish better understanding of the relationship between mechanical properties and the distribution of various particles in alloy and boron-treated steels. Specifically, the approximate compositions and sizes of the particles need to be obtained. The experiments to be conducted are mainly on the TEM (Philip's CM12, CM200 and CM30 AEM's). In the first year (1996-97) of this work, carbon extraction replicas and thin foils were examined for ten alloys of 4 different alloy grades. Results are summarized in Table 5.1.

Table 5.1. Hardness and size data of alloy and boron-treated steels

Alloys	R'C'	TiN ppt (average nm)	TiCN or other fine ppt (average nm)
S5 MOD 0.27 C	50.000	120-270 (210)	10-39 (20)
S5 MOD 0.37C	54.000	444-460 (452)	33-90 (59)
S5 MOD 0.55C	59.000	Not observed	16-106 (53)
40B30 MOD	50.000	Not observed	22-142 (45)
40B35 MOD	51.000	279-600 (440)	7-100 (28)
40B40 MOD	53.000	528-569 (549)	14-173 (70)
40BV30 MOD	50.000	Not observed	6-129 (31)
40BV35 MOD	51.000	Not observed	4-98 (25)
S5 MOD fast cool	45-48	160-400 (258)	5-50 (11)
S5 MOD slow cool	41-43	80-320 (176)	4-40 (10)

We have only scratched the surface of what needs to be done to understand the operative mechanisms. Without that understanding, it is not possible to scale up experimental alloys to production or to apply the mechanism to other materials.

Nanu Menon, AlliedSignal Engines, "Tensile Cyclic Fatigue and Compression Creep Behavior of NT154 Si_3N_4" [FEL95-27(19)-5I]

MCAUC

Status:

1. Cyclic fatigue:

Ceramic turbine blades are often subjected to cyclic loading in their applications. Crack growth under cyclic loading has been observed to be faster than that under-static loading at intermediate temperatures.[5.1] The objective of this part of the research is to understand the cyclic fatigue phenomenon in silicon nitrides.

Fifteen AS800 specimens have been tested at the following conditions: temperature = 1300°F, stress ratio (R_s) = 0.1, max. stress = 500 MPa – 600 MPa, and frequency (ν) = 50 Hz. The results are shown in Table 5.2.

Table 5.2. Results of axial cyclic fatigue testing

Specimen ID	Max/Min stress	Cycles to failure	Fractography	Remarks
35835	500/50	10,000,000	Further tested	
35835	550/55	10,000,000	Further tested	
35844	550/55	10,000,000	Further tested	
35836	550/55	20,084,630	Pore, surface	Ran out at 20E6, taken out of machine and retested
35827	550/55		Pore, internal	Broke at ≈513 MPa during loading of 1st cycle
35819	550/55	34,928	Pore, surface	
35820	550/55	3,279,547	Pore, internal	
35811	550/55		Pore, internal	Broke at ≈514 MPa during loading of 1st cycle
35812	550/55		Pore, surface	Broke at ≈451 MPa during loading of 1st cycle
35860	570/57	689,570	Pore, internal	
35828	570/57	48,237	Pore, internal	
35804	570/57		Pore, internal	Broke at ≈454 MPa during loading of 1st cycle
35852	570/57	4,998	Pore, surface	Broke while tuning: max stress ≈561 MPa
35859	570/57		Pore, surface	Broke at ≈447 MPa during loading of 1st cycle
35851	570/57	17,193	Pore, surface	Broke while tuning: max stress ≈549 MPa
35835	600/60	7,208	Pore, internal	Tested at 500 and 550 MPa prior
35867	600/60		Pore, internal	Broke at ≈576 MPa during loading of 1st cycle
35844	600/60	2,332	Pore, internal	Tested prior at 550 MPa; broke while tuning at 583 MPa

The information includes results from the SEM fractography. All specimens failed from pores/white spots.

2. Compressive creep:

Compressive creep rates in Si_3N_4 are considerably lower than tensile creep rates.[5.2] Hence, compressive creep models are needed for accurate estimation of stress redistributions in Si_3N_4 components subjected to elevated temperatures. In addition, if compressive creep models are available, flexure creep can be modeled using finite element methods. Since flexure creep tests involve much lower cost than the tensile creep tests, a considerable cost saving could be realized in production lot testing if flexure specimens are employed in place of the current tensile specimens as a bench mark for assurance of the right sintering conditions in product lot testing.

Test matrix for compressive testing is given Table 5.3. The key results are shown in Table 5.4.

A model for secondary creep has already been established. The viscoelastic part of the compressive strains are now being analyzed.

Table 5.3. NT154 specimen test matrix for compressive creep

Temperature, °C	Stresses, MPa (one specimen at each stress)
1316	125, 200, 300, 400, 500
1343	300, 400, 500
1371	30, 100, 200, 300, 400, 500
1399	25, 50, 100, 200, 300

Table 5.4. Minimum creep rates in compression measured at the end of approximately 150 h, or after approximately 100 h of steady-state creep

Temperature (°C)/(°F)	Applied compressive stress (MPa)/(ksi)	Minimum creep rate ($\times 10^{-10}$ s^{-1})
1316/2400	300/43.5	2.7
1316/2400	400/58.0	9.3
1316/2400	500/72.5	10.0
1343/2450	300/43.5	9.3
1343/2450	400/58.0	12.0
1343/2450	500/72.5	16.0
1371/2500	100/14.5	5.3
1371/2500	200/29.0	12.0
1371/2500	300/43.5	11.0
1371/2500	400/58.0	18.0
1371/2500	500/72.5	13.0
1399/2550	50/7.3	8.4
1399/2550	100/14.5	10.0
1399/2550	200/29.0	16.0
1399/2550	300/43.5	21.0

[5.1]C. J. Gilbert, R. H. Dauskardt, and R. O. Ritchie, "Behavior of Cyclic Fatigue Cracks in Monolithic Silicon Nitride," *J. Am. Ceram. Soc.* **78**[9], 2291–2300 (1995).

[5.2]M. K. Ferber, M. G. Jenkins, and V. J. Tennery, "Comparison of Tension, Compression and Flexure Creep for Alumina and Silicon Nitride Ceramics," *Ceram. Eng. Sci. Proc.* **11** [7-8], 1028–1045 (1990).

Krishnan Narasimhan, Valenite, Inc., "Study of Physical and Metallurgical Properties of CVD Hard Coatings on Cutting Tools and Modeling of Response of Multilayered Coated Tools in Machining" [FEL96-39(23)-101]

MCAUC/MAUC

Chemical vapor deposition (CVD) coatings (monolayers and multilayers) for cutting tools are being developed at Valenite for various machining applications for a wide spectrum of materials. Cutting tools encounter severe adverse conditions during machining, being subjected to high stresses, deformation, thermal, and mechanical stress cycling, and chemical reactions. Temperatures as high as 1000°C can be encountered at the cutting tool edge. Thus, CVD coatings on cutting tools demand significant mechanical and thermal integrity. Our goal is to measure the mechanical and thermal properties of various monolayer and multilayer CVD coatings, in addition to evaluating the lattice relationships and structures of thin multilayer CVD coatings, using TEM. Coating property measurements can then aid in the judicious choice of coating designs for specific work-piece machining applications to complement our own in-house testing program for various coated cutting tools.

Hardness and elastic modulus properties of multilayered coatings were compared with conventional coatings using the nanoindenter. Figure 5.1 illustrates that high carbon multilayered TiCN-TiN coatings exhibit higher hardness compared to conventional CVD coatings. Pin-on disk abrasion tests carried out using the tribometer and diamond (pin) indenter under dry, sliding wear conditions, showed that multilayered coatings offer increased abrasive wear resistance (Fig. 5.2). We have recently started evaluating fracture toughness (K_{Ic}) properties of various coatings using nanoindentation (cube corner indenter). Optimum loads need to be determined to establish the threshold for cracking.

In-house machining tests conducted at Valenite showed that multilayer coatings offer significant improvements over conventional coatings in milling steels where flank/nose wear and chipping are the dominant failure modes. These findings seem to correlate well with the hardness, elastic modulus and abrasion properties measured at HTML.

FIB techniques (focused ion beam milling) are being used to generate TEM samples for analyzing the structure and lattice relationships of multilayered coatings.

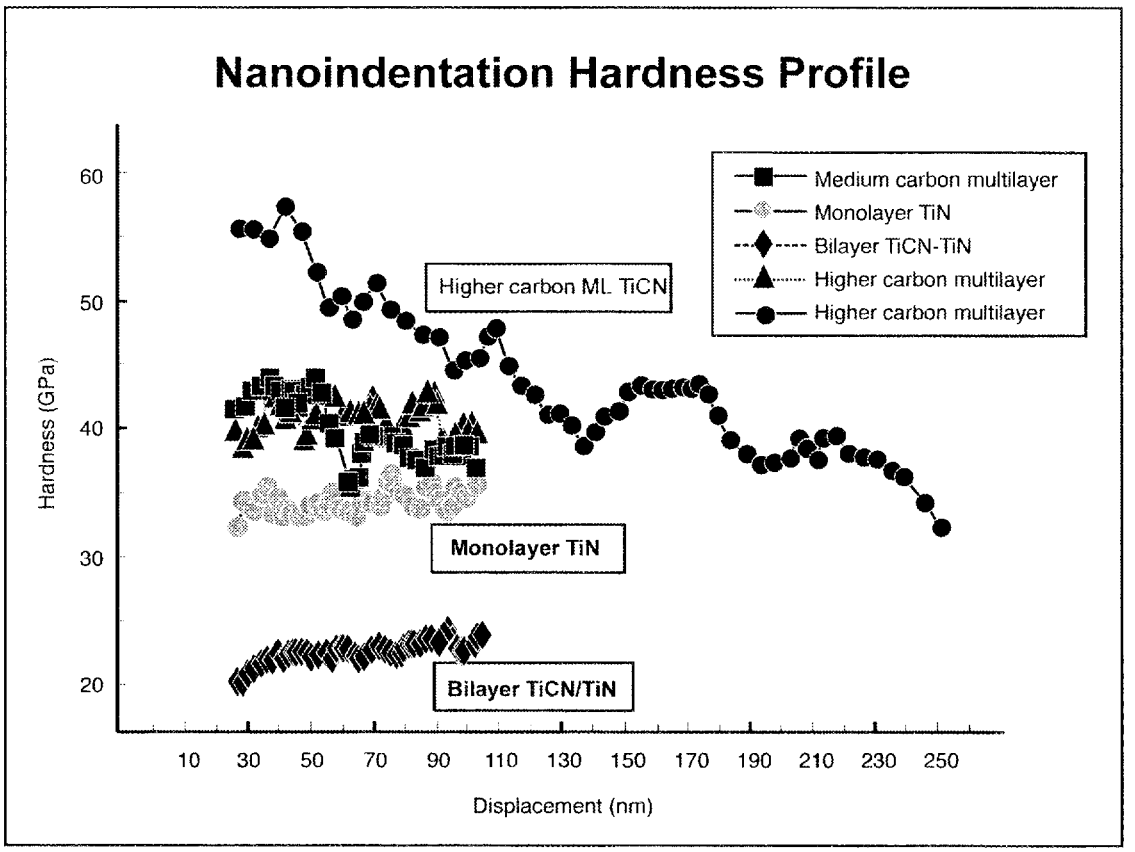

Fig. 5.1. Nanoindentation hardness profile.

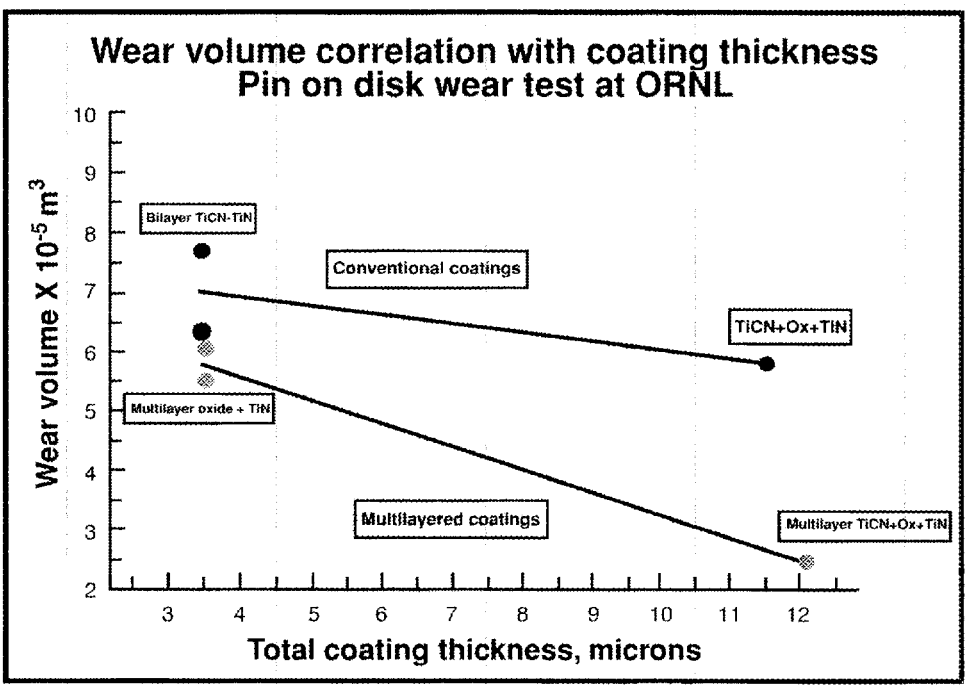

Fig. 5.2. Wear volume correlation with coating thickness. (Pin on disk wear test at ORNL.)

Chaitanya Narula, Ford Motor Company, "Sol-Gel Precursors and the Oxygen Storage Capacity of PrO_2-ZrO_2 Materials" [FEL95-33(20)-7I]

MAUC

The gels derived from a mixture of $Pr(O^iC_3H_7)_3$ and $Zr(O^iC_3H_7)_4$. $^iC_3H_7OH$ upon hydrolysis and sintering furnish PrO_2-ZrO_2 materials crystallized in fluorite phase. The PrO_2-ZrO_2 materials can be deposited on alumina particles as coatings or on alumina coupons as thin films from a solution of parent alkoxides modified with 2,4-pentanedione in THF. The X-ray powder diffraction of coated alumina particles shows only alumina diffraction peaks due to the low loading of the PrO_2-ZrO_2 phase. Thermal evolution of the PrO_2-ZrO_2 phase in films can be followed in the X-ray diffraction of films deposited on alumina coupons. The fluorite phase in films evolves at 750°C and remains stable up to 1200°C.

The precursor plays an important role in the phase evolution of the PrO_2-ZrO_2 materials. PrO_2-ZrO_2 prepared from a new single source heterometallic alkoxide, $Pr_2Zr_6(\mu_4\text{-}O)_2(\mu\text{-}OAc)_6(\mu\text{-}O^iPr)_{10}(O^iPr)_{10}$ does not show evidence for the fluorite phase.

In order to determine microstructure of the materials, we investiagted the samples by TEM. An important conclusion of this study is that the PrO_2-ZrO_2 is dispersed on the alumina particles as a thin coating. This prevents the reaction of PrO_2 with alumina to form praseodymium aluminates that contains Pr^{3+} stabilized and cannot undergo Pr_2O_3-PrO_2 interconversion.

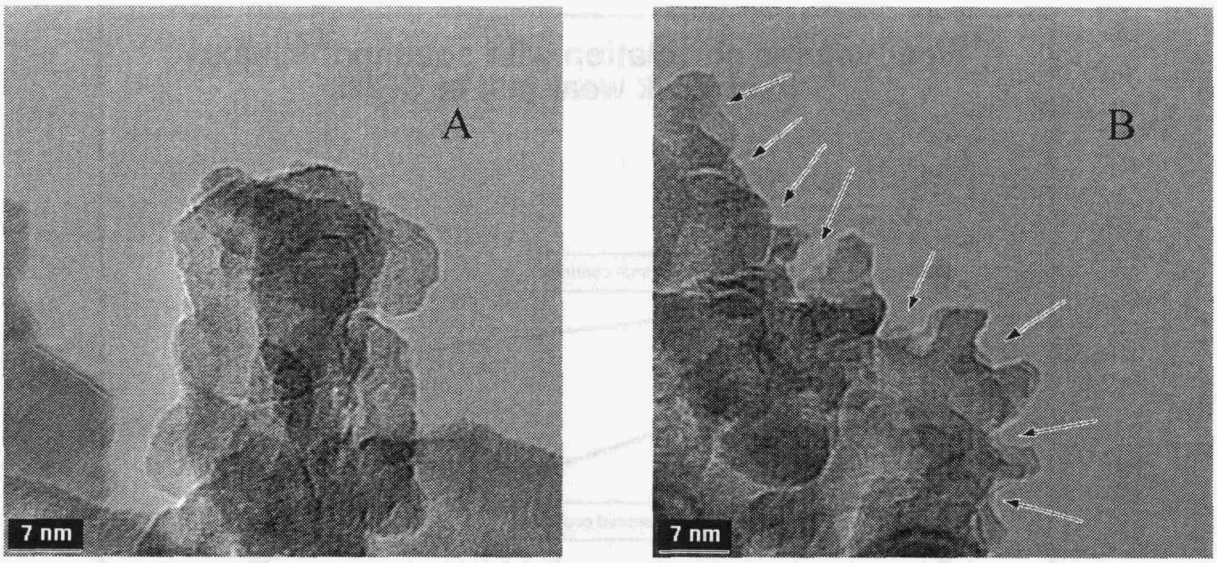

Fig. 5.3. High resolution electron micrograph of (a) PrO_2-ZrO_2 coated alumina particles and (b) the arrows showing damage to the particle during EDS measurements.

Jian Zhang, Caterpillar Inc, "Characterization of Thin Film Coatings" [FEL95-37 (21)-8I]

MCAUC/MAUC/DUC/TPUC

Caterpillar is investigating thin film coatings for improving the reliability and durability of components. The purpose of this project is to obtain a relationship between the mechanical properties of a thin film coating and its microstructure and performance.

In the second year of this program, the hardness, elastic modulus, chemical composition, phase and residual stress of nitride, carbide and carbon based thin film coating samples have been measured at HTML, using nanoindentation, Auger electron spectroscopy, and X-ray diffraction techniques. The data collected at HTML have been used for coating selection and modeling at Caterpillar.

Figure 5.4 shows how the nanoindentation load and displacement curve was used to calculate nanohardness and elastic modulus.

The microstructure and chemistry of nitride coating specimens have been examined using cross-section TEM. Focused ion beam technique was used to overcome the difficulties of thin film coating sample preparation.

Thermal property measurement of thin film coating has been started at TPUC by using the 3 Omega technique to measure thermal conductivity of insulate coatings.

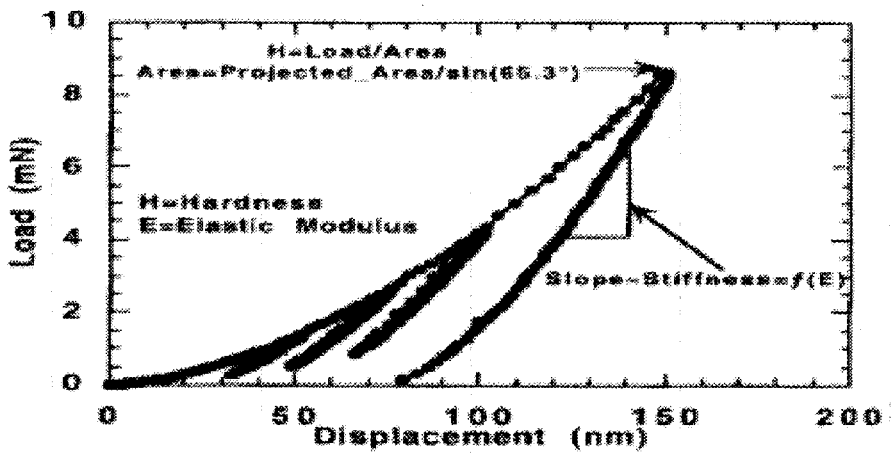

Fig. 5.4. Nanoindentation loading/displacement curve of the TiN thin film coating sample.

5.2 GRADUATE FELLOWSHIPS

For graduate students the following criteria are applicable:

- The student must be a U.S. citizen and be studying in an engineering department having ABET accreditation of the undergraduate program.
- The candidate must be prepared to conduct a substantial part of his or her thesis research in residence at HTML.
- The candidate must have an undergraduate grade point average of at least 3.5 in a 4.0 system.
- A standard nonproprietary user agreement must be in place.

The student's thesis research progress is evaluated once a year by the HTML director, the HTML staff advisor, and the student's professor to determine whether significant progress has been made and to establish future research goals. This meeting also serves as a mechanism to determine whether funding is to continue. An HTML staff member serves as an on-site advisor and is a member of the student's dissertation committee at the university. Each graduate student receives a stipend of approximately $2200 per month for the duration of the fellowship appointment.

E. C. Dickey, Northwestern University, "The Role of Interfaces and Residual Stress on the Fracture Behavior of Directionally Solidified Eutectics" [FEL95-26(18)-15G]

RSUC/DUC/MAUC

In situ oxide-oxide composites can be produced through directional solidification of pseudo-binary eutectic phases [e.g., $NiO-ZrO_2(Y_2O_3)$]. Because of their potential applicability as high-temperature structural materials, the mechanical behavior of these directionally solidified eutectics (DSEs) has been the focus of several studies. Typically, DSEs show an increased work-to-fracture over that of the two constituent phases, but at room temperature they do not behave as classical composites in that little interface debonding occurs between the two phases. Because the two phases in a eutectic system have different thermal expansion properties, residual stresses may build up during processing as the sample cools from the solidification, or stress-free, temperature. Such residual stresses—compressive in one phase and tensile in the other—will certainly affect the mechanical properties of these in-situ composites, so it is important to measure and understand the residual stress state. Under the HTML Graduate Fellowship program, two aspects of $NiO-ZrO_2(Y_2O_3)$ DSEs were

addressed. First, the interfaces between the two phases were studied on an atomic scale by various electron imaging and spectroscopy techniques, and, secondly, the residual stress and strain tensors of the two phases were measured by X-ray diffraction techniques. From the two studies, conclusions were drawn about the role of the interface structure on the interface bonding and its role in the accumulation of residual stresses in the composite system.

In the first phase of the research, the interface structure and chemistry were elucidated on an atomic scale by TEM techniques including high resolution electron microscopy (HREM), which was performed at Northwestern University. Z-contrast scanning transmission electron microscopy (STEM) and electron energy loss spectroscopy (EELS) were performed in collaboration with the SSD at ORNL. Figure 5.5 presents a Z-contrast image of the NiO-$ZrO_2(Y_2O_3)$ interface with a structural model superimposed. The atomically abrupt transition between the two phases is facilitated by an oxygen plane at the interface that is shared by both NiO and ZrO_2. EELS profiles taken across the interface in steps of interplanar spacing (see Fig. 5.6) indicate that the interface is also chemically abrupt with no significant mutual solid solubility. The interface atomic structure leads to electrostatic bonding between the cation and anion planes across the boundary and rationalizes the mechanical integrity of the interfaces.

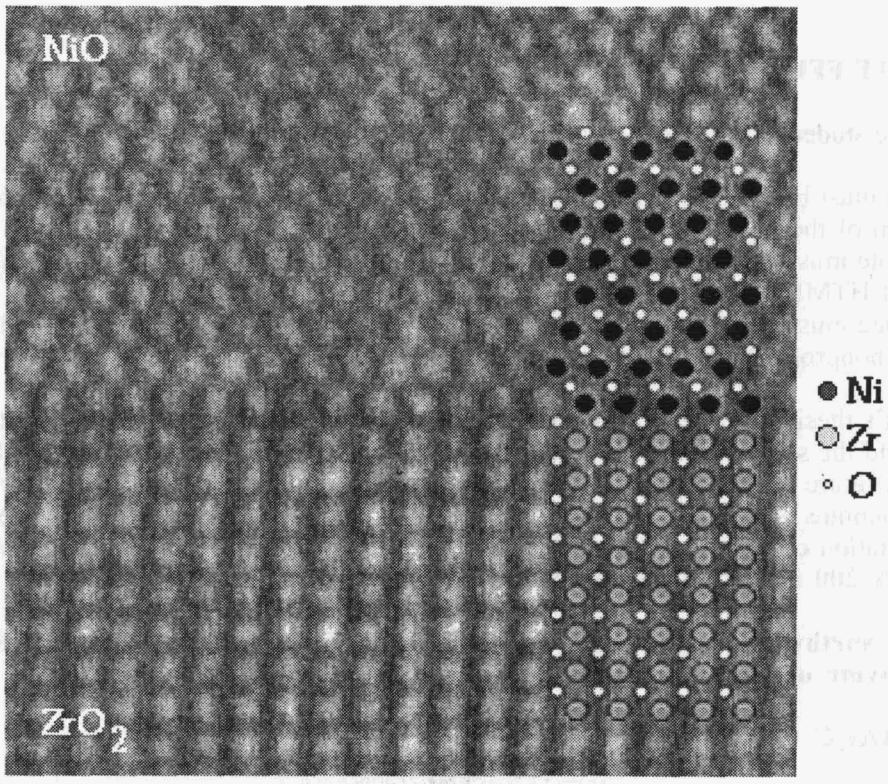

Fig. 5.5. Z-contrast STEM image of NiO-$ZrO_2(Y_2O_3)$ interface with structural model superimposed.

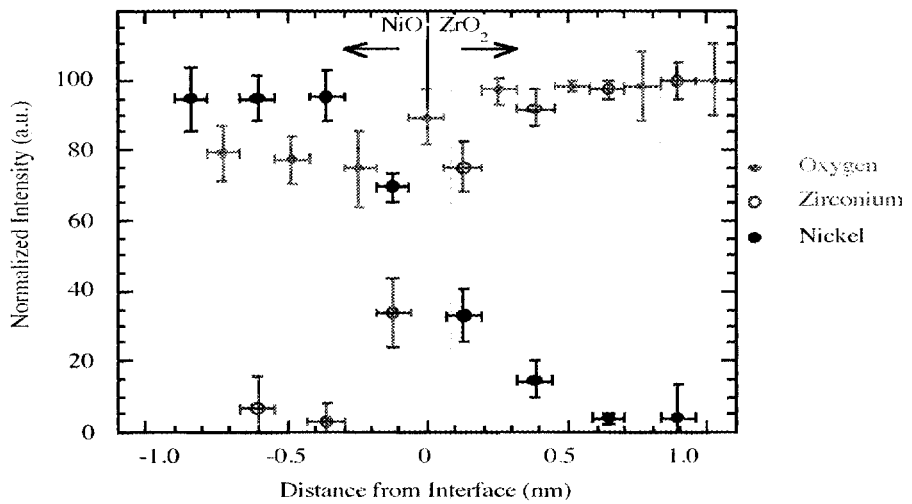

Fig. 5.6. Profiles of Ni, Zr, and O normalized EELS intensities taken across the NiO-ZrO_2 interface in steps of interplanar spacing.

In the second phase of the research, interlamellar residual stresses because of thermal expansion mismatches were measured in lamellar NiO-ZrO_2(cubic) DSEs. The triaxial strain tensors of both phases were measured using single-crystal X-ray diffraction techniques on isolated grains of the DSE. From the strain tensors, the stress tensors were calculated, taking into account the full elastic anisotropy of the phases. The resulting stress tensors indicate that very large compressive stresses accumulate in ZrO_2, while large tensile stresses build up in NiO parallel to the lamellae during the solidification process (see Fig. 5.7 and Fig. 5.8). The large magnitude of the stresses indicates that the interfaces between the lamellae are very well bonded and do not facilitate slip or other stress-relieving processes.

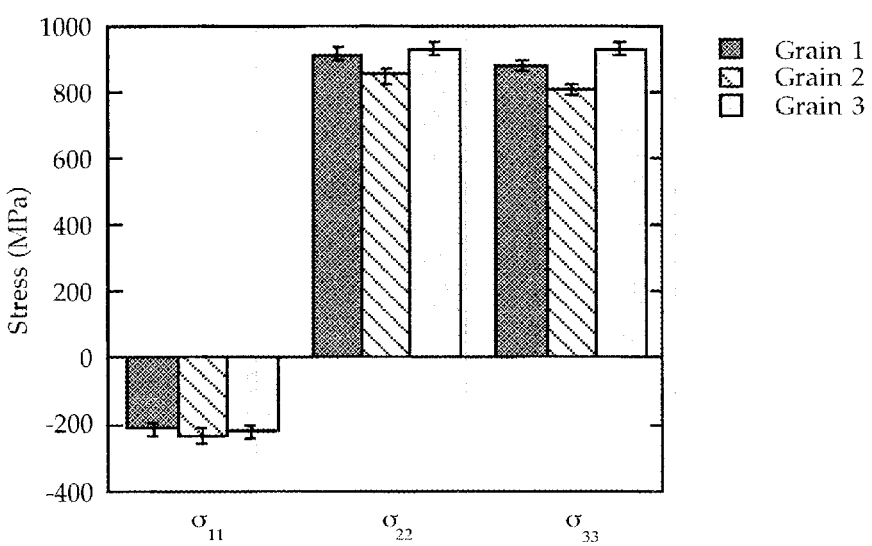

Fig. 5.7. Normal stresses in NiO lamellae. σ_{11} is perpendicular to the lamellae. σ_{22} and σ_{33} are parallel to the lamellae.

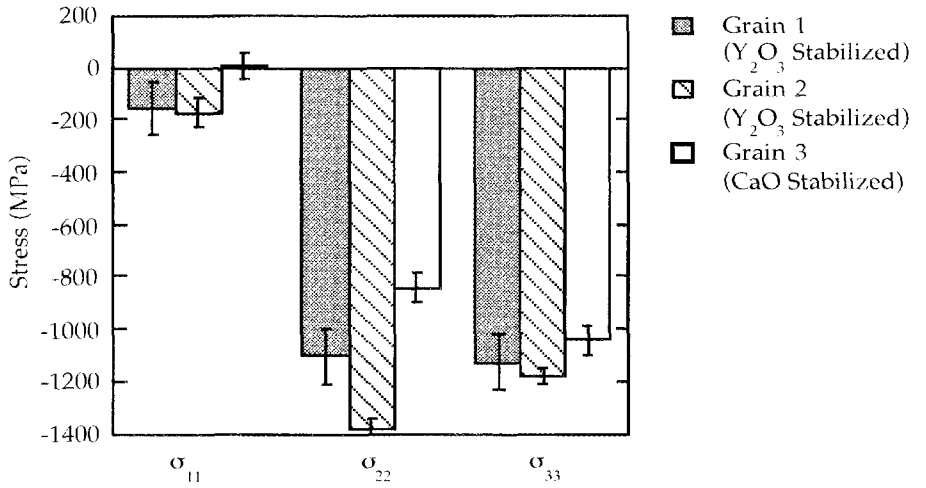

Fig. 5.8. Normal stresses in ZrO_2 (cubic) lamellae. σ_{11} is perpendicular to the lamellae. σ_{22} and σ_{33} are parallel to the lamellae.

J. Allen Haynes, University of Alabama at Birmingham, "Oxidation and Degradation of Thermal Barrier Coating Systems" [FEL93-09(5)-4G]

MCAUC/TPUC/MAUC

TBC systems are currently used to protect hot-section superalloy hardware in gas turbine engines. A typical TBC consists of an oxidation-resistant metallic bond coating overlaid with a thermally insulating Y_2O_3-stabilized ZrO_2 (YSZ) top coating applied by either air plasma-spray (APS) or electron beam physical vapor deposition (EB-PVD). Although it is well documented that thermocyclic failure of ceramic top coatings is accelerated by growth of an Al_2O_3 scale along the bond coat/top coat interface, the mechanisms by which oxidation degrades top coating integrity are not well defined for APS TBCs. In the case of EB-PVD TBCs, the interfacial scale is clearly the weak link in the system since the predominant failure mode is thermomechanical fracture or delamination of the Al_2O_3. Thus, scale growth kinetics and mechanical properties are critical life-determining factors in EB-PVD TBC durability. However, the fracture behavior and mechanical properties of Al_2O_3 scales are not well understood, and are strongly influenced by numerous factors including substrate chemistry and surface morphology, oxide-metal bond strength, scale microstructure and internal void content, reactive element additions, residual stresses, and growth stresses. The purpose of this study was to investigate the isothermal oxidation and thermocyclic degradation of various TBC systems (both APS and EB-PVD) with particular emphasis on the growth kinetics, microstructures, flaw content, fracture behavior, and micromechanical properties of the interfacial Al_2O_3 scales that formed on APS TBCs.

Isothermal oxidation kinetics of superalloy discs coated with (1) bare MCrAlY (M = Ni and/or Co) bond coatings or (2) APS or EB-PVD TBCs were measured and compared by high-mass thermogravimetric analysis at 950–1150°C. Thermocyclic behavior of TBCs was evaluated by furnace thermal cycle testing at 1150°C. Coating and scale microstructures, phases, and chemistries were evaluated by field emission gun-scanning electron microscopy, energy dispersive spectroscopy, X-ray diffraction, and electron microprobe analysis. Coating and oxide scale mechanical properties (hardness and Young's modulus) were measured by mechanical properties microprobe.

The isothermal oxidation kinetics of plasma-sprayed Ni-22Cr-10Al-1Y bond coatings were not influenced by the presence of an APS YSZ top coating at 1150°C. However, as shown in Fig. 5.9, the steady-state isothermal oxidation rate constants (as measured by continuous thermogravimetry) of low pressure plasma-sprayed Ni-22Co-18Cr-12Al-0.3Y bond coatings were increased by a factor of 2 at 950, 1050, and 1150°C when overlaid with a layer of commercial EB-PVD YSZ. This effect has not been previously reported. It was not transient in nature and was constant at up to 200 h testing. The mechanism(s) by which the presence of the TBC caused the accelerated oxidation rates were not resolved because of complications related to internal oxidation of the bond coatings.

The APS TBCs displayed average lifetimes of 360 1-h cycles at 1150°C. Interrupted thermocyclic testing revealed that failure of APS TBCs occurred by progressive YSZ fracture and crack link-up above and near to the bond coat interface, as was reported in previous studies. Severe localized fracture, buckling, and multilayering of the interfacial Al_2O_3 scales occurred during thermal cycling, resulting in localized scale thickness of more than 20 μm. Although the localized scale damage initiated prior to 25% of TBC lifetime, it did not induce rapid failure of APS TBCs. Extensive microstructural evaluation of the interfacial Al_2O_3 scales on APS TBCs after various levels of thermal cycling revealed the following: (1) thermocyclic scale damage often occurred by internal fracture across the columnar Al_2O_3 grains (see Fig. 5.10), indicating a high intrinsic oxide-metal bond strength, (2) Al_2O_3 scale crack healing by sintering occurred at 1150°C (see Fig. 5.11), (3) surfaces with a sharp radius of curvature induced less Al_2O_3 damage than gradually convex surfaces, (4) scale void growth was significantly accelerated by a combination of thermal cycling and convex surfaces, (5) higher void contents were observed in scales that formed on convex surfaces, and (6) Al_2O_3 scales on APS Ni-22Cr-10Al-1Y displayed much better thermocyclic stability/fracture resistance than scales on vacuum plasma-sprayed Ni-22Cr-10Al-1Y, possibly because of the lower strength of the APS NiCrAlY.

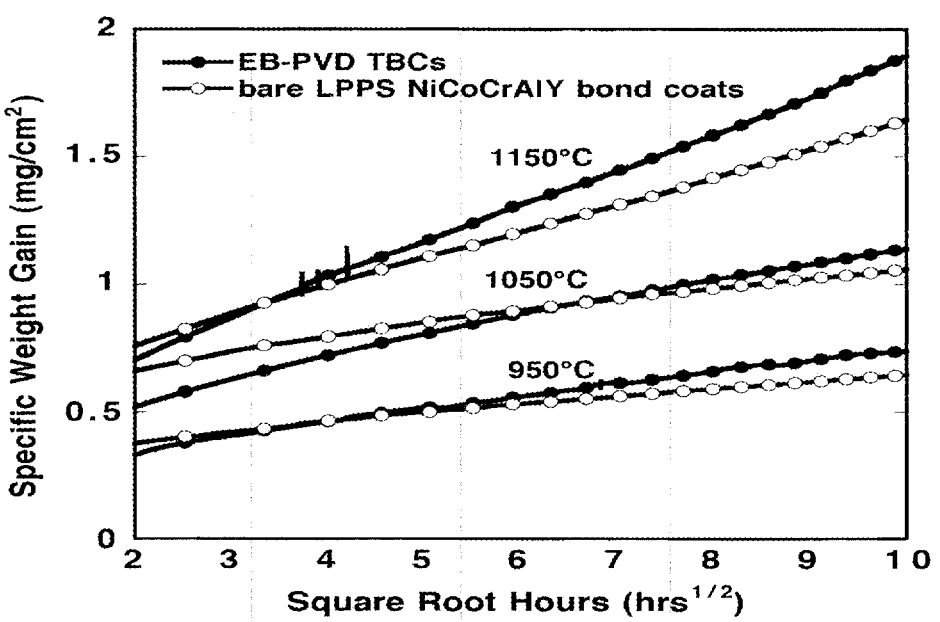

Fig. 5.9. Parabolic plot of continuous thermogravimetry measurements comparing the steady-state oxidation kinetics (at 950–1150°C) of bare LPPS Ni-22Co-18Cr-12Al-0.3Y bond coatings with the same bond coatings coated with a 125-mm TBC (a commercial EB-PVD TBC system). Note that the NiCoCrAlY oxidation rates were accelerated by the presence of the EB-PVD YSZ top coating at each temperature (k_p increased by approximately 2X). Replicate specimens of 50- and 200-h duration gave similar results.

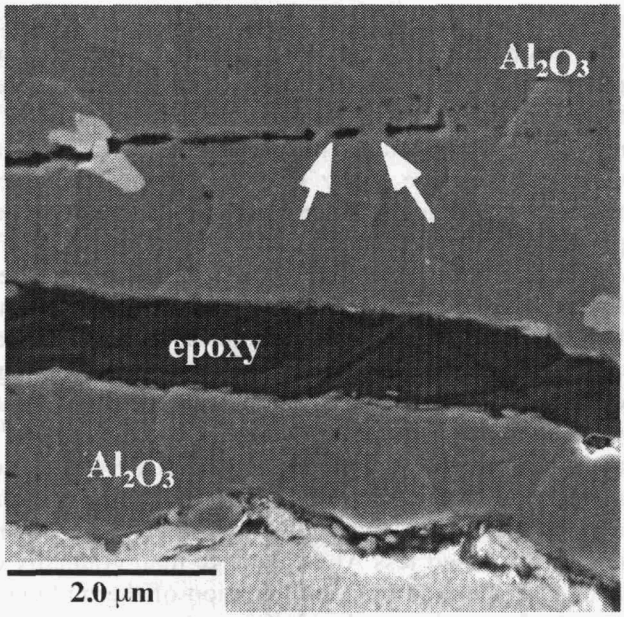

Fig. 5.10. Metallographic section showing internal fracture of an interfacial Al_2O_3 scale on a failed APS TBC (100 h + 270 1-h cycles at 1150°C). Fracture occurred across the columnar grains in preference to interfacial delamination, and grain structures match on both sides of the crack (indicating internal fracture instead of delamination and sub-scale growth) . No cracking was observed after identical preparation of isothermally grown scales. Evidence of crack healing by sintering is indicated by the arrows.

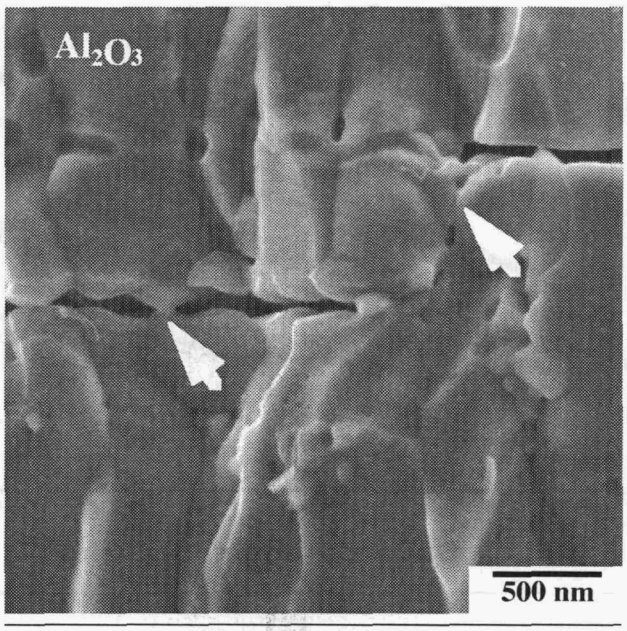

Fig. 5.11. Fracture section of an interfacial Al_2O_3 scale (exposed by YSZ spallation) on an APS TBC showing microstructural evidence of localized Al_2O_3 scale healing by sintering across an internal crack (arrows); 360 1-h cycles at 1150°C.

There were no significant changes in the hardness or Young's modulus of the Al_2O_3 scales and individual APS YSZ splats (as determined by mechanical properties microprobe) due to time-at-temperature or thermal cycling (at 1150°C). The hardness of the NiCrAlY bond coating decreased rapidly during the first cycle to a relatively constant value (out to 360 cycles). The morphologies of the bond coat and superalloy interdiffusion zone were significantly different after similar time periods of isothermal and cyclic aging. It was concluded that failure of APS TBC systems is not intrinsically dependent on the mechanical properties or adherence of the interfacial Al_2O_3 scale.

Results of this study have provided significant improvements in understanding of Al_2O_3 scale thermocyclic fracture and time-dependent mechanical properties, and have provided a foundation for future studies that will develop methods of optimizing scale adherence. The identification of a possible YSZ-Al_2O_3 interaction to increase oxidation rates in EB-PVD TBCs requires further study, since thermomechanical stresses in brittle interfacial scales are proportional to their thickness, which is in turn determined by growth kinetics. Thus, phenomena that affect interfacial scale growth rates have important implications in modeling the long-term durability of EB-PVD TBC systems.

A dissertation entitled "Oxidation and Degradation of Thermal Barrier Coating Systems" was accepted by the graduate school at the University of Alabama at Birmingham, and a Ph.D in Materials Engineering was granted to the graduate fellow in December 1997. Three related journal articles are in the process of being submitted for publication.

Michael Lance, Rutgers University—Dept. of Ceramics, "Piezospectroscopy of Ceramics" [FEL95-22(14)-11G]

MCAUC

Piezospectroscopy is a new field of stress measurement that applies spectroscopic techniques (luminescence, Raman, or FTIR spectroscopy) to measure stress in ceramics with a high spatial resolution. In the case of piezo-Raman and piezoluminescence, the spatial resolution is about 1 micron, which is far superior to either X-ray or neutron diffraction. Also, data acquisition is fast, and interpretation is relatively simple. The theory of piezoluminescence has already been derived in the literature. In this work, a similar analysis is used to extend the theory of piezo-Raman to polycrystalline ceramics. In addition piezospectroscopy has been used to measure macro- and micro-stresses in thermal barrier coatings and thermally grown oxide scales on alumina-forming metal substrates.

The effect of stress and strain on the splittings and shifts of Raman peaks of various materials was determined theoretically using a mathematical program and a UNIX station at HTML. For polycrystalline ceramics, it was determined that piezo-Raman can be used for measuring the mean hydrostatic stress within a material. The splittings of doubly and triply degenerate peaks are dependent upon the deviatoric strains (or stresses). This is the first phenomenological description of piezo-Raman for polycrystalline ceramics.

Piezospectroscopy is particularly useful for analyzing the failure behavior of thermal barrier coatings since stress can be measured in both the zirconia thermal barrier and the oxide scale that forms at high temperatures. For plasma-sprayed TBCs, the bulk compressive stress in the zirconia gradually decreases with the number of cycles indicating cracking during cooldown. Tensile stresses normal to the interface at the peaks of asperities in the bond coat were measured indicating that cracking in the zirconia is highly dependent upon interface roughness. Similar results were obtained for TBCs produced by PVD with the bulk compressive stress in the zirconia gradually decreasing with the number of thermal cycles. A bimodal stress distribution was measured in the oxide scale; either stress was close to zero or over 2 GPa of compression for delaminated or intact scales, respectively. This shows that piezospectroscopy can be used to measure damage accumulation nondestructively in thermal barrier coatings. This work was performed in conjunction with HTML fellow Allen Haynes.

Michael Lance, Rutgers University—Dept. of Ceramics, "Piezospectroscopy of Ceramics, [FEL95-22(14)-11G]

MCAUC

Piezospectroscopy is a new field of stress measurement that applies spectroscopic techniques (luminescence, Raman, or FTIR spectroscopy) to measure stress in ceramics with a high spatial resolution. In the case of piezo-Raman and piezoluminescence, the spatial resolution is about 1 micron, which is far superior to either X-ray or neutron diffraction. Also, data acquisition is fast and interpretation is relatively simple. The theory of piezoluminescence has already been derived in the literature. In this work, a similar analysis is used to extend the theory of piezo-Raman to polycrystalline ceramics. In addition, piezospectroscopy has been used to measure macro- and micro-stresses in thermal barrier coatings and thermally grown oxide scales on alumina-forming metal substrates.

The effect of stress and strain on the splittings and shifts of Raman peaks of various materials was determined theoretically using a mathematical program and a UNIX station at HTML. For polycrystalline ceramics it was determined that piezo-Raman can be used for measuring the mean hydrostatic stress within a material. The splittings of doubly and triply degenerate peaks are dependent upon the deviatoric strains (or stresses). This is the first phenomenological description of piezo-Raman for polycrystalline ceramics.

Piezospectroscopy is particularly useful for analyzing the failure behavior of thermal barrier coatings since stress can be measured in both the zirconia thermal barrier and the oxide scale that forms at high temperatures. For plasma sprayed TBCs the bulk compressive stress in the zirconia gradually decreases with the number of cycles indicating cracking during cooldown. Tensile stresses normal to the interface at the peaks of asperities in the bond coat were measured indicating that cracking in the zirconia is highly dependent upon interface roughness. Similar results were obtained for TBCs produced by PVD with the bulk compressive stress in the zirconia gradually decreasing with the number of thermal cycles. A bimodal stress distribution was measured in the oxide scale; either stress was close to zero or over 2 GPa of compression for delaminated or intact scales, respectively. This shows that piezospectroscopy can be used to measure damage accumulation nondestructively in thermal barrier coatings. This work was performed in conjunction with HTML fellow Allen Haynes.

Sharon Robinson Mrotek, Rutgers University, "Microstructural Control of Silicon Carbide Via Liquid Phase Sintering" [FEL95-24(16)-13G]

MAUC

Silicon carbide ceramics with various microstructures were fabricated by controlling the amount and composition of a Y_2O_3-Al_2O_3 liquid phase, the crystallographic phase of the starting powders, the trace impurities in those powders, and the time and temperature of sintering and post-sintering heat-treatments. Alpha and beta SiC "seeds" were used to control the phase conversion and grain growth during sintering.

The grain size distribution and aspect ratio of the grains was determined through computer-assisted microstructural analysis on SEM images of polished and etched samples. TEM was used in conjunction with EDS to determine the distribution of the sintering aids in the grains and the grain boundaries. Additionally, the final phase content of the samples was determined via X-ray diffraction. The fracture toughness and hardness were measured by the indentation method in order to evaluate the relative effects of the microstructural variations on the mechanical properties.

Alpha silicon carbide samples exhibited a fine grained, equiaxed microstructure. Under appropriate conditions, samples prepared from beta SiC powders underwent a phase transformation to alpha SiC accompanied by the growth of elongated platelet grains. The addition of alpha seeds to the beta powder reduced the size of the platelets compared to unseeded samples of the same composition. If the beta to alpha phase transformation did not occur, samples prepared from beta

powders developed an equiaxed microstructure. The grain size of all samples decreased with increasing amounts of sintering additives.

The beta to alpha phase transformation was required to obtain an elongated grain microstructure and was catalyzed by the presence of a sufficient amount of aluminum metal. If there was insufficient Al impurity present in the initial silicon carbide powder, purposeful additions of Al metal could induce the phase transformation. Examination of the sintering progression over time indicated that the phase transformation occurred late in the sintering process and appeared to occur via a solution/reprecipitation mechanism.

Post-sintering heat treatments were also used to encourage the beta to alpha phase transformation. However, heat treatments were accompanied by large weight loss and volatilization of significant amounts of alumina from the liquid phase. This resulted in large surface flaws that were expected to degrade the mechanical properties.

Since fracture toughness was a function of the final grain morphology, the formulation of large interlocking platelets via either an Al catalyst or heat treatment was critical in obtaining the desired high toughness values. The results of this project are currently being written up as a doctoral thesis and will be presented at the annual meeting of the American Ceramic Society.

M. A. Stough, The Pennsylvania State University, "Diffusivity and Solid Solubility in an Alumina-Zirconia Binary System" [FEL95-25(17)-14G]

MAUC

In the high-temperature ceramic composite field, polycrystalline zirconia (ZrO_2) has been investigated as a potential interfacial barrier in the sapphire-fiber-reinforced alumina (Al_2O_3) matrix system. Because of their intimate contact at temperatures of fabrication and use between 1000°C to 1600°C, a fundamental understanding of the mutual solid solubility and diffusivity between these oxides is important. This research project is one step in the process of understanding the solid-state behavior.

Ion-implanted single crystal specimens and interdiffusion specimens were used in conjunction with field-emission analytical electron microscopy (AEM), energy dispersive spectroscopy (EDS), and secondary ion mass spectroscopy (SIMS, Penn State) to determine cation impurity diffusion coefficients and solid solution concentrations. The solubility of ZrO_2 in sapphire between 1200°C and 1600°C was found to be approximately 0.014 to 0.027 wt% based on SIMS data but could be as high as 0.11 wt% based on AEM observations of precipitates in the sapphire. A higher solubility of Al_2O_3 in cubic zirconia allowed a more complete characterization of solubility using the Cliff-Lorimer analysis of EDS spectra; the results are presented in Fig. 5.12 below.

Diffusion coefficients were determined by applying the Crank-Nicolson numerical solution of Fick's Second Law of diffusion to the SIMS data. Other analytical approaches were modeled to fit the data, all assuming diffusivity is a constant at a given temperature. Generally, zirconium diffusion in sapphire was found to be of the order 10^{-17} to 10^{-15} cm^2/s between 1200°C and 1600°C while aluminum diffusion in cubic zirconia is nearly two orders of magnitude faster (10^{-15} to 10^{-13} cm^2/s) in the same temperature region. Further work in the area of diffusion coefficient measurement is warranted as evidence exists to suggest concentration-dependent diffusion is probable in this binary system.

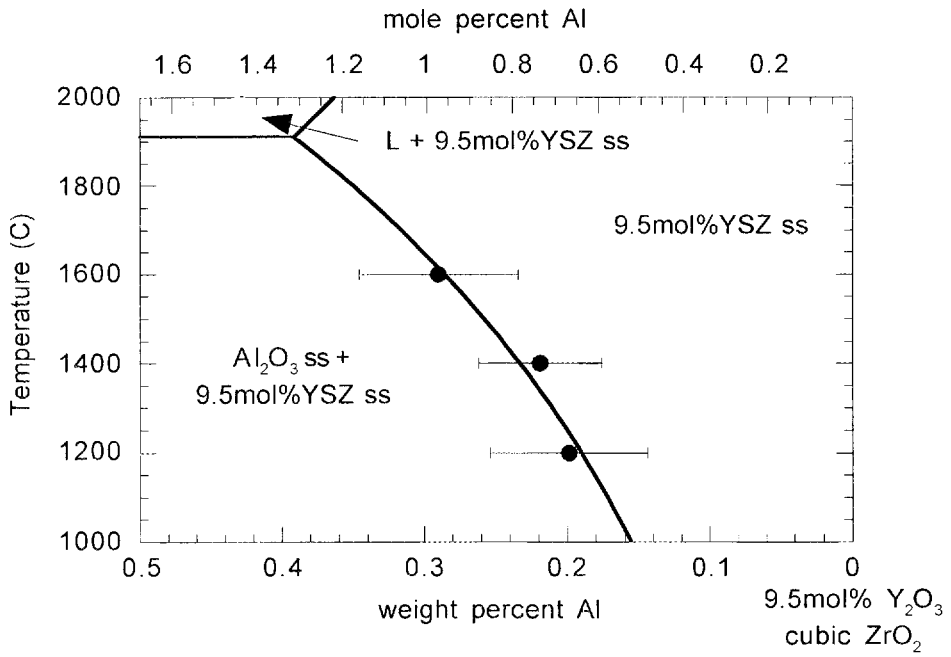

Fig. 5.12. A portion of the alumina-cubic zirconia phase diagram as determined in this investigation. The solvus line was fit using a logarithmic curve.

5.3 FACULTY FELLOWSHIPS

5.3.1 Background

Faculty fellowships are intended for faculty departments accredited by the Accrediting Board for Technology (ABET) to conduct special problem research in the HTML. The research problem must be related to at least one of DOE's areas of interest as defined for the fellowship program. The research application for faculty fellowships must be reviewed and approved by the HTML Fellowship Review Committee before the research can begin.

E. C. Dickey, University of Kentucky, "Oxidation of PtAl Bond Coats" [FEL97-54(36)-13F] (Sponsored by the Office of Industrial Technologies)

MAUC

This research program aims to understand the chemical attributes that govern oxide scale adhesion on NiPtAl and PtAl alloys. These alloys are used as bond coats in thermal barrier coating systems and must therefore be resistant to severe oxidation. Furthermore, the oxide scale that does inevitably form must be well adhered to prevent scale spallation. It is found that small additions of certain elements, termed "reactive elements," have a profound effect on the oxidation kinetics and scale adhesion in these systems. To understand the role of the reactive elements in the oxidation process, analytical electron microscopy studies were conducted.

Model oxidation studies were performed on cast NiPtAl and PtAl alloys, some of which contain small additions of reactive elements (e.g., Zr or Hf). Both isothermal and cyclic oxidation studies were performed on the various bond-coat compositions to assess the oxidation kinetics. Complementary microstructural and chemical studies were carried out by SEM, EDS, and STEM to gain a phenomenological understanding of the different oxidation behaviors.

In the case of the Zr-doped PtAl, Zr segregation to the alumina grain boundaries was observed using spatially resolved EDS. Figure 5.13 presents a bright-field TEM image of the columnar Al_2O_3 grains grown isothermally at 1200°C on PtAl-Zr. EDS spectra, shown in Fig. 5.14, show that Zr is present at the Al_2O_3 grain boundaries but not in the bulk of the Al_2O_3 grains. The improved adherence of the oxide scale in the Zr-doped aluminides appears to be associated with segregation of the Zr to the Al_2O_3 grain boundaries.

Similar studies on other doped alumindes will be conducted to gain a generalized understanding of the role of reactive elements in the oxidation process. This knowledge will enable us to design alloy compositions with improved oxidation resistance.

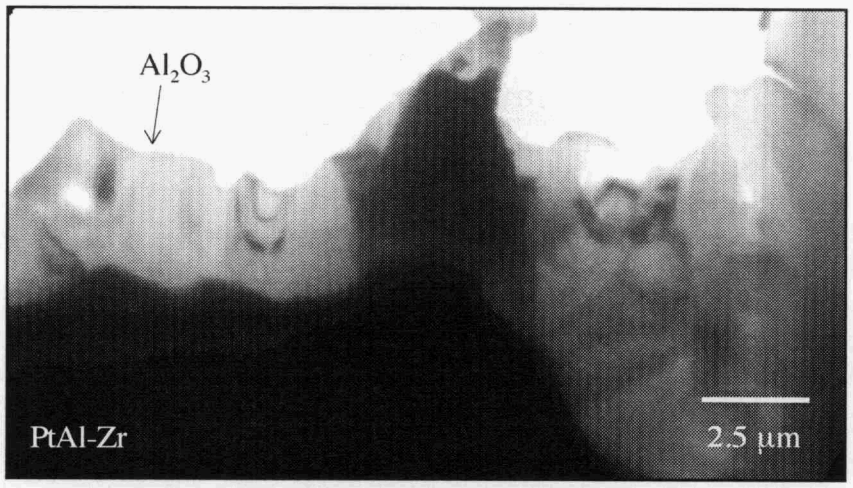

Fig. 5.13. Bright-field TEM image of alumina scale on isothermally oxidized PtAl+Zr.

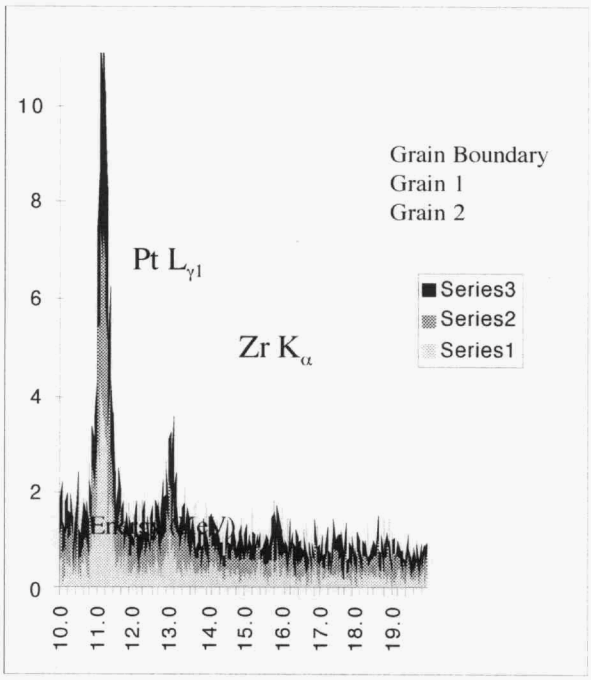

Fig. 5.14. EDS spectra from alumina grains and grain boundary showing segregation of Zr to grain boundaries. The intensities of the three spectra are offset for clarity. Traces of Pt are also detected in the alumina grains and grain boundaries.

APPENDIX A

STANDARD NONPROPRIETARY USER AGREEMENTS

APPENDIX A. STANDARD NONPROPRIETARY USER AGREEMENTS

U. S. Industry—211

Alabama

Monarch Tile, Inc. (Florence)
United Defense LP (Anniston)
Southern Research Institute (Birmingham)

Arizona

Advanced Ceramics Research (Tucson)
AlliedSignal (Phoenix)
Materials Focus Inc. (Tucson)

California

AlliedSignal EMRC (Los Angeles)
Alzeta Corp. (Santa Clara)
Amercom Inc. (Chatsworth)
Applied Materials, Inc. (Santa Clara)
Ceradyne, Inc. (Costa Mesa)
CERCOM, Inc. (Vista)
FMC Corp., (Santa Clara)
Guidance & Control Systems/Litton Ind. (Woodland Hills)
IBM Almaden Research Center (San Jose)
Lockheed Martin Skunk Works (Palmdale)
Membrane Technology Research (Menlo Park)
Northrop Corp. (Pico Rivera)
Nuclear & Aerospace Materials Corp. (Poway)
Rohr Inc. (Chula Vista)
Solar Turbines, Inc. (San Diego)
SRI International (Menlo Park)
Sullivan Mining Corp. (San Diego)
Sundstrand Power Systems (San Diego)
Ultramet (Pacoma)

Colorado

Coors Ceramics Company (Golden)
Golden Technologies Co. (Golden)
Quantum Peripherals (Louisville)
Schuller Int'l. Inc. (Littleton)
TDA Research Inc. (Wheat Ridge)

Connecticut

ABB C-E Services, Inc. (Windsor)
Steven Winter Associates, Inc. (Norwalk)
Torrington Co. (Torrington)
United Technologies/Pratt & Whitney (East Hartford)

Delaware

E. I. DuPont de Nemours (Wilmington)
E. I. DuPont de Nemours (Fluorochemicals)
Guidance & Control Systems-Litton
Rodel, Inc. (Newark)

District of Columbia

SPI/SPFD

Florida

GELTECH, Inc./LMES (Orlando)
Martin Marietta Elect. Info & Missile—LMES (Winter Garden)
Pratt & Whitney (W. Palm Beach)
Westinghouse Electric Corp. (W. Palm Beach)

Georgia

Advanced Engineered Materials (Atlanta)
BRH, Inc.—LMES (Lawrenceville)
Ceradyne, Inc. (Scottdale)
Ionic Atlanta, Inc. (Atlanta)
Institute of Paper Science & Tech. (Atlanta)
ITI MOVATS—LMES (Kennesaw)
RCF Seals (Vidalia)
Rolls Royce, Inc. (Atlanta)

Illinois

A. Finkl & Sons (Chicago)
Adtech Nepth, Inc. (Oak Park)
AlliedSignal (Des Plains)
Alloy Eng. & Casting (Champagne)
Caterpillar, Inc./Tech. Ctr. (Peoria)
Wagner Castings Co. (Decatur)

Indiana

AlliedSignal (South Bend)
Allison Engine Co. (Indianapolis)
Cummins Engine Co. (Columbus)
Dana Corp. (Richmond)
GM Corporation/Delco Remy (Andersonville)

Kentucky

Florida Tile Industries (Lawrenceburg)
Machining Research, Inc. (Florence)
Stoody Co. (Bowling Green)

Maryland

Kisner Tech. (Rockville)
Krispin Tech., Inc. (Rockville)
RCMA (Rockville)
Refractory Composites Inc. (Glen Burnie)
W. R. Grace & Co. /Conn. (Columbia)

Massachusetts

American Superconductor Corp. (Westborough)
Busek Co. (Natick)
Ceramics Process Systems Corp. (Cambridge)
Chand Kare Tech. Ceramics (Worcester)
Foster-Miller, Inc. (Waltham)
GTE Laboratories, Inc. (Waltham)
Norton Co. (Northboro)
Norton/TRW Ceramics (Northboro)
Refractory Testing Associates (Chestnut Hill)
Textron Specialty Materials (Lowell)
Uniform Metal Tech. LLC (Watertown)

Michigan

Chrysler Corporation (Highland Park)
Detroit Diesel Corp. (Detroit)
Dow Corning Corp. (Midland)
Eaton Corp. (Southfield)
Energy Conversion Devices, Inc. (Troy)
Ford Motor Company (Ann Arbor)
GM AC-Rochester (Flint)
GM Research & Development (Warren)
Hoskins Mfg. (Hamburg)
Howmet (Whitehall)
Metallamics Inc. (Traverse)
Valenite, Inc. (Troy)

Minnesota

3M (St. Paul)
FMC Naval Systems Division (Minneapolis)

Mississippi

Alpha Optical Systems (Ocean Springs)

Missouri

McDonnell Douglas Corp. (St. Louis)

Montana

Anaconda Foundry Fab. (Anaconda)
Columbia Falls Alumin. (Columbia Falls)

New Hampshire

FLUENT Inc. (Lebanon)
Miniature Precision Bearings (Keene)

New Jersey

AlliedSignal (Morristown)
AT&T Bell Laboratories (Murrary Hill)
Ceramic Magnetics, Inc. (Fairfield)
Engelhard Corp. (Edison)
Exxon Research & Eng. Co. (Annadell)
INRAD (Northvale)
Materials Technology (Shrewsbury)
NEC Research Inst. (Princeton)
Phone-Poulenc, Inc. (Cranbury)
Union Camp Corp. (Princeton)

New Mexico

Eberline Instruments (Santa Fe)

New York

Advanced Refractory Tech., Inc. (Buffalo)
CMP Industries, Inc. (Albany)
Carborundum Co. (Niagara Falls)
Eastman Kodak Co. (Rochester)
General Electric (Schnectedy)
ReMaxCo Technologies, Inc. (Kenmore)
Sulzer-Metco (Westbury)
X-Ray Optical Systems (Albany)

North Carolina

Cree Research, Inc. (Durham)
Selee Corp. (Hendersonville)
Teledyne Allvac (Monroe)

Ohio

Applied Sciences, Inc. (Yellow Springs)
Eaton Corp. (Willoughby Hills)
Edison Welding Institute (Columbus)
Doehler-Jarvis Tech. (Toledo)
GE Aircraft Engines (Cincinnati)
Goodyear Tires & Rubber Co. (Akron)
Lincoln Electric (Cleveland)
LTV Steel Co. (Independence)
Owens Corning Tech. Ctr. (Granville)
Park-Ohio Trans. (Cleveland)
Proctor & Gamble (Cincinnati)
Sandusky Int'l. (Sandusky)
Rhenium Alloys, Inc. (Elyria)
Tosoh SMD, Inc. (Grove City)
Universal Energy Systems, Inc. (Dayton)
Western Environmental (Franklin)

Pennsylvania

AHT, Inc. (Chicora)
Advanced Technology Materials, Inc. (University Park)
Alcoa Tech. Center (Alcoa Center)
Aluminum Co. of America (Alcoa Ctr.)
Bethlehem Steel Corp. (Bethlehem)
Calgon Corp. (Pittsburgh)
Certainteed Corp. (Valley Forge)
Concurrent Technologies Corp. (Johnstown)
J&L Specialty Steel (Pittsburgh)
Kennametal, Inc. (Latrobe)
Leroy A. Landers (Philadelphia)
PPG Industries, Inc. (Lancaster)
SB&TD Business Systems (Lancaster)
Thermacore, Inc. (Lancaster)
Westinghouse Science & Tech Ctr (Pittsburgh)

Rhode Island

Quadrax Corp. (Portsmouth)

Tennessee

Alliance Engines (Maryville)
American Matrix, Inc. (Knoxville)
AMS (Knoxville)
Barrett Firearms Mfg., Inc. (Murfreesboro)
Browne Tech. (Nashville)
Cavin Consulting Services (Knoxville)
Church & Dwight Co., Inc. (Knoxville)
Complete Machine Co. (Clinton)
Computational Mechanics Corp. (Knoxville)
Computational Systems (Knoxville)
Coors Electronic Package (Chattanooga)
CTI, Inc. (Knoxville)
DG Trim Products (Alcoa)
Eastman Kodak/Chemical (Kingsport)
Environment Systems Corp.—LMES (Knoxville)
Forged Performance Products, Inc. (Oak Ridge)
ForMat Industries—LMES (Oak Ridge)
Gaylon's Machine Shop (Sweetwater)
Great Lakes Research (Elizabethon)
IMTech Company (Knoxville)
IntraSpec, Inc. (Oak Ridge)
J. A. Martin (Knoxville)
Jeffrey Chain Corp. (Morristown)
Materials Eng. & Testing (Oak Ridge)
Microbial Insight, Inc. (Knoxville)
Nano Instruments, Inc. (Knoxville)
Oak Ridge Housing Authority (Oak Ridge)
Oxyrase (Knoxville)
ReMaxCo Technologies (Kingston)
SENES Oak Ridge, Inc. (Oak Ridge)
Smith & Nephew (Memphis)
Standard Aero (Maryville)
Status Technologies (Knoxville)
Technology for Energy Corp. (Knoxville)
Textron Specialty Materials Div. Avco (Nashville)
Tennessee Center for R&D (Knoxville)
Third Millenium Tech., Inc. (Knoxville)
Vamistor Corp. (Sevierville)

Texas

Agriboard Industries (Electra)
CarboMedics, Inc. (Austin)
Electrospace Systems, Inc.—LMES (Richardson)
Exxon Corp. (Houston)
Ludlum Measurement Inc. (Sweetwater)
Robert Hageman (Austin)
Southwest Research Institute (San Antonio)
Stone & Webster Eng. (Houston)
Texas Instruments (Dallas)

Utah

LoTEC, Inc. (Salt Lake City)
Mantic Corp. (Salt Lake City)

Virginia

B&W Nuclear Technologies (Lynchburg)
Babcock & Wilcox (Lynchburg)
Institute for Defense Analyses (Alexandria)
Energy Recovery, Inc. (Virginia Beach)
E. R. Johnson Associates, Inc. (Fairfax)
Hy-Tech Res. Corp. (Radford)
Materials Technologies of Virginia (Blacksburg)
Philip Morris (Richmond)
Reynolds Metals Company (Richmond)
Soil and Land Use Tech. (McLean)

Washington

Kyocera Industrial Ceramics Corp. (Vancouver)
Weyerhauser Co. (Tacoma)

Wisconsin

Waukesha Electric Systems

Other Government Facilities—12

Federal Highway Administration (Virginia)
NASA Langley Research Ctr. (Virginia)
NASA Lewis Research Ctr. (Ohio)
National Highway Traffic Safety (DC)
Naval Post Graduate School (California)
Naval Research Laboratory (DC)
NIST (Maryland)
U.S. Army Research Lab
U.S. Bureau of Mines (New York)
U.S. FDA (Maryland)
U.S. Naval Academy (Maryland)

Universities—143

Alabama

University of Alabama (Birmingham/ Tuscaloosa)
Alabama A&M (Normal)
Auburn University (Auburn)
Tuskegee Univ. (Tuskegee)

Arizona

Arizona State (Tempe)
Univ. of Arizona (Tucson)

California

California Inst. of Tech. (Pasadena)
California State Univ. (Los Angeles)
Stanford Univ. (Stanford)
Univ. of Calif., Berkeley
Univ. of Calif., Irvine
Univ. of Calif., Los Angeles
Univ. of Calif., San Diego
Univ. of Calif., Santa Barbara
Univ. of Calif., Santa Cruz
Univ. of S. Calif. (Los Angeles)

Colorado

Colorado School of Mines (Golden)
Univ. of Denver

Connecticut

Univ. of Connecticut (Storrs)
Yale Univ. (New Haven)

Delaware

Univ. of Delaware (Newark)

District of Columbia

Howard University

Florida

Florida A&M Univ. (Tallahassee)
Florida Atlantic Univ. (Boca Raton)
Florida International Univ. (Miami)
Florida Solar Energy Center (Cape Canaveral)
Florida State Univ. (Tallahassee)
Univ. of Central Fl. (Orlando)
Univ. of Florida (Gainesville)

Georgia

Georgia Inst. of Tech. (Atlanta)

Hawaii

Univ. of Hawaii (Honolulu)

Illinois

Illinois Inst. of Tech. (Chicago)
Northwestern Univ. (Evanston)
S. Ill. Univ. (Carbondale)
Univ. of Ill. (Urbana)

Indiana

Purdue Univ. Calumet (Hammond)
Purdue Univ. (West Lafayette)
Univ. of Notre Dame (South Bend)

Iowa

Iowa State Univ. (Ames)

Kansas

Kansas State Univ. (Manhatten)

Kentucky

Berea College (Berea)
Eastern Ky. State (Richmond)
Univ. of Ky. (Lexington)

Louisiana

Louisiana State Univ./A&M College (Baton Rouge)
Southern Univ. (Baton Rouge)

Maine

Univ. of Maine (Orono)

Maryland

Johns Hopkins Univ. (Baltimore)
Univ. of Maryland (College Park)

Massachusetts

Boston Univ. (Boston)
Clark Univ. (Worcester)
Harvard Univ. (Cambridge)
Mass. Inst. of Tech. (Cambridge)
Mt. Holyoke College (South Hadley)
Northeastern (Boston)
Tufts Univ. (Medford)
Univ. of Mass. (Amherst)

Michigan

Michigan State Univ. (East Lansing)
Michigan Tech. Univ. (Houghton)
Univ. of Michigan (Ann Arbor)
Wayne State Univ. (Detroit)
Western Michigan Univ. (Kalamazoo)

Minnesota

Univ. of Minnesota (Minneapolis)

Mississippi

Mississippi College (Clinton)
Mississippi State Univ. (Starkville)

Missouri

Lincoln Univ. (Jefferson City)
Univ. of Missouri (Columbia)
Univ. of Missouri (Rolla)
Washington Univ. (St. Louis)

Montana

Univ. of Montana (Missoula)

Nebraska

Univ. of Nebraska, Lincoln

Nevada

Univ. of Nevada, Reno

New Hampshire

Dartmouth Collge (Hanover)

New Jersey

New Jersey Inst. of Tech. (Newark)
Princeton Univ. (Princeton)
Rutgers Univ. (Piscataway)
Stevens Inst. of Tech. (Hoboken)

New Mexico

NM Inst. of Mining & Tech. (Socorro)
New Mexico State (Las Cruces)
Univ. of NM (Albuquerque)

New York

Alfred Univ. College of Ceramics (Alfred)
Clarkson Univ. (Potsdam)
Cornell Univ. (Ithaca)
Polytechnic Univ. (Brookland)
Rensselaer Polytechnic Inst. (Troy)
Rochester Inst. of Tech. (Rochester)
State Univ of NY (Stonybrook)
Univ. of Rochester (Rochester)

North Carolina

Appalachian State Univ. (Boone)
Duke Univ. (Durham)
North Carolina A&T State Univ. (Greensboro)
North Carolina State Univ. (Raleigh)
Univ. of North Carolina (Chapel Hill)
UNC School of Dentistry (Chapel Hill)

North Dakota

Univ. of North Dakota/Energy & Environmental Research (Grand Forks)

Ohio

Case Western Reserve Univ. (Cleveland)
Denison Univ. (Granville)
John Carroll Univ. (University Heights)
Kent State Univ. (Kent)
Ohio State Univ. (Columbus)
Ohio Univ. (Athens)
Univ. of Cincinnati (Cincinnati)
Univ. of Akron (Akron)
Univ. of Dayton (Dayton)
Wright State Univ. (Dayton)

Oklahoma

Oklahoma State Univ. (Stillwater)
Univ. of Oklahoma (Oklahoma City)

Oregon

Oregon Graduate Institute (Portland)
Oregon State Univ. (Corvallis)
Portland State Univ. (Portland)

Pennsylvania

Carnegie Mellon Univ. (Pittsburgh)
Drexel (Philadelphia)
Lehigh Univ. (Bethlehem)
Pennsylvania State Univ. (University Park)
Univ. of Pennsylvania (Philadelphia)
Univ. of Pittsburgh (Pittsburgh)

Rhode Island

Brown Univ. (Providence)

South Carolina

Clemson Univ. (Clemson)
Univ. of S. Carolina (Columbia)

South Dakota

S. Dakota State Univ. (Brookings)

Tennessee

East Tennessee State Univ. (Johnson City)
Fisk Univ. (Nashville)
Jacksboro State Area Vocation School (Jacksboro)
Maryville College (Maryville)
Tennessee State Univ. (Nashville)
Tennessee Tech. Center (Knoxville)
Tennessee Tech. Univ. (Cookeville)
Univ. of Memphis (Memphis)
Univ. of Tennessee (Knoxville)
Vanderbilt Univ. (Nashville)

Texas

Rice Univ. (Houston)
Texas A&M Univ. (College Station)
Univ. of Houston (Houston)
Univ. of North Texas (Denton)
Univ. of Texas (Arlington, Austin)

Utah

Univ. of Utah (Salt Lake)

Virginia

VPI & State Univ. (Blacksburg)
Univ. of Virginia (Charlottesville)
Washington & Lee Univ. (Lexington)

Washington

Univ. of Washington (Seattle)
Washington State Univ. (Pullman)

West Virginia

West Virginia Univ. (Morgantown)

Wisconsin

Marquette Univ. (Milwaukee)
Univ. of Wisconsin (Madison)

APPENDIX B

FY 1997 NONPROPRIETARY RESEARCH PROPOSALS

APPENDIX B. FY 1997 NONPROPRIETARY RESEARCH PROPOSALS

97-001 NP	SALUT (01) SHASHIDHAR, NAGA	DUC	Thermal Expansion of Ettringite
97-002 NP	DIVERSIFIED DIAMOND (01) DILLON, MARY	MIRUC	Diamond Life/tm Coatings—Advantages on Electroplated Products Versus Non-Coated Electroplated Products
97-003 NP	ARMCO INC. (01) DOUTHETT, JOSEPH A. WHITE, JAMES	MCAUC	The Strain Rate Sensitivity of Various Stainless Alloys
97-004 NP	UNIVERSAL ENERGY SYS. (02) BHATTACHARYA, RABI	MIRUC	Tribological Properties of Solid Lubricant Coatings Over a Wide Range of Temperature
97-005 NP	ALFRED UNIVERSITY (09) TAYLOR, JENIFER	DUC	Phase Identification of Metallic Impurities in Aluminum Nitride Powder
97-006 NP	GRACE, W.R. & CO (02) TOMCZAK, DOUGLAS	MAUC	Sub-Micron EDS/EELS Characterization of FCC Catalysts Using HRES TEM
97-007 NP	ADTECH NEPTH INC. (01) SINHA, SHOME N.	MAUC	Characterization of Grain Boundaries and Interfaces in Interpenetrating YAG-Alumina Composites
97-008 NP	STEVENS INST. OF TECH. (02) LIBERA, MATTHEW CHOU, TSENG	MAUC	Mean Inner Potential Measurements by Quantitative Transmission Electron Holography
97-009 NP	ADTECH NEPTH INC. (02) SINHA, SHOME	DUC	In Situ Observation of Formation of Orthorhombic YBa2Cu307-x (Y123 Superconductor) from BaCuO2.5 Contained in NEPTH
97-010 NP	SO. ILLINOIS UNIV. (03) MARX, DAVID	TPUC	Use of the Fast Infrared Camera in the Measurement of Surface Temperatures During Dynamometer Brake Studies
97-011 NP	UNIV. OF MAINE (01) LAD, ROBERT MOULZOLF, SCOTT	MIRUC	Tribology Studies of Oxide and Oxynitride Thin Films Grown by Molecular Beam Epitaxy Techniques
97-012 NP	UNIV. OF DAYTON (05) HECHT, NORMAN RUH, ROBERT	DUC	The Investigation of a Methodology for Producing Nanophased Reinforced Composites from the SiC-AIN

			System
97-013 NP	ADV. TECH. MATERIALS (03) KOZACZEK, KRIS	RSUC	Stress Depth Profiles in Shot Peened 2024 Series Aluminum-Depth Resolved X-ray Diffraction Measurement Using Deep Penetrating Radiation
97-014 NP	CUMMINS ENGINE CO. (10) ENGLAND, ROGER	RSUC	Residual Stress Variations in the Interface Between a Fine Tempered Martensite Case and Large Grain Size Core
97-016 NP	GM/DELCO REMY (DELPHI) (02) LEE, KWANGJIN (MIKE)	TPUC	An Experimental Observation of Frictionally-Excited Thermoelastic Instability in Automotive Disk Brakes
97-017 NP	SMITH & NEPHEW (01) LONG, MARC	MCAUC	Nano-Indentation Testing of Oxidized Zirconium Surfaces
97-018 NP	FORD RESEARCH LAB (08) HECHT, RENA	TPUC	Thermal Transport Properties of Aluminum Metal matrix Composites Used for Automotive Brake Hardware
97-019 NP	CUMMINS ENGINE CO. (11) SHIH, JAU-MIN	MIRUC	Grinding of Combined Zirconia/M2 Tool Steel Using CBN Wheel
97-020 NP	LEHIGH UNIV. (02) WILLIAMS, DAVID B.	MAUC	Undergraduate Teaching of Electron Microscopy Using TelePresence Microscopy
97-021 NP	UNIV. OF CENTRAL FL. (01) KAR, ARAVINDA	RSUC	Measurements of Residual Stresses in Components Manufactured by Laser Assisted Direct Rapid Prototyping
97-022 NP	ALFRED UNIVERSITY (10) MISTURE, SCOTT HALUSKA, MIKE	RSUC	Field-Induced Strain Mapping of Piezoelectric and Electrostrictive Materials Using Neutron Diffraction
97-023 NP	UNIV. OF KENTUCKY (11) DICKEY, ELIZABETH	MAUC	NiO-Y2O3 Interface Structure and Chemistry
97-024 NP	KENNAMETAL INC. (01) YECKLEY, RUSSELL	MCAUC	High Temperature Contact Fatigue
97-025 NP	GENERAL ELECTRIC CORP. (05) MOGRO-CAMPERO, A.	TPUC	Thermal Conductivity of Thermally Treated Zirconia Thermal Barrier Coatings
97-026 NP	UNIV. OF CINCINNATI (05) BLUE, CHARLES T.	RSUC	Neutron Diffraction Study of High Strain Materials
97-027 NP	ALFRED UNIVERSITY (11) SPRIGGS, R.	MCAUC	Nano-Indentation of ITO Films Fabricated by Plasma Deposition Technique

97-028 NP	ILLINOIS INST. OF TECH. (01) SELMAN, J. ROBERT	TPUC	Characterization of Lithium Ion Battery Components and Materials
97-029 NP	UNIV. OF ALABAMA (10) KLEMMER, TIMOTHY VARGA, LAJOS	RSUC	X-ray Diffraction Studies of (110) Oriented FeTaN Epitaxial Thin Films
97-030 NP	3M COMPANY (01) BESSER, MICHAEL LINK, BILL	MIRUC	Quantification of the Effects of Machining Variables, Water Fixturing Methods, and Residual Stress on the Properties
97-031 NP	CORNING INC. (03) WIGHT, JOHN F. JR.	TPUC	IR Imaging of Refractory Foam Production and Thermal Diffusivity Measurements of Ceramic Foams
97-032 NP	LEHIGH UNIV. (03) WILLIAMS, DAVID B.	MCAUC	Analysis of Subsurface Plastic Deformation During Solid Particle Erosion of Ductile Alloys
97-033 NP	UNIV. OF ALABAMA (11) LITTLETON, HARRY E. MOLIBOG, T.	TPUC	Thermal Diffusivity of Refractory Sands and Coatings for the Lost Foam Coasting Process
97-034 NP	UNIV. OF CINCINNATI (06) SINGH, RAJ N. WANG, YU-LIN	MCAUC	Effect of Thermal Shock Damage on Elastic Properties of CFCC's Determined by Resonant Ultrasound Spectroscopy
97-035 NP	N.C. STATE UNIV. (13) KASICHAINULA, JAG	TPUC	Multilayer Diamond Coatings
97-036 NP	UNIV. OF CONNECTICUT (02) PEASE, DOUGLAS	RSUC	An X-ray Diffraction Study of the Bond Coat in EB-PVD and Plasma-Sprayed Thermal Barrier Coatings
97-037 NP	CATERPILLAR INC. (06) LONG, MICHAEL C.	MCAUC	Determination of Calcium-Magnesium-Zirconium-Phosphate (CMZP) Mechanical Properties
97-038 NP	PPG INDUSTRIES (02) ZIBERT, MICHAEL	MCAUC	Spalling of Glass Substrates
97-039 NP	UNIV. OF MASS. (05) JAKUS, KARL	RSUC	High Temperature Residual Stress Measurement of SiC-Reinforced BMAS Glass-Ceramic Matrix Composite
97-040 NP	DOW CHEMICAL CO. (05) CISNEROS, MARK RIGHTOR, ED	MAUC	Metal Particle Growth on Catalyst Supports

97-041 NP	GEORGIA TECH. (26) MCDOWELL, DAVID L.	TPUC	The Effective Thermal Properties of Damaged Composites
97-042 NP	WESTERN MICHIGAN UNIV. (01) OLOWE, ABI	DUC	Thermal Stability of Conductive Layered Hydroxides
97-043 NP	BROWNE TECHNOLOGY, INC. (01) BROWNE, JIM	TPUC	Microscopic Thermal Conductivity Analysis of a Die Attachment Adhesive
97-045 NP	DREXEL UNIV. (01) BARSOUM, MICHEL W.	DUC	High Temperature X-ray Characterization of Ti3SiC2 and Ti2AIN
97-046 NP	ORNL (03) MATHIS, JOHN E.	MAUC	Surface Characterization of Superconductors and Buffer Layers Deposited on Rolling Assisted Biaxial Textured Substrates
97-047 NP	MATERIALS FOCUS, INC. (01) LEASKEY, LORI A.	MAUC	Characterization of Silicon Carbide Composite Systems
97-048 NP	LOUISIANA STATE UNIV. (06) LIAO, WARREN	MIRUC	Wear Mechanisms of a Resinoid Diamond Wheel with Fine Abrasives and Associated Responses in Creep-Feed Grinding
97-050 NP	ORNL (04) DEPAOLI, DAVID	DUC	Synthesis and Characterization of Nanosized and Nanophase Ceramic Materials
97-051 NP	BUSEK CO./STONE & WEBSTER (01) CARNAHAN, DAVID L. GONDOLFE, JOSEPH	MCAUC	High Temperature Properties of Superalloy to Silicon Carbide Braze Joints
97-052 NP	UNIV. OF WISCONSIN (04) GAJDARDZISKA-JOSIFOV, M. SCHOFIELD, M.	MAUC	Energy Filtered Off-Axis Electron Holography
97-053 NP	CUMMINS ENGINE CO. (12) KLEPSER, CHERYL ANN ENGLAND, ROGER	MAUC	Characterization of Iron Nitride
97-054 NP	KYOCERA IND. CER. CORP. (01) KRAFT, EDWIN H. ITALIANO, DAVID	MCAUC	Effect of Grinding and Testing Procedures on Measured MOR of SN282
97-055 NP	UNIV. OF TENN. (49) GERARD, DAVID MARKS, MURRAY	MAUC	Dietary Reconstruction Based on Dental Microwear Analysis
97-057 NP	HY-TECH RES. CORP. (01) KLEPPER, CHRIS	MAUC	Fabrication of Ribbon Load for Soft-X-ray Sources

97-058 NP	SOUTHERN UNIVERSITY (03) MIRSHAMS, REZA A.	MCAUC	High Temperature Tensile Property of the Super Alloy IN738LC
97-059 NP	TORRINGTON COMP. (02) WALTON, HARRY W.	RSUC	Residual Stress Measurement in Precision Bearing Components at Various Stages of Manufacture
97-060 NP	CUMMINS ENGINE CO. (13) SHIH, JAUMIN	MIRUC	High Speed Cylindrical Grinding of Silicon nitride Fuel System Component Using CBN Wheel
97-061 NP	NORTON COMPANY (12) LICHT, ROBERT H.	RSUC	Evaluation of Residual Stress in Silicon Nitride Ground with a New "Innovative Grinding Wheel"
97-062 NP	UNIV. OF NEW MEXICO (04) DATYE, ABHAYA	DUC	X-ray Diffraction Studies of Active Phases in Fischer-Tropsch Catalysts at Elevated Temperature in the Slurry Matrix
97-063 NP	ORNL (06) METALS AND CERAMICS MAZIASZ, PHIL J.	RSUC	Residual Stress Measurements on Rapidly Formed H-13 Die Steels
97-064 NP	UNIV. OF PITTSBURGH (2) J. R. BLACHERE	RSUC	Growth and Residual Stresses in TBC
97-065 NP	GEORGIA TECH. (27) MILKOTE, SHREYES	RSUC	Surface Generation Mechanisms in Hard Turning
97-066 NP	CATERPILLAR INC. (07) READEY, MICHAEL J.	MAUC	Self-Assembling Molecular Templates for Textured Thin Films
97-067 NP	ADV. TECH. MATERIALS (04) KOZACZEK, KRIS	RSUC	Depth Profiling of Shot Peen Induced Residual Stresses by Neutron Diffraction
97-068 NP	ORNL (05) CHEMICAL TECHNOLOGY DIV. HU, MICHAEL. Z.-C.	TPUC	XRD Study of the Stability and Thermal Properties of Perovskite-Type Materials at High Temperatures
97-069 NP	FORD RESEARCH LAB. (09) HARTSOCK, DALE	TPUC	Examination of Hot Spot Formation and Movement in Automotive Brake Rotors
97-070 NP	REMAXCO TECHNOLOGIES (05) NIXDORF, RICHARD DEAN	MAUC	Microwave Sensitive Silicon Carbide Fiber
97-071 NP	UNIV. OF ILLINOIS (15) GOGOTSI, YURY	MCAUC	Nanoindentation Studies of Phase Transformations in Semiconductors and Ceramics

97-072 NP	INCO ALLOYS INTERNATIONAL, INC. (1) FAHRMANN, MICHAEL	MCAU C	Stress Effects on Dimensional Changes of Age-Hardenable Superalloys
97-073 NP	GEORGIA TECH. (28) DANYLUK, STEVEN	MCAU C	The Mechanical and Thermophysical Properties of Titanium Aluminide (Gamma)
97-074 NP	RUTGERS UNIVERSITY (03) SAFARI, A.	DUC	High Temperature X-ray Diffraction Studies of Crystallite Size Effects in Ferroelectric Powders
97-075 NP	UNIV. OF N. DAKOTA (02) FOLKEDAHL, BRUCE C.	DUC	Crystallization of Coal Ash Slags Near the Temperature of Critical Viscosity
97-077 NP	PPG INDUSTRIES (03) WALCK, SCOTT	MAUC	Thin Film Characterization of Mixed Cobalt, Iron, and Chromium Oxides Deposited on Glass Substrates
97-078 NP	TEXAS A&M UNIVERSITY (3) HARTWIG, K. T. SIMONE LEIPERT	RSUC	Texture Development in Tantalum Processed Through Equal Channel Angular Extrusion

APPENDIX C

FY 1997 RESEARCH PROJECT SUMMARIES, INDUSTRIES AND UNIVERSITIES

APPENDIX C. FY 1997 RESEARCH PROJECT SUMMARIES
INDUSTRIES

Advanced Ceramics Research, Inc., "The Thermal Conductivity of Zirconium and Hafnium Diboride/Boron Nitride 'Fibrous Monolithic' Composites," *S. Nowell* and *G. Hilmas*, HTML No. 96-019

TPUC

Advanced Ceramics Research has completed a Phase II SBIR contract with NASA Marshall Space Flight Center to develop ZrB_2- and HfB_2-based ceramics. These materials are required to withstand temperatures in the vicinity of 3000 K, while exhibiting excellent thermal shock resistance. Diboride based "fibrous monolith" ceramic matrix composite (CMC) materials were developed at Advanced Ceramics Research (ACR) Inc., as a relatively inexpensive alternative to continuous fiber reinforced ceramic composites (CFCCs) for use by the aerospace industry in high-temperature applications. Thermal conductivity of the composites is very difficult to predict due to a very complex microstructure and a high degree of thermal anisotropy in the interpenetrating boron nitride matrix material.

The thermal diffusivity of ZrB_2/BN and HfB_2/BN "fibrous monolithic" composites was measured along three orthogonal axes, from room temperature to 2100°C. Room temperature measurements were made using the xenon flash apparatus, and elevated temperature measurements were made using the laser flash apparatus. Using published specific heat data for the individual phases, thermal conductivity was calculated in each orientation for both diboride/BN composite materials. The thermal conductivity of the ZrB_2/BN composite ranged from 95 W/m-K^{-1} parallel to the long axis of the cells to 50 W/m-K^{-1} parallel to the hot pressing direction, at room temperature. Similar anisotropy was noted in the HfB_2/BN composite with values of 100 W/m-K^{-1} and 56 W/m-K^{-1}, respectively. The measurement of the thermal properties of the composites in three dimensions, at elevated temperatures, allowed ACR to closer predict their values at service temperatures for numerous aerospace applications.

Fibrous monolithic (FM) processing technology was employed to improve the fracture toughness and reduce the thermal shock sensitivity of the diboride materials. ACR has produced prototype solar thermal-propulsion-related components, and other aerospace-related components from diboride-based "fibrous monolithic" material.

AlliedSignal, "Machining-Tolerant Ceramics," *C. W. Li*, HTML No. 95-024

MIRUC

The reliability and lifetime properties of typical monolithic structural ceramic components are very sensitive to the flaw distributions, which are strongly correlated with the machining conditions for the components. Consequently, reliability and lifetime prediction remains as one of the major challenges in applying monolithic ceramics for structural components.

Toughened ceramics present a promising solution to improve reliability and lifetime predictability. AS800 is an in situ toughened silicon nitride with R-curve behavior. It is anticipated that the material will show a better damage tolerance property, and its strength will be less sensitive to the machining condition variations when compared to the fine-grained, low-toughness material.

The purpose of this study is to use the design-of-experiment (DOE) approach to examine how machining parameters affect the strength of AS800. The two factors selected are the grit size of the machining wheel (resin bond, 100 concentration diamond grit) and its downfeed. A total of five grit sizes from 80 to 600 and five downfeed levels from 0.0001 in. to 0.0033 in. were employed. Other machining

conditions such as crossfeed (0.071 in.), table speed (8 in. per min) and spindle speed (5260 rpm) were fixed for all the runs. For each machining condition, a total of 20 MOR bars were machined in transverse direction so that the grinding direction was perpendicular to the long axis of the bars. To date, the 4-point bending strength data for all the bars have been collected. The preliminary results indicate that the grit size has a significant effect on the average strength property, and the Weibull strength distribution is affected by the machining conditions.

ATMI, "Depth Profiling of Shot Peen Induced Residual Stresses by Neutron Diffraction," *K. J. Kozaczek*, HTML No. 97-067

RSUC

The objective of this work was to determine subsurface profiles of residual stresses due to shot peening of aluminum alloys. Deep penetrating Mo K-alpha radiation was used (mean absorption weighted penetration depth is 320 microns) on 6061T6 aluminum alloy shot peened to Almen intensity 0.016 in. The penetration depth was controlled by changing the inclination angle of the incident X-ray beam with respect to the sample surface. An unpeened sample was used as a reference material in order to determine the unstressed lattice parameter. The poor quality of the X-ray diffraction signal hindered the measurements. The initial data analysis indicates that the results are not usable. Neutron diffraction stress mapping is planned.

Browne Technology, Inc., "Microscopic Thermal Conductivity Analysis of a Die Attachment Adhesive," *J. M. Browne*, HTML No. 97-043

TPUC/DUC

Under a Small Business Innovative Research (SBIR) Phase II program sponsored by the Ballistic Missile Defense Organization, Browne Technology, Inc., is developing a high thermal conductivity polymeric adhesive for use as a die attachment adhesive to bond high power integrated devices to their packages. The goal is to have the high heat transfer capability of solder with a low processing temperature typical of epoxy adhesives. The adhesive consists of mesophase pitch-based carbon fibers that are anisotropically aligned through the thickness of an epoxy adhesive film. Initial thermal conductivity data on this adhesive is 20 to 50 times greater than current polymeric adhesives. Optimization of the heat flow properties of the adhesive will require understanding in detail how heat is transferred between the end of a fiber and the surface of a substrate.

Feasibility work has been completed at HTML that indicates that the Scanning Thermal Conductivity Microscope (STCM) is an outstanding tool for examining thermal conductivity details on the surface of the adhesive. Adhesive films were cured in a manner that duplicated die bonding and separated from the substrate surface. Scans on these samples showed a rich variety of thermal contrast details that could be correlated with features seen by optical and scanning electron microscope examination. The importance of many of these features to thermal conductivity performance was not appreciated before this work. Polished specimens were also examined by the STCM. Individual fiber ends clearly showed thermal contrast patterns indicating structural details and heat flow patterns. Examination of a copper-coated fiber showed changes in the heat flow in the fiber and into the surrounding matrix.

<u>Busek Company Inc. and Stone and Webster Engineering Corp.</u>, "High Temperature Properties of Superalloy to Silicon Carbide Braze Joints," *D. L. Carnahan* and *D. Tribbey*, HTML No. 97-051

MCAUC/RSUC

To provide for the replacement of Incoloy 800HT tubes in ethylene processing with silicon carbide, a suitable joining technique is required. Busek researched the use of six braze materials for suitability between Hexoloy SA silicon carbide (Carborundum Corp) and Incoloy 800HT (Inco Alloys). These braze materials included binary compositions Au-Ni, Au-Pd, Pd-Co, Pd-Ni, Cu-Ni as well as pure nickel. Preliminary screening was conducted using silicon carbide to tungsten joints, then full joints were produced using the remaining brazes. Silicon carbide—tungsten—800HT joints were produced for shear testing at room temperature and bend testing at elevated temperatures. To quantify the stress state of the joint interface, an X-ray diffraction stress analysis technique was employed at Oak Ridge National Laboratory (ORNL). Based on the results obtained, Busek concludes that the suitable alloys for the high temperature brazing of silicon carbide are Nickel and the Au-Ni alloys. The use of the gold-nickel alloy restricts the braze exposure temperature to 900°C, but these are the strongest joints tested. The use of nickel (T_m = 1450°C) is restricted to the joint between the tungsten and the silicon carbide, as it is too high melting for the 800HT alloy. The other alloys are acceptable at the tungsten—800HT interface. The Au-Ni alloy is acceptable at both joint interfaces. Both the Au-Ni alloy and the nickel braze were tested extensively at ORNL.

<u>Caterpillar, Inc.</u>, "Self-Assembling Molecular Templates for Textured Thin Films," *J. E. Crumpacker*, HTML No. 97-066

MAUC/MCAUC/DUC

The goal of this research is to determine whether textured thin film coatings offer improved tribological performance compared to coatings having a more uniform structure. For example, textured coatings could affect the bearing ratio known to be important in wear of materials. To this end, we are studying a novel process of creating textured coatings using self-assembling organic molecules (SAMs) as a template, which is later removed by thermal decomposition. For simplicity, we are studying titania coatings on glass slides, a model system, with fatty acids acting as the SAM template. However, before experimenting with the SAM templating process, it was necessary to determine the best coating parameters for the glass slides. Several slides were coated with titanium alkoxide solutions using a variety of coating temperatures and alkoxide concentrations. After drying, the coatings were characterized at the nanoscale level using Oak Ridge National Laboratory's Atomic Force Microscope (AFM). The slides were examined to determine if the slides were successfully coated with titania and if the coating was uniform. Using the results obtained from the AFM, identification of key coating/processing parameters to be used in further research can be accomplished. Without the use of an AFM, it would have been difficult to differentiate between the coated glass slides and thus determine which parameters were appropriate for the desired results. Currently, the next step in developing the organic SAM template is being investigated.

<u>Concurrent Technologies Corporation</u>, "Thermophysical Properties Measurements of HY-100 Steel and Al-Ni-Bronze," *J. Jo* and *L. S. Knipple*, HTML No. 94-054

TPUC

Thermophysical properties of the base metal, heat-affected zone (HAZ), and weld metal in an HY-100 weldment (Fig. C.1) were needed by the Navy as input to the numerical simulation of welding. The thermophysical properties determined at HTML were thermal diffusivity, specific heat, and thermal

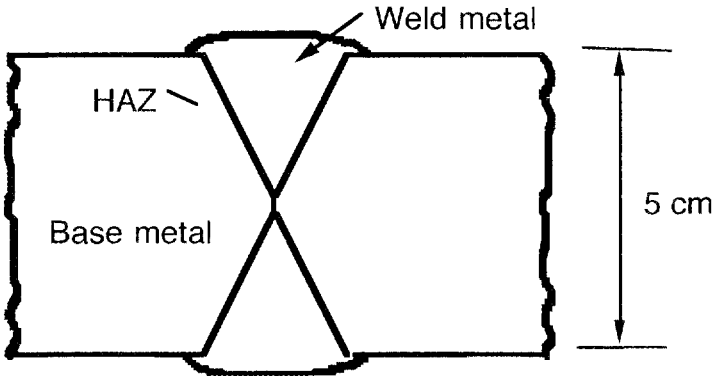

Fig. C.1. The geometry and pass sequence of weld.

expansion using the laser flash technique, differential scanning calorimeter and a dilatometer, respectively. The specimen of the laser flash system was heated in the 4-in. hot zone provided by the ultra-high temperature graphite furnace. For thermal diffusivity measurements at molten state, a special graphite sample holder was designed for this system. Eight small grooves were cut at the edges of the top and bottom sapphire windows. These grooves allowed excessive metal to escape in the molten region and kept the thickness of the specimen constant.

As shown in Fig. C.2, from room temperature to 750°C, the thermal conductivities of the base metal, HAZ, and weld metal exhibit a decrease with temperature. From 750°C up to around 1500°C, the thermal conductivity increases with temperature, and then, between 1500°C and 1550°C, it decreases rapidly. Above 1550°C, the thermal conductivity slowly increases. The thermal conductivities of the three metals were approximately 0.18 W/cmK at 650°C and was approximately 0.3 W/cmK at about 1400°C. It is believed that the valleys in thermal conductivities around these two temperatures were generated by the ferrite-austenite and solid-liquid transformations. The variation of thermal conductivity with temperature was most influenced by thermal diffusivity, and as a result the thermal conductivity—temperature curve resembles the thermal diffusivity—temperature curve.

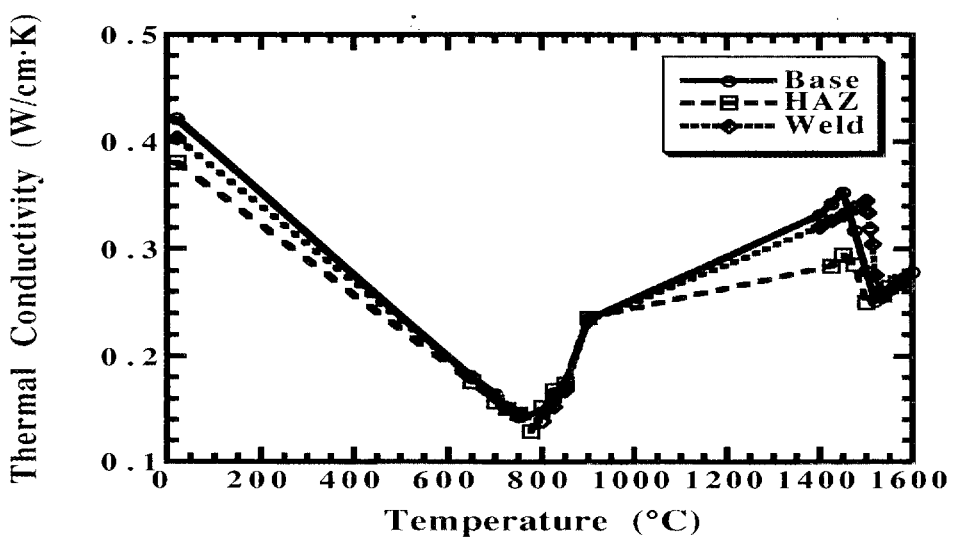

Fig. C.2. Thermal conductivity of the base metal in an HY-100 weldment.

<u>Corning, Inc.</u>, "Measurement of Stress Gradients in Metal Refractory Films on Glass Substrates," *H. J. Holland*, HTML No. 96-054

RSUC

Sputtered films of refractory metals are of importance to the video display industry for active matrix liquid crystal displays. From preliminary experimental data, it was indicated that stress gradients were present in Mo-Ta thin films sputtered on glass. The stated object of the proposal submitted to HTML was to measure this gradient.

A number of films were examined by XRD both at HTML, using the Scintag PTS goniometer, and at the ORNL/HTML synchrotron beam line. GIXD (grazing incidence X-ray diffraction) indicated the presence of stress gradients. The $\sin^2\Psi$ method showed the presence of large compressive and tensile stresses in films sputtered at low and high sputtering pressures, respectively. The direction of the XRD stress, but not the magnitude, was found to be in agreement with photoelastic stress data obtained at Corning. The presence of two body-centered cubic (bcc) phases is likely. These and a number of issues remain regarding interpretation of some of the observed XRD data. Results from stress, composition, orientation, and morphology data from the films were presented and will be published in the proceedings of the 1997 Denver X-ray conference.

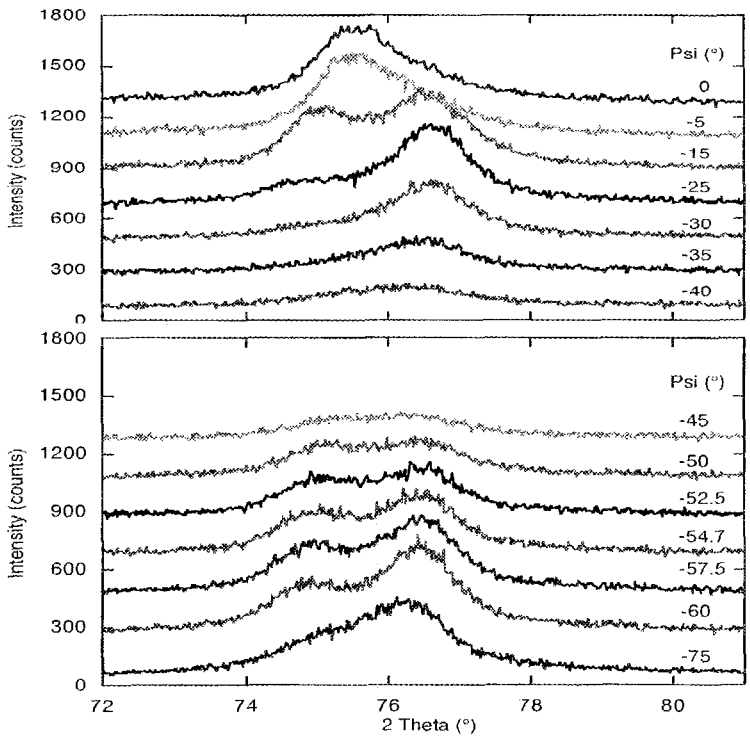

The diffraction pattern of a Mo-Ta film deposited at 15 mTorr as a function of tilt angle, psi. The selected 2Θ regions show the (211) reflections. The unusual splitting (e.g., psi = –15 and below –50°) indicates that two bcc phases coexist in the film.

<u>Cummins Engine Company</u>, "Neutron Residual Strain Mapping of a Cummins Diesel Engine Forged Component," *R. England*, HTML No. 97-014

RSUC

In the past, forgings have been normalized, and then quenched and tempered after the hot forging process. As a cost saving, industry is working toward the elimination of these heat treatment operations and going directly to the use of controlled cooling of the as-forged parts. This has produced parts with a very large prior austenite grain size in the core and a fine-grained induction-hardened martensite case microstructure. High tensile residual stresses are anticipated in the subsurface transition zone between the martensitic case and the ferritic/pearlitic core. These stresses have a high probability of reducing the fatigue endurance limit of the part. Neutron residual strain scanning has been used as a non-destructive method of mapping strain distributions at various depths, particularly in critical regions of a component with the objective of defining the residual stresses operating in the region of the microstructural transition between the martensite and ferrite/pearlite. The presence of martensite is clearly revealed in double diffraction peaks arising from the ferrite and martensite phases. The behavior of the residual stresses down to about 1/2 in., as indicated in one of the strain components, shows a clear tendency to vary between compressive character at the surface to a tensile character in the interior. The large size of the test sample presented a challenge of finding a way of probing this critical area. Without alteration to the test piece, neutrons would have to probe the critical region through so long a material beam path that no scattering signal could be measured. Neutron beam access was improved by drilling and milling small amounts of material well away from the critical area. Results show that these machining operations affected measurements over a few millimeters and, in the present case, did not affect the residual strain measurement. Comparison of neutron strain measurements and X-ray residual stress measurements show reasonable consistency. More detailed work is to be continued. It is clear that the neutron scanning measurements will yield a clearer picture of the mechanical state of the case-hardened forging. Improving endurance limits for high performance forgings are expected through a better understanding of subsurface residual stress.

<u>Cummins Engine Co.</u>, "Grinding of Combined Zirconia/M2 Tool Steel Using CBN Wheel," *Albert J. Shih*, HTML No. 97-019

MIRUC

The objectives of this project are to evaluate the potential benefits of high-speed grinding over conventional-speed grinding for production of heavy-duty diesel engine components and to establish a production-viable, high-speed grinding process suitable for both ceramic and steel materials, using a vitreous-bond, cubic-boron-nitride (CBN) grinding wheel.

The performance of a vitreous-bond CBN grinding wheel was evaluated by conducting a series of experiments under controlled conditions on the instrumented Weldon cylindrical grinding machine at HTML. The variables investigated were grinding wheel speed (v_w), truing speed ratio (q_d), type of workpiece material, and coolant flow rate. The grinding process was evaluated by measuring the effect of each of the four input variables on specific normal and tangential grinding forces, specific grinding energy, surface finish, and roundness.

As shown in the table below, 16 experiments were conducted for zirconia and M2 workpiece materials. Two additional experiments were conducted at a wheel speed of 127 m/s to investigate the effects of high coolant flow rate.

Wheel speed at truing, m/s	Wheel speed at grinding (v_w), m/s				
	35	61	91	127	q_d
19.3	x	x	x	x	0.661
25.4	x	x	x	x, H	0.503
33.9	x	x	x	x, H	0.381
35.0	x (q_d = 0.364)				Same wheel speed for truing and grinding
61.0		x (q_d = 0.209)			
91.0			x (q_d = 0.140)		
127.0				x (q_d = 0.101)	

x: Selected for the test; **H**: High coolant flow rate tested

The grinding results have been reported in a paper and submitted to the 26th North American Manufacturing Research Conference. The benefits of using high speed grinding to reduce both normal and tangential grinding forces and the grinding force ratio were verified. It gave Cummins valuable data to specify the requirements for ceramic grinding machines. The process of performing wheel truing operations at a slower grinding wheel speed was shown to reduce grinding forces, especially for M2 tool steel. A high coolant flow rate was shown to be important. The concept of using CBN to grind both ceramic and steel materials was verified.

<u>Cummins Engine Company</u>, "Characterization of Iron Nitride," *R. England* and *C. A. Klepser*, HTML No. 97-053

RSUC

Gas and ion nitriding have become common practice in diesel engine components where wear is critical. The high hardness and the wear resistance of nitrided steels provide an attractive engineering alternative. The first stage of the nitriding heat treatment process involves building a nitrogen rich sink, or "white layer," on the surface of the component. Nitrogen from this white layer is driven into the substrate during the second stage of the process. The white layer, a mixture of Fe and N, is often removed in post-heat treatment machining, thus very little physical property data has been collected or published.

Cummins Engine Company is seeking a better understanding of the crystallographic nature and mechanical properties in iron nitride layers, as little information is available. Since several critical engine components are nitrided and other applications of nitriding are being evaluated, the physical properties of this white layer are necessary to the calculations for accurate life predictions of these components.

A scientist from Cummins Engine Company visited the Residual Stress User Center to determine the phases, X-ray elastic constants, and residual stresses in the white layer of two different substrate steels, H13 and 501. The components of interest to this study did not receive a post-heat treatment finish machining. The white layer is composed predominantly of Fe_3N. Our goal was to determine the X-ray elastic constants. To accomplish this, first a strain gage was mounted onto a nitrided sample. Next, the sample was placed in four point flexure with a mechanical testing machine, and the load/strain calibration curve was generated. Next, the sample was placed in the same flexure jig, loaded, and then attached to the goniometer. The X-ray elastic constant can be determined as it is the relation between the applied stress, determined from the calibration curve, and the resulting strain, measured via X-ray diffraction. Finally, the residual stresses were determined both with the conventional $\sin^2\Psi$ technique and grazing incidence X-ray diffraction and were found to be tensile in the white layer. Data collection and analysis are continuing on this interesting problem.

Dana Corp., "Investigation of the Effects of Composition, Heat Treatment, and Finishing Method on Friction and Wear of Camshaft Alloys," *K. Kaiser*, HTML 96-046

MIRUC

Because camshafts are currently manufactured with several different processes, there is a need to determine whether or not the manufacturing process affects performance and reliability. The objective of this project was to develop data to predict the life expectancy of camshafts for large diesel engines. Engine builders would like to increase the design stress of the cam but want to increase the life of the cam also.

The Plint TE-53 tester was used to load sample camshaft materials under conditions similar to their true operating conditions. A disk on disk configuration was used with 5.1% and 22.22% sliding ratios. In every case but one, the results did not produce the type of failure expected in real life. In the one case, the failure began in the matting component and not the cam material. Figure C.3 shows data from published literature and the most significant data point generated from testing. To date, the test results are surprising in that they indicate the materials performance greatly exceeds expected performance. The fact that we can not replicate real world wear condition has prevented us reaching our gold of developing data to predict performance and reliability of various cam processing methods. Currently we are exploring additional information to improve the testing procedure so the data can be generated.

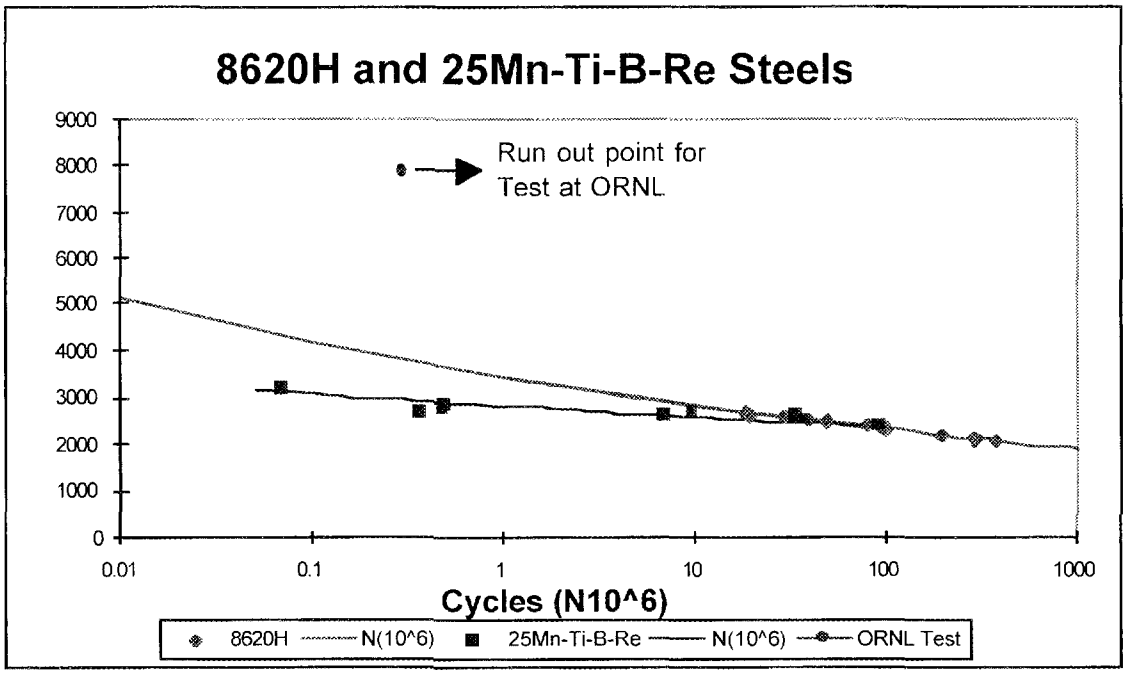

Fig. C.3. Shows failure data points for two different materials and a run-out point (not a failure) from the current testing method.

<u>The Dow Chemical Company</u>, "Metal Particle Growth on Catalyst Supports," *M. Cisneros*, HTML No. 97-040

MAUC

The activity and selectivity of catalytic processes are directly coupled with the dynamics of the catalyst morphology. Many of these processes use supported metal catalysts, and understanding the interaction that the metal has with local environmental parameters is essential for the energy efficiency of the process. In particular, metal sintering on catalyst supports is the focus of this study, and ex situ transmission electron microscopy (TEM) analysis was chosen to simulate the local environment of specific catalytic processes.

In 1997, our project team visited the HTML twice. The establishment of the experimental protocol and initial data on 0.5 wt% Pt and Pd on alumina, silica, and carbon were completed. The initial observations indicated the need for further background study using the ex situ TEM cell. Specifically, a temperature calibration of the cell was required and completed during a second visit. Also, the ex situ cell TEM grid holder material of construction was required to change from copper to nickel or other suitable metal.

Our next scheduled visit will be during the first quarter of 1998. Our initial experimental design will be repeated to evaluate the benefits from the temperature calibration and the change in the grid holder material of construction. Work will proceed on the determination of the required local environment to induce and extend metal sintering on catalyst supports.

<u>Edison Welding Institute</u>, "Stress-Free Lattice Parameters Determination for Al Welded Specimens," *Z. Feng*, HTML No. 96-029

RSUC

Neutron diffraction was used to determine the stress-free lattice parameters in an aluminum welded specimen prepared for residual stress analysis. Because the base plate and filler metal used in the weld specimen are different aluminum alloys, there is a compositional change in the heat-affected zone, which results in a change in the stress-free lattice parameters. High resolution neutron powder diffraction patterns were recorded for 10 coupons cut at various positions and depths from the weld specimen. The diffraction data were analyzed using the Rietveld analysis method to yield the lattice parameters for each coupon. Results from this study, shown in Fig. C.4, confirmed that the stress-lattice parameter in the heat-affected zone is substantially different from that in the base metal. This difference, if not corrected, will lead to a false strain value by as much as 1×10^{-3}, ten times the typical precision in strain/stress mapping experiments. The stress-free lattice parameters obtained here allow the correction for the strain maps measured in an earlier experiment, so that an accurate comparison with finite element calculations can be made.

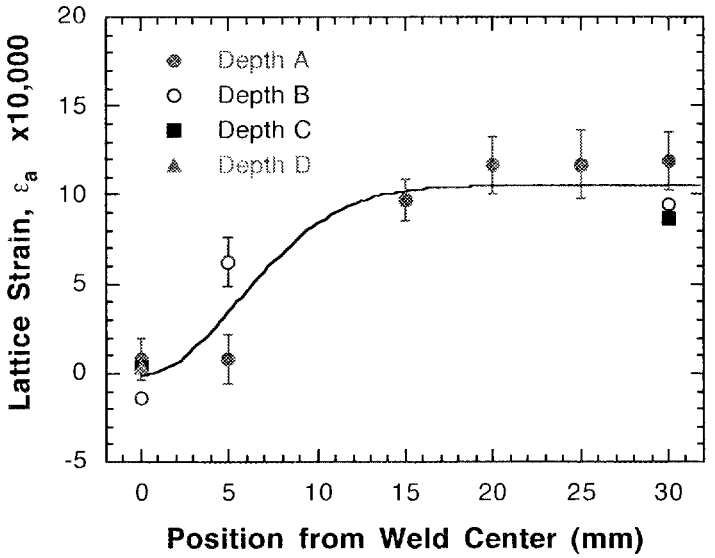

Fig. C.4. Lattice strains due to change in composition in the aluminum weld specimen.

<u>Ford Motor Company, Ford Scientific Research Laboratories</u>, "Thermal Transport Properties of Aluminum Metal Matrix Composites Used for Automotive Brake Hardware," *R. Hecht*, HTML No. 97-018

TPUC

For several years, aluminum metal matrix composite (Al MMC) materials have been considered for automotive brake applications, driven by the possibility of vehicle weight reduction and of lower brake operating temperatures. Currently, Al MMCs are used for several low-volume commercial brake applications, but their viability for more widespread use has yet to be demonstrated. A key step in the development of brake systems is modeling thermal events; material properties such as thermal diffusivity, thermal conductivity, and heat capacity are inputs to most finite element and analytical models for brakes.

At HTML, thermal diffusivity and specific heat were measured on several Al MMC materials currently used or suggested for use in automotive brake hardware. The goal was to investigate the effects of particle reinforcement type, particle volume fraction, and elevated temperature exposure on thermal transport in these materials. Specimens were cut from brake hardware provided by two manufacturers, representing six different materials: 4 SiC particle-reinforced MMCs and 2 Al_2O_3 particle-reinforced MMCs. (Four additional materials will be investigated in the coming months.) Thermal diffusivity was measured by the laser flash technique from room temperature up to 475°C. The specific heat capacity was determined via differential scanning calorimetry. Using these quantities, thermal conductivity as a function of temperature was calculated.

Room temperature thermal diffusivity varied from 0.89 cm^2/s for the SiC-reinforced materials to 0.43 cm^2/s for the Al_2O_3-reinforced materials. Thermal diffusivities of both types of materials dropped by 35% from their room temperature values at 475°C, as seen in Fig. C.5. The specific heat capacity of the Al MMCs measured via differential scanning calorimetry ranged from approximately 0.212 cal/g/°C at 100°C to 0.256 cal/g/°C at 425°C. This collection of thermal transport data provides materials properties for finite element and heat transfer modeling of new Al MMC automotive brake components.

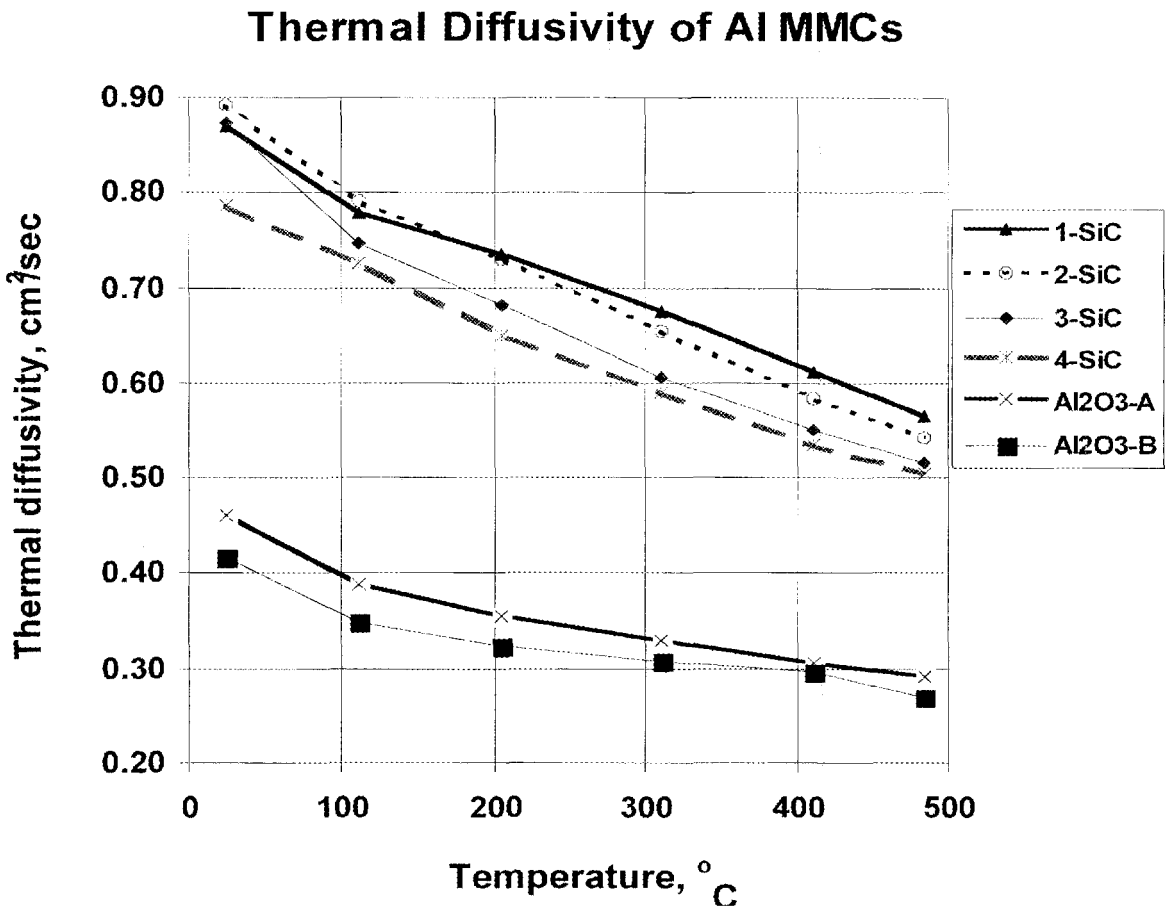

Fig. C.5. Average values of thermal diffusivity for several Al MMCs measured via laser flash.

<u>General Electric Corporate Research and Development</u>, "Effect of Gas Pressure on the Thermal Conductivity of Zirconia Coatings," *A. Mogro-Campero*, HTML No. 96-021

TPUC

Thermal barrier coatings (TBCs) are used in turbines at elevated temperatures and at gas pressures exceeding 1 atm. Because TBCs contain open porosity, their effective thermal conductivity is a function of gas pressure. There is no recent data on this effect and on its consequence for high gas pressures. This study addressed these issues.

This project originated in the last fiscal year and was completed during this fiscal year. Air plasma-sprayed samples were prepared in free-standing form, and thermal diffusivity was measured in the laser flash equipment as a function of temperature and gas pressure.

The results showed that a definite increase in thermal conductivity was observed when comparing data taken in vacuum to that at 1 atm of nitrogen. For example, the increase was 10% at 500°C. A model in the literature was used to extrapolate results to the high pressures of interest, with the result that a 30% increase can be expected at 10 atm of nitrogen. Thus, a significant effect has been shown to exist and should be taken into account when considering TBC thermal conductivity at high gas pressure.

The results have been written up and will appear shortly (A. Mogro-Campero, C.A. Johnson, P.J. Bednarczyk, R.B. Dinwiddie, and H. Wang, "Effect of Gas Pressure on Thermal Conductivity of Zirconia Thermal Barrier Coatings," *Surface and Coatings Technology*, **94-95**, pp. 102–105 (1997).

General Electric Corporate Research and Development, "Thermal Conductivity of Curved Zirconia Thermal Barrier Coatings," *A. Mogro-Campero*, HTML No. 96-041

TPUC

Thermal barrier coatings are typically applied to parts with various radii of curvature, such as nozzles and buckets. The deposition of zirconia coatings by air plasma spraying results in different microstructures of the coating depending on the radius of curvature of the part. In turn, microstructure is known to affect thermal conductivity. Published values for thermal conductivity of zirconia TBCs are for planar samples. Values of thermal conductivity for curved samples and their variation with radius of curvature are much closer to application needs, and thus more useful to designers.

Before TBCs were measured, the laser flash technique had to be tested to verify whether thermal conductivity of samples with the same microstructure but different radii of curvature give the same value. The best way to obtain these samples has been by tape casting zirconia, starting with zirconia powder. These tape cast samples proved that the laser flash method is capable of producing the same value of thermal conductivity down to at least a radius of curvature of 1 cm.

TBC samples from curved surfaces were prepared as free-standing samples and measured in the laser flash apparatus. The precision of the method is not as good as with planar samples due to polishing difficulties with curved samples. Nevertheless, the measurements showed that within experimental error, there was no difference in thermal conductivity between samples with radius of curvature down to 3 cm (the lowest that could be handled in this experiment). This conclusion applies whether the samples came from a concave or convex surface.

In actual parts of interest, there are some areas with a radius of curvature smaller than 3 cm, and these are still of concern, but we were not able to address these in this study. Nevertheless, the results obtained apply to most of the areas of interest and are important for applications. In view of the results, no publication is planned.

Kennametal, Inc., "High Temperature Contact Fatigue," *R. Yeckley*, HTML No. 97-024

MCAUC/MAUC

Cutting tool performance depends on a number of material characteristics such as hardness, chemical stability, toughness, creep resistance, and thermal expansion. Cutting tools experience temperatures in excess of 1000°C at the tool tip. Currently, high temperature deformation is evaluated by hot hardness. This technique uses a vicker indenter. Stresses with this technique are 14 GPa. These stresses are much higher than the cutting tool experiences during metal cutting. The relationship of these hot hardness tests to cutting performance is questionable. In this project, the mechanical properties group will develop a high temperature contact fatigue technique. Contact fatigue stresses in the range of 2 to 10 GPa will be used. A 1/2 in. diam SiC pin with a hemispherical end will be the indenter. Sample heating may be done with a furnace or quartz lamps. The quartz lamps would develop a temperature gradient in the sample similar to the actual application. Contact diameter dependence on time at applied stress or load will be measured. The contact fatigue stress field is similar to the stress in the cutting application. The new contact fatigue test will enable observation of fatigue differences between cutting tool materials. The fatigue performance will be compared to cutting performance. The microstructural mechanisms will be investigated using SEM and TEM. This user program will focus on evaluation of deformation resistance of silicon nitride cutting tools. The technique developed will not be limited to silicon nitride. This technique may provide unique insights into the coated cutting tool performance.

Project activity is limited to experimental setup. Room temperature evaluation of the loading rig and extensometer setup has been completed. High temperature tests will begin during the first quarter of 1998.

<u>Kyocera Industrial Ceramics Corporation</u>, "Effect of Grinding and Testing Procedures on Measured MOR of SN 282," *D. Italiano*, HTML No. 97-054

MCAUC

The purpose of this work was to perform a preliminary assessment of the sensitivity of RT MOR testing results on the test bar preparation and testing facility. Though our material SN 282 is manufactured in only two locations, ground surfaces may be either prepared and/or evaluated by a third party, such as a customer or outside vendor. When trying to provide a product having a critical material property, it is important to be certain that all evaluations of that property are accurate. For this reason, we have analyzed this issue by using Kyocera Industrial Ceramics Corporation (KICC), Chand Kare, and Kyocera Corporation (KC) as test bar preparation facilities, and KICC, KC, and ORNL as evaluation sites.

All of the test bars used in this study were longitudinally ground according to the standard grinding procedure of the grinding facility. In each case, the grinding prodedure is better than or equal to the surface quality intended by the ASTM C 1161-94 standard.

The presence of potential machining damage was investigated using two methods. Scanning accoustic microscopy was used to image subsurface cracking due to grinding. It was determined that surface roughness limits imaging ability. Improved sample preparation is expected to improve resolution and future analysis results. Resonant ultrasound spectroscopy was also unable to detect the presence of machining damage.

Grinding was evaluated by measuring surface profiles perpendicular to the grinding direction. Table C.1 shows that room temperature MOR is essentially independent of grinding within the reported range. This data represents lot 1 of the material tested at KICC with the same JIS fixture.

Flexural strength was measured at three locations using two fixture types: the ASTM C 1161-94 design was used at ORNL and KICC, while the Japanese Industrial Standard (JIS) design was used at KC and KICC. The data represent material lot 2. The difference in measured flexural strength was 21 MPa for the JIS fixture and 79 MPa for the ASTM test fixture, as shown in Table C.2. However, this level of disagreement is not surprising, as it was found to be typical, as reported in the 1993 ORNL publication, "Study of Flexural and Tensile Strength of US Silicon Nitrides." The Daytronics/microstrain gage method used in that study was employed in this study to show the effect of fixture alignment on true stress distribution. It has been determined that further analysis of this type is needed on all fixtures used in this study.

Table C.1. Surface profilometry

Grinding location	Profilometry, Ra (mic)	RT MOR (MPa)		
		Avg.	SD	n
KC	0.448	648	81	10
KICC	0.0705	634	11	10
Chand Kare	0.4175	691	88	10

Table C.2. Test

Testing Location	ASTM RT MOR (MPa)			JIS RT MOR (MPa)		
	Avg.	SD	n	Avg.	SD	n
KC				684	59	10
KICC	728	80	10	705	76	10
ORNL/HTML	649	59	9			

Materials Focus, Inc., "Characterization of Silicon Carbide Composite Systems," *L. A. Leaskey*, HTML No. 97-047

MAUC/MCAUC/TPUC/DUC

The purpose of the visit to the HTML User Center was to evaluate two different SiC-based systems as follows:

- First system: Commercial SiC-Si products

  1. to evaluate the progress relating to development of intended commercial products through measurement of strength and microstructural analyses and
  2. to further refine processing

- Second system: Potential new SiC-molybdenum silicide composites

  1. perform phase analyses to establish the presence of molybdenum silicides and
  2. compare diffusion of iron (Fe) through silicon (Si) vs molybdenum disilicide ($MoSi_2$) to evaluate potential for long term purity

For the first system, information was obtained that verified that the product development is progressing as expected and within the development schedule. The data obtained using the STA regarding volatilization of organics in our preforms allowed for modification of furnace cycles, resulting in faster and more cost effective pyrolyzation runs.

For the second system, XRD analyses verified the presence of $MoSi_2$ without any other molybdenum silicides.

The diffusion study using the electron microprobe was conducted with Si and $MoSi_2$ disks that were coated with Fe and heat-treated at 1200°C for 1 h. As shown in Figs. C.6 and C.7 for $MoSi_2$ and Si, respectively, the concentration of Fe decreases rapidly in both substrates. Also, Fe is detected in $MoSi_2$ (as represented by data points above "0 counts") only to ~50 μm below the surface, with no evidence of diffused Fe beyond that depth. For Si, Fe is detected to depths of at least 130 μm but is also clearly evident to depths of even 300 μm. Accordingly, the diffusion rate of Fe in Si is greater than through $MoSi_2$. These results could indicate improved long term purity for $MoSi_2$ as compared to Si in applications where diffusion of contaminants such as Fe is critical.

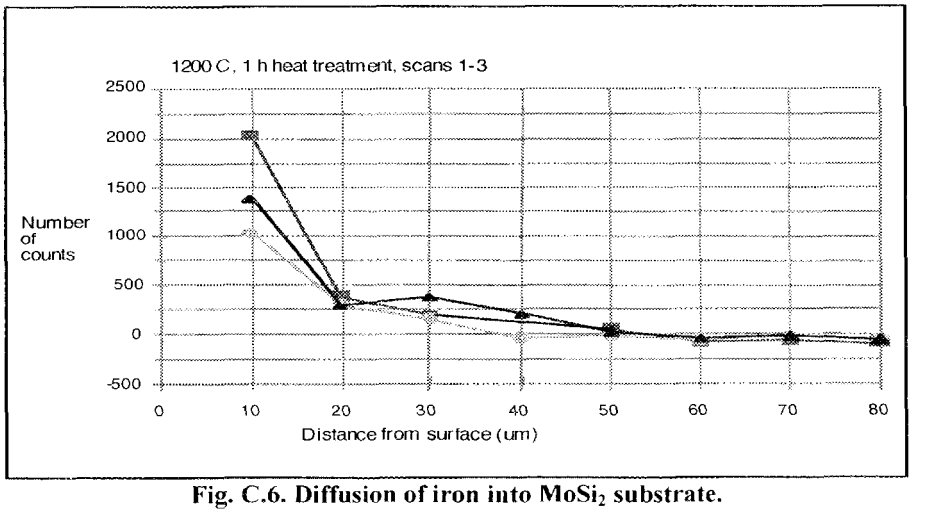

Fig. C.6. Diffusion of iron into $MoSi_2$ substrate.

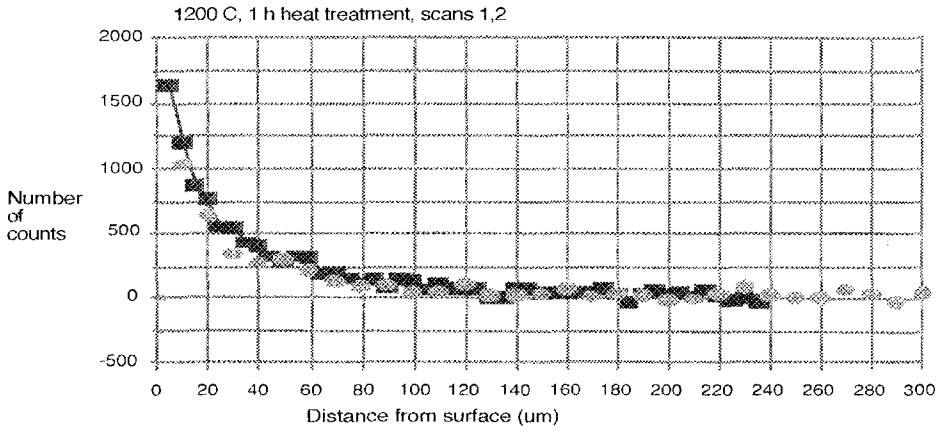

Fig. C.7. Diffusion of iron into Si substrate.

<u>Oak Ridge National Laboratory</u>, "Surface Characterization of Superconductors and Buffer Layers Deposited on Rolling Assisted Biaxial Textured Substrates (RABiTS™)," *J. E. Mathis*, HTML No. 97-046

MAUC

High temperature superconductors hold great promise in significantly reducing this nation's energy consumption. Methods are now being developed to fabricate wires of practical lengths employing these superconductors. The problem of producing HTSC wires is that the high temperature superconductors must be laid down epitaxially onto a flexible substrate. Recently, researchers at ORNL developed a method for cold rolling nickel such that the required biaxial texture is achieved. This method is called RABiTS™ for Rolling-Assisted Biaxial Textured Substrate. One of the HTSCs currently being studied at ORNL as a candidate for deposition onto RABiTS™ is barium yttrium cuprate, $YBa_2Cu_3O_7$, also known as YBCO.

Because nickel reacts with YBCO, buffer layers must be inserted between the two. These buffer layers must be nonreactive and have nearly the same lattice constants as the YBCO's. Presently, we are using CeO_2 capped with yttrium-stabilized zirconia (YSZ) as the buffer layers. The YBCO layer is deposited by pulsed laser ablation. However, the degree of 00l alignment as revealed by XRD in the YBCO is not as great with RABiTS™ as with a control substrate such as $SrTiO_3$. Moreover, the amount of current per unit area (J_c) that the YBCO/RABiTS™ combination can carry is less than for YBCO/$SrTiO_3$. It is thought that sulfur contamination on the nickel surface might be a contributing factor, as well as impurities in the buffer layers.

To determine the effect of contamination on the 00l orientation and the current-carrying capability of the HTSC, it is proposed to use Auger spectroscopy to examine the surfaces of the metal and the buffer layers before the YBCO is deposited. The plan consisists of three steps. First, after the nickel is rolled, the surface will be examined by auger spectroscopy for the presence of sulfur or other impurities. Second, the buffer layers will be applied and also subsequently examined by auger spectroscopy and XRD. Finally, the YBCO will be laid down onto the buffer layers, processed, and characterized as to its superconducting properties. Examination of the YBCO surface by SEM is also likely.

A negative correlation between the degree of contamination on the various surfaces and the critical current of the superconductor is expected to be observed. The contaminants probably will create

discontinuities and weak links in the YBCO layer, reducing the amount of current the superconductor can carry.

Thus far, we have determined by scanning auger spectroscopy that some of the nickel does indeed have contaminants on the surface. We are still evaluating whether these contaminants have a deleterious effect on the transport properties of the superconductor. We are also examining the chemical composition of the buffer layers by auger depth profile analysis to determine the degree of chemical reactivity between them.

Oak Ridge National Laboratory, "Synthesis and Characterization of Nanosized and Nanophase Ceramic Materials," *Michael Z.-C. Hu*, HTML No. 97-050

DUC

The proposed research is a project supported by a BES materials sciences program titled "Nucleation, Growth, and Transport Phenomena in Homogeneous Precipitation." This research program involves (1) fundamental studies of chemical reactive systems for synthesis of ultrafine (nanosized), monodispersed particles/powders via mainly sol-gel and chemical processing and (2) characterization of the resulting powders, gels/glasses, and nanostructured materials that are derived from the powders and gels under controlled conditions. It is anticipated that the results of this project will have significant impact upon development of advanced materials for structural and electronic applications.

The current research goal is focused on developing a new zirconia particle synthesis process that allows higher kinetics and good capability in particle morphology control. Forced hydrolysis of aqueous solutions of zirconyl salt shows the potential of generating nanocrystalline zirconia powders. Our recent studies showed that under thermal hydrolysis conditions, the aqueous-alcohol mixture solutions of inorganic salts can be analog (or alternative) systems to alkoxide systems that are usually kinetically efficient for sol-gel processing. Preliminary results showed that the addition of isopropanol into zirconyl salt aqueous solutions improved dramatically the process kinetic performance by decreasing induction period and increasing particle growth rate. Second, addition of alcohol solvent can be a method to control particle morphology. Instead of cube-shaped particles, perfect spherical particles can be produced from thermal hydrolysis aqueous-alcohol solutions. In addition, alcohol introduction into aqueous solution decreased the process thermal energy requirement because the temperature to induce the homogeneous nucleation/precipitation dropped significantly with increasing alcohol concentration. This new alternative powder synthesis route by inorganic salts opens up great opportunity in efficient production of diversified ceramic precursor powders. The microstructure and properties of the resulting powders or nanophase ceramics are closely related to the synthesis methods and processing conditions.

The HTXRD is extensively utilized for characterization of powder materials produced from various homogeneous precipitation routes, including hydrolysis/condensation of alkoxide, forced hydrolysis, and homogeneous nucleation and growth in inorganic salt solution of mixed alcohol-water system. The sample powders may be either amorphous or crystalline, depending on the synthesis conditions. We need to know the similarities or differences among these powder samples, in terms of (1) phases existing for various nanosized ceramic precursor powders, (2) size determination of primary crystallite if the particles are polycrystalline, and (3) phase transformation with temperatures.

The results showed that cube-shaped zirconia powder from forced hydrolysis is monoclinic, while the microsphere powders from alkoxide or from the mixed solvent system are amorphous. With increasing temperature from room temperature to 1200°C, the cube-shaped powder showed unique nucleation and monoclinic nanocrystal growth. No tetragonal phase was observed until 1200°C. This new finding on the monoclinic phase evolution with temperature is different from the traditional zirconia phase transformation pathway. For the microsphere powders produced by alkoxide/ethanol, only tetragonal phase appeared during heating from 600 to 1400°C. Phase transformation of microsphere powders synthesized by the homogeneous precipitation in inorganic salt solutions of mixed alcohol-water strongly depends on the synthesis conditions. Less aged powders or gels (produced at short incubation and low RH

conditions) showed the evolution of co-existing monoclinic and tetragonal phases with increasing the calcination temperature from 400 to 1400°C. However, the well-aged powders (produced after long incubation and at high RH conditions) showed the evolution of only tetragonal phase from ~400 to 1400°C. This work was presented in the 22nd Annual Cocoa Beach Conference & Exposition, January 20–24, 1998, Cocoa Beach, Florida.

Oak Ridge National Laboratory, "Residual Stress Measurements on Rapidly Formed H-13 Die Steels," *P. J. Maziasz*, HTML No. 97-063

RSUC

Direct fabrication of functional tooling and die components with superior properties from commercial die-steels like H-13 is one of the objectives of a unique joint effort involving the ORNL, Sandia National Laboratory (SNL), and the Idaho National Environmental and Engineering Laboratory (INEEL). INEEL has developed a process for spraying molten metal, while SNL has developed a process based on laser welding of fine powder sprays [laser engineering net shaping (LENS)]. ORNL characterizes and interprets the properties behavior of these new directly fabricated steel parts.

There is a distinct need for optimizing the combination of deposition rate and final surface detail when the two direct fabrication processes are combined, with LENS material being deposited on spray-formed material. However, despite good properties for steel made by each native process, there has been a tendency toward cracking at the interface when the two are combined. The objective of this project has been to use the unique neutron-diffraction residual strain measurement facilities at ORNL to determine the role that residual stresses might play in such interfacial behavior. A piece of spray-formed H-13 steel with LENS deposits of the same material on both surfaces is shown in Fig. C.8. Neutron-diffraction measurements of micro-strains across this specimen show very large strain (and hence stress) differences across the interfaces in Fig. C.9, which would contribute to cracking. These H-13 die-steel have yield-strengths at lower temperatures of 240–270 ksi (1660–1870 MPa), so that enormous elastic strains can build up due to processing-induced thermal gradients. This project will conclude by comparing these measured strains to the native processing-induced residual strains found in monolithic LENS and spray-formed materials.

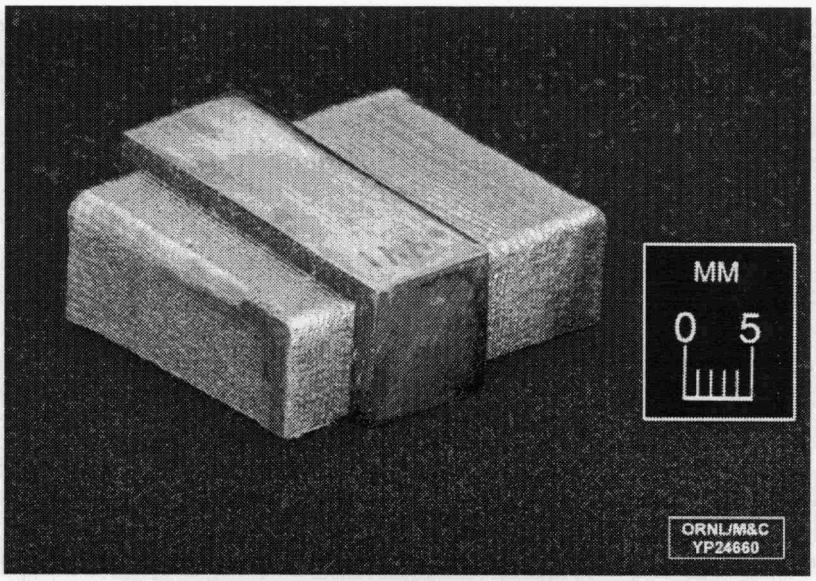

Fig. C.8. Composite sample of spray-formed H-13 steel (center) with LENS deposits of H-13 on polished (left) and as-formed (right) spray-formed surfaces.

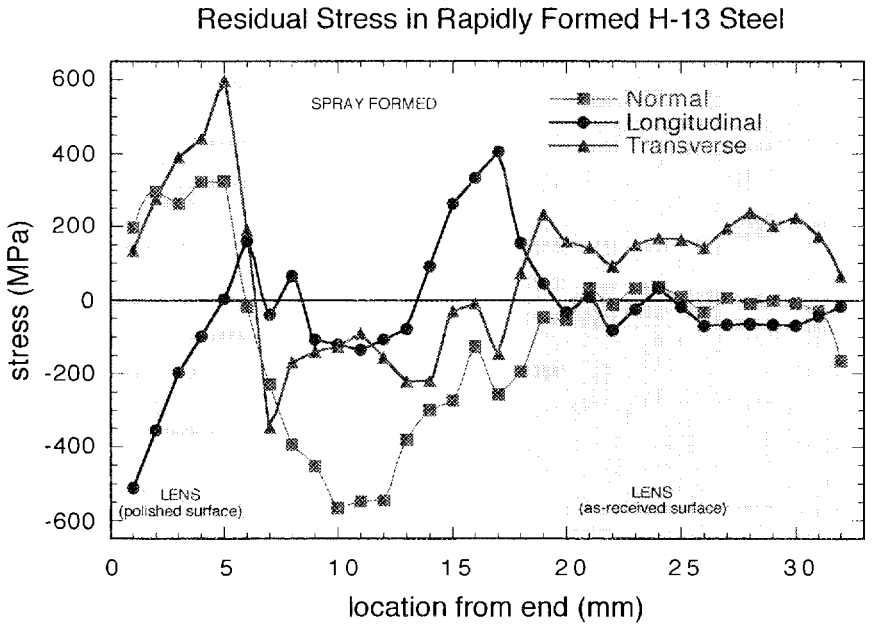

Fig. C.9. Residual stresses determined by neutron diffraction in LENS-spray-LENS composite. The stress gradients are much higher at the polished interface (left) than the as-formed interface (right) between the LENS-formed and spray-formed material.

<u>Oak Ridge National Laboratory</u>, "XRD Study of the Stability and Thermal Properties of Perovskite-Type Materials at High Temperatures," *M. Z.-C. Hu*, HTML No. 97-068

TPUC/DUC

The perovskite-type materials have many uses ranging from structural to functional ceramics. Many technological devices or processes that utilize the perovskite-type materials operate at elevated temperatures. The perovskite-type materials incorporate oxide sublattices required to sustain high oxygen fluxes. At elevated temperatures, perovskite-type membranes are semipermeable to oxygen while being impervious to other gaseous components. Examples include mixed conductors for ceramic membranes designed to separate oxygen from air, oxide electrodes for solid oxide fuel cell, electrolyses, oxygen pumps, and amperometeric oxygen monitors.

The stability and thermal properties of these perovskite-type materials at high temperatures are very important. Generally, the perovskite-type materials are not very stable at high temperatures and have large thermal expansion coefficients. During preparation of inorganic membranes used in membrane reactors for simultaneous catalysis and separations, chemical compatibility of perovskite-type material top layer to the support material is another challenging issue. These properties of perovskite-type materials have limited their applications.

The current research goal is focused on developing perovskite-type materials with good stability and low thermal expansion coefficients by optimization of composite powder preparation and material compositions.

Various powders of $La_{1-x}Sr_xCo_{1-y}Fe_yO_3$-based perovskites with different compositions have been prepared by solid reactions and citric acid coprecipitation routes. The powder size and size distribution were controlled. The powders were then calcined at high temperature to form the specimens to be characterized by HTXRD in order to investigate the following issues:

- the stability of materials in air at different temperatures (30 to 1400°C);
- the effects of oxygen concentration on the stability of materials at different temperatures;
- the effects of preparation method of powder on the stability of materials; and
- the thermal expansion of materials.

Data analysis showed that the presence of zirconia in the perovskite materials seems to improve the thermal stability. In oxygen-deficient atmosphere, the perovskite lost its stability after sequential heating from room temperature to 1350°C. The lattice thermal expansion coefficients were determined by analyzing XRD data. However, further data are needed to elucidate the mechanisms that are responsible for the thermal stability and expansion.

The proposed research is one of the projects that are supported by a BES materials sciences program titled "Nucleation, Growth, and Transport Phenomena in Homogeneous Precipitation." The results of this study will help improve the lifetime and catalytic property of the perovskite-based inorganic membrane reactor.

PPG Industries, Inc., "Compressive Creep Testing of Fusion-Cast Alpha-Beta Alumina Material," *G. A. Pecoraro*, HTML No. 94-061

MCAUC

There has been a need to rate competitive magnesite (MgO) refractory products for resistance to linear subsidence under load because of more aggressively operated glass furnace regenerators (crowns and checker packing). Because these materials are subjected to elevated temperatures and stresses during service, engineering data representing the deformation behavior are needed for accurate superstructure design and confident prediction of furnace life expectancy. The test conditions offered by each refractory supplier are sometimes not comparable to others, and often there is the question of precision and credibility of the published results. The HTML user gave PPG materials engineers the resources to accomplish this work using state-of-the-art equipment and highly qualified personnel. The compressive creep responses of commercially available magnesia refractories were measured in ambient air in excess of 1400°C (2550°F).

The creep measurements were taken using a high-temperature extensometer in conjunction with a load-train rack. The resolution of the extensometer was approximately 0.00004 in. at temperature. Much time and effort was expended to achieve a stable signal. A closed-loop, self-dedicated water chiller was installed into the cooling system.

The creep resistance of so-called equivalent magnesia refractories was found to vary substantially. At the lowest stress level, the creep rate of the most resistant refractory was more than an order of magnitude better than the worst. At the highest stress, the slowest creep rate was still about four times slower than the fastest. The stress exponents for all the magnesite refractories was approximately unity. The two most creep-resistant brands had the combination of largest grain size and widest grain size distribution.

The impact of this research is a screening out of inferior products from the subsidence-under-load standpoint. PPG now has more information on which to base its selection of magnesite refractories for checker applications.

Quantum Peripherals Colorado, Inc., "Measurements of Intrinsic Film Stress, Crystallographic Texture, and Crystallite Size in Sputtered Permalloy-Based Thin Films," *J. Doyle* and *E. L. Brown*, HTML No. 95-055

RSUC

Magneto-restrictive heads are often fabricated with Permalloy™, which is a permanent magnet material. Thin-film (<1 μm) Permalloy-based compositions are deposited in multilayer configurations. As

device technology advances, production tolerances become more stringent, and demands upon material performance increase. Thus, crystallographic texture and residual stress all impact the magnetic properties of these thin films and are of concern to device fabricators. The objective of this research was to determine the orientation, intrinsic film stress and crystallite size of NiFe-based sputtered thin films as a function of chemical composition and film thickness.

In this study, the Ta layers in NiFe/Ta, NiFeMo/Ta and Ta/NiFe/Ta/NiFeMo/Ta thin-film specimens were characterized at ORNL/HTML's X-14A beamline at the National Synchrotron Light Source at BNL. The high intensity of the synchrotron X-ray source allowed for adequate signal from the thin Ta layers in these specimens, which could not be achieved with conventional laboratory sources. The Ta layers deposited on an alumina substrate (NiFe, NiFeMo) possess either an α or β-Ta crystal structure in either a (110) or (202) preferred orientation, respectively. In contrast, deposition of Ta on a (111) NiFe(Mo) substrate would seem to result in the formation of a (200) β-Ta texture component. This result represents either a crystal structure or orientation transition with substrate type. This information will be correlated with magnetic property and TEM measurements in an effort to understand and manipulate deposition conditions to obtain films with enhanced magnetic properties. This study is complete.

Soil and Land Use Techologies, Inc., "Thermal Expansion of Ettringite," *N. Shashidhar*, HTML No. 97-001

DUC

The thermal expansion of the mineral ettringite is thought to contribute to the deterioration of concrete structures. Consequently, temperature-dependent changes in the ettringite crystalline lattice are of interest to organizations such as the Federal Highways Administration in order to understand the contributing factors to the high maintenance of the national transportation network.

HTXRD was used to examine the lattice parameters of the mineral at temperatures from 25–80°C. At higher temperatures, or at moderate temperatures over time, dehydration of the crystal collapsed the structure. Refinement of the lattice parameters was possible over a limited temperature range. Additional XRD experiments will be undertaken at temperatures from 0–25°C, utilizing a newly acquired thermoelectric cooling stage for the X-ray diffractometer, in order to more fully characterize the thermal expansion.

TEC, Inc., "Near-Surface Neutron Residual Stress Measurements in a 40-mm Diameter Fatigue Test Reference Specimen," *E. B. S. Pardue*, HTML No. 96-043

RSUC

One materials test used in the development of heavy equipment calls for an SAE standard fatigue test of large diameter steel rods. The steel fatigue specimens under investigation are induction-heat-treated to form a partially penetrating martensitic layer. The presence of heat-treating residual stress in the fatigue specimen has a big influence on fatigue test results. Hole drilling methods for determination of residual stress below the surface have recently been developed. The present work is part of a residual stress validation effort with intercomparison of X-ray diffraction, holographic hole drilling methods, and neutron residual stress methods.

Neutron measurements can give results that overlap the near surface X-ray residual stress measurements and the relatively new interior measurements with holographic hole-drilling methods. With a 40-mm diam fatigue specimen, a novel geometry must be used to achieve the required spatial resolution in the neutron method to make comparison with the X-ray and holographic methods. Two perpendicular strains parallel to the surface were measured with a plate-like gage volume 3 × 3 mm by 0.5 mm thick, with the plate parallel to the specimen surface. The strain perpendicular to the surface was measured with

a tall gage volume 1 × 1 mm by 5 mm tall. Test points were chosen at depths to 2.5 mm and at several positions along the length of the fatigue specimen in the gage section.

The neutron residual stresses showed small variation with depth and little variation along the length of the gage section. The axial and circumferential stress components were about 550 ± 100 MPa in compression with no obvious difference between the two components. The surface normal stress was zero within a spread of ±100 MPa. There were two weak trends in the residual stresses within the estimated variance. The circumferential stress was slightly less compressive than the axial stress, and both these stresses became less compressive with depth.

The X-ray and holographic residual stresses differ from neutron results in several ways. In the X-ray results, axial stresses are about 850 MPa, and the circumferential stresses are about 450 MPa. Holographic hole drilling stress results were measured over 1 mm depth. The ratio of the two orthogonal in-plane stresses was about half the equivalent ratio found in the X-ray results. The holographic stresses (500 MPa to more than 800 MPa) were larger than the neutron stresses. The absence of differences between the axial and circumferential stresses measured with neutrons suggests that further consideration of the use of a plate-like sampling volume parallel to a cylindrical surface may be required.

UES, Inc., "Tribological Properties of Solid Lubricant Coatings Over a Wide Range of Temperature," *R. S. Bhattacharya*, HTML No. 97-004

MIRUC

Advanced jet engines require lubricants that can function over a wide range of temperature, subambient to 800°C. Lubrication at such wide temperature range can only be attained by using appropriate solid lubricants. The maximum useful temperature for most common solid lubricants such as MoS_2, WS_2, etc., are limited to about 400°C under favorable conditions in air atmosphere. Some oxides and fluorides have been identified for higher temperature applications. These are: MoO_3, TiO_x, CoO, ZnO, ZrO_2, LiF, CaF_2, and BaF_2. Use of oxides and fluorides has been limited because of their lubricating ability within a narrow temperature range. Also, the friction coefficient of most of these oxides even at high temperatures is rather high, ~0.2-0.4. The objective of this work is to explore the concept of encapsulation of low temperature lubricants such as MoS_2 and WS_2 with high-temperature oxide lubricants. It is expected that the oxide lubricant phase will protect MoS_2 or WS_2 from oxidation at high temperature, while providing a low-friction corresponding to that of MoS_2 or WS_2 by dynamic exposure of these materials in the contact region. Also, it is possible that a metal-molybdate or tungstate can form in the contact region during friction at high temperatures. Some of these molybdates and tungstates are quite stable at high temperature under oxidizing environment and can provide low friction.

Thin films of MoS_2-ZnO were prepared by sputtering on high-speed steel and Si_3N_4 substrates. Both uniformly mixed and layered structures were prepared by using deposition from two sputter sources. The films were characterized for composition by auger electron spectroscopy. Selected films were subjected to friction tests at temperatures in the range room temperature to 700°C in air utilizing the controlled-atmosphere high-temperature tribometer at HTML. Results obtained so far indicate that layered ZnO+MoS_2/ZnO coating performed better at high temperature than the mixed composite coatings. Friction coefficients were in the range 0.2 to 0.3 at temperatures below 400°C for coated M50 substrate against uncoated ball. At higher temperatures, the friction coefficient increased to ≥0.4 for coated Si_3N_4 substrate against uncoated Si_3N_4 ball. Further measurements of friction and wear will be performed at HTML using films with optimum compositions of oxides and sulfides.

Westinghouse Power Generation, "Thermal Conductivity Measurements on Thermal Barrier Coatings," *Evan Ludeman, K. Sloan*, and *Ramesh Subramanian*, HTML No. 96-027

TPUC/RSUC

Westinghouse Power Generation conducted thermal diffusivity measurements on their alternative TBCs at TPUC. Eighteen specimens were tested by the laser flash diffusivity system. The specimens were free-standing coatings, about one-half inch in diameter and 300 μm to 500 μm thick. Submicron graphite coatings were applied to both sides of the specimen to make it opaque. At room temperature, the as-sprayed specimens showed very low thermal diffusivity values, ranged from 0.005 to 0.006 cm^2/s. Thermal aging at 1200°C to 1300°C for 24, 72, and 240 hours were performed at Westinghouse. Thermal diffusivity of the thermally-aged specimens were found to be increased as a function of aging temperature and time.

The as-sprayed coatings and thermally-aged coatings were both tested to 1200°C in argon. The effects of aging were observed on these alternative coatings. Thermal diffusivity decreased as a function of temperature up to 600°C and showed a slight increase after 600°C dependent on the previous heat treatment. Thermal diffusivity vs temperature curves of a stabilized zirconia are shown in Fig. C.10. The hysterisis effect was observed in as-sprayed specimens. Thermal diffusivity increased nearly 60% after aging. The thermal aging is believed to be a result of grain growth and further densification of the ceramic coatings at elevated temperatures. Understanding of the aging effect on thermal conductivity of TBCs is very important to the engine designers. The results provided valuable information to Westinghouse in selecting the best candidate for high performance TBCs.

Specific heat capacities were measured at HTML using the differential scanning calorimeter (DSC). Specimens consisted of 4-mm diam, 2-mm thick disks that were heated at 20°C/min. Heat capacities were calculated using the ratio method with sapphire as the reference standard.

In RSUC, the phases within the ceramic top coats deposited via EB-PVD and air plasma spray were determined for as-received and heat-treated samples.

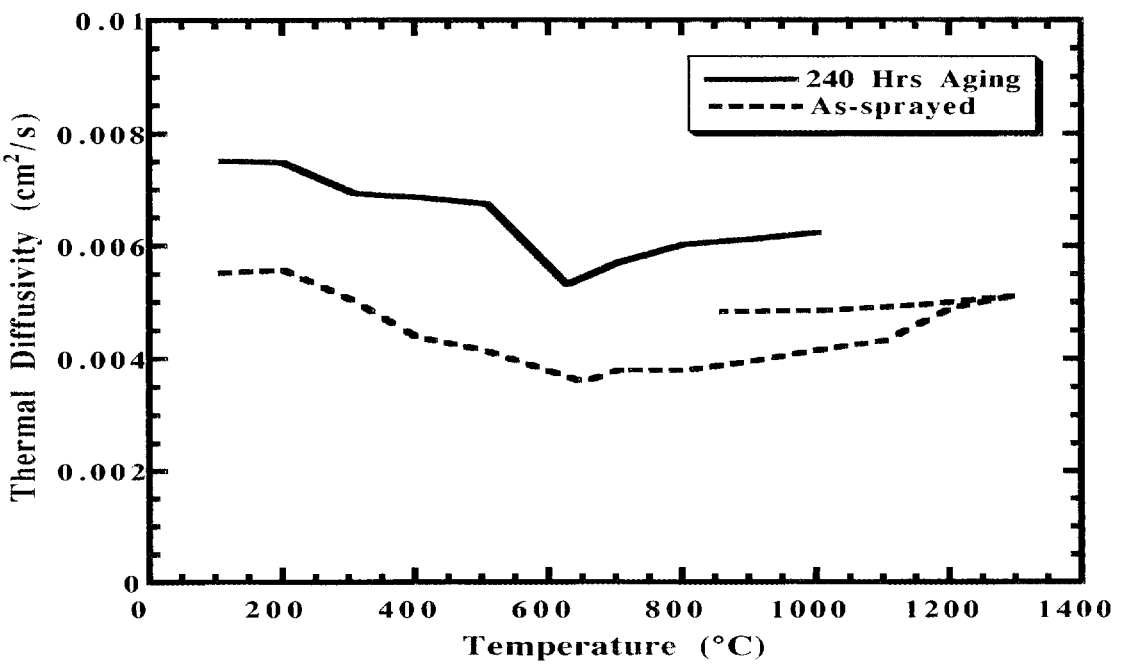

Fig. C.10. Thermal diffusivity of APS coatings before and after thermal aging.

Westinghouse Electric Corporation, "Life Determination of Thermal Barrier Coatings in Fatigue," ***M. Arana*****, HTML No. 96-047**

MCAUC

Thermal Barrier Coatings (TBCs) are an integral technological component of advanced energy efficient low-emission combustion turbine technology. As design strategies progress from using TBCs primarily for the life extension to taking full advantage of the TBC in thermal design, requirements for TBC reliability will increase markedly. To address the development of advanced, high reliability TBC systems, Westinghouse has been contracted by DOE to develop improved compositions, application processes, and life prediction models. The subject of this user project is to generate fatigue life data on TBC specimens to assist in development and validation of the TBC life prediction model.

The approach taken here will use a compression/compression fatigue on a tubular substrate/bond coat/thermally grown oxide (TGO)/TBC in a strain controlled mode to a series of preselected strains at two temperatures. Failures are expected to consist of coating spallation. Failure detection will be by infrared camera system. The principle data required will be cycles to failures vs strain range.

Successful acquisition of these data points will imply a step forward to the final decoupling between fatigue and diffusion-induced failure modes. This is a key step in the future development of a life prediction model. Simultaneously, determination of the cycles to TBC spallation under fatigue conditions will form the baseline of a database to determine refurbishing and inspection periods.

UNIVERSITIES

Alabama A&M University, "X-ray Study of MeV Ion Bombarded GaAs/AlGaAs Quantum Layers," *A. T. Taylor* and *D. Ila*, HTML No. 96-014

RSUC

A scientist from Alabama A&M University visited the Residual Stress User Center to measure changes in lattice parameters of GaAs single crystal due to 8.0 MeV C bombardment and relate these changes in the measured index of refraction. The region of interest is the electronically damaged region (top 5 μm) of the implanted crystal. Mechanisms for these changes could be atomic mixing due to localized heating from the implantation event, defects, and/or residual stress. After sample orientation, the GaAs peak positions of (220), (311), and (620) were measured for the ion-implanted and the as-received sample. This project is complete.

Alfred University, "Characterization of Fe Impurities in AlN Using EXAFS," *T. C. Bruss, S. T. Misture*, and *J. A. Taylor*, HTML No. 97-005

DUC

Aluminum nitride is of great interest in the field of electronic ceramics because of its unique combination of high thermal conductivity and high electrical resistivity. Direct nitridation of Al is a low cost alternative to traditional sol-gel processing. However, this processing technique typically produces AlN powders with Fe impurities that originate in the Al metal. Metallic impurities have a detrimental effect on the aforementioned properties. A first step in removal of these impurities is identification of the chemical state of the impurities. Since the impurity levels are rather small (<500 ppm), X-ray diffraction techniques from laboratory instruments were unable to detect Fe or any Fe-containing compound, possibly because the phase is amorphous.

Extended X-ray Absorption Fine Structure (EXAFS) is a powerful technique for identification of phases and compounds containing a specific element as well as determination of the local structure (short-range order) about a given atomic center in all states of matter. EXAFS has been used to detect Fe impurities in silicon nitride and Ti impurities in AlN, for example. EXAFS data was collected at ORNL/HTML's X14A beamline located at the National Synchrotron Light Source at Brookhaven National Laboratory. EXAFS analysis and absorption edge positions were used to unambiguously determine that metallic iron is present in AlN produced by direct nitridation. Based on these results, vapor-phase acid leaching was used to remove the Fe without significant degradation of the AlN.

Alfred University, "Field-Induced Strain Mapping of Piezoelectric and Electrostrictive Materials Using Neutron Diffraction," *S. Misture*, HTML No. 97-022

University of Cincinnati, "Neutron Diffraction Study of High Strain Materials," *C. T. Blue*, HTML No. 97-026

RSUC

Recent studies on electrostrictive materials have led to the use of $Pb(Mn_{1/3}Nb_{2/3})O_3$-$PbTiO_3$-$(Ba,Sr)TiO_3$ (PMN-PT-BT) in major transducer systems. Such electrostrictive materials are considered good candidates to replace piezoelectrics because of their increased strain response with electric field. However, the application of these materials has been limited by poor electromechanical coupling, and there are many unanswered questions regarding the performance and power generation capabilities of the PMN material.

These two projects were very similar in scope, and, with the agreement of both users, a collaborative experimental plan was established. Experiments were undertaken using the neutron strain-mapping facilities at the High Flux Isotope Reactor to determine the dc field dependent strains under applied electric fields for piezoelectric PZT and electrostrictive PMN samples produced by Lockheed Martin Ocean, Radar, & Sensor Systems Company. Neutron diffraction provides a means of determining strain as a function of direction and *hkl* within bulk electrostrictive materials under applied dc fields, which was used to correlate microscopic strains with macroscopic strains measured using strain gages. Strain components normal and parallel to the field were measured as a function of applied field up to 1.2 kV/mm. The (400), (220), (310), and (222) reflections of PMN were measured and used to determine the maximum microscopic strain response of polycrystalline PMN. The neutron diffraction strain data has been compared to the macroscopically-measured strains determined using strain gauges as an initial step towards understanding the poor electromechanical coupling of PMN materials.

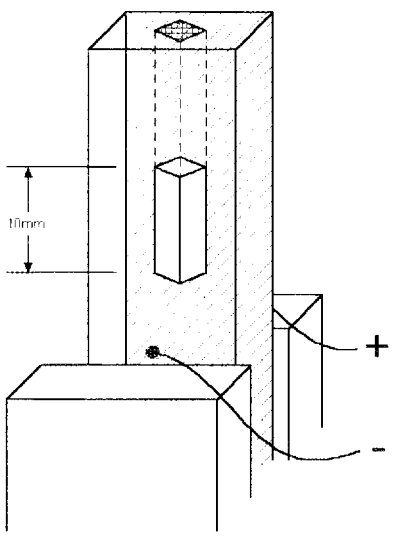

Fig. C.11. Experimental layout.

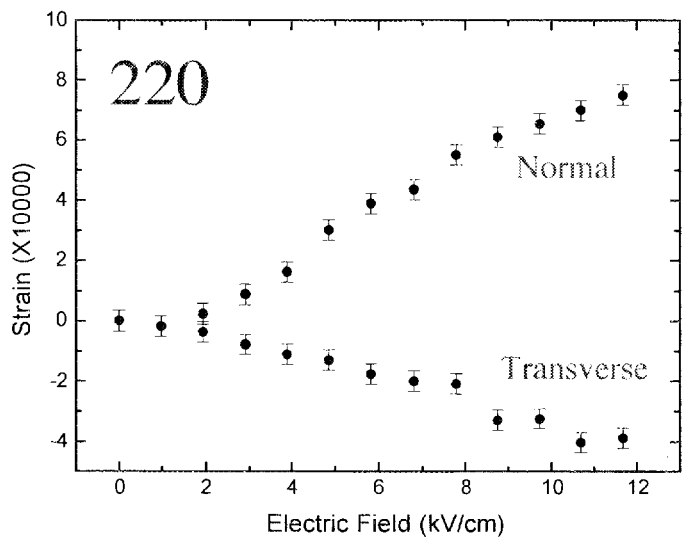

Fig. C.12. Strain in the <220> direction measured normal and transverse to the applied field direction.

<u>Drexel University</u>, "High Temperature X-ray Characterization of Ti_3SiC_2 and Ti_2AlN," *M. W. Barsoum* and *T. El-Raghy*, HTML No. 97-045

DUC

The objectives of this proposal are twofold. The first is to refine the structures of Ti_3SiC_2 and Ti_2AlN using X-ray and neutron diffraction studies. The second is to measure the lattice parameter changes in these compounds as a function of temperature.

Until recently, Ti_3SiC_2 had not been available in fully dense form, single-phase bulk quantities, and therefore its potential for high temperature applications was unknown. Recently we fabricated fully dense, predominately single-phase samples of Ti_3SiC_2, and preliminary characterization has shown it to be a ternary compound with a unique set of properties: machinability similar to that of graphite; oxidation resistance at 1000°C comparable to chromium; a compressive yield strength of about 500 MPa at 1300°C accompanied by significant high temperature ductility; and nonsusceptibility to thermal shock. Needless to say, this combination of properties render this material an attractive candidate for a variety of high-temperature structural applications and creates the immediate need for a detailed characterization study to

understand the physical origin of these properties. Clearly, knowledge of the exact crystal structure and how it varies with temperature is of great value for understanding the structure/property relationships in these materials.

Since our first reports on Ti_3SiC_2 we have also shown that, as a class, the closely related 211 phases or M_2BX, where M is a transition metal, B is B-group element, and X is either carbon or nitrogen, have a lot in common with Ti_3SiC_2. The two structures are compared in Fig. C.13; both are hexagonal with one or two layers of the transition metal carbide or nitride alternating with two dimensional hexagonal nets comprised of the B-group element.

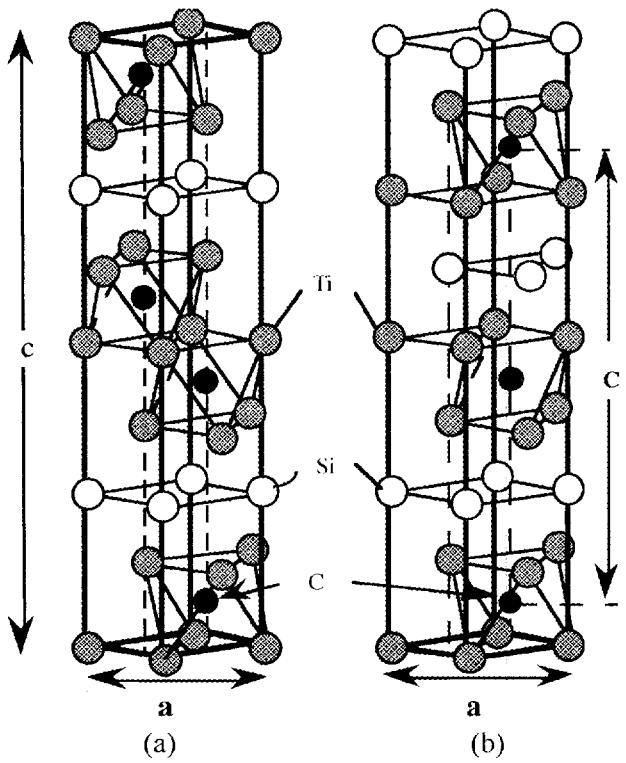

Fig. C.13. Unit cells of (a) 312 and (b) 211 phases. In the 312 phases, there are three layers of the transition metal; in the 211 phases, there are only two.

The initial aim of this work was to carry out a detailed X-ray diffraction study on Ti_3SiC_2 and Ti_2AlN. Fabrication of the latter, however, was complicated by its dissociation. Consequently, Ti_2AlC, which was much less prone to dissociation, was chosen instead. The X-ray powder diffraction data for Ti_3SiC_2 and Ti_2AlC have been collected and are currently being analyzed.

Using X-ray powder diffraction, we have identified that both samples contain at least three phases. The Rietveld analysis of Ti_3SiC_2 has confirmed the known structure. It is worth noting that we have confirmed discrepancies between the observed X-ray powder diffraction pattern and the ICDD-PDF card. Our X-ray powder diffraction pattern calculated from the structure fits our collected data. Thus the Rietveld analysis with a new powder diffraction pattern will result in at least one archival journal publication plus a revised reference pattern for the PDF. At this stage, it is premature to explore site occupancies. The latter will be determined from the planned synchrotron X-ray and neutron diffraction studies.

The effect of temperature on the lattice parameters is shown in Fig. C.14. A least square fit of the results indicated that the lattice expansion is quite linear with:

$$\alpha_c = 7.9 \times 10^{-6}\ °C^{-1} \text{ and } \alpha_a = 6.7 \times 10^{-6}\ °C^{-1}$$

It is not too surprising that there is an anisotropy in the lattice thermal expansion coefficients. However, given the extent of anisotropy in elastic constants, that preliminary results have shown to be at least an order of magnitude lower along the c-direction than along the a-direction, the anisotropy in thermal expansion is quite modest. The reason for this state of affairs is unclear at this time.

Based on these results, the average calculated polycrystalline linear thermal expansion coefficient of Ti_3SiC_2 is $\approx 7.1 \times 10^{-6}\ °C^{-1}$. This value is lower than the thermal expansion coefficients we have previously measured for bulk samples of Ti_3SiC_2. Another important conclusion of this work is that we have ruled out any high-temperature structural transformations in Ti_3SiC_2, at least up to 1200°C.

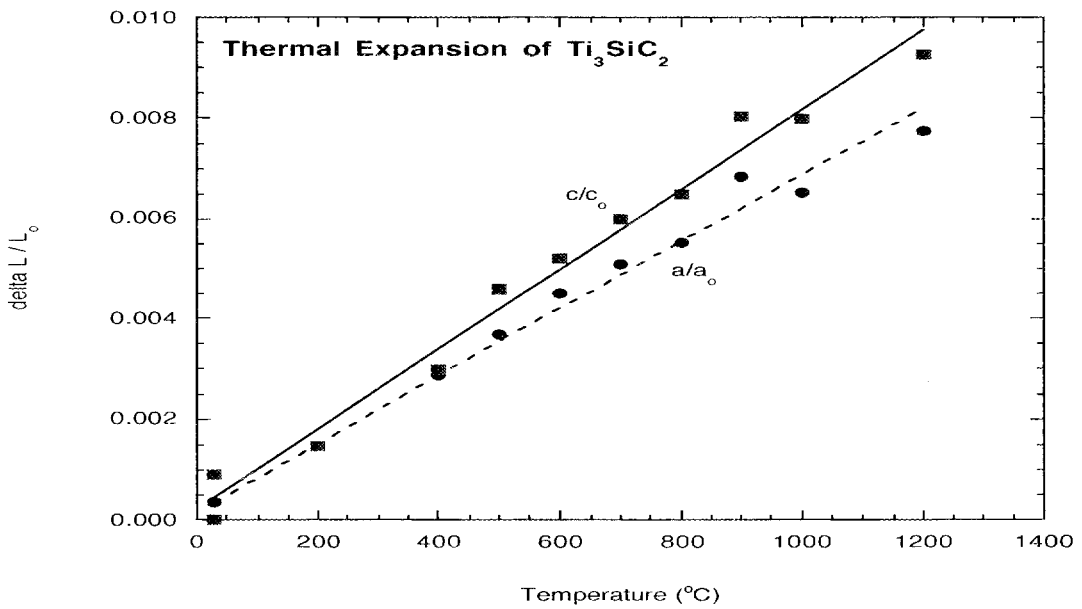

Fig. C.14. Lattice parameter changes as a function of temperature for Ti_3SiC_2.

<u>Georgia Institute of Technology</u>, "The Effective Thermal Conductivity of Damaged Composites," *D. McDowell*, HTML No. 95-092.

TPUC

Continuous fiber-reinforced ceramic composites are currently under development to extend the performance and efficiency of gas turbine and rocket engines. Even under normal operation, these materials undergo irreversible deformation processes or damage. These processes act to dissipate stored strain-energy in the material, thus providing a measure of toughness. Such inherent processes not only affect the mechanical properties, but also the thermal properties of the material. Because of the high temperature applications of these materials, it is desirable to understand the changes in thermal conductivity with damage. The degradation of thermal conductivity may lead to increased temperature gradients and thermal stresses in these materials. The augmentation of thermal stresses may influence crack stability in damage-affected zones. For accurate life prediction, it is imperative to understand the

role that degraded thermal conductivity plays in the coupled thermomechanical behavior of advanced materials at high temperatures.

An experimental program is under way that will characterize the change in thermal conductivity for carbon-coated Nicalon™-reinforced lithium aluminosilicate glass and silicon carbide-boron nitride-coated Nicalon-reinforced barium magnesium aluminosilicate glass composites. Damage in the form of matrix microcracking, fiber matrix debonding, and fiber breaks are being introduced into the materials through fatigue deformation.

A new experimental procedure has been developed at HTML based upon the radial flash technique whereby the in-plane thermal properties of a composite can be measured nondestructively. The technique involves numerically fitting the temperature ratio of two points as a function of time following localized heating of the sample. This procedure will facilitate unique experiments whereby the diffusivity of fatigue-damaged samples can be measured while under static and fatigue loading.

An experimental validation of the in-plane thermal diffusivity measurement technique has been completed. Measurements were then made on SiC-BN-Nicalon/BMAS to determine the principal in-plane thermal diffusivities (see Fig. C.15). A comparison of the experimental results were made with the standard flash thermal diffusivity techniques. The experimental data were obtained at room temperature using the xenon flash system. The in-plane diffusivity method predicted a diffusivity value of 0.0099 cm^2/s in the fiber direction, while the one-dimensional technique provided a value of 0.0098 cm^2/s. Transverse to the fibers, the in-plane method predicted a thermal diffusivity of 0.0086 cm^2/s, whereas the one-dimensional technique provided a value of 0.0085 cm^2/s. These results show that the nondestructive in-plane diffusivity measurement technique is a viable procedure whereby the thermal diffusivity can be obtained for principal in-plane directions.

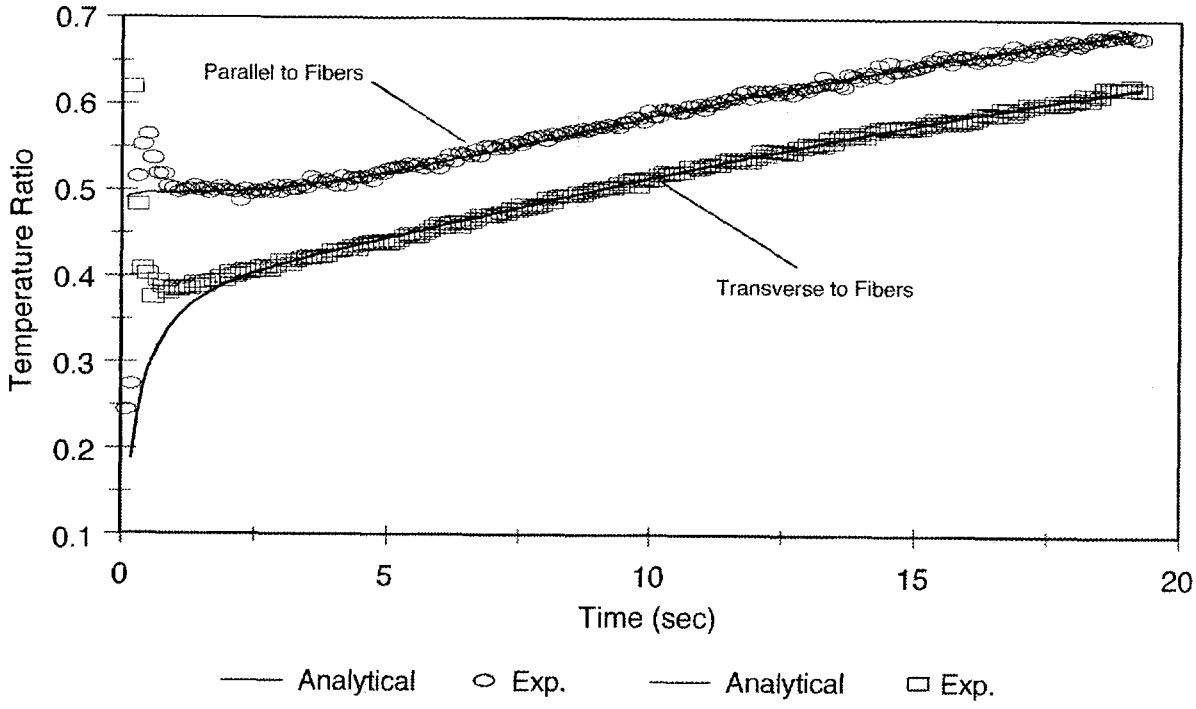

Fig. C.15. Experimental and predicted in-plane temperature ratios of SiC-BN-Nicalon/BMAS.

Illinois Institute of Technology, "Thermal Properties of Lithium Ion Battery and Components," *Hossein Maleki, Said Al Hallaj, Jong-Sung Hong*, and *J. R. Selman*, HTML 97-028

TPUC

Illinois Institute of Technology conducted studies of the thermal properties of lithium ion battery materials at TPUC. Thermal properties values (Cp and a or k) are needed in order to model the thermal behavior of a battery system for high-power applications. To our knowledge, no detailed experimental thermal diffusivity or thermal conductivity data are available in the public domain for the Sony US-18650 lithium-ion battery and components.

The main objective of thermal analysis is to arrive at designs that avoid significant heat accumulation, in particular when scaling up to sizes suitable for power tools and electric vehicles. This means that the heat transport properties of electrode materials of the candidate battery should be determined. Battery systems of 100Wh/kg density and 100W/kg power density suitable for electric vehicle applications are being developed. The lithium-ion system of ($Li_xC/Li_{1-x}CoO_4$) would be suitable if the capacity could be two/three orders of magnitude higher than its present value of 1.37Ah.

A successful rechargeable battery technology of high-energy density has been developed based on the lithium-ion battery (rocking chair cell). This cell consists of a negative electrode (NE), a positive electrode (PE) and a porous separator (Sp). On charging, lithium ions deintercalate from the PE and intercalate into the NE; the reverse takes place on discharging.

Two different methods of Cp measurement applied to the Sony battery were used: transient temperature measurement and adiabatic calorimetry. Two methods were used to obtain k values for components of the same battery. In the first method, the cross-sectional k was determined by applying a known heat flux across the surface of PE/Sp/NE layers, and sampling the temperature difference at a known location between the stacked layers. In the second method, both cross-sectional and in-plane k values were calculated from cross-planar and planar-thermal diffusivity values measured by the xenon flash technique with and without electrolyte.

The heat capacity of this battery depends on its state of charge and increases by 8% as open circuit voltage (OCV) changes from 2.75 V to 3.75 V. Thermal conductivity of the NE material depends more strongly on the state of charge than that of the PE material. The cross-sectional thermal conductivity of an electrolyte-filled PE/Sp/NE assembly is 3.4 W/mK. Thermal conductivity along the planar direction of the stacked layers of all the battery components is higher than that in the perpendicular direction by nearly one order of magnitude. This increase may be attributed to a higher thermal conductivity, related to the electrical conductivity along the basal plane of flake-like particles of the NE material (in this case, possibly a graphitizable carbon, but not necessarily graphite) and presence of the current collector. Finally electrolyte [EC-DMC (1:1 wt%)/1M $LiPF_6$] increases the thermal conductivity of the stacked layers of PE/Sp/NE by nearly 55–70%, and eliminates the OCV effects.

Louisiana State University, "Wear Mechanisms of a Resinoid Diamond Wheel with Fine Abrasives and Associated Responses in Creep-Feed Grinding of Alumina," *T. Warren Liao*, HTML No. 97-048

MIRUC

The state of the wheel surface is a very important factor in machining ceramic materials. Unfortunately, the effect of wheel wear on ground workpiece quality has not been fully investigated. This project intends to study the wear mechanisms of a resinoid wheel with 320 mesh and 100 concentration diamond abrasives in creep-feed grinding of AlliedSignal GS44 silicon-nitride material. The grinding conditions of 36.84 m/s wheel speed, 5.08 mm/s work speed, 1.5- and 1.0-mm depth of cut and 13.2-mm grinding width (full width of the wheel) were used. Wheel wear states were captured using the lead tape

imprint technique, followed by SEM examinations in backscattered electron mode. Five states were traced during the transition stage including the as-dressed state and after grinding 2.14, 6.41, 10.68, and 17.09 cm^3 volumes of material. To investigate the difference in the wear mechanisms, six additional states during the steady stage were also traced after continuously grinding 46.80, 49.65, 52.50, 55.35, 58.20, 62.47 cm^3 volumes of material.

The results obtained indicate that the wear mechanisms during the transition stage differ from those during the steady stage. During the transition stage, wheel preparation plays a major role other than the wheel specification, material properties, and grinding conditions. Wheel preparation weakens the grit bonding force leading to a high percentage of grit dislodgement. Due to the large protrusion after wheel preparation, the number of grits not involving in cutting is also high. The wear mechanism during the steady stage is dominated by erosive wear, caused by the abrasion between the grit and the workpiece. This is supported by the increased percentages of grits showing wear-flats and wear-flat area as more materials are removed.

Also studied is the effect of grinding width on uneven wear on wheel surface, which in turn might have an effect on the resultant workpiece quality in terms of strength and surface texture. The ceramic material studied in this case is Coors AD995 CAP-3.

Michigan State University, "Modeling Heat Transfer for Parameter Estimation in Flash Diffusivity Experiments," *R. McMasters*, HTML No. 96-053

TPUC

Carbon-bonded carbon fiber (CBCF) is produced at ORNL for use as an insulator in atmosphere re-entry applications. Measurement of the thermal diffusivity of this material, using the flash heating method, is somewhat difficult due to its semiporous nature. The goals of this research were as follows:

- to determine the thermal properties of the material, specifically thermal diffusivity, from transient temperature measurements,
- to investigate the possibility of internal radiation as an ancillary means of heat transfer to Fourier conduction and to investigate penetration of the laser flash beyond the surface of the specimen, and
- to investigate nonradiative effects that may have been responsible for systematic disparities between the measured data and the mathematical model for the flash measurement method.

The common underlying motivation behind each of the above objectives was to develop and utilize a heat transfer model for flash diffusivity experiments that would accurately conform to the physical phenomenon observed, thereby giving greater confidence in the parameter values reported. The primary means of evaluating the degree of success achieved in this endeavor was the extent to which reductions were achieved in the residual signatures, from those evident in previous analyses. These signatures indicated an inadequacy in the models used previously that, in turn, implied some unreliability in the estimated parameters.

The nonpenetrating model utilized ordinary least squares to minimize the difference between calculated and measured temperatures from the flash diffusivity experiments. Three simultaneous parameters were determined using this model: thermal diffusivity (mm^2/s), heat flux magnitude (joules/mm^2), and the dimensionless heat transfer coefficient, biot number. Table C.3 shows the thermal diffusivity and biot number along with the residual standard deviation of fitting the temperature rise data.

Table C.3. CBCF samples measured at ORNL 800°C analysis with the nonpenetrating model

Sample	Diffusivity	Biot number	Residual std. dev.
1.0mm(a)	0.294	2.164	0.017
1.0mm(b)	0.263	2.436	0.014
1.2mm(a)	0.352	2.300	0.018
1.2mm(b)	0.317	2.706	0.013

The penetration model assumed an exponentially distributed temperature profile in the material at the instant of flash, due to the penetration of the flash. The same least squares method was used to determine the extinction coefficient of the laser flash as well as the same three parameters of the nonpenetrtion model fit (see Table C.4). This new analysis method, incorporating a correction for penetration, achieved a higher level of agreement between samples when comparing the estimated parameters measured at one temperature. In contrast, the results obtained using the simpler model produced a wider range of values under the same conditions. The observed reduction in the magnitude of the residuals is a validation of the higher order model.

Table C.4. CBCF samples measured at ORNL at 800°C analysis with the penetrating model

Sample	Diffusivity	Biot number	Penetration	Residual std. dev.
1.0mm(a)	0.252	2.999	0.080	0.009
1.0mm(b)	0.228	3.307	0.077	0.013
1.2mm(a)	0.313	2.959	0.085	0.006
1.2mm(b)	0.288	3.327	0.075	0.008

The value of the main parameter of interest, thermal diffusivity, is shown to be sensitive to the type of model used. Approximately a 12% reduction in a was found for these CBCF specimens when the penetration model was employed. The magnitude of the estimated value can be affected by as much as 20%. The results generated by the refined models can be reported with greater confidence, as demonstrated by the improvements noted above, and are therefore more reliable for use in design-related work with these materials.

North Carolina State University, "Residual Stresses in Diamond and Diamond Composite Films," *J. Kasichainula*, HTML No. 95-039

RSUC

The purpose of this work was to determine the sign and magnitude of residual stresses in a system of coatings on molybdenum. Single-layer diamond films and multilayer diamond films were scanned using the PTS-rotating anode X-ray diffraction instrument. The diffraction patterns showed the presence of a carbide layer between the molybdenum substrate and the diamond layer. Texture was observed within the carbide layer and the diamond layer, and pole figures were measured to quantify this observation. The diamond layer and the carbide intermediate layer were found to be under tensile residual stress while the molybdenum substrate was under a compressive residual stress at the interface (e.g., see Fig. C.16 below). This interesting and unexpected result fostered a further study (97-035).

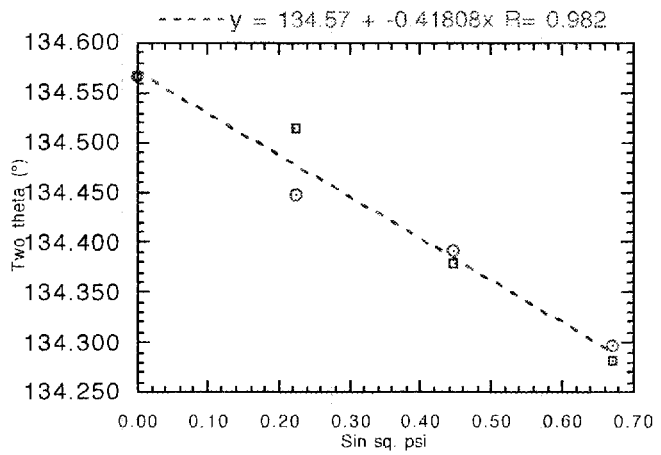

Fig. C.16. A $\sin^2\psi$ plot showing tensile stresses in the Mo_2C layer using the (213) reflection.

North Carolina State University, "Residual Stresses in a Multilayer System of Coatings," *A. J. McGinnis* and *J. Kasichainula*, HTML No. 97-035

RSUC

Residual stresses present in coatings may adversely affect coating adhesion and wear resistance, particularly in diamond coatings. Insertion of an appropriate intermediate layer between the coating and substrate has been used to improve adhesion and wear resistance. In this study, the multilayer structures consisted of diamond/molybdenum carbide/molybdenum (substrate) and diamond/diamond-aluminum nitride-molybdenum carbide/molybdenum (substrate). Diamond was deposited via hot filament chemical vapor deposition (HFCVD), and AlN was deposited by laser physical vapor deposition (PLD). Raman analysis was used to measure thermal residual stress within diamond. X-ray diffraction (XRD) was used to measure thermal residual stresses within Mo and Mo_2C phases. The residual stresses measured with XRD were compared to theoretical calculations.

The residual stresses were measured using the PTS 4-axis goniometers. The sign of residual stresses in the diamond, Mo_2C, and Mo were all consistent with the expected sign based on the phase thermal-expansion mismatch and estimated temperature of deposition. Further, an interposing AlN layer in a multilayer diamond sample provided a benefit for a given stress level relative to a sample without this interposing layer. Empirically, the multilayer diamond sample did not delaminate, suggesting enhanced adhesion between the diamond coating and the Mo_2C/Mo substrate. The data also suggests that in the single-layer diamond samples, the residual stress increases with coating thickness. The residual stresses in the discontinuous diamond sample are the smallest measured, likely because of the lack of an in-plane constraint between the islands of diamond.

Table C.5. Sample identification and layer description

Sample ID	Microstructure (Top/.../bottom)
Multilayer diamond	Diamond/AlN+diamond islands/Mo_2C/Mo substrate
Discontinuous diamond	Diamond islands/Mo_2C/Mo substrate
Single diamond	Diamond/Mo_2C/Mo substrate
AlN/diamond	AlN/diamond islands/Mo_2C/Mo substrate

Table C.6. Hydrostatic stresses measured by X-ray diffraction and macro-Raman spectroscopy

Sample ID	Diamond layer thickness (μm)	Mean hydrostatic stress (GPa)			
		Unidentified phase *	(321) Mo	(213) Mo_2C	Diamond†
Multilayer diamond	5	0.63 (0.11)**	–0.07 (0.06)	0.49 (0.06)	–4.5
Discontinuous diamond	1	0.43 (0.07)	–0.14 (0.06)	0.38 (0.06)	–1.5
Single diamond	2	0.76 (0.13)	–0.10 (0.06)	0.39 (0.09)	–3.0
Single diamond	8.5	0.17 (0.07)	–0.08 (0.07)	0.53 (0.05)	–4.5
AlN/diamond	1.5	0.32 (0.07)	–0.07 (0.07)	0.46 (0.05)	—

*Young's Modulus and Poisson's ratio for Mo_2C were used.
†Macro-Raman data.
**( )Denotes standard deviation.

<u>Pennsylvania State University</u>, "The Effects of Grain Size, Porosity, and Yttria Content on the Thermal Conductivity of Nanocrystalline Zirconia," *S. Raghavan* and *M. Mayo*, HTML No. 95-094

TPUC

Thermal conductivity of nanocrystalline zirconia with varying grain size, porosity, and yttria content has been determined in an effort to evaluate its potential for thermal barrier applications. In pure, dense monoclinic zirconia (grain size ≈63 nm), the temperature dependence of the thermal conductivity indicates that phonon-phonon scattering still controls thermal conductivity, even down to such small grain sizes. The temperature dependence of thermal conductivity in doped zirconias (grain size = 30 nm–400 nm and 60–100% dense) is flat, which is representative of phonon scattering by defects. Subsequent comparison of data for different grain sizes and yttria contents shows that the responsible defects are yttria-induced oxygen vacancies, not grain boundaries. A comparison of the thermal conductivities of nanocrystalline zirconia doped with 8 wt.% yttria and currently available thermal barrier coatings shows approximately equal values.

Thermal diffusivities, α, were measured by the laser flash technique at HTML on a flash thermal diffusivity system. Prior to measuring the thermal diffusivity, all the samples were sputter coated with 1000 Å of platinum or gold-palladium alloy on both sides to make them opaque and then with a thin layer of colloidal graphite to ensure complete and uniform absorption of the laser pulse and similar surface emissivity in all samples. All the measurements were carried out from 100 to 1000°C in 100 degree intervals, in nitrogen.

Specific heat capacities were measured at HTML using the differential scanning calorimeter (DSC). Specimens consisted of 4-mm diam, 2-mm thick disks that were heated at 20°C/min. Heat capacities were calculated using the ratio method with sapphire as the reference standard.

The effect of yttria content on the thermal conductivity vs temperature plots is shown in Fig. C.17. Atomic defect scattering is responsible for the insensitivity of thermal conductivity to temperature in the 8 and 15 wt.% yttria samples. At a given temperature, the decrease in thermal conductivity with larger yttria contents is consistent with oxygen vacancies playing the dominant role in phonon scattering. It is noteworthy that while there is a relatively large drop in conductivity in going from 5.8 to 8 wt.% yttria, further increase in yttria content to about 15 wt.% does not cause a proportionate decrease in conductivity. Thermal conductivity values for the monoclinic zirconia were calculated using values of specific heat from the literature. It is stressed that the monoclinic zirconia is pure zirconia with a grain size of 63 nm, with no stabilizer additions and having impurity contents similar to the indigenously produced 5.8 wt.% nanocrystalline tetragonal zirconia. The strong temperature dependence of thermal conductivity in the monoclinic material shows that in the absence of oxygen vacancies, defect scattering is not the dominant mechanism.

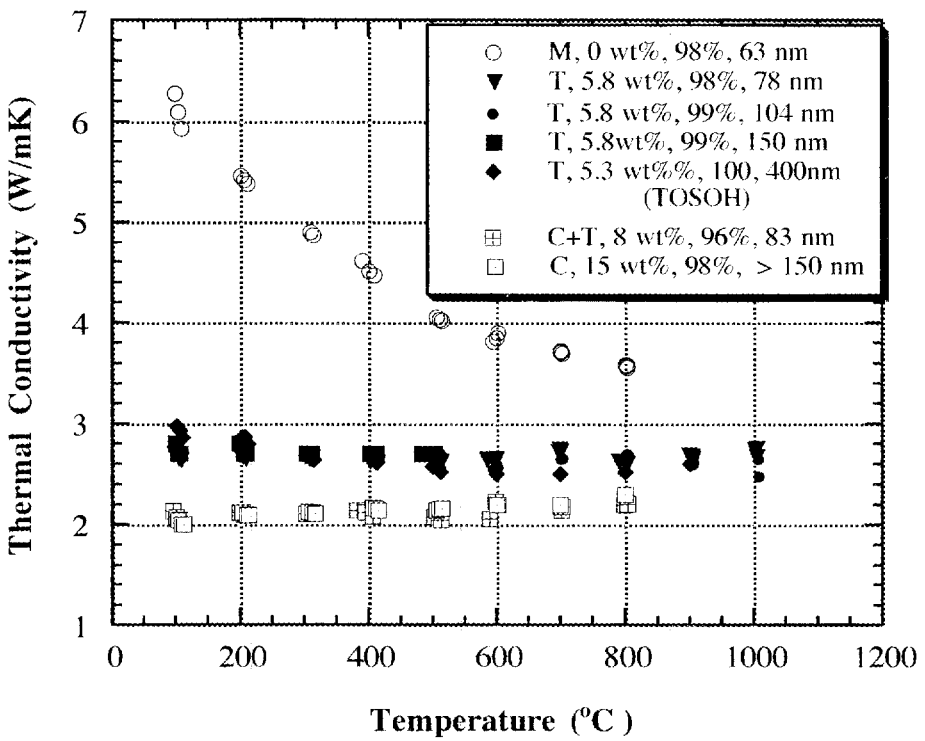

Fig. C.17. Effect of yttria content on thermal conductivity.

<u>Southern University</u>, "High Temperature Tensile Property of the Super Alloy IN738LC," *R. A. Mirshams*, HTML No. 97-058

MCAUC

IN738LC is a Ni-base precipitate strengthened superalloy. The precipitate phase in this alloy is the γ', $Ni_3(Al,Ti)$ with the $L1_2$ superlattice. This superalloy has promising features for applications in gas turbines and aerospace engines. The yield strength of the superalloy increases with increasing temperature and reaches a peak value around 750°C. The morphology and distribution of the precipitates in the matrix affect the mechanical properties. For this reason, different precipitate microstructures were developed to test for tensile properties at high temperatures in the range 650–1200°C. The study confines the microstructure development and the effect of the microstructure on the selected high temperature mechanical properties. The microstructures developed are the ones containing: (1) fine ppts. (50–70 nm), (2) medium ppts. (450 nm), (3) coarse ppts. (700 nm), and (4) duplex-size ppts., a mixture of 1 and 2. IN738LC shows a stable fine precipitate microstructure at 1200°C. Therefore, it is possible that this microstructure may show some good mechanical properties at this high temperature. Because of this distinct feature of the superalloy, collecting the tensile and creep data at 1200°C would be very beneficial

to contribute to the development of IN738LC superalloy. Currently, no mechanical property data are available on this superalloy at this temperature.

Four specimens were tested at 1200°C in the tensile test facilities at the HTML at ORNL. The round tensile specimens were machined and heat-treated to produce the fine ppt. microstructure. Two different strain rates were used, and two specimens were tested at each strain rate. Some other lower temperature testings were conducted at Southern University, Baton Rouge, Louisianna.

The preliminary study on the tensile test data was done, and it was observed that the tensile strength of the superalloy is almost 1/100 at 1200°C compared to the strength obtained in the range 650–850°C. Further analysis is in progress.

Texas A&M University, "Texture in Cubic Metals Processed Through Equal Channel Angular Extrusions," *K. T. Hartwig* and *M. A. Gibbs*, HTML No. 95-093

RSUC

A novel method of modifying the microstructure of metals, called equal channel angular extrusion (ECAE), has been developed recently. This new processing method has the capability of introducing large amounts of plastic strain into bulk material in a relatively uniform manner without a reduction in workpiece cross section. The processing concept is elegant: press a block of solid material through a constant cross-section tunnel composed of two intersecting channels. The material undergoes simple shear in a thin zone at the crossing plane of the channels. Because workpiece dimensions are nearly the same before and after processing, multiple extrusions of the same workpiece in the same tooling are possible. By controlling workpiece orientation relative to the tooling crossing plane during multiple extrusion operations, different microstructures can be developed. The purpose of this HTML project is to determine which kinds of texture are developed by three basic schemes of multipass ECAE.

Pure iron was ECAE-processed and examined by X-ray diffraction analysis for texture. The investigation included extrusions at room temperature on 25 × 25 × 120 mm blocks of annealed relatively untextured polycrystalline material. Billet orientation was controlled during multiple extrusion steps in order to promote the development of conventional textures similar to those arising from rolling, drawing, and torsion. These textures were confirmed. Continuing work (HTML Proposal No. 97-078) involves comparing texture in ECAE processed materials with those found in rolled and drawn products. Early results demonstrate another dimension of the versatility possible with this innovative method for introducing large effective strains to bulk material by simple shear.

The University of Alabama, "X-ray Diffraction Studies of (110) Oriented FeTaN Epitaxial Thin Films," *L. Varga, T. J. Klemmer*, and *H. Jiang*, HTML No. 97-029

RSUC

High moment soft magnetic FeTaN films are promising candidates for pole materials in the next generation inductive write heads used with high-density media. There has been a great interest in this and other reactively sputtered polycrystalline FeXN materials during the last few years, and much information has been accumulated on its nanocrystalline state. However, the effect of nitrogen on the fundamental magnetic properties, magnetocrystalline anisotropy (K_1) and magnetostriction (λ_{100},λ_{111}), has not been studied experimentally.

In order to study these fundamental physical properties, a film of the FeTaN material must be grown with very few crystallographic orientations and these orientations must be completely characterized. In this investigation epitaxial FeTaN films (~1500 Å) were grown by reactive sputtering and as a function of nitrogen flow rate on epitaxial Cu(001) buffer layers (~2000 Å) on Si(001) single crystal substrates. The crystallographic orientations and the relationship between the films and the substrate were thoroughly

characterized using pole figure analysis carried out on a Scintag four-circle X-ray diffractometer. The FeTaN films were found to obey the Pitsch orientation relationship with the buffer layer [FeTaN(110)||Cu(001) and FeTaN<111>||Cu(110)], which allows four different in-plane variants to coexist in the film (shown in Fig. C.18). These four variants can be observed distinctly in the Fe (110) pole figure in Fig. C.19a and the in-plane spread of the orientations increases with increasing nitrogen as shown in Figs. C.19a-d.

By taking into consideration the different orientations present in the films, the fundamental magnetic properties could be measured. The values of K_1 decreased slightly with increasing nitrogen from ~5 to 4×10^5 ergs/cc. The magnetostriction constant λ_{100} also decreased slightly, staying around $+20 \times 10^{-6}$ while λ_{111} increased and eventually changed sign from -20×10^{-6} to $+2 \times 10^{-6}$. The change in these intrinsic properties along with the microstructure (i.e., grain size and stress) of the nanocrystalline FeTaN films should give a more complete understanding of the soft magnetic properties observed in these materials.

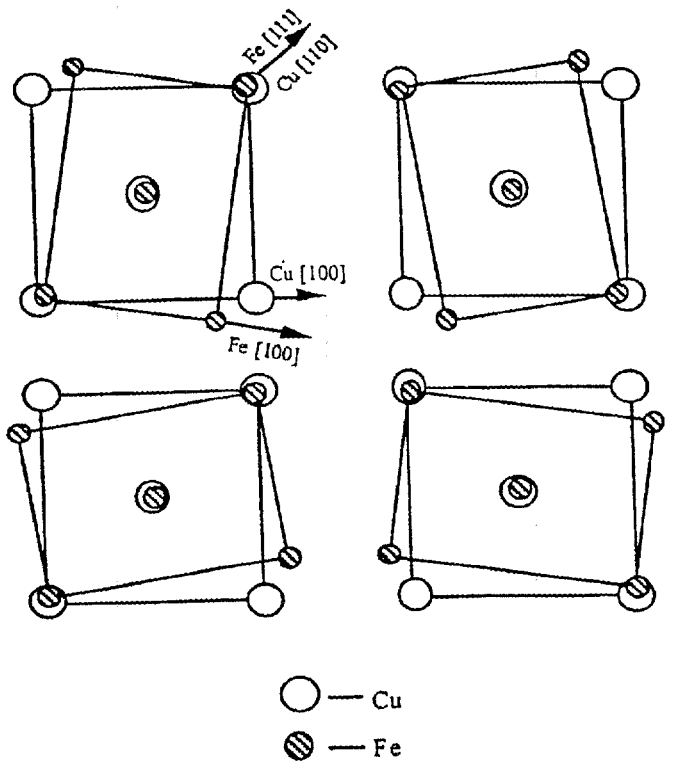

Fig. C.18. The atomic configurations consistent with the Pitsch orientation relationship between Fe and Cu, where A, B, C, and D denote the four possible in-plane orientations.

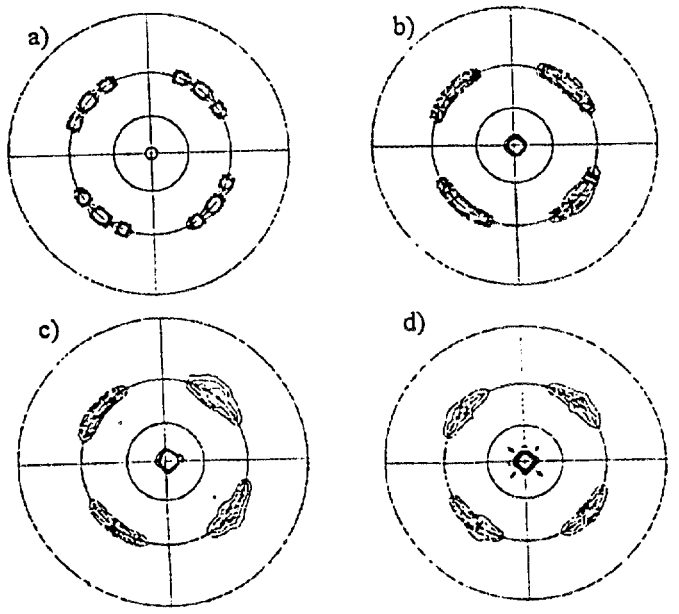

Fig. C.19. Comparison of the (110) pole figures for (a) Fe, (b) FeTa, and (c)-(d) FeTaN epitaxial films.

<u>University Of Alabama at Birmingham</u>, "Thermal Diffusivity of Refractory Sands and Coatings for the Lost Foam Casting Process," *T. Molibog*, HTML No 97-033

TPUC

Computer modeling of the lost foam (LF) casting process requires the thermophysical properties of refractory coatings and foundry sands over a wide temperature range (RT-1400°C). The thermo-physical properties required are density, thermal heat capacity, and thermal conductivity.

The purpose of this work was to study the thermophysical properties of coatings used in the LF casting process and foundry sands in the temperature range RT-~1000°C. The coatings studied were 510 and 533, whose main component was aluminum silicate, and StyroCoat 27 and StyroCoat 400, whose main components were silica and mica, respectively. The sands studied were Mullite 30/50, Mullite 30/60, Olivine, and silica sands. The thermophysical properties studied in the experiments were thermal diffusivity and specific heat capacity. Thermal diffusivity and specific heat capacity were later used to calculate thermal conductivity. The diffusivity measurements were conducted on the laser flash thermal diffusivity (LFTD) apparatus. The specific heat measurements were done by the use of the differential scanning calorimeter (DSC), and the results for the casting sands are shown in Fig. C.20.

The thermal conductivity data of these coatings (Fig. C.21) show that coating composition may change the value of thermal conductivity by a factor of 2–3. Thermal conductivity of LF coatings controls the heat transfer from the metal to the sand that in turn has significant effect on the solidification rate and fluidity of metal and defect formation in the casting.

The thermal diffusivity of sands was not possible to measure by the LFD method mainly because of the physical properties of loose sand (low thermal diffusivity, transparency to laser light, etc.). Experiments based on the hot disk method are currently being designed to obtain conductivity values for sands.

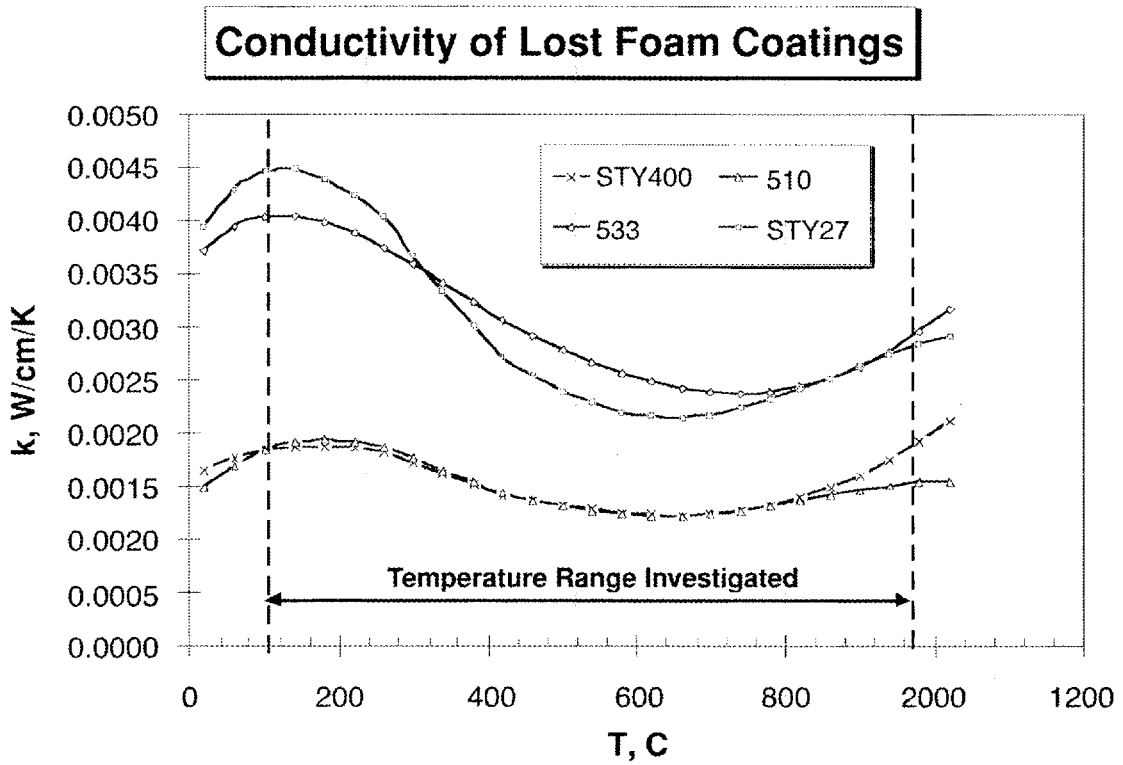

Fig. C.20. Conductivity of lost foam coatings.

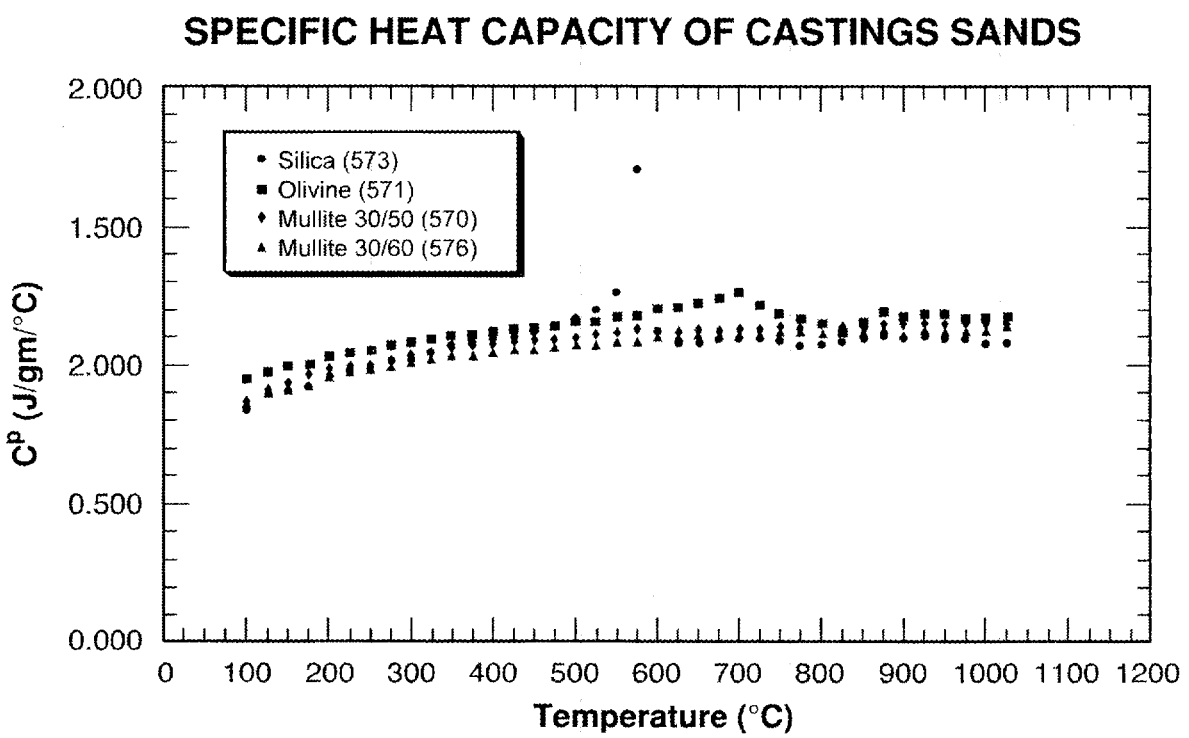

Fig. C.21. Specific heat capacity of casting sands.

<u>University of Central Florida</u>, "Measurements of Residual Stresses in Components Manufactured by Laser Assisted Direct Rapid Prototyping," *A. Kar* and F. *Kahlen*, HTML No. 97-021

RSUC

A scientist from University of Central Florida (UCF) visited the Residual Stress User Center to measure the residual stresses in the walls of 3-D structures fabricated by a new rapid prototyping process. At UCF, a metal powder is fed to the laser beam where the powder is melted. As the substrate is moved horizontally under the laser beam, planar, two-dimensional geometries are formed. After completing the geometry in the plane, the substrate is displaced in the vertical direction, and a new layer of material is placed on top of the just completed deposit. By continuous repetition of this process, 3-D parts are created. The goal is to develop a new metal-based rapid prototyping process.

Several of the stainless steel samples were examined with both X-ray and neutron diffraction. The as-deposited metal contained ferritic and austenitic phases. The overall stress in the surface of the sample was tensile. The specimens contained very large grains, extremely rough sample surface (±0.5 mm), and thin walls (~1 mm). These features obtained in the first deposition studies precluded meaningful X-ray and neutron stress measurements. A future visit is planned to look at an improved sample.

<u>University of Connecticut</u>, "X-ray and Neutron Diffraction Study of Thermal Barrier Coating Material," *D. Pease* and *V. Krishnakumar*, HTML No. 96-026

RSUC

The Residual Stress and Diffraction User Centers worked with two users from the University of Connecticut at the X14A beamline within the National Synchrotron Light Source (NSLS) at Brookhaven National Laboratory to further explore methods to characterize nondestructively the long range residual stresses in the ceramic top coat and the metallic bond coat in a TBC-protected super alloy turbine blade specimen. Here, proof-of-principle was sought to show that diffraction peaks from the bond coat could be observed in situ underneath 300 μm of yttria stabilized zirconia. Both high flux and energy (or wavelength) tuneability were required in order to succeed. X-rays having an energy just below the absorption edge of zirconia were successfully used to observe diffraction peaks from the in situ bond coat. Further work is planned at NSLS.

<u>University of Dayton</u>, "The Investigation of a Methodology for Producing Nanophased Reinforced Composites from the SiC-AlN System," *A. Lubis*, HTML No. 96-036

MAUC/RSUC

Solid solutions of SiC-AlN (25, 50, and 75 mol% AlN) were formed via hot pressing at 2100°C for 1 h soaking time under a pressure of 35 MPa in vacuum. Heat treating these three 2H-würtzite SiC-AlN specimens at 1750°C for 150 hours in a flowing nitrogen atmosphere resulted in modulated tweed-type structures indicative of a spinodal decomposition process. The spinodal decomposition process is also expected to produce compositional modulation accompanying the modulated tweed-type structures. No qualitative or quantitative evidence on the presence of the nanosized compositional modulation on the heat-treated SiC-AlN system has ever been reported.

In this work, high resolution transmission electron microscopy (HRTEM) was used to resolve the presence of the nanosized modulated feature that occurred on the three heat-treated specimens. The combination of the HRTEM and a very fine EDS probe with 1-nm resolution was used to resolve nanosized compositional modulation throughout the modulated tweed-type structure. Nano precipitates with typical modulated tweed-type structures were found through the $[2\bar{1}\bar{1}0]$ zone axis on the three

heat-treated compositions. Compositions associated with the modulated structures were also successfully found to modulate around average compositions within nanointervals. These two significant results strongly confirmed the formation of in situ nanophased reinforced composites from the SiC-AlN system.

Two significant findings associated with characterization of the modulated structures were established. The first significant finding was a method for precise determination of modulation orientation that occurred on each heat-treated composition. This method requires: (1) Khachaturyan-Mayo-Tsakalakos approach that predicts one of the possible modulation orientation minimizing elastic energy function, **Y(n)** is lying on a cone surface that makes an angle to [0001]; (2) TEM images and their corresponding selected area diffraction (SAD) patterns; and (3) lattice parameter data. The modulation orientations observed for the three test specimens were orthogonal to $\{01\bar{1}2\}$ planes that make angles of 46.70°, 46.90°, and 47.12° towards [0001] for 25, 50, and 75 mol% AlN, respectively. The second significant finding was utilizing the combination of the HRTEM and the EDS probe data to successfully resolve the compositional modulation. In addition, X-ray diffraction residual stress measurements were also conducted on the hot-pressed and the heat–treated specimens. The results showed no significant differences between the specimens and little spot-to-spot variations as indicated by the replicate measurements. Further, the level of residual stress is very low in all samples. Although more study is needed, spinodal decompositions may be a way to produce macroscopically uniform samples without significant residual stress.

Based on the results obtained, nanophased reinforced composites from the SiC-AlN system can be produced by heat treatment within the spinodal decomposition zone.

Material	Condition	Residual stress (MPa)
SiC-25 mol% AlN	As-hot pressed	–2 (±40)*
		–10 (±20)
		–14 (±22)
SiC-25 mol% AlN	As-heat treated	–26 (±29)
		– 5 (±20)
		–22 (±21)
SiC-50 mol% AlN	As-hot pressed	31 (±29)
		–5 (±17)
		9 (±19)
SiC-50 mol% AlN	As-heat treated	–24 (±25)
		–30 (±17)
		2 (±19)
SiC-75 mol% AlN	As-hot pressed	24 (±29)
		–24 (±17)
		–27 (±17)
SiC-75 mol% AlN	As-heat treated	6 (±27)
		–25 (±17)
		–39 (±19)

*Numbers in parentheses are standard deviation values

Fig. C.22. Results summary of residual stress analyses of the hot-pressed and the heat-treated SiC-AlN specimens.

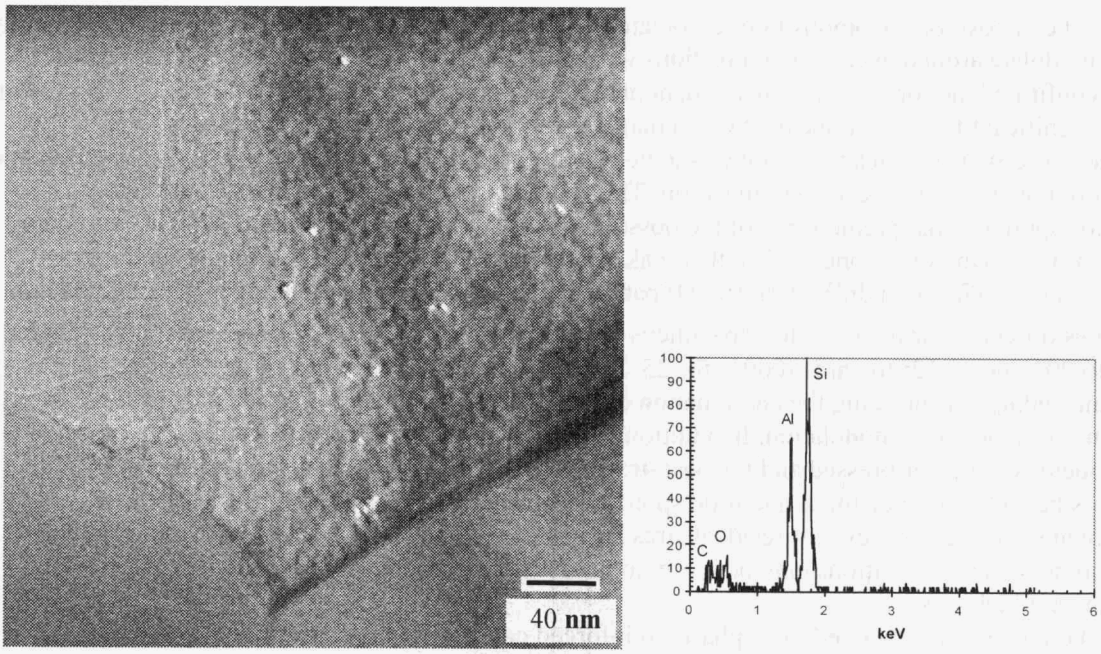

Fig. C.23. Lattice image of the heat-treated SiC-25 mol% AlN with its corresponding EDS spectra from different locations.

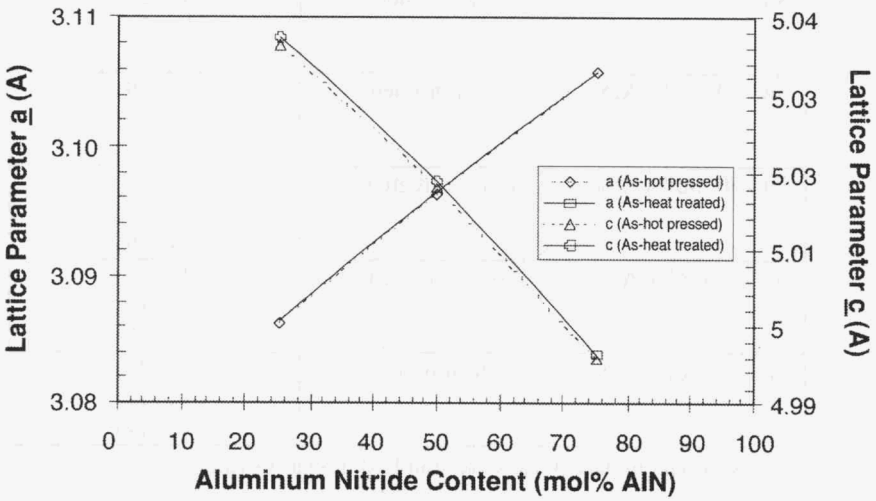

Fig. C.24. Differences in lattice parameters a and c for the hot pressed and the heat-treated SiC-AlN specimens.

University of Kentucky, "High Temperature X-ray Diffraction Studies of Metals Promoted ZrO_2," *R. Srinivasan* and *B. H. Davis*, HTML No. 96-013

DUC

Sulfated zirconia superacid catalysts exhibit activity and selectivity for skeletal isomerizations of alkanes at low temperatures. The presence of noble metal crystallites (such as Pt) in the sulfated zirconia catalyst formulation enhances their activity and stability, but why this is so is not well understood. Attempts have been made to utilize less expensive metals with a similar activity and stability. A new class of solid superacid catalysts with Fe and Mn impregnated onto sulfated zirconia has been reported to have suitable activity.

The states of iron and manganese, impregnated onto sulfated zirconia, were studied using the in situ high temperature X-ray diffraction technique, in both activated and reducing conditions. The aim of the investigation was to study the states of iron and manganese on these catalysts after activation and during reaction conditions. When the catalyst is activated in air at 725°C for 1–2 h, Fe_2O_3 forms and has been found to be a stable phase during and after cooling to room temperature.

After activation, the catalyst was heated in flowing hydrogen at 100, 150, 200 and 250°C. At temperatures up to 200°C, the catalyst retained the Fe_2O_3 phase and only at 250°C was the Fe_2O_3 phase reduced to metallic Fe. The activation energy for the crystallization is 468 kJ/mol for the sulfated zirconia, while this is ~23.2 kJ/mol for zirconia without sulfate.

No X-ray diffraction peaks were observed to permit characterization of the state of manganese species in this study.

University of Kentucky, "Interface Structure and Chemistry of NiO-Y_2O_3 Directionally Solidified Eutectics," *E. C. Dickey*, HTML No. 97-023.

MAUC

Presently, the factors that govern the atomic structure of crystalline interfaces between two dissimilar ionic materials are not thoroughly understood. This research program aims to elucidate the structural and chemical aspects of internal interfaces in a model ionic heterophase system, NiO-Y_2O_3 directionally solidified eutectics.

Initial studies on the NiO-Y_2O_3 interface were performed by HRTEM on a 400-kV JEOL-4000EX to identify the morphology and atomic structure of the interfaces. HRTEM images taken along the $[110]_{NiO}//[010]_{Y2O3}$ zone axis (see Fig. C.25) show an abrupt transition between NiO and Y_2O_3 at their interface. Although interfacial defects such as steps are present to accommodate global variations in the interface plane normal, the local interface plane along the step ledges is $(111)_{NiO}//(100)_{Y2O3}$ suggesting that this is a low-energy interface plane.

Based on the initial HRTEM data, a model of the NiO-Y_2O_3 was developed (see Fig. C.26). As a consequence of the crystallographic orientation relationship and the local interface plane orientation, alternating planes of cations and anions lie parallel to the interface in both phases. As proposed in the interface model, this anion-cation sequence is maintained across the interface plane via a common oxygen plane that is shared by both phases. This scenario, similar to that observed at NiO-ZrO_2 interfaces, facilitates electrostatic bonding across the interface.

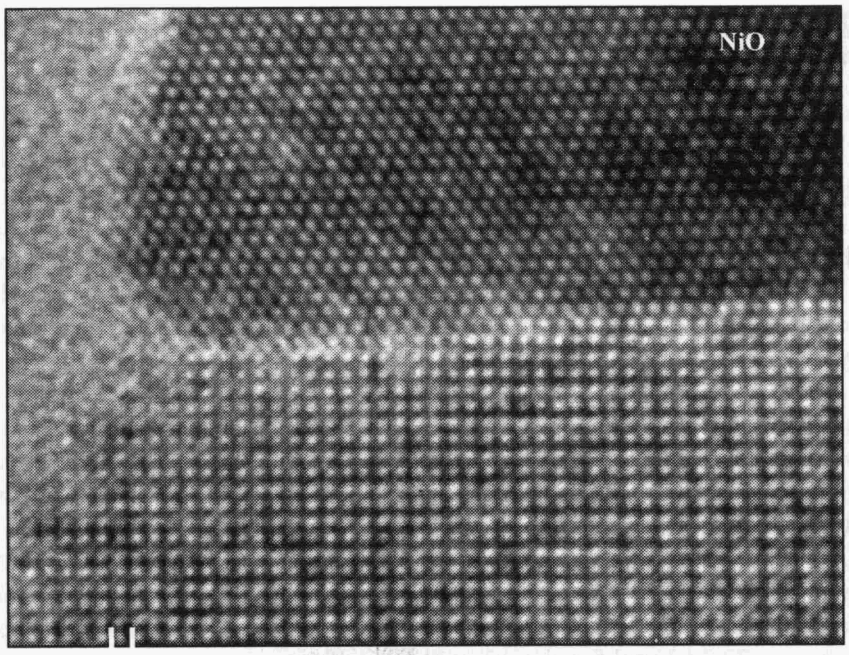

Fig. C.25. HREM image of NiO-Y_2O_3 interface showing an atomically abrupt transition between the two phases.

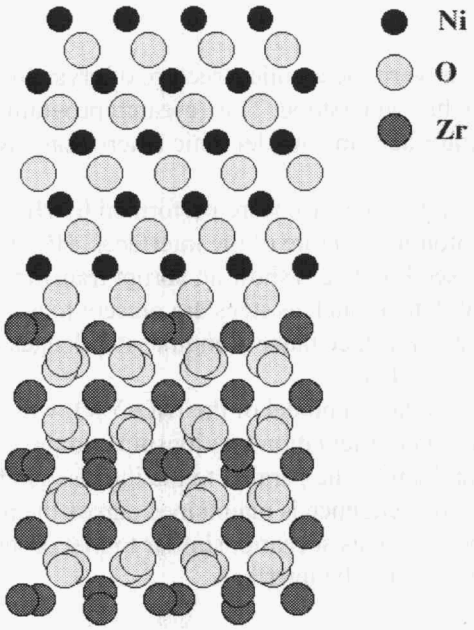

Fig. C.26. Model of NiO-Y_2O_3 interface in which the phases share a common oxygen plane.

University of Massachusetts at Amherst, "High-Temperature Residual Stress Measurement of SiC-Fiber-Reinforced BMAS Glass-Ceramic Matrix Composite," *K. Jakus* and *S. Widjaja*, HTML No. 97-039

RSUC

When a fiber-reinforced ceramic matrix composite is creep-conditioned such that the applied load transfers from the matrix to the fibers and when the composite is cooled under load, a compressive residual stress is induced in the matrix as a result of a constrained elastic rebound. This compressive residual stress increases the ultimate matrix cracking stress of the composite (see HTML Proposal No. 95-043). X-ray diffraction residual stress analysis results show that the residual stress in the matrix of Nicalon™/BMAS glass-ceramic matrix composite increased from –71 MPa (as-received specimen) to –124 MPa for a specimen creep-conditioned at 1100°C for 12 h under a stress of 75 MPa, and to –190 MPa for a specimen treated at 1100°C for 30 h under a stress of 90 MPa. The residual stress measurement of the BMAS matrix was based on the peak shift of the (8 2 4) plane of barium osumilite phase. The compressive residual stress in the as-received specimen is because of the thermal expansion mismatch between the fibers and matrix upon cooling. The increase in the residual stress in the matrix of creep-conditioned specimens is attributed to the effectiveness of creep-load transfer technique.

The purpose of this study was to better understand the behavior of residual stress induced in the Nicalon™/BMAS glass-ceramic matrix composite at high temperature. High temperature residual stress measurements would provide data to characterize the compressive residual stress in the matrix with respect to temperature. The HTXRD residual stress measurements were done at temperatures of 300°C and 550°C, where the matrix does not creep. A problem arose at elevated temperature in that the barium osumilite (8 2 4) reflection was no longer observable in the X-ray pattern because of the thermal motion of the atoms reducing the scattered intensity. Further work is being considered for NSLS.

University of Massachusetts at Amherst, "Creep-Induced Residual Stress Strengthening in Fiber Reinforced Ceramic Matrix Composites," *K. Jakus* and *S. Widjaja*, HTML No. 95-043

MCAUC/RSUC

High temperature creep-conditioning of continuous fiber-reinforced ceramic matrix composites, in which the fibers are more creep-resistant than the matrix, causes the matrix to transfer its load to the fibers. Upon removal of the load after cooling to room temperature, a compressive residual stress is induced in the matrix by the elastic recovery of the fibers. This compressive residual stress in the matrix causes an increase in the matrix cracking stress of the composite, improving the reliability of the materials. The objective of this research was to study the effectiveness of high temperature creep conditioning in improving the matrix cracking stress.

Laminated 0°/90° Nicalon™ fiber-reinforced BMAS glass-ceramic matrix composite specimens were creep-conditioned in tension at 1100°C under constant stress, cooled under load to room temperature, and then unloaded. The applied creep stress ranged from 35 MPa to 90 MPa, and the creep times varied from 12 h to 100 h. The resulting room temperature tensile stress-strain behavior was determined, and acoustic emission activity was monitored during the tensile test to detect cracking activity. The residual stresses in the matrix of the as-received and creep-conditioned specimens were independently measured with X-ray diffraction.

Creep-load transfer results showed that the increase in the proportional limit (i.e., the onset of significant matrix cracking) of the creep-conditioned specimens was attributed to the effectiveness of the creep-load transfer treatment in inducing a compressive residual stress in the matrix. Figure C.27 illustrates the tensile stress-strain behaviors of the as-received and crept specimens, showing a significant increase in the proportional limit of the specimen creep-conditioned under 75 MPa for 12 h. The acoustic emission and X-ray diffraction data confirmed that the increase in the observed proportional limit of the

crept specimens was due to an increase in the compressive residual stress in the matrix. The compressive residual stress in the matrix was found to be dependent upon the applied creep stress; however, it was not significantly affected by the creep time. Fractography using SEM revealed that the creep-conditioned specimens exhibited similar fiber pull-out behavior to that of the as-received specimens, indicating that the creep-load transfer treatment did not embrittle the fiber/matrix interface, and hence, the "graceful" failure behavior of the composite was preserved.

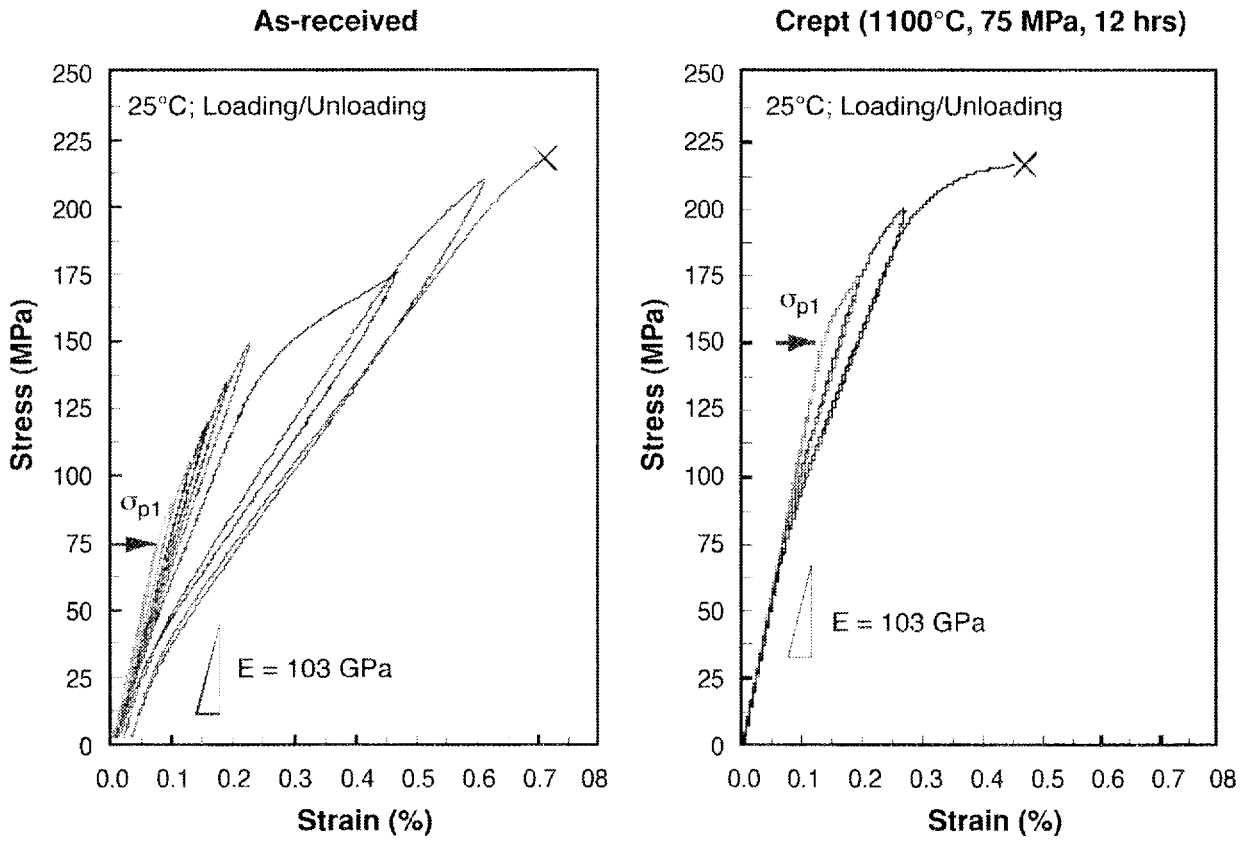

Fig. C.27. Tensile stress-strain behaviors of the as-received and crept specimens.

<u>University of Maine</u>, "Tribology Studies Of Tungsten Trioxide Thin Films Grown By Molecular Beam Epitaxy Techniques," *O. D. Greenwood* and *R. J. Lad*, HTML No. 97-011

MIRUC

Tungsten trioxide (WO_3) thin films offer potential as tribological coatings for use in high temperatures and oxidizing environments. Friction and wear experiments were performed on well-characterized WO_3 films in order to determine the effect of film microstructure upon tribological performance.

Five hundred-nm-thick WO_3 films were grown by electron cyclotron resonance (ECR) plasma-assisted e-beam evaporation of WO_3, and analyzed in situ using RHEED and XPS. Stoichiometric WO_3 films grown on R-sapphire exhibited amorphous, polycrystalline or epitaxial microstructure, depending on the substrate temperature in the range 50°C to 600°C. Pin-on-disk tests were performed on films having these different microstructures using sapphire and stainless steel ball bearing sliders, a 1-N load,

and a sliding speed of 0.1 m/s. Friction microprobe linear single pass tests for the same slider-film combinations were also carried out (0.1-N load, 10 μ/s sliding speed) to study initial sliding behavior.

Pin-on-disk experiments showed that the friction coefficient for sapphire sliders on amorphous WO_3 films ($\mu \sim 0.6$) was twice that of epitaxial WO_3 films ($\mu \sim 0.3$). In addition, the friction coefficients were higher for steel sliders than for sapphire sliders on all the films. Microprobe friction coefficients, which emphasize the initial stages of sliding contact, were lowest for epitaxial films ($\mu \sim 0.2$), varied strongly with slider material on amorphous WO_3 films ($\mu \sim 0.2$ to 0.4), and were highest on polycrystalline WO_3 films ($\mu \sim 0.3$ to 0.5). Optical micrographs and profilometry of wear tracks indicate that greater film wear occurred for the steel/WO_3 system than for sapphire/WO_3. In all cases, the lowest friction coefficients and wear rate occurred for epitaxial WO_3 films, indicating a strong effect of microstructure upon WO_3 thin film tribology.

University of Maine, "Tribology Studies of Zirconia Thin Films Grown by Molecular Beam Epitaxy Techniques," *S. C. Moulzolf* and *R. J. Lad*, HTML No. 97-011

MIRUC

Zirconia films have great potential for advanced materials applications since they possess many desirable characteristics such as a high melting point, resistance to oxidation, low thermal conductivity, and high hardness. In addition to these characteristics, the tribological properties (friction and wear) of a zirconia coating may determine whether it is suitable for a particular application. The microstructure of a synthesized zirconia film is determined by the particular substrate, deposition method, and deposition parameters. In this study, the Friction and Wear Analysis Facility at HTML was utilized to study the microstructural effect on the friction and wear of several zirconia films grown at the University of Maine.

Stoichiometric zirconia films of varying microstructure characterized by in situ RHEED were deposited on r-cut sapphire via electron beam evaporation of Zr in the presence of an ECR oxygen plasma. Polycrystalline films with nanometer-sized grains are formed at deposition temperatures below 300°C. Above 475°C, highly textured zirconia films are produced that contain coexisting phases of cubic and monoclinic zirconia.

A pin-on-disk tribometer at HTML was used to measure friction coefficients and wear rates of the zirconia films using sapphire and stainless steel pins in air at 25°C. The polycrystalline films exhibited low friction coefficients (0.2–0.3) but appear to be unsuitable for unlubricated tribological applications because of high wear rates ($> 2.5 \times 10^{-5}$ mm^3 N^{-1} m^{-1}). The wear rates on the highly textured films were extremely small; the wear tracks were too shallow to be measured by profilometry. The textured films also had dramatically different pin-on-disk friction characteristics depending on the relative percentage of cubic vs monoclinic phase. For the films containing primarily the monoclinic phase, the pin-on-disk traces exhibited abrupt transitions to high friction coefficients (>0.8) due to the generation of third-body particulates. However, highly textured films containing primarily the cubic phase had low, relatively constant friction coefficients (~0.3) and exhibited anisotropic microcracking during scratch testing at the HTML with a conical diamond at a 10-N load. The initial friction characteristics for the same pin/film combinations were also studied using the friction microprobe at the HTML. Friction microprobe traces from the films reveal qualitatively different initial friction coefficients and features related to stick-slip events.

University of Nevada-Reno, Department of Chemical and Metallurgical Engineering Mackay School of Mines, "Thermal Conductivities of Plastic Crystals," *D. Chandra*, HTML No. 95-036

TPUC

The electrical conductivity of polyalcohols and amines show an increasing trend from 10^{-9} to 10^{-5} $ohm^{-1}cm^{-1}$ with increasing temperature. Select polyalcohols and amines are being considered for thermal energy storage as there is a low temperature ordered and a high temperature, disordered transformation The specific heat capacity jumps significantly at the transition. The objective of this research is to measure the thermal conductivity of these materials and to correlate the thermal conductivity, electrical conductivity, ionic mobility, and temperature. We have already published the electrical conductivity data, which show an increasing trend from 10^{-9} to 10^{-5} ohm^{-1} cm^{-1} with increasing temperature, a behavior opposite to that in metals. We would like to develop a $\kappa/\sigma=\psi T$ type relationship, where ψ is the ionic mobility factor for a family of plastic crystals such as polyalcohols, and T is the temperature.

Polyalcohols, such as pentaerythritol ($C_5H_{12}O_4$), pentaglycerine ($C_5H_{12}O_3$), neopentylglycol ($C_5H_{12}O_2$), neopentylalcohol ($C_5H_{12}O_2$), and amines such as 2 amino-2methyl,1,3 propanediol ($C_4H_{11}O_2N$), and Tris-hydroxymethyl aminomethane ($C_4H_{11}O_3N$) are some of the plastic crystals that are being considered for thermal energy storage. The low temperature phase II structure of these plastic crystals is either layered or chain type and is ordered, whereas the high temperature phase I is cubic and is orientationally disordered.

We initiated the thermal conductivity studies using the laser flash thermal diffusivity method during the summer of 1997 with Dr. Ralph Dinwiddie. However, we experienced problems with the very low thermal conductivity of the samples. Although some experiments were performed on neopentylglycol ($C_5H_{12}O_2$) and neopentylalcohol ($C_5H_{12}O$), we had difficulty in obtaining data. In these feasibility tests, powders of the samples were compacted and used for measurements. It was concluded that the sample thickness, approximately 2 to 3 mm, was too thick. However, it will be possible to make measurements with thinner samples. We are now in a process of developing new methods to prepare very thin samples for thermal conductivity experiments. We will resume our studies in June 1998.

University of North Dakota—Energy and Environmental Research Center, "Transmission Electron Microscopy of Nanometer-Scale Inorganic Components in Coal and Char Enriched in Selected Organic Microstructures," *J. Hurley, F. Karner*, and *C. G. Tomforde*, HTML No. 96-009

MAUC

Sticky ash, which may cause filters in coal-fired power plants to malfunction, is dependent on size distribution and compositional variation of ash particles. These depend on the occurrence of inorganic components in coal. In addition, maceral content may play a major role in ash characteristics. We examined how natural assemblages of macerals and lithotypes influenced combustion.

First, organic microstructures concentrated in certain macerals may affect nanometer-scale inorganic particles in coal. The organic microstructures are affected by the original plant matter and coalification processes, and may contain voids that are filled by the precipitation of nanometer-scale inorganic components. Secondly, some macerals are more reactive, and produce porous or vesicular charforms after partial combustion. Less reactive macerals may produce dense charforms. During combustion, dense charforms may shed fine ash particles that produce a sticky cake on hot-gas cleanup filters. Fine ash might adhere to the surface of porous char where coalescence of ash particles occurs. In a combustion system, this will produce coarser ash that is easier to remove than fine ash.

The HF-2000 Field Emission Gun Analytical Electron Microscope was used at HTML to study bright and dull lithotypes of different rank coals and on char produced from bituminous and subbituminous coals. Energy dispersive spectroscopy (EDS) determined elemental information on inorganic inclusions. Thin sections of dull and bright lithotypes of bituminous, subbituminous, and lignitic coals were prepared

to determine with the TEM if there were certain mineral types and sizes, specifically nanometer-scale inorganic components that were enriched in each sample. Char produced from the bituminous and subbituminous coals was also examined to ascertain with AEM char morphology and the physical and chemical characteristics of nanometer-scale inclusions.

Nanometer-scale inclusions observed in the subbituminous bright lithotype with a nonanalytical TEM at University of North Dakota (UND) were not evident at Oak Ridge. They were apparent in the char samples. The char produced by the UND—Energy and Environmental Research Center (EERC) pressurized fluidized-bed reactor were named: bituminous bright, bituminous dull, subbituminous bright, and subbituminous dull char. The small inclusions range in size from 5 to 70 nm in diameter. They are not abundantly disseminated in the char particles, but occur as groups of 10 to 30 inclusions within isolated areas of each char particle. Titanium peaks are dominant on all EDS spectra obtained from analysis of nanometer scale inorganic components in bright and dull bituminous char. Aluminum appears to be very significant in the small inorganic components occurring in the bituminous bright char. Iron peaks are prevalent on all of the EDS spectra obtained from nanometer-scale inorganic components in bright and dull subbituminous char. Calcium peaks are characteristic of the tiny inorganic components in all of the char particles.

The work conducted at Oak Ridge and at UND shows that coal lithotypes and coal rank control char morphologies, coal lithotypes have little impact on the formation of fine ash in a pressurized fluidized-bed combustor, and nanometer-scale inclusions are present in coal and char. The small inclusions examined in the char are inorganic components, but may be mesophase inclusions (liquid crystals, an intermediate phase in the conversion of vitrinite to coke by heating) in the subbituminous bright lithotype. Although it appears that lithotype reactivity does not influence ash liberation in a PFBR, it may influence ash liberation in other modes of combustion (i.e., pulverized coal combustion).

University of Wisconsin—Milwaukee, "Residual Stress Analysis in Cryogenically Treated Steels," *J. J. Bruckner* and *T. L. Barr*, HTML No. 96-042

RSUC

Cryogenic treatment of steel is a growing industry in the United States. Although an improved part lifetime and performance is often attributed to stress relief, the effects of this treatment on the residual stresses are poorly documented. In this neutron and X-ray diffraction study, samples of 4140 steel, 416 stainless steel, and 6061 aluminum alloy were examined. In each case, one sample was prepared by 300Below Ltd using their commercial cryogenic process, and one sample was untreated. No discernable differences in the diffraction peak profiles or positions were observed between the treated and untreated samples. This implies that any differences in the service lifetime of these materials cannot be attributed to alteration of the micro- or macro-stresses. Additional characterizations of hardness and microstructure are being undertaken by the user, and additional measurements on austenitic and ferritic steel samples are planned.

Western Michigan University, "Thermal Stability of Conductive Layered Hydroxides," *A. A. Olowe*, HTML No. 97-042

DUC

Sandwiched Layered Hydroxides (SLHs) are inorganic materials that have a general formula: $[M^{2+}_{1-x}M^{3+}_{x}(OH)_2]^{x+}[X^{n-}_{x/n} \cdot mH_2O]$ where X is an anion and x varies from 0 to 0.333. The cations M^{n+} are usually from Cu, Ca, Al, Mg, Mn, Zn, Ni, Fe, Cr, Ni, and Co. Several SLHs have been found as naturally occurring minerals (e.g., pyroaurite and hydrotalcite), as corrosion products (e.g., green rusts), but most must be synthesized. A variety of names have been used to refer to them; some are "pyroaurite-type compounds," or "hydrotalcites," or Òhydrotalcite-like compounds (HTLC)," although the general

use of specific mineral names to describe SLHs is not quite appropriate. The crystal structure of SLHs have common features: (1) they form classes having a similar X-ray diffraction pattern with comparable lattice parameters and (2) they possess positively charged metal hydroxide blocks separated by negatively charged mobile layers of the hydrated anion X^{n} . The two most widely studied classes of SLHs are the pyroaurite and sjögrenite types where the hydroxide blocks are single and the anion, X^{n-}, is CO_3^{2-} in each case; both composed of the same elements with the same M^{2+}:M^{3+} ratio. The main difference between the pyroaurite and sjögrenite type structures is that the former is rhombohedral 3-R polytype,while the latter is hexagonal 2-H polytype.

High temperature X-ray diffraction at HTML confirmed that the pyroaurite type structure collapses as the hydration water molecules are removed from the interlayer. HTXRD shows that the *a*-lattice parameter is nearly constant, whereas the reduction in the *c*-lattice parameter is quite significant as the temperature increases. The hydration water appeared to be completely removed at about 175°C for all the three samples studied, confirming previous results. Also, at around 400°C, a new crystal starts to form from the collapsed structure. This information is important for application of these materials as thermally activated catalysts.

APPENDIX D

PUBLICATIONS AND PRESENTATIONS

APPENDIX D. PUBLICATIONS AND PRESENTATIONS

Note: Asterisks indicate HTML staff members.

D.1 PUBLICATIONS

Beck, J. V., and R. B. Dinwiddie,* "Measurement of Thermal Diffusivity in Flash Tests with Simultaneous Estimation of Heat Transfer Coefficients on Each Side," in *Thermal Conductivity* **23**, ed. K. E. Wilkes, R. B. Dinwiddie, and R. S. Graves, Technomics Publishing Co., 1996.

Braski,* D., and R. B. Dinwiddie,* *The Characterization of High Explosive Material Residues Using Atomic Force Microscopy*, Final Report for Interagency Agreement DOE No. 1866-1098-A1, Navy No. NO464A96MPO5566 (1997).

Breder,* K., and V. J. Tennery, "Dynamic Fatigue Behavior of Two SiC and a SiCp Reinforced Al_2O_3 at Elevated Temperatures," *J. European Cer. Soc.* **17**, 1579–86 (1997).

Calderón Moreno, J. M., M. R. Elizalde, and E. Lara-Curzio,* "Push-out Tests on Small Fibers and Interfacial Properties of a Fiber-Reinforced Ceramic Matrix Composite," *Key Eng. Mater.* **127–131**, 617–22 (1997).

Dickey, E. C., *Interface Structure and Interfacial Phenomena in NiO-ZrO_2(cubic) Directionally Solidified Eutectics*, Ph.D. Dissertation, Northwestern University, UMI Co. #9731243 (1997).

Dickey, E. C., and V. P. Dravid, "Atomic Structure Determination of NiO-Y_2O_3 Interfaces by HRTEM," *Microscopy and Microanalysis* **3**, S2, 649–50 (1997).

Dickey, E. C., and V. P. Dravid, "Rigid-Body Translation (RBT) in a NiO-ZrO_2(cubic) Bicrystal and its Implications for Interface Atomic Structure," in *Proceedings of Microscopy and Microanalysis 1996*, ed. G. W. Bailey et al., San Francisco Press, Inc., San Francisco, 1996.

Dickey, E. C., V. P. Dravid, P. Nellist, and D. J. Wallis, "A Combined Techniques Approach to Studying Heterophase Interfaces Using HREM, Z-Contrast Imaging and EELS," *Materials Research Society Symposium Proceedings* **466**, 45–50 (1997).

Dickey, E. C., V. P. Dravid, P. Nellist, D. J. Wallis, N. Browning, and S. J. Pennycook, "Atomic Structure Determination of NiO-ZrO_2(CaO) and Ni-ZrO_2(CaO) Interfaces Using Z-Contrast Imaging and EELS," in *Proceedings of Microscopy and Microanalysis 1996*, ed. G. W. Bailey et al., San Francisco Press, Inc., San Francisco, 1996.

Dickey, E. C., V. P. Dravid, P. Nellist, D. J. Wallis, and S. J. Pennycook, "Three-Dimensional Atomic Structure of NiO-ZrO_2(cubic) Interfaces," *Acta Materialia* (in press).

Dickey, E. C., V. P. Dravid, P. Nellist, D. J. Wallis, S. J. Pennycook, and A. Revcolevschi, "Structure and Bonding at Ni-ZrO_2(cubic) Interfaces Formed by the Reduction of NiO-ZrO_2(cubic) Composite," *Microscopy and Microanalysis* **3**, 443–50 (1997).

Dickey, E. C., C. R. Hubbard,* and V. P. Dravid, "Interlamellar Residual Stresses in Single Grains of NiO-ZrO_2(cubic) Directionally Solidified Eutectics," *J. Am. Ceram. Soc.* **80**(11), 2773–80 (1997).

Dinwiddie,* R. B., S. C. Beecher,* W. D. Porter,* and B. A. Nagaraj, "The Effect of Thermal Aging on the Thermal Conductivity of Plasma Sprayed and EB-PVD Thermal Barrier Coatings," in *Proceedings of the International Gas Tubine and Aeroengine Congress and Exhibition*, Birmingham, UK, ASME, 96-GT-282 (1996).

Dinwiddie,* R. B., G. E. Nelson, and C. E. Weaver, "Effect of Sub-Minute High Temperature Heat Treatments on the Thermal Conductivity of Carbon-Bonded Carbon Fiber (CBCF) Insulation," in *Thermal Conductivity* **23**, ed. K. E. Wilks, R. B. Dinwiddie, and R. S. Graves, Technomics Publishing Co., 1996.

Dinwiddie,* R. B., H. Wang,* W. D. Porter,* J. Jo, and P. L. Knipple, "Thermophysical Properties of an HY-100 Weldment," *24th International Conductivity Conference Proceedings*, Pittsburgh, 1997.

Dragoi, D., T. R. Watkins,* and K. J. Kozaczek* "Interpreting Oscillatory Bragg Peak Positions," *J. Appl. Cryst.* **29**, 493–94 (1996).

Ghasemi-Nejhad, M. N., M. V. Chandramouli, and A. A. Wereszczak,* "Processing and Performance of Continuous Fiber Ceramic Composites by Filament Winding and Pre-Ceramic Polymer Pyrolysis," *Extended Abstracts, Proc. of ASME/IMECE Product Realization Through Processing*, Atlanta, November 1996 (in press).

Guo, Changsheng, Ronald H. Chand, and Samuel B. McSpadden,* "Diamond Wheel Specification and Ceramic Grinding," published in the *Proceedings of the 2nd International Machining and Grinding Conference*, SME, Dearborn, Michigan, September 8–11, 1997.

Hannel, S. E., K. Breder,* and D. L. Joslin,* "Effects of Coal Slag Corrosion on the Mechanical Properties of Sintered α-Silicon Carbide," *Cer. Eng. Sci. Proc.* **18**(3), 513–23 (1997).

Haynes J. A., E. D. Rigney, and M. K. Ferber,* "Oxidation and Degradation of a Plasma-Sprayed Thermal Barrier Coating System," *Surf. Coat. Tech.* **87-8**(1-3), 102–108, Part 1 (1996).

Hecht, R., R. B. Dinwiddie,* H. Wang,* and W. D. Porter,* "Thermal Transport Properties of Grey Cast Irons," in the *Proceedings of the SAE Brake Colloquium*, New Orleans, 926126, October 1996.

Holland, H. J., T. R. Watkins,* and G. F. Foster, "Characterization of Mo-Ta Films," *Proceedings of the 1997 Denver X-Ray Conference* (in press).

Hsieh, K. C., and E. A. Kenik, "Characterization of Precipitate Distributions in Modified S5 Tool Steels," *Microscopy and Microanalysis* **3**, Supplement 2, Proceedings, 1997.

Jagannadham, K., and T. R. Watkins,* "A Comparative Study of Residual Stresses in Single and Multilayer Composite Diamond Coatings," *Proceedings MRS Symposium* **505**, Boston, 1997.

Jenkins, M. G., J. P. Piccola, and E. Lara-Curzio,* "Onset of Cumulative Damage and the Effects of Test Parameters on the Tensile Behavior of Continuous Fiber-Reinforced Ceramic Composites (CFCC)," *Fracture Mechanics of Ceramics* **12**, 267–82, ed. R. C. Bradt, D. P. H. Hasselman, D. Munz, M. Sakai, and V. Y. Shevchenko, Plenum Publishing Corp., 1996.

Jones, M. C., E. Lara-Curzio,* A. Kopper, and D. C. Martin, "Lateral Deformation of Crosslinkable PPXTA Fibers," *J. Mater. Sci.* **32**(11), 2855–71 (1997).

Knepfler, C. A., K. T. Faber, J. Weertman, G. B. Olson, C. R. Hubbard,* O. B. Cavin,* and N. Packan, "High Temperature Stability and Thermal Expansion Behavior of Molybdenum-Chromium M_2C Carbides," *J. Alloy Compd.* **248** (1–2), 139–42 (1997).

Kozaczek,* K. J., C. R. Hubbard,* T. R. Watkins,* X.-L. Wang,* and S. Spooner, "Diffraction Techniques in Engineering Applications," *Mat. Sci. Forum*, 210–213, 703–710 (1996).

Lance, M. J., J. A. Haynes, W. R. Cannon, and M. K. Ferber,* "Piezospectroscopic Characterization of Thermal Barrier Coatings," in *Ceramic Transactions: Nondestructive Evaluation of Ceramics*, ed. C. H. Schilling and J. N. Gray, American Ceramic Society, Inc. **89**, Westerville, Ohio, 1997.

Lara-Curzio,* E., "Oxidation-Induced Stress-Rupture of Fiber Bundles," Paper 97GT332, **ASME Turbo Expo '97**, Orlando, Florida, June 2–5, 1997.

Lara-Curzio,* E., "Stress-Rupture of Nicalon™/SiC Continuous Fiber Ceramic Composites in Air at 950ßC," *J. Am. Ceram. Soc.* **8**(12), 3268–72 (1997).

Lara-Curzio,* E., and R. P. Boisvert, "Time-Dependent Deformation of Polymer-Derived CFCCs," *CFCC Newsletter*, No. 9, 13–15 (1997).

Lara-Curzio,* E. and M. K. Ferber,* "Stress Rupture of Nicalon™/SiC CFCCs at Intermediate Temperatures," *J. Mater. Sci. Lett.* **16**(1), 23–26 (1997).

Lara-Curzio,* E., M. K. Ferber,* and P. F. Tortorelli, "Interface Oxidation and Stress-Rupture of Nicalon™/SiC CFCCs at Intermediate Temperatures," *Key Eng. Mater.* 127–131, 1069–82 (1997).

Lara-Curzio,* E., and C. M. Russ, "Redistribution of Internal Stresses and Residual Stresses in Composites: An Approach for Increasing the Matrix Cracking Stress," *Ceram. Eng. and Sci.* **18**, 437–46 (1997).

Lara-Curzio,* E., P. F. Tortorelli, and K. L. More,* "Stress-Rupture of CFCCs at Intermediate Temperatures," *Ceram. Eng. and Sci.* **18**, 209–19 (1997).

Lee, Deok-Hyung, Hyukjae Lee, Byungwoo Park, David B. Poker, and Laura Riester,* "The Effect of Implantation Temperature on the Surface Hardness, Elastic Modulus and Raman Scattering in Amorphous Carbon," *Appl. Phys. Lett.* **70**, June 1997.

Li, K., T. W. Liao, G. P. Fang, J. E. Mayer, Jr., and K. Breder,* "Creep-Feed Grinding of Al_2O_3 and Si_3N_4 Under Widely Different Conditions," Presented at *NAMRC, XXV* May 97, Lincoln, Nebraska, *Technical Papers of the North American Manufacturing Research Institution*, 45–50, Published by Society of Manufacturing Engineers, Dearborn, Michigan, 1997.

Li, K., T. W. Liao,* L. J. O'Rourke,* and S. B. McSpadden,* "Wear of Diamond Wheels in Creep-Feed Grinding of Ceramic Materials. II. Effects on Process Responses and Strength," *Wear* **211**, 104–112 (1997).

Li, M., J. A. Brooks, D. G. Atteridge, and W. D. Porter,* "Thermophysical Property Measurements on Low Alloy High Strength Carbon Steels," *Scripta Mater.* **3**(12), 1353–59 (1997).

Liao, T. W., K. Li, and K. Breder,* "Flexural Strength of Ceramics Ground with Widely Different Conditions," presented at the *ASME IMECE Symposium on Advanced Machining and Finishing Process for Ceramics, Composites and High Temperature Alloys*, 1996 (to be published in *J. Materials Processing Technology*, 1997).

Liao, T. W., K. Li, S. B. McSpadden, Jr.*, and L. J. O'Rourke,* "Wear of Diamond Wheels in Creep-Feed Grinding of Ceramic Materials I. Mechanisms," *Wear* **211**, 94–103 (1997).

Makinson, J. D., H. Wang,* and R. B. Dinwiddie,* "Thermal Diffusivity of Nanocrystalline Copper-Iron Prepared by Mechanically Alloying," *Third International Conference on Nanostructured Materials*, 1996.

Maleki, H., L. R. Holland, and G. M. Jenkins, "Maximum Heating Rates for Producing Undistorted Glassy Carbon Ware Determined by Wedge-shaped Samples," *J. Mater. Res.* **11**(9), 2368–75 (1996).

Martukanitz, R. P., P. R. Howell, E. A. Payzant,* S. Spooner,* and C. R. Hubbard,* "Neutron Diffraction Study of Welds of Aerospace Aluminum Alloys," *Nondestructive Evaluation and Materials Properties III*, ed. P. K. Liaw, O. Buck, R. J. Arsenault, and R. E. Green, Jr., TMS, Warrendale, Pennsylvania, 89–95, 1996.

McCormack, R., M. Asta, J. J. Hoyt, B. C. Chakoumakos, S. T. Misture,* J. D. Althoff, and D. D. Johnson, "Experimental and Theoretical Investigations of Order-Disorder in Cu_2AlMn," *Comp. Mater. Sci.* **8**, 39–45 (1997).

McGinnis, A. J., T. R. Watkins,* and K. Jagannadham, "Residual Stresses in a Multilayer System of Coatings," *Proceedings Denver X-Ray Conference*, August 1997.

Mogro-Campero, A., C. A. Johnson, P. J. Bendarczyk, R. B. Dinwiddie,* and H. Wang,* "Effect of Gas Pressure on Thermal Conductivity of Zirconia Thermal Barrier Coatings," *Surface and Coatings Technology* **94–95**, 102–105 (1977).

Narasimhan, K., and W. C. Russell, "Properties and Performance of Multilayered CVD Coatings," in *Proceedings of the 14th International Plansee Seminar* **3**, 290–303, ed. G. Kneringer, P. Rî dhammer, and P. Wilhartitz, Plansee AG, Reutte, 1997.

Ott, R. D., K. Breder,* T. R. Watkins,* M. K. Ferber,* and J. M. Rigsbee, "Characterization of Machining-Induced Sub-Surface Damage of a High Strength Silicon Nitride," *Cer. Eng. Sci. Proc.* **18**(4), 93–104 (1997).

Pasto,* A. E., and B. J. Russell,* "High Temperature Materials Laboratory—Eighth and Ninth Annual Reports: October 1994 through September 1996," ORNL/TM-13431, October 1997.

Payzant,* E. A., and H. W. King, "High Temperature Electrical Resistivity of Solid Solution $LaSr(Cu,M)O_4$ Ceramics," *J. Can. Ceram. Soc.* **65**, 67–71 (1996).

Payzant,* E. A., S. Spooner,* X. Zhu,* C. R. Hubbard,* S. T. Rosinski, and J. Dowicki, "Experimental Determination of Residual Stress by Neutron Diffraction in a Boiling Water

Reactor Core Shroud," *NDE Engineering Codes and Standards and Materials Characterization,* **PVP-322/NDE-15**, 55–61, ASME, New York, 1996.

Pennycook, S. J., P. D. Nellist, M. F. Chisholm, N. D. Browning, D. J. Wallis, and E. C. Dickey, "Determination of Atomic Structure at Surfaces and Interfaces by High-Resolution STEM," *Materials Research Society Symposium Proceedings* **466**, 3–12 (1997).

Raghuraman, S., E. Lara-Curzio,* and M. K. Ferber,* "Modeling of Flexural Behavior of CFCCs Using Finite Element Analysis," *Ceram. Eng. and Sci.* **17**(4), 147–56 (1996).

Raine,* D., C. R. Hubbard,* P. M. Whaley, M. Wright, and D. Hutchinson, "Neutron Radiography and Computed Tomography at Oak Ridge National Laboratory," *ASNT Fall Conference Proceedings, Materials Evaluation*, 1174–78 (1997).

Riester,* L., M. K. Ferber,* K. Breder,* and R. J. Bridge, "Elastic Modulus Calculations from Load/Displacement Curves Using Spherical and Pointed Indenters," to be published in *Proceedings of the Symposium of Non-Destructive Evaluation of Ceramics and Glasses*, 99th Annual Meeting, American Ceramic Society, 1997.

Saigal, A., G. G. Leisk, S. T. Misture,* and C. R. Hubbard,* "Neutron Diffraction Measurements of Residual Strains in Tungsten Fiber-Reinforced Kanthal Composites," *Scripta Mater.* **34**, 1309–13 (1996).

Spooner,* S., E. A. Payzant,* C. R. Hubbard,* W. T. Donlon, and G. M. Vyletel, "Neutron Scattering Residual Stress Measurements on Gray Cast Iron Brake Discs," in *Quenching and the Control of Distortion Proceedings of the 2nd International Conference*, 491–94, ASM, Materials Park, Ohio, 1996.

Spooner, S., and X.-L. Wang,* "Diffraction Peak Displacement in Residual Stress Samples Due to Partial Burial of the Sampling Volume," *J. Appl. Cryst.* **30**, 449–55 (1997).

Stough, M. A, *Diffusivity and Solid Solubility in an Alumina-Zirconia System,* Ph.D. Dissertation, The Pennsylvania State University, 1997.

Stroud, R. M., K. F. Kelton, and S. T. Misture,* "High Temperature X-ray and Calorimetric Studies of Phase Transformation in Quasicrystalline Ti-Zr-Ni Alloys," *J. Mater. Res.* **12**, 434–38 (1997).

Stroud, R. M., A. M. Viano, P. C. Gibbons, K. F. Kelton, and S. T. Misture,* "Stable Ti-based Quasicrystal Offers Prospect for Improved Hydrogen Storage," *Appl. Phys. Lett.* **69**, 2998–3000 (1996).

Togami, T. C., S. Spooner,* E. A. Payzant,* X. Zhu,* and C. R. Hubbard,* *Residual Stress Measurements Performed on the Grand Gulf Nuclear Power Station Reactor Core Shroud,* Sandia Report SAND97-0034, Sandia National Laboratory, Albuquerque, New Mexico, 1997.

Wang,* H., and R. B. Dinwiddie,* "Advanced Thermal Imaging of Composite Materials," *Advances in Ceramic-Matrix Composites III, Ceramic Transactions* **74**, 609–618 (1996).

Wang,* H., and R. B. Dinwiddie,* "Thermal Diffusivity Mapping of 4-D Carbon-Carbon Composites," *Materials and Structures* **18**(4 B), 755–62 (1997).

Wang,* H., R. B. Dinwiddie,* and P. A. Gaal, "Multiple Station Thermal Diffusivity Instrument," *Thermal Conductivity* **23**, 119–27, ed. K. E. Wilkes, R. B. Dinwiddie, and R. S. Graves, Technomic Publishing Co., 1996.

Wang,* X.-L., "Diffraction Peak Displacement in Residual Stress Samples Due to Partial Burial of the Sampling Volume," *J. Appl. Cryst.* **30**, 449–55 (1997).

Wang,* X.-L., E. A. Payzant,* B. Taljat, C. R. Hubbard,* and J. R. Keiser, "Experimental Determination of the Residual Stresses in a Kraft Recovery Boiler Tube," in *Approximate Methods in the Design and Analysis of Pressure Vessels and Piping Components*, **PVP-347**, 165–71, ASME, New York, 1997.

Wang,* X.-L., E. A. Payzant,* B. Taljat, C. R. Hubbard,* and J. R. Keiser, "Experimental Determination of the Residual Stresses in a Spiral Weld Overlay Tube," *Mat. Sci. Eng. A.* **232**, 31–38 (1997).

Webb, J. E., R. N. Singh, H. Cai, and M. K. Ferber,* "Characterization of Thermal Shock in a 2D-Woven Fiber CVI SiC Composite Using Resonant Ultrasound Spectroscopy," *Proceedings of the Symposium on Ceramic Matrix Composites*, held in conjunction with the 1996 Annual Meeting of the American Ceramic Society.

Wereszczak,* A. A., M. K. Ferber,* T. P. Kirkland,* and C.-K. J. Lin, "Effect of Cyclic Loading on the Creep Performance of Silicon Nitride," *ASME J. Eng. Gas Turbines Power* **118**(4), 251–56 (1996).

Wereszczak,* A. A., and T. P. Kirkland,* "Creep Performance of Candidate Si_3N_4 and SiC Materials for Land-Based, Gas Turbine Engine Components," *J. Eng. Gas Turbines and Power, Transactions of the ASME* **119**(10), 799–806 (1997).

Wereszczak,* A. A., T. P. Kirkland,* M. K. Ferber,* and M. J. Andrews, "Prediction of SiAlON Diesel Valve Failure Probability Using AlliedSignal's *CERAMIC* and *ERICA* Life Prediction Codes," *Cer. Eng. Sci. Proc.* **18,** 475–84 (1997).

Wereszczak,* A. A., T. P. Kirkland,* H.-T. Lin, M. K. Ferber,* C.-W. Li, and J. A. Goldacker, "Tensile Creep Performance of a Developmental, In-Situ Reinforced Silicon Nitride," *Cer. Eng. Sci. Proc.* **18**, 45–55 (1997)

Wereszczak,* A. A., A. Parvizi-Majidi, and M. K. Ferber,* "Directional Dependence of Fracture Toughness in Hot-Pressed SiC-Whisker Reinforced Alumina at Room and Elevated Temperatures," *J. Compos. Mater.* **31**(19), 1905–20 (1997).

Widjaja, S., *Creep-Induced Residual Stress Strengthening in a Laminated 0°/90° Nicalon-Fiber-Reinforced BMAS Glass Ceramic Composite*, Ph.D. thesis, Department of Mechanical Engineering, University of Massachusetts at Amherst (1997).

Widjaja, S., K. Jakus, J. E. Ritter, E. Lara-Curzio,* E. Y. Sun, T. R. Watkins,* and J. J. Brennan, "High-Temperature Load Transfer in Nicalon™/BMAS Glass-Ceramic Matrix Composites," *Ceram. Eng. Sci. Proc.* **18**(3), 681–88 (1997).

D.2 PRESENTATIONS

Bruss, T., J. Taylor, S. Misture,* and T. R. Watkins,* "Characterization of Fe Impurities in Aluminum Nitride Using EXAFS," presented by T. Bruss at the 99th Annual Meeting of the American Ceramic Society, Cincinnati, Ohio, May 6, 1997.

Dickey, E. C., and V. P. Dravid, "Rigid-Body Translation (RBT) in a NiO-ZrO_2(cubic) Bicrystal and Its Implications for Interface Atomic Structure," presented at the 54th Annual Meeting of the Microscopy Society of America, Minneapolis, 1996.

Dickey, E. C., V. P. Dravid, and C. R. Hubbard,* "Interlamellar Stresses in NiO-ZrO_2(cubic) Directionally Solidified Eutectics," presented at the 99th Annual Meeting of the American Ceramic Society, Cincinnati, Ohio, May 4–7, 1997.

Dickey, E. C., V. P. Dravid, P. Nellist, and D. J. Wallis, "A Combined Techniques Approach to Studying Heterophase Interfaces Using HREM, Z-Contrast Imaging and EELS," presented at the Materials Research Society 1996 Fall Meeting, Boston, 1996.

Dickey, E. C., V. P. Dravid, P. Nellist, and D. J. Wallis, "Z-Contrast STEM Imaging and EELS Studies of Ni-ZrO_2(cubic) Interfaces Formed by the Reduction of NiO- ZrO_2(cubic) Composites," presented at the ASU Winter Workshop on Atomic Structure of Interfaces, Tempe, Arizona, 1997.

Dickey, E. C., V. P. Dravid, P. Nellist, D. J. Wallis, N. Browning, and S. J. Pennycook, "Atomic Structure Determination of NiO-ZrO_2(CaO) and Ni-ZrO_2(CaO) Interfaces Using Z-Contrast Imaging and EELS," presented at the 54th Annual Meeting of the Microscopy Society of America, Minneapolis, 1996.

Dinwiddie,* R. B., and H. Wang,* "Thermal Transport Properties and Infrared Imaging of Thermal Barrier Coatings," TBC Workshop, Fort Mitchell, Kentucky, May 19–21, 1997.

Ferber,* M. K., E. Lara-Curzio,* and A. A. Wereszczak,* "Time-Dependent Failure of Structural Ceramics and Ceramic Matrix Composites at Elevated Temperatures," presented at the 99th Annual Meeting, an Exposition of the American Ceramic Society, Cincinnati, Ohio, May 4–7, 1997.

Greenwood, O. D., R. J. Lad, and P. J. Blau,* "Tribological Testing of WO_3 Thin Films," poster at the 1997 Spring New England Meeting of the American Physical Society.

Holland, H. J., T. R. Watkins,* and G. F. Foster, "Characterization of Mo-Ta Films," presented by H. J. Holland at the 46th Annual Denver Conference, Steamboat Springs, Colorado, August 5, 1997.

Hubbard,* C. R., X.-L. Wang,* T. R. Watkins,* B. H. Rabin, R. L. Williamson, and H. A. Bruck, "3-D Nondestructive Residual Stress Mapping in an Al_2O_3-Ni Joint Bonded with a Composite Layer," presented by C. R. Hubbard at the 99th Annual Meeting of the American Ceramic Society, Cincinnati, Ohio, May 5, 1997.

Hubbard,* C. R., E. C. Dickey, and V. P. Dravid, "Crystallography and Interlamellar Stresses in NiO-ZrO_2(cubic) Directionally Solidified Eutectics," American Crystallographic Association 1997 Annual Meeting, July 19–25, 1997.

Hubbard,* C. R., W. Wong-Ng, and J. Rodgers, "Assessment of the Completeness of the PDF Database for Engineering Ceramic Materials," 46th Annual Denver X-ray Conference Steamboat Springs, Colorado, August 4–8, 1997.

Jagannadham, K., T. R. Watkins,* and J. Narayan, "Residual Stresses in Single and Multilayer Composite Diamond Coatings," presented by K. Jagannadham at the Fall Meeting of the Materials Research Society, Boston, December 2–5, 1996.

Jakus, K., S. Widjaja, J. E. Ritter, E. Lara-Curzio,* E. Y. Sun, T. R. Watkins,* and J. J. Brennan, "Creep-Induced Residual Stress Strengthening in Fiber-Reinforced Glass-Ceramic Composites," presented by K. Jakus at the 1996 Joint Fall Meeting of the American Ceramic Society, San Antonio, Texas, Oct. 30–Nov. 2, 1996.

Jakus, K., S. Widjaja, J. E. Ritter, E. Lara-Curzio,* T. R. Watkins,* E. Y. Sun, and J. J. Brennan "Creep-Load Transfer Characteristics of SiC-Fiber-Reinforced BMAS Glass-Ceramic Matrix Composite," presented by K. Jakus at the 99th Annual Meeting of the American Ceramic Society, Cincinnati, Ohio, May 7, 1997.

Jakus, K., S. Widjaja, J. E. Ritter, E. Lara-Curzio,* E. Y. Sun, T. R. Watkins,* and J. J. Brennan, "High-Temperature Load Transfer in Nicalon™/BMAS Glass-Ceramic Matrix Composites," presented by K. Jakus at the 99th Annual Meeting and Exposition of the American Ceramic Society, Cincinnati, Ohio, May 4–7, 1997.

Kupp, E. R., E. Lara-Curzio,* D. P. Stinton, and T. M. Besmann, "Screening of Interface Coating Materials Using Minicomposites," presented at 21st Annual Conference on Composites, Advanced Ceramics, Materials and Structures, Cocoa Beach, Florida, January 14, 1997.

Lara-Curzio,* E., "A Model for the Stress-Rupture of Fiber-Reinforced Ceramic Composites at Intermediate Temperatures," presented at the 4th International Conference on Composite Engineering ICCE/4, Kohala Coast, Hawaii, July 7–11, 1997.

Lara-Curzio,* E., "Oxidation-Induced Stress-Rupture of Fiber Bundles," paper 97GT332 presented at ASME Turbo Expo 1997, International Gas Turbine Institute Meeting, Orlando, Florida, June 2–5, 1997.

Lara-Curzio,* E., and C. M. Russ, "Redistribution of Internal Stresses and Residual Stresses in Composites: An Approach for Increasing the Matrix Cracking Stress," presented at 21st Annual Conference on Composites, Advanced Ceramics, Materials and Structures, Cocoa Beach, Florida, January 14, 1997.

Lara-Curzio,* E., P. F. Tortorelli, and K. L. More,* "Stress-Rupture of Nicalon™/SiC at Intermediate Temperatures," presented at 21st Annual Conference on composites, Advanced Ceramics, Materials and Structures, Cocoa Beach, Florida, January 15, 1997.

Lee, W. Y., K. M. Cooley, E. Lara-Curzio,* and K. L. More,* Preparation of Silica and Zirconia Coatings by CVD for Nicalon™/SiC Composites," presented at 99th Annual Meeting and Exposition of the American Ceramic Society, Cincinnati, Ohio, May 4–7, 1997.

Lee, W., K. M. Cooley, E. Lara-Curzio,* T. R. Watkins,* S. T. Misture,* E. Kupp, and K. L. More,* "Phase Transformation as a Means for Promoting Weak Interfacial Behavior in Ceramic Matrix Composites," presented at 21st Annual Conference on Composites, Advanced Ceramics, Materials and Structures, Cocoa Beach, Florida, January 14, 1997.

McGinnis, A., "Residual Stresses in a Multilayer System of Coatings," XRD Poster Session, Best Poster Award at the 1997 Denver X-Ray Conference.

Misture, S. T., S. M. Pilgrim, E. A. Payzant,* C. R. Hubbard,* "Neutron Diffraction Strain Measurements of Electroactive Ceramics Under D. C. Fields," presented at the 46th Annual Denver X-ray Conference, Steamboat Springs, Colorado, Aug. 4, 1997

Mogro-Campero, A., C. A. Johnson, P. J. Bendarczyk, R. B. Dinwiddie,* and H. Wang,* "Effect of Gas Pressure on Thermal Conductivity of Zirconia Thermal Barrier Coatings," presented at International Conference on Metallurgical Coatings and Thin Films, San Diego, California, April 21–27, 1977.

More,* K. L., P. F. Tortorelli, H. T. Lin, E. Lara-Curzio,* A. Clark, and R. A. Lowden, "Stability of BN Interfaces in Several CFCC Systems during Oxidation," presented at 21st Annual Conference on Composites, Advanced Ceramics, Materials and Structures, Cocoa Beach, Florida, January 15, 1997.

Narasimhan, K., and W. C. Russell, "Properties and Performance of Multilayered CVD Coatings," poster presented at the 14th International Plansee Seminar (1997).

Ott, R. D., K. Breder,* T. R. Watkins,* M. K. Ferber,* and J. M. Rigsbee, "Characterization of Machining-Induced Sub-Surface Damage of a High Strength Silicon Nitride," presented by R. D. Ott at the 21th Annual Meeting of the Engineering Ceramic Division of the American Ceramic Society, Cocoa Beach, Florida, January 12–16, 1997.

Payzant,* E. A., C. R. Hubbard,* S. T. Misture, S. M. Pilgrim, "Neutron Diffraction Strain Measurements of Electrostrictive Ceramics," presented at the International Conference on Neutron Scattering, Toronto, Ontario, Canada, August 18, 1997

Payzant,* E. A., M. A. Gibbs, K. T. Hartwig, and R. E. Goforth, "Texture Formation in Iron Processed by Equal Channel Angular Extrusion," poster presented at Materials Week/TMS Fall Meeting, Indianapolis, Indiana, September 14, 1997

Pennycook, S. J., P. D. Nellist, N. D. Browning, E. C. Dickey, and V. P. Dravid, "Prospects of Z-Contrast Imaging STEM for Ceramic Science," invited paper presented at the 98th Meeting of the American Ceramic Society, Indianapolis, Indiana, 1996.

Pennycook, S. J., P. D. Nellist, M. F. Chisholm, N. D. Browning, D. J. Wallis and E. C. Dickey, "Determination of Atomic Structure at Surfaces and Interfaces by High-Resolution STEM," presented at the Materials Research Society 1996 Fall Meeting, Boston, 1996.

Raine,* D., P. M. Whaley, M. Wright, and C. R. Hubbard,* "Designs for Neutron Radiography and Computed Tomography at Oak Ridge National Laboratory," 46th Annual Denver X-ray Conference, Steamboat Springs, August 4–8, 1997.

Riester,* L., M. K. Ferber,* K. Breder,* R. J. Bridge, "Elastic Modulus Calculations from Load/Displacement Curves using Spherical and Pointed Indenters," poster presentation, 99th Annual Meeting of the American Ceramic Society, Cincinnati, Ohio, May 6, 1997.

Rightor, Ed, "Metal Particle Growth on Supported Catalysts," interim presentation at the HTML Users Forum, July 1997.

Spooner, S., E. A. Payzant,* C. R. Hubbard,* W. T. Donlon, and G. M. Vyletel, "Neutron Scattering Residual Stress Measurements on Gray Cast Iron Brake Discs," 2nd International Conference on Quenching and the Control of Distortion, Cleveland, Ohio, November 4–11, 1996.

Stinton, D. P., E. R. Kupp, E. Lara-Curzio,* R. A. Lowden, and T. M. Besmann, "Fiber Protection Layers for Continuous Fiber Ceramic Matrix Composites," presented at the 99th Annual Meeting and Exposition of the American Ceramic Society, Cincinnati, Ohio, May 4–7, 1997.

Stough, M. A., "Phase Equilibria And Diffusional Aspects Of A Zirconia/Sapphire System," presented at the 99th Annual Meeting and Exposition of the American Ceramic Society, Cincinnati, Ohio, May 4–7, 1997.

Voelkl,* E., L. F. Allard,* J. Bruley, V. J. Keast, and D. B. Williams, "The Teaching of TEM by Telepresence Microscopy Over the Internet," *Inst. Phys. Conf. Ser. No. 153: Section 2*, paper presented at Electron Microscopy and Analysis Group Conf. EMAG97, Cambridge, 1997.

Wang,* H., R. B. Dinwiddie,* F. A. Modine, L. A. Boatner, M. Bartkowiak, and G. D. Mahan, "Thermal-Boundary Resistance at Solid-Solid Interfaces Studied by High-Resolution Infrared Imaging," presented at the Thirteenth Symposium on Thermophysical Properties, Boulder, Colorado, 1997.

Wang,* H., R. B. Dinwiddie,* and B. A. Nagaraj, "The Effects of Thermal Aging on Thermal Conductivities of Thermal Barrier Coatings," 2nd Annual Surface Engineering Symposium, Materials Week '96, Cincinnati, Ohio, October 7, 1996.

Wang,* X.-L., "Characterization of Residual Stresses Using Neutron Diffraction," Institut Max Von Laue–Paul Langevin, Grenoble, France, June 25, 1997.

Wang,* X.-L., C. R. Hubbard,* and S. Spooner, "Residual Stresses Due to Processing of Composite Tubes" The Fifth International Conference on Residual Stresses, ICRS-5, Linkoping, Sweden, June 16–18, 1997.

Wang,* X.-L., C. R. Hubbard,* and S. Spooner, "Residual Stresses within Composite Boiler Tubes," 46th Annual Denver X-ray Conference Steamboat Springs, Colorado, August 4–8, 1997.

Wang,* X.-L., E. A. Payzant,* B. Taljat, C. R. Hubbard,* and J. R. Keiser, "Experimental Determination of the Residual Stresses in a Kraft Recovery Boiler Tube," presented at the 1997 ASME Pressure Vessels and Piping Conference, Orlando, Florida, July 23–31, 1997.

Wang,* X.-L., E. A. Payzant,* B. Taljat, C. R. Hubbard,* and J. R. Keiser, "Measurement and Modeling of the Residual Stresses in a Spiral Weld Overlay Tube," The Fifth International Conference on Residual Stresses, ICRS-5, Linkoping, Sweden, June 16–18, 1997.

Wang,* X.-L., B. H. Rabin, R. L. Williamson, H. A. Bruck, T. R. Watkins,* and C. R. Hubbard,* "3-D Nondestructive Residual Stress Mapping in an Al_2O_3-Ni Joint Bonded with a Composite Layer," The American Ceramics Society's 99th Annual Meeting & Exposition, Cincinnati, Ohio, May 4–7, 1997.

Wang,* X.-L., S. Spooner, and C. R. Hubbard,* "Scattering Physics of the Peak Shift Anomaly Due to Partial Burial of the Sampling Volume in Neutron Diffraction Residual Stress Measurements," The International Conference on Neutron Scattering Toronto, Ontario, Canada, August 17–21, 1997.

Wang,* X.-L., S. Spooner, and C. R. Hubbard,* "Theory of the Peak Shift Anomaly Due to Partial Burial of the Scattering Volume in Neutron Diffraction Residual Stress Measurements," The Fifth International Conference on Residual Stresses, ICRS-5, Linkoping, Sweden, June 16–18, 1997.

Watkins,* T. R., and C. R. Hubbard,* "High Temperature Residual Stress Measurement in Thermal Barrier Coatings," presented at the 99th Annual Meeting of the American Ceramic Society, Cincinnati, Ohio, May 6, 1997.

Watkins,* T. R., and C. R. Hubbard,* "Residual Stress Measurements in Thermal Barrier Coatings," presented at the TBC Workshop, Cincinnati, Ohio, May 20, 1997.

Watkins,* T. R., A. J. McGinnis, and K. Jagannadham, "Residual Stresses in a Multilayer System of Coatings," presented at the 46th Annual Denver Conference, Steamboat Springs, Colorado, August 5, 1997.

Wereszczak,* A. A., "Compressive Creep Behavior of Fusion-Cast Alumina Refractories," Advances in the Fusion and Processing of Glass, Toronto, July 30, 1997.

Wereszczak,* A. A., "Compressive Creep Performance of Glass Furnace Crown Refractories," University of Missouri-Rolla Ceramic Engineering Department Seminar Series, Rolla, Missouri, October 10, 1996.

Wereszczak,* A. A., "Compressive Creep Resistance of Magnesia Refractories at Temperatures ≥1400°C (2550°F)," Advances in the Fusion and Processing of Glass, Toronto, July 30, 1997.

Wereszczak,* A. A., "Dynamic Fatigue Characteristics of Electronic Ceramic Films," 99th Annual Meeting of The American Ceramic Society, Cincinnati, Ohio, May 5–7, 1997.

Wereszczak,* A. A., "Failure Probability Prediction of Fast-Fractured NT451 SiAlON Diesel Valves," ASME Turbo Expo '97, Orlando, Florida, June 4, 1997.

Wereszczak,* A. A., "High Temperature Deformation of an AZS Refractory," Advances in the Fusion and Processing of Glass, Toronto, July 30, 1997.

Wereszczak,* A. A., "High Temperature Mechanical Properties and Corrosion Resistance of Refractories," 2nd Industrial Energy Efficiency Expo, Arlington, Virginia, February 27, 1997.

Wereszczak,* A. A., "Life Prediction and Reliability Analysis of Load-Bearing Ceramics," Lehigh University, Bethlehem, Pennsylvania, October 23, 1996.

Wereszczak,* A. A., "Prediction of SiAlON Diesel Valve Failure Probability Using AlliedSignal's *CERAMIC* and *ERICA* Life Prediction Codes," 21st Annual Conference on Composites and Advanced Ceramics, Cocoa Beach, Florida, January 12–16, 1997.

Wereszczak,* A. A., "Tensile Creep Performance of a Developmental, In-Situ Reinforced Silicon Nitride," 21st Annual Conference on Composites and Advanced Ceramics, Cocoa Beach, Florida, January 12–16, 1997.

Widjaja, S., K. Jakus, J. E. Ritter, E. Lara-Curzio,* E. Y. Sun, T. R. Watkins,* and J. J. Brennan, "High-Temperature Load Transfer in Nicalon™/BMAS Glass-Ceramic Matrix Composites," presented at 21st Annual Conference on Composites, Advanced Ceramics, Materials and Structures, Cocoa Beach, Florida, January 16, 1997.

INTERNAL DISTRIBUTION

1. Central Research Library
2–3. Laboratory Records-OSTI
4. Laboratory Records-RC
5. K. B. Alexander
6. L. F. Allard
7. P. Angelini
8. B. R. Appleton
9. J. B. Ball
10. R. L. Beatty
11. T. M. Besmann
12. P. J. Blau
13. E. E. Bloom
14. R. A. Bradley
15. D. N. Braski
16. K. Breder
17. D. W. Coffey
18. D. F. Craig
19. D. DePaoli
20. R. B. Dinwiddie
21. L. B. Dunlap
22. M. K. Ferber
23. R. G. Gilliland
24. H. W. Hayden
25. A. Haynes
26. C. Hoffmann
27. L. L. Horton
28. M.-C. Hu
29. C. R. Hubbard
30. M. A. Janney
31. D. R. Johnson
32. D. Joy
33. M. A. Karnitz
34. T. Kirkland
35. M. Lance
36. E. Lara-Curzio
37. Gail Ludtka
38. J. E. Mathis
39. P. Maziasz
40. S. B. McSpadden
41. P. A. Miller
42. W. H. Miller, Jr.
43. K. L. More
44. T. A. Nolan
45–46. A. E. Pasto
47. E. A. Payzant
48. W. D. Porter
49. M. Rawlins
50. C. Rawn
51. L. Riester
52–53. B. J. Russell
54. A. C. Schaffhauser
55. S. Spoone
56. E. Voelkl
57. L. Walker
58. H. Wang
59. X.-L. Wang
60. T. R. Watkins
61. A. A. Wereszczak
62. S. Widjaja
63. R. E. Ziegler

EXTERNAL DISTRIBUTION

64–67. 3M Company, Advanced Ceramics Program, 1425 Parkway Drive, Menomonie, WI 54751

M. J. Besser
E. Kahler
C. Dye
B. Link

68–70. Advanced Ceramics Research, Inc., 841 E. 47th St., Tucson, AZ 85713

H. Denham
K. Stuffle
S. Nowell

71–72. Advanced Technology Materials Inc., Suite A #2, 3006 Research Drive, State College, PA 16801

K. J. Kozaczek
D. Kurtz

73–78. Alabama A&M University, Center for Irradiation of Materials, P.O. Box 1447, Normal, AL 35762-1447

D. Ila
Y. Qian
E. Williams
L. Evelyn
T. Taylor
R. L. Zimmerman

79. AlliedSignal Engines, M/S 93-77/301-227, 111 S. 34th Street, PO Box 52181, Phoenix, AZ 85072-2181

M. N. Menon

80–81. AlliedSignal, Inc., Box 1021, Morristown, NJ 07962-1021

C.-W. Li
P. Whalen

82. AlliedSignal, Inc., Ceramic Components, 2525 West 190th St., Box 2960, Torrance, CA 90509-2960

M. L. Savitz

83. ANI Adtech Nepth Inc., 220 N. Lombard Avenue, Oak Park, IL 60302-2504

S. N. Sinha

84–87. Automotive Mkt. and Prod. Development, ARMCO Inc., 705 Curtis Street, Middletown, OH 45044

D. M. Bench
B. A. Kneveppel
J. A. Douthett
J. E. White

88. Browne Technology, Inc., 315 10th Avenue, N. STE 100, Nashville, TN 37203

J. Browne

89. Busek Company, 11 Tech Circle, Natick, MA 01760

D. Carnahan

90–95. Caterpillar—Technology Center, P.O. Box 1875, Tech Center Bldg E, Peoria, IL 61656-1875

M. H. Haselkorn
M. C. Long
J. Rockwood
C. Hsieh
M. J. Readey
J. Zhang

96–97. Chand Kare Technical Ceramics, 2 Coppage Drive, Worcester MA 01603-1252

R. Chand
C. Guo

98. Coors Electronic Package Co., 923 W. Sawmill Road, Quakertown, PA 18951

E. Winters

99. Corning Inc., Sullivan Park, SP-DV-01-09, Corning, NY 14831

J. F. Wight, Jr.

100. Corning Inc., Sullivan Park, SP.FR.18, Corning, NY 14831

H. J. Holland

101-107. Cummins Engine Co., Mail Code 50183, 1900 McKinley Ave., Columbus, IN 47201

A. Y. Cheung
R. D. England
J. Patten
J.-M. Shih
J. A. Denton
C. A. Klepser
S. P. Raebel

108. Dana Corporation, 2001 Sanford Street, P.O. Box 1208, Muskegon, MI 49443

Mr. R. Hite

109. DOE, Office of Assistant Secretary for Defense Programs, Forrestal Building, 1000 Independence Avenue, Washington, DC 20585-0121

D. Byrd

110–111. DOE, Office of Assistant Secretary for Energy Efficiency and Renewable Energy, Office of Transportation Technologies, EE-30, Forrestal Building, 1000 Independence Avenue, Washington, DC 20585-0121

T. J. Gross
A. Hegnauer

112-114. DOE, Office of Assistant Secretary for Energy Efficiency and Renewable Energy, Office of Transportation Technologies, Office of Advanced Automotive Technologies, EE-32, Forrestal Bldg., 1000 Independence Ave., Washington, DC 20585-0121

D. Haught
P. Patil
T. Maréchaux

115–116. DOE, Office of Assistant Secretary for Energy Efficiency and Renewable Energy, Office of Transportation Technologies, Office of Heavy Vehicle Technologies, EE-33, Forrestal Building, 1000 Independence Avenue, Washington, DC 20585-0121

S. Diamond
J. Eberhardt

117. DOE, Office of Assistant Secretary for Energy Research, Forrestal Building, 1000 Independence Avenue, Washington, DC 20585-0121

T. Vojnovich

118–119. DOE, Oak Ridge Operations Office, P.O. Box 2008, Oak Ridge, TN 37831-6269

E. G. Cumesty M. H. Rawlins

120–122. The Dow Chemical Co., LA Highway 1, Plaquemine, LA 70765

J. Blackson M. Cisneros
E. Rightor

123–124. Drexel University, Department of Materials Engineering, Philadelphia, PA 19104

M. W. Barsoum T. El-Raghy

125. Edison Welding Institute, 1250 Arthur E. Adams Dr., Columbus, OH 43221

Mr. Zhili Feng

126. Energy Recovery, Inc., P. O. Box 65157, Virginia Beach, VA 23467-5157

Mr. Leif J. Hauge

127. Ford Motor Company, Mail 3182-Rm 2172A-SRL, 20000 Rotunda Dr, P.O. 2053, Dearborn, MI 48121-2053

J. W. Fash

128–129. Ford Motor Company, Ford Research Laboratory, 20000 Rotunda Drive, MD 3182, SRL, P. O. Box 3053, Dearborn, MI 48121-2053

D. L. Hartsock R. Hecht

130. Ford Motor Company, Ford Research Laboratory, Department of Chemistry, P.O. Box 2053 - MD 3083, Dearborn, MI 48121-2053

C. Narula

131. Ford Motor Company, Ford Research Laboratory, P.O. Box 2053 - MD 3135, Dearborn, MI 48121-2053

A. M. Sherman

132. Ceramics Laboratory, General Electric Corporate, Research and Development (GE CRD), One Research Circle, K1-1C43, Niskayuna, NY 12309

A. Mogro-Campero

133–134. Georgia Institute of Technology, Manufacturing Research Center, 813 Ferst Drive, NW, Atlanta, GA 30332-0560

S. Danyluk L. Nelson

135–138. Georgia Institute of Technology, Woodruff School of Mechanical Engineering, Rm. 437, Manufacturing Res. Center, 813 Ferst Drive, N. W., Atlanta, GA 30332-0405

S. Graham, Jr.
S. Melkote
D. L. McDowell
J. Thiele

139–142. Georgia Institute of Technology, Atlanta, GA 30332-0245

W. B. Carter
A. Saxena
R. H. Norris
F. Yang

143. GM Delphi Chassis Systems, Bldg 7, 1 GM Road, MC: 483-307116, Milford, MI 48380-3726

K. M. Lee

144. W. R. Grace & Co-Conn., Washington Research Center 7500 Grace Drive, Columbia, MD 21044

D. C. Tomczak

145. Hy-Tech Research Corp., 104 Centre Court, Radford, VA 24141

C. Klepper

146–147. Illinois Institute of Technology, 10 W. 33rd Street, Department of Chemical Engineering, Chicago, IL 60616

H. Maleki
J. R. Selman

148. Inco Alloys International, Inc., 3200 Riverside Drive, Huntington, WV 25705

M. Fahrmann

149. Kennametal, Inc., Route 981 South, Latrobe, PA 15650

R. Yeckley

150. Kyocera Industrial Ceramics Corp., 5713 E. 4th Plain Blvd., Vancouver, WA 98661

E. H. Kraft

151–152. Lehigh University, Dept. of Materials Science & Engineering, 5 E. Packer Avenue, Bethlehem, PA 18015-3195

B. F. Levin
D. B. Williams

153–154. Louisiana State University, 117 Davis Boyd Hall, Baton Rouge, LA 70803

K. Li
T. W. Liao

155. Machining Research Inc., 7785 Foundation Drive, Suite 1, Florence, KY 41042

G. Hughes

156. Materials Data, Inc., 1224 Concannon Blvd., Livermore, CA 94550

X.-J. Zhu

157. Materials Focus, Inc., 2100 N. Wilmot Road, #214, Tucson, AZ 85712

L. A. Leaskey

158–159. Michigan State University, Engineering Services, Physical Plant, East Lansing, MI 48824

Dr. James V. Beck
Robert L. McMasters

160–161. North Carolina State University, Department of Materials Science and Engineering, 7916 Burlington Hall, Raleigh, NC 27695-7916

J. Kasichainula
A. J. McGinnis

162–163. Norton Company, Northboro R&D Center, Goddard Road, Northboro, MA 01532

R. H. Licht
D. Murphy

164–166. NY College of Ceramics at Alfred University, 2 Pine Street, Alfred, NY 14802

T. C. Bruss
S. T. Misture
J. Taylor

167. NY College of Ceramics at Alfred University, 1 Saxon Drive, Alfred, NY 14801

R. Spriggs

168. Osram Sylvania Products, 131 Portsmouth Ave., Exeter, NH 03833

M. Stough

169–171. The Pennsylvania State University, 220 Steidle Building, University Park, PA 16802

S. M. Ferrell
P. R. Howell
M. J. Mayo

172–177. PPG Industries, Inc., Glass Technology Center, P.O. Box 11472, Pittsburgh, PA 15238

W. Curtis
H. Hughes
E. Kruppa
G. A. Pecoraro
M. Tenhover
M. Zibert

178. Refractory Composites, Inc., 107 N. Langley Rd., Glen Burnie, MD 21060

F. Lauten

179. ReMaxCo Technologies, Inc., 10425 Dogdill Road, Suite B, Knoxville, TN 37932

R. D. Nixdorf

180–181. Rutgers University, Department of Ceramic & Materials Engineering, PO Box 909, Brett and Bowser Roads, Piscataway, NJ 08855

E. K. Akdogan A. Safari

182. Scientific Ecology Group (SEG), 1560 Bear Creek Road, QCEP Operations, West Gate, Oak Ridge, TN 37831

J. T. Duncan

183–184. Smith and Nephew, 1450 Brooks Road, Memphis, TN 38116

G. Hunter M. Long

185–186. Soil and Land Use Technology, Inc., 6300 Georgetown Pike, McLean, VA 22101

R. Livingston N. Shashidhar

187. Southern Illinois University, Ctr. Adv. Friction Studies, Carbondale, IL 62901-4343

D. T. Marx

188–189. Southern University, Dept. of Mechanical Engineering, P.O. Box 9987, Baton Rouge, LA 70813

E. Balikci R. A. Mirshams

190–192. Stevens Institute of Technology, Materials Sci. and Engineering, Castle Point on the Hudson, Hoboken, NJ 07030

T. M. Chou M. R. Libera
Y. C. Wang

193–194. Stone & Webster Engineering Corp., 1430 Enclave Parkway, Houston, TX 77077

J. Gondolfe D. Tribbey

195. 113 Newell Lane, Oak Ridge, TN 37830

V. J. Tennery

196–198. Texas A&M University, Department of Mechanical Engineering, College Station, TX 77843-3123

M. Gibbs
K. T. Hartwig
S. Leipert

199. The Torrington Co., P.O. Box T, Rutherfordton, NC 28139

H. W. Walton

200. United Defense, 2101 West 10th Street, Box 1030, Anniston, AL 36202

J. Boggan

201. Universal Energy Systems, Inc., 4401 Dayton-Xenia Road, Dayton, OH 45432-1894

R. S. Bhattacharya

202–204. University of Alabama, 1016 15th Street South, Materials Engineering Annex, Birmingham, AL 36294-4552

C. T. Bates
H. E. Littleton
T. V. Molibog

205–207. University of Alabama, Center for Materials for Information Technology, Box 870209, Tuscaloosa, AL 35487-0209

H. Jiang
T. Klemmer
L. Varga

208–209. University of Central Florida, Cntr. for Res. & Edu. in Optics and Lasers, Laser Assisted Mtrls. & Mechan. Processing Laboratory, P.O. Box 162700, Orlando, FL 32816-2700

F. J. Kahlen
A. Kar

210–212. University of Cincinnati, Dept. of Materials Sci. & Eng., Cincinnati, OH 45221-0012

R. N. Singh
Y.-L. Wang
J. E. Webb

213. University of Cincinnati, M. L. 30, Dept. of Electrical Engineering, Cincinnati, OH 45221

C. T. Blue

214–216. University of Connecticut, Department of Physics, Storrs, CT 05269

D. M. Pease
K. Vaidyanathan

217–219. University of Dayton, Chemical & Materials Eng. Dept, 300 College Park, Dayton, OH 45469-0172

N. L. Hecht
A. H. Lubis
R. Ruh

220–221. University of Illinois at Chicago, Department of Mechanical Engineering, 842 West Taylor Street, Chicago, IL 60607

C. Y. Baek
Y. Gogotsi

222. University of Illinois at Urbana, 2214 S. Lynn St., Urbana, IL 61801

W. S. Williams

223. University of Kentucky, 177 Anderson Hall, Lexington, KY 40506-0046

E. Dickey

224–225. University of Kentucky, Center for Applied Energy Research, 3572 Iron Works Pike, Lexington, KY 40511-8433

B. H. Davis
R. Srinivasan

226–228. University of Maine, Laboratory for Surface Science & Technology 5764 Sawyer Research Center, Orono, ME 04469-5764

O. D. Greenwood
R. J. Lad
S. C. Moulzolf

229. University of Massachusetts, Dept. of Mech. Eng., Engineering Laboratory Building, Amherst, MA 01003

K. Jakus

230. University of Nevada, Department of Chemical and Metallurgical Engineering, Mackay School of Mines, Mail Stop 170, Reno, Reno, NV 89557

D. Chandra

231–232. University of New Mexico, UNM-NSF Center for Micro-Engineered Ceramics, 209 Farris Engineering Center, Chemical and Nuclear Engineering Department, Albuquerque, NM 87131-1341

A. K. Datye
L. D. Mansker

233–236. University of North Dakota, 15 N. 23rd St., Box 9018, Grand Forks, ND 58202-9018

B. C. Folkedahl
J. Hurley
F. R. Karner
C. G. Tomforde

237–238. University of Pittsburgh, 848 Benedum Hall, Materials Science & Engineering Department, Pittsburgh, PA 15261

J. R. Blachere
G. H. Meier

239–241. University of Tennessee Medical Center, Department of Oral Surgery, Oral & Maxillofacial Surgery, POB 3, Suite 335, 1930 Alcoa Highway, Knoxville, TN 37920-1514

D. Gerard
M. K. Marks
M. Muendel

242–243. University of Virginia, Department of Materials Science and Engineering, Thornton Hall, Charlottesville, VA 22903-2442

Mr. M. H. Ettenberg
Dr. William A. Jesser

244–245. University of Wisconsin at Milwaukee, 3203 North Downder Ave., Mitchell Hall, Milwaukee, WI 53201

Dr. Tery L. Barr J. J. Bruckner

246–248. University of Wisconsin - Milwaukee, Department of Physics, P.O. Box 413, 1900 E. Kenwood Blvd., Milwaukee, WI 53201

M. Gajdardziska-Josifovska R. Plass
M. Schofield

249. Valenite, Inc., 1711 Thunderbird, Troy, MI 48084

K. Narasimhan

250. Western Michigan University, College of Engineering and Applied Science, Kalamazoo, MI 49008

A. A. Olowe

251. Westinghouse Power Generation, 4400 Alafaya Trail MC 303, Orlando, FL 32826

M. Arana